FisEs'26

XXVI CONFERENCIA DE
FÍSICA ESTADÍSTICA

Libro de resúmenes

TARRAGONA · 2026

UNIVERSITAT ROVIRA i VIRGILI

CÀTEDRA de CIÈNCIA i HUMANISME
UNIVERSITAT ROVIRA i VIRGILI

Real Sociedad Española de Física
R.S.E.F.

DIFENSC
DIVISIÓN DE FÍSICA ESTADÍSTICA, NO LINEAL Y SISTEMAS COMPLEJOS

Índice general

Historia iv

Comités v

Programa vi

1. Charlas Invitadas 1
Antonioni, Alberto . . . 2
Dominguez Garcia, Virginia . . . 3
Guardia, Elvira . . . 4
Ibañes Miguez, Marta . . . 5
Luque Serrano, Bartolo . . . 6
Manrubia, Susanna . . . 7
Olmi, Simona . . . 8
Rodriguez Parrondo, Juan Manuel . . . 9
Sánchez de Andrés, Álvaro . . . 10
Sartori, Pablo . . . 11
Tarazona Lafarga, Pedro . . . 12

2. Charlas Cortas 13
Aguilar Sánchez, Javier . . . 14
Alsina, Adolfo . . . 15
Bel Bordes, Gemma . . . 16
Buceta Fernandez, Javier . . . 17
Capitán Gómez, José Ángel . . . 18
Echeverría Huarte, Iñaki . . . 19
Faraudo, Jordi . . . 21
Franco Oñate, María José . . . 22
García Pantaleón Tarifa, María Jinxue . . . 23
González-Casado, Miguel A. . . . 24
González Méndez, David . . . 25
Grande, Mar . . . 26
Grasa Lainez, Marta . . . 27
Gutiérrez Arroyo, Adrián . . . 29
Hidalgo Aguilera, Jorge . . . 30
Ibáñez García, Miguel . . . 32
Llabrés Rubio, Jaume . . . 33
Mayo León, Manuel . . . 34
Palermo, Giovanni . . . 35
Pascual-García, Alberto . . . 36
Santalla, Silvia . . . 37
Sanz Arqué, Verónica . . . 38
Seoane Bartolomé, Beatriz . . . 39
Viader Godoy, Xavier . . . 40

3. Pósteres 41
Alonso Muñoz, Sergio . . . 42
Ares, Saúl . . . 43
Artime Vila, Oriol . . . 44
Bartolucci, Giacomo . . . 45
Bellisardi, Federico . . . 46
Benito Calvino, Guillermo . . . 47
Borondo Benito, Javier . . . 48
Briñas, Natalia . . . 49
Burgio, Giulio . . . 50
Campos Moreno, Daniel . . . 51
Cao García, Francisco Javier . . . 52
Carpio Rivas, David Mateo . . . 53

Castioni, Piergiorgio . . . 55
Castro, Luis . . . 56
Castro Ponce, Mario . . . 57
Chamorro Burgos, Miguel Ángel . . . 58
Colet, Pere . . . 60
Coterillo Ruisánchez, Raúl . . . 61
Cristin, Javier . . . 63
De Leonardis, Matteo . . . 64
Diaz Moreno, Alejandro . . . 65
Diez, Jonathan . . . 66
Dilisante, Francesca . . . 67
Fernandez Garrido, Pablo . . . 68
Fernández Peralta, Antonio . . . 70
Franzese, Giancarlo . . . 71
Galeano, Javier . . . 72
Galeano, Javier . . . 73
Galeano, Javier . . . 74
Gallarta Sáenz, Pablo . . . 75
Gancio, Juan . . . 76
García de Lamo, Elena . . . 77
García Inglés, Jorge . . . 78
García-Muelas, Rodrigo . . . 79
García Ortiz, Enrique . . . 80
Ghivarello, Sara . . . 81
Guzmán Schiller, Gabriel Mallku . . . 82
Hernandez Arnal, Violeta . . . 84
Hernández-Fernández, Antoni . . . 85
Hernandez Garcia, Emilio . . . 87
Iribas de la Puerta, Juan . . . 88
Jarillo Díaz, Javier . . . 89
Jiménez Flores, Daniel . . . 90
Jiménez González, Pedro . . . 91
Khalil Rodríguez, Nagi . . . 92
Kim, Jungho . . . 93
Lamata Otín, Santiago . . . 94
Lamata Otín, Santiago . . . 95
Lázaro Sánchez, Teresa . . . 97
Leyva, Inmaculada . . . 98
López, Juan Manuel . . . 99
López Zancajo, Judith . . . 100
Losada, Juan Carlos . . . 101
Losada, Juan Carlos . . . 103
Maire, Raphaël . . . 104
Mampel, Jorge . . . 105
March Pons, David . . . 106
March Pons, David . . . 107
Marinelli, Dimitri . . . 108
Martínez Ratón, Yuri . . . 109
Martínez Saiz, Pedro . . . 110
Martins Cano, Marina . . . 111
Matias, Manuel A. . . . 112
Maza Cuello, Mara . . . 113
Maza Ozcoidi, DIego . . . 114
Megías Fernández, Alberto . . . 115
Mejía Monasterio, Carlos . . . 117
Mejía Parra, Oscar Ricardo . . . 118
Mendívil Carboni, Marco . . . 120
Miguel López, María del Carmen . . . 121
Molas, Daniela . . . 122

Montero Martinez, Ana Maria . . . 123
Muñoz Ortega, Francisco Javier . . . 124
Muñoz Puente, Fernando . . . 125
Nadal Rosa, Adrián . . . 127
Nieto Vargas, Eduardo . . . 128
Ocio Moliner, Mikel . . . 129
Oliver Bonafoux, Sara . . . 130
Ortiz del Campo, David . . . 131
Patti, Alessandro . . . 132
Pérez González, Federico . . . 133
Perez Mariño, Ines . . . 134
Perez Muñuzuri, Alberto . . . 135
Pérez Muñuzuri, Vicente . . . 136
Prat Pou, Arnau . . . 137
Ramírez de la Piscina Millán, Laureano . . . 138
Reguera, David . . . 140
Revuelta Peña, Fabio . . . 141
Ríos Monje, Carlos . . . 142
Rodríguez Cabanillas, Juan Carlos . . . 143
Rodríguez-Laguna, Javier . . . 145
Rojas Navarrete, Consuelo . . . 147
Rosillo Rodes, Pablo . . . 148
Rosillo Rodes, Pablo . . . 149
Rozas Garcia, Enrique . . . 151
Sánchez Díez, Marta . . . 152
Sánchez Rego, Paula . . . 153
Santos, Andrés . . . 154
Sendiña Nadal, Irene . . . 155
Sevostianov, Ivan . . . 156
Silvano, Nathan . . . 157
Sintes Olives, Tomas . . . 158
Suárez Román, Manuel . . . 159
Tajuelo Valbuena, Ángela . . . 160
Téllez Calle, Daniel . . . 161
Toral, Raul . . . 162
Torres-Hugas, Lluís . . . 163
Torres Serra, Sergi . . . 164
Trigal, Lucas . . . 166
Valencia Díaz, Yolanda . . . 167
Velasco Falguera, Núria . . . 168
Vivet Parés, Arnau . . . 169

Lista de participantes **170**

Historia

La Reunión de Física Estadística se viene celebrando en intervalos de año y medio desde 1987, año en el que tuvo lugar la primera edición en Barcelona. Desde 1996 esta reunión es conocida también como FisEs. Con FisEs'26 se cumplirán, por tanto, 39 años de reuniones.

Ha sido organizada siempre por distintos grupos de investigación, repartidos por toda la geografía nacional, y ha reunido a una media de 150 investigadores y a conferenciantes invitados de primera talla mundial.

En torno a FisEs se creó, en el año 2001, el Grupo Especializado de Física Estadística y No Lineal (GEFENOL), dentro del marco de la Real Sociedad Española de Física. Su principal objetivo es promover la Física Estadística y No Lineal en España y el intercambio científico y académico entre los grupos que investigan en estas disciplinas. Recientemente (en la Junta Ordinaria de la RSEF celebrada el 20 de diciembre de 2024) se aprobó la transformación del Grupo Especializado en Física Estadística y No Lineal (GEFENOL) a División con el nombre de División de Física Estadística, No Lineal y Sistemas Complejos (DIFENSC), por lo que la reunión FisEs pasa a estar enmarcada como una actividad dentro de esta división.

La edición de este año la organiza el Alephsys Lab, de la Universitat Rovira i Virgili (URV).

Reuniones FisEs realizadas hasta la fecha

I Física Estadística'87
Barcelona, Mayo 1987

II Física Estadística'88
Palma de Mallorca, Septiembre 1988

III Física Estadística'90
Badajoz, Mayo 1990

IV Física Estadística'91
Gijón, Septiembre 1991

V Física Estadística'93
El Escorial, Mayo 1993

VI Física Estadística'94
Sevilla, Octubre 1994

VII Física Estadística, FisEs'96
Zaragoza, Mayo 1996

VIII Física Estadística, FisEs'97
Getafe, Septiembre 1997

IX Física Estadística, FisEs'99
Santander, Mayo 1999

X Física Estadística, FisEs'00
Santiago de Compostela, Septiembre 2000

XI Física Estadística, FisEs'02
Tarragona, Mayo 2002

XII Física Estadística, FisEs'03
Pamplona, Octubre 2003

XIII Física Estadística, FisEs'05
Madrid, Junio 2005

XIV Física Estadística, FisEs'06
Granada, Septiembre 2006

XV Física Estadística, FisEs'08
Salamanca, Marzo 2008

XVI Física Estadística, FisEs'09
Huelva, Septiembre 2009

XVII Física Estadística, FisEs'11
Barcelona, Junio 2011

XVIII Física Estadística, FisEs'12
Palma, Octubre 2012

XIX Física Estadística, FisEs'14
Ourense, Abril 2014

XX Física Estadística, FisEs'15
Badajoz, Octubre 2015

XXI Física Estadística, FisEs'17
Sevilla, Marzo 2017

XXII Física Estadística, FisEs'18
Madrid, Octubre 2018

XXIII Física Estadística, FisEs'22
Zaragoza, Mayo 2022

XXIV Física Estadística, FisEs'23
Pamplona, Octubre 2023

XXV Física Estadística, FisES'25
Santiago de Compostela, Junio 2025

XXVI Física Estadística, FisES'26
Tarragona, Octubre 2026

Comités

Comité organizador

- Alex Arenas (coordinador)
- Clara Granell
- Sergio Gómez
- David Soriano-Paños

Comité científico

- Alex Arenas (Universitat Rovira i Virgili)
- Rosa María Benito (Universidad Politécnica de Madrid)
- Giancarlo Franzese (Universitat de Barcelona)
- María Isabel García de Soria (Universidad de Sevilla)
- Eva González Noya (Instituto de Química Física Rocasolano, CSIC)
- Jesús Gómez Gardenes (Universidad de Zaragoza)
- Manuel Matías (Institut de Física Interdisciplinària i Sistemes Complexos, UIB-CSIC)
- Carlos Pérez Espigares (Universidad de Granada)
- Alberto Pérez Muñuzuri (Universidade de Santiago de Compostela)
- Clara Prats Soler (Universitat Politècnica de Catalunya)
- Irene Sendiña (Universidad Rey Juan Carlos)
- Iker Zuriguel Ballaz (Universidad de Navarra)

Comité local

- Lluis Arola-Fernández
- Piergiorgio Castioni
- Jordi Duch
- Roger Guimerà
- Mattia Mattei
- Marta Sales-Pardo
- Lluís Torres-Hugas
- Arnau Vivet

Programa

Miércoles 14 de octubre de 2026

14:00 – 15:00	**Registro**
15:00 – 15:15	**Presentación**
15:15 – 16:00	**Juan M. R. Parrondo** *¿Es objetiva la irreversibilidad?*
16:00 – 16:15	**Verónica Sanz-Arqué** *Stochastic resetting with limited information.*
16:15 – 16:30	**Beatriz Seoane** *RBMs, powerful modeling machines*
16:30 – 17:00	**Coffee break**
17:00 – 18:00	**Poster Session 1**
18:00 – 18:45	**Marta Ibañes** *Resource limitation and Criticality in Developmental Pattern Formation*
18:45 – 19:00	**Gemma Bel-Bordes** *Detecting Shared Functional Groups of Neurons Across Connectomes*

Nota: los títulos de las contribuciones se han mantenido en el idioma en el que se han recibido. Este idioma puede coincidir o no con el idioma en el que se imparte la charla.

Actualización indicada en el programa original: 25/09/2026, 18:19.

Programa

Jueves 15 de octubre de 2026

09:00 – 09:45	**Susanna Manrubia** *Universality of hierarchical organization in viral populations*
09:45 – 10:00	**Jorge Hidalgo** *Delayed reproduction in fluctuating environments*
10:00 – 10:15	**José Ángel Capitán** *Robust coexistence in ecological communities dominated by competition*
10:15 – 10:30	**Adrián Gutiérrez-Arroyo** *The role of space in explaining macroecological patterns of microbial abundance*
10:30 – 11:00	**Simona Olmi** *The π-transition: A tipping point for the Kuramoto model with triadic repulsive interaction*
11:00 – 11:30	**Coffee break**
11:30 – 12:00	**Alberto Antonioni** *Synchronization as a Social Dilemma: From Complex Networks to Mobile Populations*
12:00 – 12:15	**Miguel A. González-Casado** *Detailed balance from social rules: a model for the evolution of social relationships*
12:15 – 12:30	**Giovanni Palermo** *Beyond the Wisdom of the Crowd: How Network Topology Distorts Collective Perception*
12:30 – 12:45	**Jaume Llabrés** *Reducibility of higher-order to pairwise interactions: Social impact models on hypergraphs*
12:45 – 13:00	**Mar Grande** *Leveraging Complex Networks for Portfolio Optimization and Risk Management in Finance*
13:00 – 14:30	**Lunch**
14:30 – 15:15	**Álvaro Sánchez** *The latent simplicity of ecological interactions*
15:15 – 15:30	**Alberto Pascual-García** *Towards the identification of principles for the design of stable microbial communities*
15:30 – 15:45	**Xavier Viader-Godoy** *Learning and adaptive dynamics in bacteria under precise microfluidic control*
15:45 – 16:00	**María Jinxue García-Pantaleón** *Information dynamics and learning in gene regulatory networks*
16:00 – 16:30	**Coffee break**
16:30 – 17:30	**Poster Session 2**
17:30 – 18:00	**Pablo Sartori** *Thinking matter: multifarious systems in and out of equilibrium*
18:00 – 18:15	**Jordi Faraudo** *Statistical physics tools to improve cancer immunotherapy*

Programa

Viernes 16 de octubre de 2026

09:00 – 09:45	**Pedro Tarazona** *La Mecánica Cuántica como un problema de Física Estadística*
09:45 – 10:00	**David González Méndez** *Kinetic theory of transport and segregation in confined granular mixtures*
10:00 – 10:15	**Manuel Mayo** *Collisional Cooling Induces Phase Separation Of Active Particles*
10:15 – 10:30	**Marta Grasa** *Stronger is Slower: Decoupling speed and pushing in evacuations through a bottleneck*
10:30 – 11:00	**Elvira Guardia** *Fingerprints of structural transitions in liquid water at high temperatures and pressures*
11:00 – 11:30	**Coffee break**
11:30 – 11:45	**Iñaki Echeverría-Huarte** *Pedestrian rotations may render obstacles ineffective in competitive evacuations*
11:45 – 12:00	**Miguel Ibáñez** *Memory-inspired acceleration of electro-orientation in nanoparticle suspensions*
12:00 – 13:00	**Tesis 'Gran Reserva'** *Con la inestimable participación de: Javier Brey, Albert Díaz-Guilera, Miguel Rubí, Maxi San Miguel, Anxo Sánchez, José María Sancho.*
13:00 – 14:30	**Lunch**
14:30 – 15:00	**Virginia Domínguez-García** *Using Complex Networks to Understand Ecological Communities*
15:00 – 15:15	**Adolfo Alsina** *Robust bilateral symmetry in the zebrafish retina emerges from stochastic differentiation dynamics*
15:15 – 15:30	**Javier Buceta** *Growth-induced buckling as a mechanochemical switch for patterning and division-site memory in bacterial filaments*
15:30 – 15:45	**María José Franco Oñate** *Active wetting transition in cellular aggregates*
15:45 – 16:45	**Poster Session 3**
16:45 – 17:15	**Coffee break**
17:15 – 17:30	**Javier Aguilar** *The Limits of Inference in Complex Systems: When Stochastic Models Become Indistinguishable*
17:30 – 17:45	**Silvia N. Santalla** *Beyond pairs: higher-order entanglement hyperlinks*
17:45 – 18:15	**Bartolo Luque** *La emergencia de vida compleja fue el resultado inevitable de una transición de fase algorítmica*
18:15 – 18:30	**Entrega de premios y clausura**

Charlas Invitadas

Synchronization as a Social Dilemma: From Complex Networks to Mobile Populations

Alberto Antonioni
Grupo Interdisciplinar de Sistemas Complejos (GISC),
Department of Mathematics, Carlos III University of Madrid
Avenida de la Universidad 30, Leganés, Spain

Synchronization is a paradigmatic example of collective behavior: interacting units adjust their rhythms and spontaneously develop macroscopic order. The Kuramoto model provides a foundational framework for understanding how this collective order emerges in populations of coupled oscillators [1]. From biological oscillators to technological infrastructures, understanding synchronization also requires accounting for the structure of interactions. Its study on complex networks has revealed how topology shapes the emergence of coherence, extending classical descriptions based on regular lattices or all-to-all coupling [2]. Yet interactions are often assumed to occur unconditionally, overlooking the individual effort required to achieve a collective benefit.

In this talk, I will explore synchronization through the lens of evolutionary game theory. In the Evolutionary Kuramoto Dilemma, oscillators can either cooperate, paying a cost to adjust their rhythms to those of their neighbors, or defect, avoiding this effort while potentially benefiting from the adjustments made by others [3]. Synchronization thus becomes a social dilemma, with collective coherence depending on the evolution of individual willingness to contribute. Network structure critically affects the outcome: stronger coupling does not necessarily improve coordination, and increasing interaction costs can undermine both cooperation and synchronization. Moreover, spatial networks can sustain cooperative, locally synchronized clusters without achieving global phase coherence.

I will then present recent work extending this framework to mobile populations, where movement continuously reshapes proximity-based interactions [4]. We find that intermediate displacement relative to the interaction radius can enable cooperation and global synchronization to emerge together. Mobility connects otherwise separated local groups while preserving interactions long enough to support coordination. At low mobility, coherence remains largely local; at high mobility, rapid neighborhood turnover narrows the parameter region supporting sustained cooperation and synchronization. Collective order therefore depends on a balance between mixing, interaction persistence, and individual costs.

These findings suggest potential design principles for decentralized systems such as drone swarms and mobile sensor networks, where coordinating activity requires costly communication or adjustment. In particular, tuning mobility relative to interaction range may help sustain collective coordination without centralized control.

[1] Y. Kuramoto, *Cooperative Dynamics of Oscillator Community: A Study Based on Lattice of Rings*, Prog. Theor. Phys. Suppl. **79**, 223–240 (1984).

[2] A. Arenas, A. Díaz-Guilera, J. Kurths, Y. Moreno, and C. Zhou, *Synchronization in complex networks*, Phys. Rep. **469**, 93–153 (2008).

[3] A. Antonioni and A. Cardillo, *Coevolution of Synchronization and Cooperation in Costly Networked Interactions*, Phys. Rev. Lett. **118**, 238301 (2017).

[4] M. Lambresa and A. Antonioni, *Coevolution of Synchronization and Cooperation in Mobile Populations*, under review.

Using Complex Networks to Understand Ecological Communities

Virginia Domínguez-García[1],
[1]Estación Biológica de Doñana - CSIC, Américo Vespucio sn, 41092, Sevilla

Ecosystems are not just collections of species, but webs of interactions linking organisms across multiple scales. These relationships can be represented as ecological networks, providing a powerful framework to connect interaction structure with community-level properties. In this talk, I will show how approaches from complex science can help us understand how real communities persist through time and respond to environmental change. By examining the architecture of interactions, I will illustrate how it shapes community dynamics, stability, and ecosystem functioning, offering new insights into the mechanisms that sustain biodiversity.

Fingerprints of structural transitions in liquid water at high temperatures and pressures

Elvira Guardia[1], Fausto Martelli[2,3], and Ioannis Skarmoutsos[4]
[1]Departament de Física, Universitat Politècnica de Catalunya, Campus Nord B4-B5, Barcelona E-08034, Spain
[2]Dipartimento di Fisica, Università di Roma La Sapienza, Piazale Aldo Moro 5, Rome 00185, Italy
[3] CNR-Istituto dei Sistemi Complessi, Piazzale Aldo Moro 5, Rome 00185, Italy
[4]Laboratory of Physical Chemistry, Department of Chemistry, University of Ioannina, 45110 Ioannina, Greece

A molecular-level understanding of the properties of water is fundamental to a wide range of processes in physics, chemistry, geosciences, biology, and life evolution. In this talk, I will present a classical molecular dynamics simulation study for liquid water along different high pressure isobars, covering a wide temperature range from ambient to near-critical conditions. The simulations were carried out using the TIP4P-2005 potential model [1]. Particular attention was given to the behavior of various local structural descriptors of liquid water, as well as to the corresponding dynamics and entropic quantities. The results obtained reveal the existence of two distinct structural transitions, located in the temperature range around 423.15 and 498.15 K, respectively. The observed transitions have been characterized by local extrema and crossovers in many of the above-mentioned quantities. Significant changes of the hydrogen bond network were also observed across these transitions. These structural rearrangements are reflected in the calculated intermolecular vibrational and librational dynamics, as evidenced by clear modifications in the spectral densities of atomic velocity correlation functions and in the translational and rotational densities of states. Figures 1 and 2 show some recently published results for the 50 MPa isobar [2].

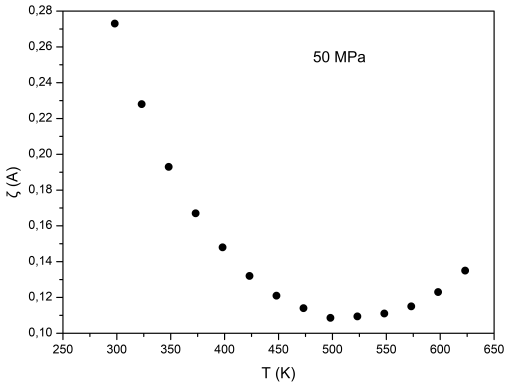

Fig. 1: Temperature dependence of the Tanaka's structural descriptor ζ [3, 4] along the 50 MPa isobar.

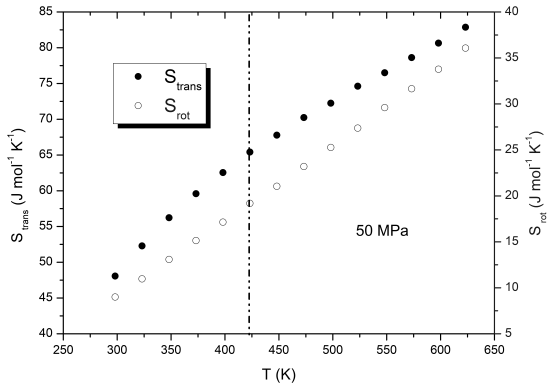

Fig. 2: Temperature dependence of the translational S_{trans} and rotational S_{rot} components of the total entropy of liquid water along the 50 MPa isobar. S_{trans} and S_{rot} were evaluated using the two-phase thermodynamic (2PT) model [5–7].

[1] J. L. F. Abascal and C. Vega, J. Chem. Phys. **123**, 234505 (2005).
[2] I. Skarmousos, F. Martelli, and E. Guardia, J. Chem. Phys. **164**, 054503 (2026).
[3] J. Russo and H. Tanaka, Nat. Commun. **5**, 3556 (2014).
[4] H. Tanaka, H. Tong, R. Shi and J. Russo, Nat. Rev. Phys. **1**, 333 (2019).
[5] S.-T. Lin, M. Blanco and W. A. III Goddard, J. Chem. Phys. **119**, 11792 (2003).
[6] S.-T. Lin, P.K. Maiti and W. A. III Goddard, J. Phys. Chem. B **114**, 8191 (2010).
[7] I. Skarmoutsos, J. Samios and E. Guardia, J. Phys. Chem. Lett. **13**, 7636 (2022).

Resource limitation and Criticality in Developmental Pattern Formation

Josep Mercadal[1,2,3], Sergio Casajús[1,2,4], Enrique García-Ortiz[1,2], Mar Ferreira-Guerra[5,4], Ana I. Caño-Delgado[5] and Marta Ibañes[1,2]
[1]Departamento de Física de la Materia Condensada, Universidad de Barcelona, Martí i Franqués 1, 08028 Barcelona, Spain
[2]Institute of Complex Systems (UBICS), Barcelona, Spain
[3] Present affiliation: Dept. Plant Developmental Biology, Max Planck Institute for Plant Breeding Research, Cologne, Germany
[4] Present affiliation: other.
[5]Department of Molecular Genetics, Centre for Research in Agricultural Genomics (CRAG), CSIC-IRTA-UAB-UB, Campus UAB (Cerdanyola del Vallès), 08193 Barcelona, Spain

The development of multicellular organisms relies on the spontaneous emergence of spatial patterns of gene expression that guide cell differentiation. Through this process, initially similar cells acquire distinct identities in a coordinated manner across both space and time. From a physics perspective, this represents a striking example of self-organization in a nonequilibrium many-body system, where local interactions between cells give rise to robust large-scale patterns and functional order.

The generation of these patterns requires communication between neighboring cells. Such communication can be mediated by diffusible signaling molecules, direct cell-to-cell transport, or contact-dependent interactions involving membrane-bound proteins. Through these mechanisms, cells continuously exchange information and dynamically adjust their internal states in response to their local environment. In many developmental systems, these interactions are short-ranged and produce patterns in which adjacent cells adopt distinct expression states and, consequently, different cellular fates [1].

A paradigmatic example of a short-range interaction is lateral inhibition. In this mechanism, a cell sends inhibitory signals to its neighbors, reducing their ability to signal in return. As a result, a population of initially equivalent cells can spontaneously break symmetry and organize into heterogeneous spatial patterns in which signaling and non-signaling cells alternate [2]. Lateral inhibition therefore provides a biological realization of pattern formation driven by local competitive interactions.

In this talk, I will present recent work on lateral inhibition-mediated pattern formation [3]. We develop and analyze mathematical models that quantitatively account for both publicly available experimental data and new measurements provided by our collaborators [3, 4]. The emphasis will be on how theoretical modeling can reveal the dynamical mechanisms underlying the observed patterns and phenomena and connect cellular interactions to emergent collective behavior. Our results suggest that limitation of resources can be relevant for pattern formation. In particular, I will discuss evidence suggesting that a developmental pattern is established at the onset of a critical transition. This finding raises the possibility that biological systems exploit the enhanced responsiveness and collective dynamics associated with criticality to robustly generate spatial organization during development.

[1] E. García-Ortiz, J. Mercadal, and M. Ibañes, *Dynamics of Cell Fate Patterning in Discrete Multicellular Systems*, Current Opinion in Systems Biology, 100594 (2026).

[2] JR. Collier, NA. Monk, PK. Maini and JH. Lewis, *Pattern formation by lateral inhibition with feedback: a mathematical model of delta-notch intercellular signalling*, J. Theor. Biol. **183**(4), 429-446 (1996).

[3] J. Mercadal, M. Ferreira-Guerra, AI. Caño-Delgado and M. Ibañes, *Cell-type specification at criticality underlies rhizoid patterning in the liverwort Marchantia polymorpha*, Cell Reports **45**(1), 116728 (2026).

[4] A. Thamm, TE. Saunders and L. Dolan, *MpFEW RHIZOIDS1 miRNA-Mediated Lateral Inhibition Controls Rhizoid Cell Patterning in Marchantia polymorpha*, Curr. Biol. **30**, 1905-1915.e4 (2020).

La emergencia de vida compleja fue el resultado inevitable de una transición de fase algorítmica

Bartolo Luque,
Departamenteo de Matemática Aplicada de la ETSI Aeronáuticos y de Espacio.
Universidad Politécnica de Madrid

Analizando estadísticamente las longitudes de los genes y las proteínas de 33.000 especies que recorren el árbol de la vida desde las bacterias a los humanos, hemos descubierto que sus distribuciones son log-normales, que sus longitudes medias han crecido exponencialmente a lo largo de la evolución y que existe una relación invariante de escala, una ley de potencias, entre la longitud media y la varianza de las longitudes de los genes y proteínas de todos los organismos.

En la charla mostraremos cómo todas estas características surgen de manera natural a partir de un sencillo proceso estocástico de crecimiento multiplicativo de los genes que la evolución ha mantenido desde el origen de la vida. Combinar este proceso con la proporción de intrones en los genomas nos conduce a entender la aparición de organismos multicelulares como resultado de una transición de fase algorítmica.

Esta interpretación nos permite, a partir del momento de aparición y tamaño medio del genoma de LUCA (nuestro primer ancestro común con regulación génica) predecir el momento y el tamaño medio del genoma de las primeras células eucariotas que permitieron un crecimiento espectacular de la complejidad de los seres vivos.

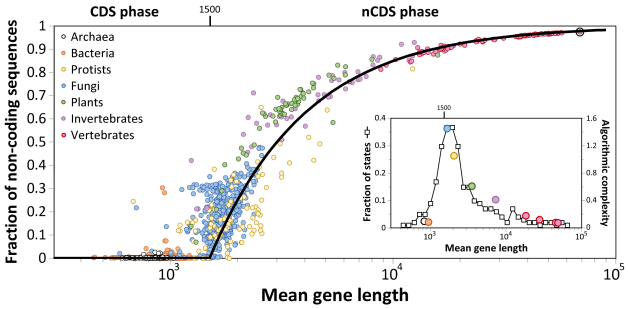

Fig. 1: Transición de fase de segundo orden en la fracción de secuencias no codificantes del gen. Cada punto representa una especie individual (n = 6.519), con Homo sapiens resaltado mediante un círculo. Los distintos colores identifican los principales clados. La línea negra representa la predicción teórica, con una longitud génica media crítica de 1.500 nucleótidos que separa las fases de secuencia codificante (CDS) y secuencia no codificante (nCDS).

[1] EM Muro, FJ Ballesteros, B Luque and J Bascompte, *The emergence of eukaryotes as an evolutionary algorithmic phase transition* , Proceedings of the National Academy of Sciences, 1820 122 (13), e2422968122, (2025).

Universality of hierarchical organization in viral populations

Susanna Manrubia
Museo Nacional de Ciencias Naturales (CSIC), c/ José Gutiérrez Abascal 2, 28006 Madrid
Grupo Interdisciplinar de Sistemas Complejos (GISC), Madrid

RNA viruses form genetically diverse populations structured as mutant spectra, or quasispecies, whose internal organization influences their evolutionary and adaptive dynamics. Recent studies have addressed the structural organization of viral populations in sequence space through the reconstruction of genotype networks. Deep sequencing data for amplicons of multiple viruses show that these networks share overall topological features, including degree distribution, assortativity and clustering, and that they organize hierarchically around the most abundant sequence at each time point.

We will present data from three viruses spanning different evolutionary contexts. First, we will show that the genotype network structure of the Qβ bacteriophage, evolving under controlled laboratory conditions, is independent of the environment. However, network comparison across environments illustrates the first stages of speciation at the molecular level [1]. Second, we will discuss data from SARS-CoV-2 obtained from infected human hosts. Comparison with Qβ reveals that, despite large differences in genome size, mutation rate, and ecological setting, both viruses share a common organization: a highly abundant central haplotype surrounded by layers of variants of diminishing abundance as Hamming distance to the central haplotype increases, resulting in a hierarchical structure [2]. Third, longitudinal data from hepatitis B virus (HBV) in patients undergoing therapy will illustrate how genotype networks help elucidate the movement and reorganization of viral populations over time, reflecting different patterns of response to therapy that can be contrasted with clinical observations [3].

The robust organization found across all viral populations analysed suggests that viruses may share a common genotype network architecture, governed by fundamental properties of sequence space explored through the generic mechanisms of replication and mutation. Genotype networks provide a unifying framework to describe viral population structure beyond conventional diversity measures and, by revealing how local constraints shape mutational search, offer insights into the predictability of viral evolution. The framework will be extended in the near future to populations of other replicating molecular systems, such as viroids, obelisks and RNA aptamers.

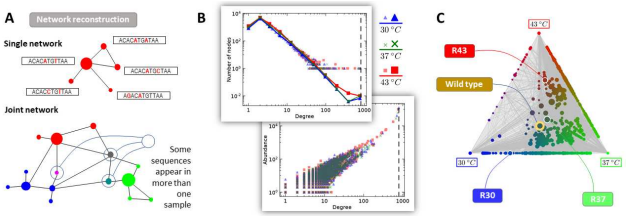

Fig. 1: Empirical genotype networks, visualization and structure. Starting with a common ancestral population, the Qβ phage has been adapted to different environmental temperatures. An amplicon (genomic fragment) has been deep sequenced, yielding tens of thousands of different sequences in each sample. **A.** Schematic of reconstruction of genotype networks. Every sequence is a node of the network; two nodes are linked if they differ in a single mutation. **B.** Replication-mutation dynamics couple sequence abundance and node degree, causing the emergence of a hierarchy that is reflected in the power-law-like degree distribution. **C.** When different experiments (networks) are joined, the corresponding populations occupy different regions in sequence space and partly overlap. This speaks for diversification, preadaptation at short evolutionary time and multiple adaptive pathways.

[1] L. F. Seoane, H. Secaira-Morocho, P. Somovilla, E. Lázaro, and S. Manrubia, *Hierarchical genotype networks and incipient ecological speciation in Qβ phage quasispecies*, Proc. Natl. Acad. Sci. USA **123**, e2512150123 (2026).

[2] S. Martínez-Alcalá, I. Atienza-Diez, P. Somovilla, B. Martínez-González, C. Perales, L. F. Seoane, E. Lázaro, and S. Manrubia, *Shared quasispecies architecture in experimental and natural RNA virus populations*, Virus Evolution, veag053 (2026).

[3] S. Manrubia, I. Atienza-Diez, S. Martínez-Alcalá, and L. F. Seoane, *Reconstructing genotype networks to elucidate HBV quasispecies evolution during treatment*, preprint (2026).

The π-transition : A tipping point for the Kuramoto model with triadic repulsive interaction

Simona Olmi[1]
[1]CNR, Consiglio Nazionale delle Ricerche, Istituto dei Sistemi Complessi, 50019 Sesto Fiorentino, Italy

We have examined the synchronization and de-synchronization transitions observable in the Kuramoto model with a standard pair-wise first harmonic interaction plus a higher order (triadic) symmetric interaction for unimodal and bimodal Gaussian distributions of the natural frequencies $\{\omega_i\}$ [1]. These transitions have been accurately characterized thanks to a self-consistent mean-field approach joined with extensive numerical simulations. The higher-order interactions favor the formation of two cluster states, which emerge from the incoherent regime via continuous (discontinuous) transitions for unimodal (bimodal) distributions. Fully synchronized initial states give rise to two symmetric equally populated bimodal clusters, each characterized by either positive or negative natural frequencies. These bimodal clusters are formed at an angular distance γ, which increases for decreasing pair-wise couplings until it reaches $\gamma = \pi$ (corresponding to an anti-phase configuration), where the cluster state destabilizes via an abrupt transition: the π-transition. Beyond this tipping point the bimodal clusters are immediateley reformed (with a smaller angle γ) and are composed of oscillators with positive and negative $\{\omega_i\}$, however the position of the oscillators with positive and negative frequencies is now exchanged (see Fig. 1). For bimodal distributions we have obtained detailed phase diagrams involving all the possible dynamical states in terms of standard and novel order parameters. In particular, the clustering order parameter, here introduced, appears quite suitable to characterize the two cluster regime. As a general aspect, hysteretic (non hysteretic) synchronization transitions, mostly mediated by the emergence of standing waves, are observable for attractive (repulsive) higher-order interactions. The survavibility and characterization of the π-transition has been investigated in detail also in three more models [2]: i) the Kuramoto model with a standard pair-wise first harmonic interaction plus two higher order (triadic) interaction terms: symmetric and antisymmetric; ii) the Kuramoto model with a standard pair-wise first harmonic interaction plus four-body interaction terms; iii) the Kuramoto model with a standard pair-wise first harmonic interaction plus three-body and four-body interaction terms.

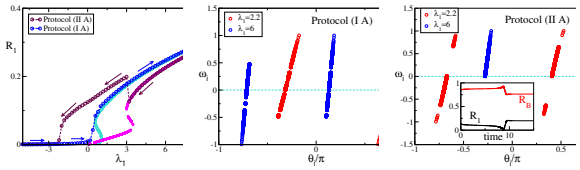

Fig. 1: Natural frequencies distributed according to an unimodal Gaussian distribution and negative triadic coupling λ_2. (a) R_1 (Kuramoto order parameter) versus λ_1 (pair-wise coupling): the blue and maroon circles refer to simulations performed by following protocols (I A) and (II A), respectively. Protocol (I) refers to simulations started with all the oscillators chracterized by random initial phases; protocol (II) refers to an initial state where all the oscillators phases are set to the same value. Furthermore, protocols (I A) and (II A) denote simulations where one of the coupling parameters is varied quasi-adiabatically. The value reported for R_1 represents the average in time over a simulation time T_S . The cyan (magenta) line refers to the self consistent evaluation of the order parameter R_1 estimated in the whole range of frequencies (restricted to positive frequencies). In panels (b) and (c) are reported snapshots of the natural frequencies ω_i versus their phases θ_i for different values of λ_1 for simulations obtained by following protocols (I A) and (II A), respectively. In the inset of panel (c) we report the instantaneous values of $R_1(t)$ (black curve) and $R_B(t)$ (red curve) versus time for $\lambda_1 = 3$ obtained by following protocol (II A).

[1] A. Carballosa, A. Muñuzuri, S. Boccaletti, A. Torcini, S. Olmi, *Cluster States and π-transition in the Kuramoto model with higher order interactions*, Chaos, Solitons and Fractals (2023).

[2] Nicolas Peteri, Synchronization transitions in the Kuramoto model with higher order interactions, Master Thesis (2025)

¿Es objetiva la irreversibilidad?

Juan M.R. Parrondo[1]
[1] Departamento de Estructura de la Materia, Física Térmica y Electrónica and GISC, Universidad Complutense de Madrid.

Las formulaciones habituales de la mecánica estadística incluyen elementos de arbitrariedad o subjetividad: macroestados, *coarse-graining* o probabilidades que reflejan la ignorancia del observador [1].

Por otro lado, hay muchos comportamientos irreversibles que lo son de forma objetiva, es decir, independientemente de la existencia de un observador con información limitada. Consideremos, por ejemplo, dos gases idénticos, etiquetados como 1 y 2 y confinados en cajas de igual volumen. Los dos gases tienen la misma densidad y sus energías internas son E_1 y E_2, con $E_1 > E_2$. Si las cajas se ponen en contacto permitiendo que los gases intercambien energía, la energía fluirá del gas 1 al gas 2 hasta que ambos alcanzan la misma energía, salvo fluctuaciones de orden $1/\sqrt{N}$, en donde N es el número de moléculas de cada gas.

Este flujo irreversible es enteramente objetivo [2]: no depende de la información accesible a un observador macroscópico, de ningún *coarse-graining*, de nuestra ignorancia sobre el estado microscópico de los gases, ni de ninguna otra característica dependiente de un hipotético observador. Es cierto que se requiere un gran número de moléculas para observar claramente la irreversibilidad. Si $\frac{E_1-E_2}{E_1} \simeq \frac{1}{\sqrt{N}}$, entonces el el comportamiento de los dos gases no mostrará ninguna flecha del tiempo claramente definida. La irreversibilidad está siempre enmascarada por fluctuaciones, pero sigue siendo un hecho objetivo de la naturaleza.

A raíz de esta observación surge un pregunta: ¿es posible formular la mecánica estadística de forma objetiva? En esta charla, basada en [4], abordaremos esta cuestión utilizando una entropía dependiente de observables utilizada por Einstein en su estudio de fluctuaciones [3]. Un estudio detallado de esta entropía, que es enteramente objetiva, nos mostrará que la irreversibilidad es independiente de la escala y nos obligará a considerar de forma separada la objetividad de conceptos como entropía, equilibrio o temperatura.

[1] J.L. Lebowitz, *Boltzmann's entropy and time's arrow*, Physics Today **46**, 32 (1993).

[2] D.Z. Albert, *The foundations of quantum mechanics and the approach to thermodynamic equilibrium*, The British Journal for the Philosophy of Science, **45**, 669 (1994).

[3] A. Einstein, Theorie der Opaleszenz von homogenen Flüssigkeiten und Flüssigkeitsgemischen in der Nähe des kritischen Zustandes, Annalen der Physik **338**, 1275 (1910).

[4] J.M.R. Parrondo, *Is entropy objective? Rethinking the foundations of irreversibility and the second law*, PNAS Nexus **5**, 288 (2026).

The latent simplicity of ecological interactions

Alvaro Sanchez[1],
[1] Institute of Functional Biology and Genomics IBFG-CSIC, University of Salamanca, 37007 Salamanca, Spain

Ecological interactions between microorganisms give rise to the collective functions and properties of the communities they form. The potential number of these interactions and their complexity pose a major challenge towards predicting microbial community function. Solving this challenge is necessary if we wish to rationally design microbial consortia. In this talk I will discuss ongoing work from our lab addressing this open problem. We have shown both experimentally and theoretically that even when pairwise and higher-order interactions exist and are strong, they are not independent from each other. Instead, they follow simple linear relationships across all interaction orders. This statistical dependency is a hallmark of low-dimensional collective behavior, where the function of a microbial community is explained by one or two emergent variables. Using consumer-resource models, we show that these collective variables can be directly connected to species traits, such as their metabolic efficiency. We validate this empirically, and show that these results are maintained over time and are robust to community dynamics. Our work provides a quantitative theoretical framework to study, predict, and ultimately engineer emergent functions in microbial communities [1].

[1] Camacho-Mateu, Jose and Quiros-Rodriguez, Isabel and Burgio, Giulio and Arrabal, Andrea and Mendana, Alfonso and de Diez, Miguel and Benitez-Dominguez, Belen and Sanchez, Alvaro, *The latent simplicity of ecological interactions*, bioRxiv 2026–07

Thinking matter: multifarious systems in and out of equilibrium

Pablo Sartori[1],
[1]Gulbenkian Institute of Molecular Medicine, Oeiras, Portugal

What distinguishes living matter from inert matter? Inside a cell thousands of different component types interact to form complex emergent structures. This is unlike classical mixtures, which are made of a few different types and show only a small number of structures. It is also unlike glasses, where every pair of individual components has a unique interaction, resulting in no specific structures at all. The cellular cytoplasm is different, it's *multifarious*, with diversity of interactions at the level of types, and not individual components. This allows the cytoplasm to encode and retrieve multitude functional structures such as crystal-like assemblies, called protein complexes, and liquid-like droplets, called biomolecular condensates (Fig. 1).

In this talk I will give an overview of our attempts in the last years to develop a theory for multifarious soft matter, both in the context of crystaline self-assembly [1–3] as well as multi-component liquids [4, 5]. In particular, I will show how an analogy between neural networks and multicomponent systems allows to treat multifarious matter as a type of associative memory. An unexpected implication is that this allows us to take ideas from soft-matter to develop new types of associative neural networks.

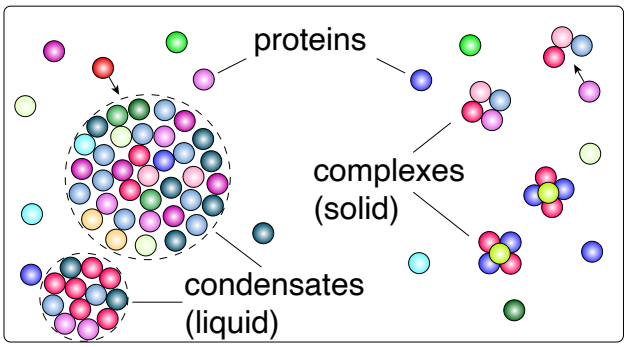

Fig. 1: Schematic of multifarious structures inside the cytoplasm.

[1] P. Sartori and S. Leibler, Lessons from equilibrium statistical physics regarding the assembly of protein complexes, Proc. Natl. Acad. Sci. USA **117**, 114–120 (2020).

[2] F. Benoist and P. Sartori, High-speed combinatorial polymerization through kinetic-trap encoding, Phys. Rev. Lett. **134**, 038402 (2025).

[3] F. Benoist and P. Sartori, Assembly Factors Resolve Speed and Encoding Bottlenecks in Multifarious Self-Assembly, Phys. Rev. X Life **4**, 033021 (2026).

[4] R. Braz Teixeira, G. Carugno, I. Neri, and P. Sartori, Liquid Hopfield model: Retrieval and localization in multicomponent liquid mixtures, Proc. Natl. Acad. Sci. USA **121**, e2320504121 (2024).

[5] R. Braz Teixeira, D. Marcato, I. Neri, and P. Sartori, Metastable phase separation and nucleation of information in multicomponent liquids, Phys. Rev. X (2026).

Quantum Mechanics as a Statistical Physics problem

Pedro Tarazona
Departamento de Física Teorica de la Materia Condensada, IFIMAC Condensed Matter Physics Center,
Universidad Autónoma de Madrid, Madrid 28049

Statistical physics describes a single system using a pair of representations: fine-grained and coarse-grained. The entropy associated to any such pair of descriptions constitutes the essential tool of statistical physics, to incorporate dissipation (the irreversible increase in entropy) as a fundamental physical law for any coarse-grained prediction. Although the physical rules at the fine-grained level may fit within a purely deterministic reductionist framework [*What would happen is fully determined by the present state, and we have the rules to predict it exactly, if we know all that is to be known*], coarse-grained predictions must incorporate dissipation as a physical effect that is (at least!) as "fundamental" as the fine-grain rules.

The physical behaviors emerging at the system's coarse-grained level can lead to a practical (thermodynamic) irreversible determinism [*What would happen is (very likely) the most probable outcome, from the present state*] or to inevitable probabilistic predictions (symmetry breaking), in which we can only calculate the probabilities of a set of possible outcomes [*We never know enough to make real the (hypothetic) fine grain determinism!*]. Challenging the reductionist view of physics, we often find that many details of the fine-grained rules prove irrelevant to coarse-grained predictions (whether deterministic or probabilistic), whereas entropy becomes essential for predicting similar behaviors in systems with vastly different fine-grained natures.

The apparent difficulty in reconciling the deterministic theories for classical and quantum mechanics, the "mysterious leap" from unitary quantum evolution to probabilistic measurement outcomes, and the description of "quantum decoherence" as a physical dissipation effect limiting the promise of emerging "quantum technologies" can all be clarified through the general perspective of statistical physics, with the quantum fine-grain and the classical coarse-grain. The difficulty to interpret the "physical reality" behind quantum mechanics and its matching with the "classical world" comes from reverting those fine/coarse grain roles, i.e. to view quantum states as a "magical coarsening" in which different fine-grain (classical) state appear to be simultaneous, rather than disjoint alternatives.

These concepts—which have given rise to formal frameworks such as Quantum Bayesianism (QBism) [1] and Quantum Darwinism [2] for interpreting quantum physics—are presented in this talk at an intuitive level suitable for undergraduate courses [3]. The talk goes through the practical handling of quantum (de)coherence in laboratories nowadays, and the theoretical descriptions (such as the Lindblad equation [4]) for quantum decoherence, as a dissipation effect within the quantum mechanics of open systems. A brief discussion on the implications for quantum technologies is included.

[1] Christopher A. Fuchs, N. David Mermin, and Rüdiger Schack *An Introduction to QBism with an Application to the Locality of Quantum Mechanics*, American Journal of Physics **82**, 749-754 (2014).

[2] Wojciech H. Zurek *Quantum Darwinism*, Nature Physics **5**, 181-188 (2009)

[3] Pedro Tarazona Lafarga *El Bayesianismo Cuántico ("Qbism"): Una interpretacion "sin misterio" para la Mecánica Cuántica* Revista Española de Física **38** 1-5 (2024)

[4] e.g. Daniel Manzano *A short introduction to the Lindblad Master Equation*, https://doi.org/10.48550/arXiv.1906.04478 (2009)

Charlas Cortas

The Limits of Inference in Complex Systems: When Stochastic Models Become Indistinguishable

Javier Aguilar[1], Miguel A. Muñoz [2], and Sandro Azaele[3,4]
[1] Quantitative Life Sciences, The Abdus Salam International Centre for Theoretical Physics (ICTP), Trieste, Italy
[2] Departamento de Electromagnetismo y Física de la Materia and
Instituto Carlos I de Física Teórica y Computacional. Universidad de Granada. E-18071, Granada, Spain
[3] Dipartimento di Fisica e Astronomia Galileo Galilei, Università degli Studi di Padova, via Marzolo 8, 35131 Padova, Italy
[4] Istituto Nazionale di Fisica Nucleare, 35131, Padova, Italy

Simple stochastic models are widely used to describe complex phenomena, as they provide an interpretable connection between minimal microscopic descriptions and macroscopic statistical patterns. A central challenge in this approach is selecting the appropriate model—and its parameters—to accurately capture specific datasets. We present a framework based on change-of-measure theory and bridge processes to perform parametric inference and assess model distinguishability using path statistics. With this tool, we identify optimal sampling protocols that minimize errors in parameter estimation, while also revealing fundamental limits of inference: the ability to discriminate between competing models is intrinsically constrained by data quality (e.g., sampling frequency and dataset size). We illustrate the framework with applications to diverse datasets (particle trapped with optical tweezers, human microbiome, topic mentions in social media, and forest population dynamics) showing how inference limits manifest in practice and inform ongoing modeling debates (see Fig. 1). Ultimately, we show that inference limits are not a failure of method, but an intrinsic property of the data-generating process itself. This contribution aims to summarize the main aspects of our work in Ref. [1].

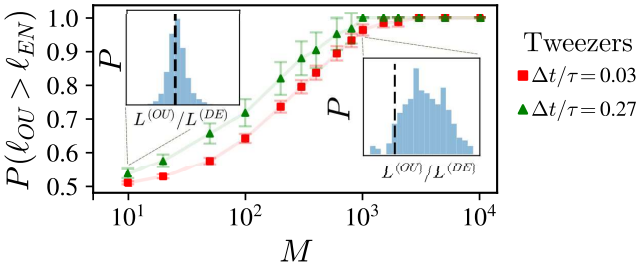

Fig. 1: Example of a distinguishability transition observed in experimental data from the position of an optically trapped particle [2]. The y-axis shows the probability of correctly identifying the underlying stochastic model, assuming additive noise consistent with the system's thermal fluctuations, while the x-axis indicates the number of sampled data points. For sufficiently large datasets, the inference procedure reliably identifies the additive-noise model. As the amount of data decreases, however, the distinguishability between additive and multiplicative noise models progressively deteriorates, eventually preventing a statistically significant discrimination between the two descriptions.

[1] Aguilar, Javier and Muñoz, Miguel A. and Azaele, Sandro, Phys. Rev. X (2026) 10.1103/tmkr-9kl2 .
[2] M. Ibáñez, C. Dieball, A. Lasanta, A. Godec & R. A. Rica Nat. Phys. 20, 135–141 (2024). https://doi.org/10.1038/s41567-023-02269-z

Robust bilateral symmetry in the zebrafish retina emerges from stochastic differentiation dynamics

Diana García Morales[1], Adolfo Alsina[2], Robert Haase[3], Guillaume Salbreux[4] and Caren Norden[1]
[1]Gulbenkian Institute of Molecular Medicine, Oeiras, Portugal
[2]GISC, Universidad Rey Juan Carlos, Móstoles, Spain
[3]Center for Scalable Data Analytics and Artificial Intelligence (ScaDS.AI), Leipzig, Germany
[4]Department of Genetics and Evolution, University of Geneva, Geneva, Switzerland

Bilateral symmetry is a fundamental feature of animal body plans, requiring paired organs to develop in a coordinated manner to ensure proper function. Whether this coordination arises from inter-organ communication or can instead emerge from stochastic developmental dynamics remains an open question.

Here, we investigate the origin of bilateral symmetry during zebrafish retinal development by combining quantitative live imaging with a theoretical model of stochastic cell differentiation. Using a fluorescent Ath5 reporter to track differentiating retinal cells, we simultaneously image both eyes of the same embryo and quantify the spatiotemporal dynamics of neurogenesis with single-cell resolution.

To characterise the observed neurogenesis dynamics, we develop a minimal stochastic model in which each cell is assigned an intrinsic differentiation time drawn independently from a position-dependent distribution along the naso-temporal axis of the retina. Differentiation is assumed to be cell autonomous, with no cell-cell interactions or inter-eye coupling (Fig. 1). By fitting the model to the measured dynamics, we show that it quantitatively reproduces multiple experimental observables, including differentiated cell counts and differentiation rates throughout retinal development in control embryos.

Strikingly, we find that the observed bilateral matching between eyes can be explained by a shared onset of neurogenesis alone, without requiring any active coordination mechanism. The measured inter-eye variability is consistent with the two eyes evolving as independent realizations of the same stochastic process (Fig. 2).

We next challenged the model by introducing perturbations that independently modify the spatial differentiation dynamics and bilateral synchronization. Altering the spatial progression of neurogenesis while preserving a synchronized onset between eyes produced a moderate increase in inter-eye variability, consistent with the model prediction for a flatter differentiation-time profile. In contrast, disrupting the synchronization of neurogenesis onset generated a strong mismatch between eyes. Accounting for the resulting onset delay restored inter-eye variability to control levels.

Together, our results suggest that bilateral matching in retinal development can emerge from stochastic differentiation dynamics combined with a shared onset of neurogenesis. Our interdisciplinary approach shows how quantitative imaging and stochastic modeling together can reveal the mechanisms underlying developmental variability.

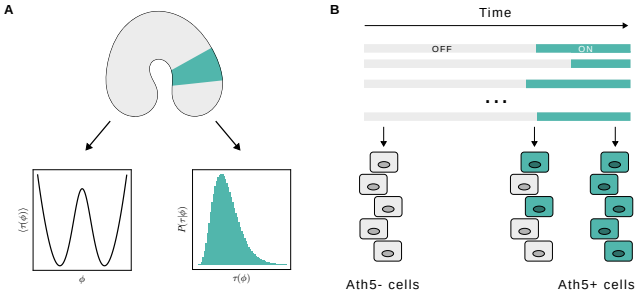

Fig. 1: Cartoon of the model. **A)** Differentiation times τ are stochastic variables drawn from a distribution $P(\tau|\phi)$ that depends on the naso-temporal coordinate ϕ. **B)** The total number of Ath5-positive cells depends on the time elapsed since the start of the experiment and the intrinsic differentiation time of each cell.

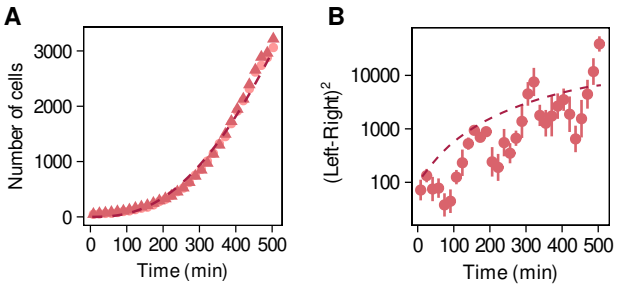

Fig. 2: **A)** Number of Ath5-positive cells over time for the left and right eyes of a representative control embryo. The dashed line shows the theoretical mean cell count computed as the average over 100 parameter combinations sampled from the posterior distribution. **B)** Squared difference in cell numbers between the two eyes of the same embryo over time averaged over all control embryos. The dashed line shows the expected squared difference, computed as the average over 200 parameter combinations sampled from the posterior distribution.

Detecting Shared Functional Groups of Neurons Across Connectomes

Gemma Bel-Bordes[1], Alec Kirkley[2], and Roger Guimerà[1,3], and Federico Battiston[4], and Marta Sales-Pardo[1]

[1]Department of Chemical Engineering, Universitat Rovira i Virgili, Tarragona, Catalonia
[2]Institute of Data Science, University of Hong Kong, Hong Kong
[3]ICREA, Barcelona, Catalonia
[4]Department of Network and Data Science, Central European University, Vienna, Austria

Before studying synapse-level structural differences across connectomes, it is essential to establish correspondences between neurons that fulfill equivalent roles across different brains. These roles are defined not solely by anatomical identity, but by patterns of connectivity. In small connectomes such as *C. elegans*, which contains only a few hundred neurons, near one-to-one neuron mappings across individuals are feasible [1]. However, this approach becomes impractical for larger systems like *D. melanogaster*. Instead, it is more meaningful to identify communities of neurons that play analogous functional roles across connectomes, regardless of their size or composition.

To formalize this, we consider K connectomes represented by adjacency matrices $\{\mathbf{A}^k\}$, each corresponding to a directed, unweighted network with N_k nodes. We assume these networks are generated from a common stochastic block model with a shared edge probability matrix $\mathscr{Q}$ with elements $q_{\alpha,\beta}$ that denotes the probability of a directed edge from block α to block β. While the interaction structure is shared, node identities and sizes may differ, so each network has its own partition $\mathbf{b}_k$.

Under this model, the likelihood of the observed connectomes can be written as

$$p(\{\mathbf{A}^k\} \mid \mathscr{Q}, \{\mathbf{b}^k\}) = \prod_{\alpha,\beta} q_{\alpha\beta}^{\sum_k n_{\alpha\beta}^{1k}} (1-q_{\alpha\beta})^{\sum_k n_{\alpha\beta}^{0k}}, \quad (1)$$

where $n_{\alpha\beta}^{1k}$ and $n_{\alpha\beta}^{0k}$ denotes the number of directed edges and non-edges from block α to block β in network k.

Applying Bayes' theorem and marginalizing over $\mathscr{Q}$ yields the posterior distribution over partitions, $p(\{\mathbf{b}^k\} \mid \{\mathbf{A}^k\})$.

We minimize the negative log-posterior using simulated annealing to infer partitions that best explain the data while enforcing consistency across networks. To improve exploration of the solution space, we incorporate collective moves such as block splits and merges [2], extended to operate jointly across connectomes. These moves help the system escape local minima.

On synthetic data, the method accurately recovers both community structure and cross-network alignment under varying conditions. Applied to real *C. elegans* connectomes across life stages, it assigns consistent block memberships to the same neurons, indicating stable functional roles. When comparing male and hermaphrodite connectomes, we find both communities composed of the same neurons and others that are topologically similar but consist of different neuron sets, suggesting functionally analogous modules implemented by distinct populations.

[1] T. Lázaro, R. Guimerà, and M. Sales-Pardo, *Probabilistic alignment of multiple networks*, Nat. Commun. **16**, 3949 (2025).

[2] T. P. Peixoto, *Merge-split Markov chain Monte Carlo for community detection*, Phys. Rev. E **102**, 012305 (2020).

Growth-induced buckling as a mechanochemical switch for patterning and division-site memory in bacterial filaments

Marta Nadal[1], Iago Grobas[1] and Javier Buceta[1],
[1]Theoretical and Computational Systems Biology Program, Institute for Integrative Systems Biology (I2SysBio), CSIC-UV, Paterna, Spain

The Min system in *Escherichia coli* is a prototypical reaction-diffusion network that generates standing or travelling waves of MinD and MinE proteins, enabling precise mid-cell division. In elongated filamentous cells this patterning leads to multiple, possible, division sites. While most studies focus on biochemical regulation, the role of cellular mechanics remains largely unexplored. In our recent work [1], we have shown that growth-induced elastic buckling acts as a direct physical modulator of patterning, introducing a mechanochemical feedback loop.

In our methodology we combine microfluidic devices, quantitative fluorescence microscopy, mechanical and signalling modeling, and patterned growth substrates. Our results reveal that proteins accumulate at buckling regions and "memory" effects that determine the division site when the source of stress causing filamentation disappears.

[1] M. Nadal, L. Guitou, I. Diez, J. Hurtado, A. Martínez, I. Grobas, Iago and J. Buceta, *E. coli filament buckling modulates Min patterning and cell division*, Nat. Comms. **16**, 8193 (2025).

Robust coexistence in ecological communities dominated by competition

Pablo Lechón-Alonso[1], Srilena Kundu[1], Paula Lemos-Costa[1], José A. Capitán[2], Stefano Allesina[1]
[1]Department of Ecology and Evolution, University of Chicago
[2]Complex Systems Group and Department of Applied Mathematics, Universidad Politécnica de Madrid

Darwin already recognized that competition is fiercest among conspecifics, a principle that later made intraspecific competition central to ecological theory through concepts such as niche differentiation and limiting similarity. Beyond shaping coexistence, strong intraspecific competition can also stabilize community dynamics by ensuring that populations return to equilibrium after disturbance.

In this contribution, we respond to a more fundamental question: how intraspecific competition influences the very existence of a steady state (feasibility) in large random ecological communities dominated by competition. For that purpose, we consider the n-species Generalized Lotka-Volterra competitive dynamics with interactions A_{ij}:

$$\dot{x}_i = x_i r_i \left(1 - \sum_{j=1}^{n} A_{ij} x_j\right). \tag{1}$$

The interaction matrix A parameterized as $A = \alpha I + B$, thus highlighting the baseline level of intraspecific competition (α) leading to species self regulation. Pairwise interactions A_{ij} and A_{ji} are assumed to be dependent with correlation coefficient $\rho \in [-1, 1]$.

We show that, in analogy with classical results on stability [1], there is a critical level of intraspecific competition above which a feasible steady state is guaranteed to exist (i.e., an *interior* equilibrium point for which all abundances x_i are positive). We prove this for arbitrary matrices $B = (B_{ij})$, and consider later the case in which the matrix B of competition excess is random (*quenched* treatment of the noise). A general expression for the probability of feasibility is derived using resolvent theory, which is asymptotically *universal* (i.e., independent of the distribution of B_{ij} in the limit of large n). The probability that the interior equilibrium point is feasible can be approximated by

$$p_F(\alpha, \sigma_{y^\star}, n) \approx \Phi\left(\frac{1}{\alpha \sigma_{y^\star}}\right)^n. \tag{2}$$

where

$$\frac{1}{(\alpha\sigma_{y^\star})^2} \approx \frac{\alpha^2 + \alpha\sqrt{\alpha^2 - 4\rho(n-1)}}{2(n-1)} - (1+\rho). \tag{3}$$

This approximation is used to prove that, asymptotically (as species number grows), the transition to stability occurs before the transition to feasibility with probability one (Fig. 1). Thus, in large competitive communities, any feasible equilibrium is automatically stable. This ordering persists even when many species in the initial pool cannot coexist and extinctions occur: the dynamics prune the community, shifting feasibility and stability thresholds but never reversing their order. These results imply that large competitive communities generically converge to a globally stable equilibrium (as illustrated in Fig. 2), making sustained oscillations or chaos unlikely—consistent with experimental observations [2].

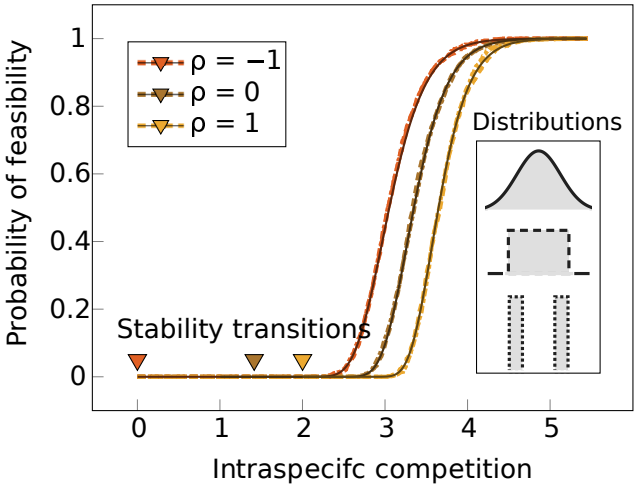

Fig. 1: Probability of feasibility as function of the scaled intraspecific competition $\alpha/\sqrt{n-1}$). The transition to feasibility occurs above the transitons to stability (triangles).

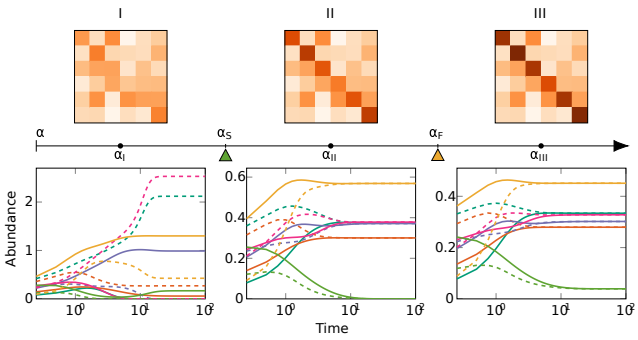

Fig. 2: Different dynamical scenarios for increasing self-regulation (darker diagonal in matrices). As α increase, different dynamics arise depending on the position of α relative to the stability (α_S) and factibility thresholds (α_F): (i) for $\alpha < \alpha_S < \alpha_F$ (case I), extintions occur and the set of coexisting species depend on initial conditions; (ii) if $\alpha_S < \alpha < \alpha_F$ (case II), the system is unfeasible, but a subset of species converge to a unique, globally stable fixed point; (iii) when $\alpha_S < \alpha_F < \alpha$ (case III), a feasible equilibrium exists, which is globally stable, and all species coexist.

[1] R. M. May. *Will a large complex system be stable?*, Nature, **238** (5364), 413–414 (1972).

[2] P. Lechón-Alonso, S. Kundu, P. Lemos-Costa, J. A. Capitán, and S. Allesina. *Robust coexistence in competitive ecological communities*, Nature Communications **17**, 2637 (2026).

Pedestrian rotations may render obstacles ineffective in competitive evacuations

I. Echeverría-Huarte[1], A. Garcimartín[1], C. Van Ham[2], A. Corbetta[2,3], I. Zuriguel[1]
[1]Dpto. de Física y Mat. Apl., Fac. Ciencias, Universidad de Navarra, Pamplona, Spain
[2]Department of Applied Physics and Science Education, Eindhoven University of Technology, Eindhoven, the Netherlands
[3]Eindhoven Artificial Intelligence Systems Institute, Eindhoven, the Netherlands

A well-known prediction of the social-force model (an agent-based description of pedestrian motion) is that placing a column-like obstacle in front of an exit in a bottleneck should ease the pressure and improve egress flow [1]. The recipe has been confirmed in inert grains, where a properly placed obstacle drastically reduces silo clogging [2], and in sheep herds passing through a narrow door [3]. The extension to humans seemed straightforward; yet controlled drills with about 200 soldiers under competitive conditions showed no measurable reduction in evacuation time for any obstacle position tested [4]. The reason for this failure remained elusive.

Here we revisit those recordings with a new observable: body orientation around the vertical axis. Inspection of the videos suggested that, with an obstacle, some evacuees spin and momentarily face away from the door. We quantify this with a fine-tuned neural network trained to recover the pose of every pedestrian during the evacuation drills.

Body orientation metric

The network locates head and shoulders of each person even under partial occlusion (Fig. 1). From these landmarks we define the **body orientation** unit vector $\hat{\mathbf{n}}$ pointing from the left to the right shoulder, and $\hat{\mathbf{d}}$ as the unit vector from the pedestrian to the centre of the exit. Alignment with the door is captured by

$$\Psi = \sin(\angle(\hat{\mathbf{d}}, \hat{\mathbf{n}})) = \hat{\mathbf{d}} \times \hat{\mathbf{n}}, \tag{1}$$

so that $\Psi = 1$ corresponds to an exit-facing posture ($\hat{n} \perp \hat{d}$), $\Psi = -1$ to the back turned to the door, and $\Psi = 0$ to a side-on stance (see the inset sketch in Fig. 2 for the geometric interpretation).

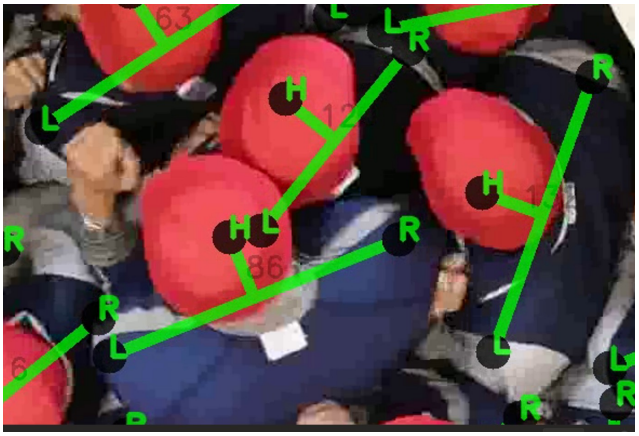

Fig. 1: Portion of a video frame showing the shoulders (L, R) and head (H) as detected with the neural network. Some shoulder locations are plausibly inferred even when not visible in the frame.

Results

We averaged Ψ over all video frames and all competitive drills on a grid covering the region in front of the door, with and without obstacle (Fig. 2). Without the obstacle, evacuees are robustly oriented towards the exit ($\Psi \approx 1$) almost everywhere, except next to the door jambs where shear with the wall enforces a side-on stance. The obstacle changes this picture qualitatively: a clear stripe with $\Psi < 0$ (bluish-green shades) appears in contact with its downstream side, signalling individuals whose backs face the door. These pedestrians, pushed by the crowd against the obstacle, end up facing it and can only exit by performing a costly rotation or by walking out backwards.

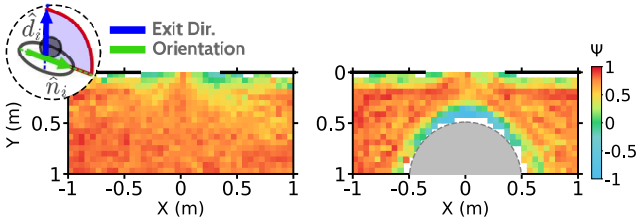

Fig. 2: Mean Ψ on a grid near the exit (*centred at* $X = 0$, $Y = 0$, *top*). *Left*: high competitiveness, no obstacle; *right*: high competitiveness, with obstacle (*gray*). Colour scale as indicated. A sketch of the Ψ alignment, showing the exit direction $\hat{\mathbf{d}}_i$ (blue) and the body orientation $\hat{\mathbf{n}}_i$ (green), is included as inset for reference.

We conclude that these undesired rotations induced by shear against the obstacle are a plausible cause for its failure in competitive human evacuations: by forcing unfavourable orientations on a fraction of pedestrians, the obstacle cancels any flow enhancement it might provide. Interestingly, grains and sheep do not have the same rotational degree of freedom as humans, so they cannot be forced into a back-facing posture. This reconciles the discrepancy with previous results and highlights the importance of considering body orientation (frequently overlooked) in the study of pedestrian dynamics.

[1] D. Helbing, I. Farkas, and T. Vicsek, *Simulating dynamical features of escape panic*, Nature **407**, 487–490 (2000).

[2] I. Zuriguel *et al.*, *Silo clogging reduction by the presence of an obstacle*, Phys. Rev. Lett. **107**, 278001 (2011).

[3] A. Garcimartín *et al.*, *Flow and clogging of a sheep herd passing through a bottleneck*, Phys. Rev. E **91**, 022808 (2015).

[4] A. Garcimartín, D. Maza, J.M. Pastor, D.R. Parisi, C. Martín-Gómez, and I. Zuriguel, *Redefining the role of obstacles in pedestrian evacuation*, New J. Phys. **20**, 123025 (2018).

Statistical physics tools to improve cancer immunotherapy

Huixia Lu, Marc Domingo and Jordi Faraudo
[1]Institut de Ciència de Materials de Barcelona (ICMAB-CSIC)
Campus UAB s/n, Bellaterra, 08193, Barcelona, Spain

Immunotherapy, a cellular therapy based on the enhancement of the patient's immune system, is considered a vital pillar of modern oncology by the World Health Organization (WHO). An important drawback of this therapy is its limited availability and access inequities due to its high cost. Hence, we urgently need to increase its efficiency and reduce costs, facilitating its use in public health systems.

Interestingly, some of the bottlenecks arising in immunotherapy are related to different fields of physics ranging from molecular interactions to active matter behaviour. In this contribution we will show how Statistical physics provides very useful tools to rationally design improvements in several critical steps involved in immunotherapy.

The first step in immunotherapy is the extraction of immune cells (T-cells) from the patient and their ex-vivo enhancement to program them to target and destroy specific cancer cells (the so called CAR T-cell therapy). This is done by a genetic modification introduced by an engineered viral vector. In the current hospital practice, the interaction between the virus and the T cells takes place in liquid solution, leading to a random (Poisson) process which is highly inefficient. This can be improved by designing porous materials that simultaneously trap the viruses and provide an appropriate environment for the cells [1, 2], as shown in Fig. 1.

Our calculations, combining Poisson-Boltzmann electrostatics and Molecular Dynamics simulations show that an appropriate strategy for the capture of the CAR gene carrier virus is to take advantage of the strong electrostatic interactions arising from highly charge proteins [3] that cover most enveloped viruses. This capture can then be realized by incorporating highly charged natural polymers present in human cells (such as heparin) into the structure of porous materials like hydrogels. This strategy, supported by our calculations, has been successfully implemented [1, 2].

Another critical step in the process is the expansion (grow and division) of the enhanced T-cells. This process can be greatly enhanced by tuning the stiffness of the substrate (hydrogel in this case) [1]. Physically, the expansion process is an active wetting process of the hydrogel substrate by the T-cells and it is known that active wetting processes by cells are governed by the stiffness of the substrate [4]. This active wetting and cell expansion process in the hydrogel can be successfully modeled by performing MonteCarlo simulations of a cellular Potts model (a generalized spin model with a modified Hamiltonian to simulate adhesive behaviour of cells [5]).

Therefore, the combination of statistical mechanical tools at the molecular level (Poisson-Boltzmann electrostatics and Molecular Dynamics) and at the cell level (Cell Potts model and MonteCarlo simulation) provides a successful tool for the understanding of key processes involved in immunotherapy and its rational optimization based on physics principles.

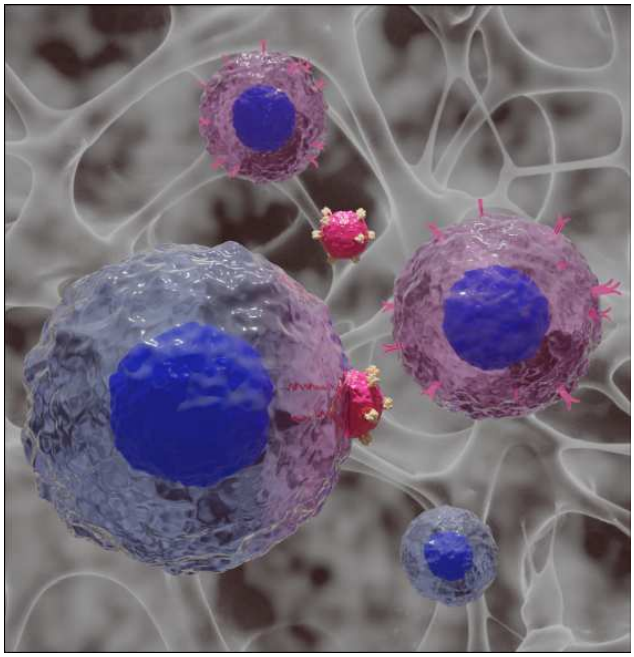

Fig. 1: Scheme of the relevant interactions taking place in the enhancement step of CAR T-cell immunotherapy. A porous material (hydrogel, in background) incorporates by electrostatic interaction viral carriers (shown in red with the charged G proteins at the surface in yellow) and transfers a CAR gene to human T cells (in blue).

[1] J. Guasch, M. Castellote, F. Merlina, J. Faraudo, M. Domingo, *Inverse opal hydrogel and its use in immunotherapy*, European Patent EP24382629 (2024). IP number WO/2025/257179.A1.

[2] M. Castellote-Borrell, M. Domingo, F. Merlina, H. Lu, S. Colell, M. Bachiller, M. Juan, S. Guedan, J. Faraudo* and J. Guasch*, ACS Applied Materials & Interfaces, **17**, 16548 (2025).

[3] M. Domingo, H.V. Guzman, M. Kanduc and J. Faraudo*, J. Chem. Inf. Model. **65**, 240 (2025).

[4] M.E. Pallares et al. Nat. Phys. **19**, 279 (2023).

[5] J. F. Graner and J. A. Glazier, Phys. Rev. Lett. **69**, 2013 (1992).

Active wetting transition in cellular aggregates

MJ Franco Oñate[1], Hanno I. Hennighausen[2], and Ricard Alert[1,2,3,4,5,6]
[1]Departament de Física de la Matèria Condensada, Universitat de Barcelona, Carrer Marti Frances 1, 08028, Barcelona, Spain
[2]Max Planck for the Physics of Complex Systems, Nothnitzer Str. 38, 01187, Dresden, Germany
[3]Center for Systems Biology Dresden, Pfotenhauerstr. 108, 01307, Dresden, Germany
[4]Cluster of Excellence Physics of Life, TU Dresden, Arnoldstraße 18, 01307, Dresden, Germany
[5]Universitat de Barcelona Institute of Complex Systems (UBICS), Carrer Marti Frances 1, 08028, Barcelona, Spain
[6]Institució Catalana de Recerca i Estudis Avançats (ICREA), Passeig de Lluís Companys 23, 08010, Barcelona, Spain

During many biological processes, such as wound healing, embryogenesis and cancer metastasis, living tissues spread on substrates. Often, they arrest at a finite contact angle rather than spreading completely, or they even shrink [1]. This behavior resembles classical droplet wetting, for which active-matter extensions have recently been proposed [2], yet the physical origin of partial wetting in these frameworks remains unclear.

Here, using an active polar fluid model of epithelial spreading, we predict a robust partial-wetting state of a cell aggregate, emerging from the competition between interfacial forces that oppose spreading and active traction stresses that promote it. We then examine how two additional ingredients reshape this picture. Substrate friction reduces the equilibrium radius and progressively suppresses the bistability between partial and total wetting. Contractility, as shown in previous work [3], actively drives dewetting and, in the low-friction regime, opens a tristable window in which total wetting, partial wetting, and dewetting coexist as stable states. Together, these results identify a minimal mechanical mechanism for partial wetting, requiring only interfacial forces and active traction, and clarify the distinct roles of friction and contractility in shaping the transitions between total, partial and de-wetting in active tissues.

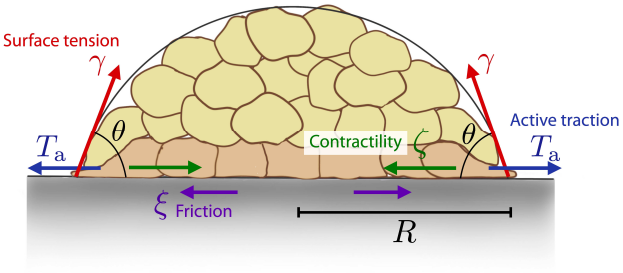

Fig. 1: Schematic of a cellular aggregate and the forces at play during the spreading process.

[1] Stéphane Douezan, Karine Guevorkian, Randa Naouar, Sylvie Dufour, Damien Cuvelier, and Françoise Brochard-Wyart, *Spreading dynamics and wetting transition of cellular aggregates*, PNAS. **108**, 18 (2011).

[2] Amir Pahlavan and Michael Murrell, *Active Wetting: Statics and Dynamics*, Ann. Rev. **17**, 257-284 (2026).

[3] Carlos Pérez-González, Ricard Alert, Carles Blanch-Mercader, Manuel Gómez-González, Tomasz Kolodziej, Elsa Bazellieres, Jaume Casademunt, and Xavier Trepat, *Active wetting of epithelial tissues*, Nat. Phys. **15**, 1 (2019).

Information dynamics and learning in gene regulatory networks

María Jinxue García-Pantaleón Tarifa[1], Francisco Prista von Bonhorst[1] and Jordi García-Ojalvo[1]
[1]Department of Medicine and Life Sciences, Universitat Pompeu Fabra, Barcelona 08003, Spain

Biological information processing begins with the idea of internal representation—how organisms encode and use external data to guide behavior. Such representations compress key environmental features without losing essential information. Although these processes are most evident in the nervous systems of multicellular organisms, similar forms of environmentally driven learning also occur in simpler systems without neural structures, including bacteria, which will be the focus of this study.

The Information Bottleneck (IB) method [1] provides a mathematical framework for finding compressed representations of an input that retain maximal information about the corresponding output. In artificial neural networks (ANNs), this compressed variable corresponds to the abstract internal representations formed in hidden layers [5], and IB has been used to analyze learning dynamics in deep neural networks (DNNs) [2, 3]. Recurrent Neural Networks (RNNs), designed for processing temporal sequences, have meanwhile been identified as key architectures for maintaining memory and internal state over time [4, 6].

In this project we suggest that in order to process information from its environment, bacteria create internal representations through their gene regulatory networks (GRNs). These networks represent the interactions that genes encounter that regulate their expression, which determine the cell state. Bacterial GRNs contain recurrent substructures that can process temporal information from their input and will have specific dynamics.

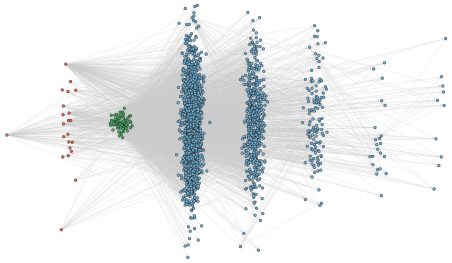

Fig. 1: Here, we represent the architecture of *E. coli* organized as follows. All recurrent nodes are grouped together in what we call the core (green). The non-recurrent nodes are then arranged in different levels: first, according to whether they are regulators (orange) or targets (blue) of core genes; and second, based on their longest distance from the core, with each layer representing a specific distance.

Therefore, we analyzed the updated *E. coli* GRN [7] and classified its nodes as either recurrent—if they participate in at least one cyclic outgoing path—or non-recurrent otherwise (See Figure 1) [4]. Then we took the recurrent nodes and used them as the hidden units of a recurrent neural network (RNN), which we then trained on a delayed AND task, which want to represent how bacteria anticipate a decrease of oxygen after a previous increase of temperature. It is important to note that in our RNN the hidden layer preserves the original GRN connectivity; therefore, during training, we masked the weight matrix to ensure that only biologically valid connections were updated.

Finally, we analyzed the information dynamics of the RNN trained on the Delayed AND task using the information bottleneck framework [1–3]. We computed the mutual information shared between the input and the predicted output, as well as the mutual information between the predicted output and the expected output throughout the training. What we have observed so far is that, similar to previous work on DNNs [2, 3], our RNN also exhibits two distinct phases during training: an initial fitting phase followed by a compression phase.

[1] N. Tishby, F. C. Pereira, and W. Bialek, *The information bottleneck method*, arXiv preprint **physics/0004057** (2000).

[2] N. Tishby and N. Zaslavsky, *Deep Learning and the Information Bottleneck Principle*, arXiv preprint **arXiv:1503.02406** (2015).

[3] R. Shwartz-Ziv and N. Tishby, *Opening the Black Box of Deep Neural Networks via Information*, arXiv preprint **arXiv:1703.00810** (2017).

[4] M. Gabalda-Sagarra, L.B. Carey and J. Garcia-Ojalvo, *Recurrence-based information processing in gene regulatory networks*. Chaos **28**, 106313 (2018).

[5] D.E. Rumelhart, G.E. Hinton and R.J. Williams, *Learning representations by back-propagating errors*. Nature **323**, 533–536 (1986). doi:10.1038/323533a0.

[6] M.S. Vidal-Saez and J. Garcia-Ojalvo, *Structural determinants of soft memory in recurrent biological networks*. Biophysical Reviews **17**, 259–269 (2025). doi:10.1007/s12551-025-01295-w.

[7] H. Salgado, S. Gama-Castro, P. Lara, C. Mejia-Almonte, G. Alarcón-Carranza, A.G. López-Almazo *et al.*, *RegulonDB v12.0: a comprehensive resource of transcriptional regulation in E. coli K-12*. Nucleic Acids Research (2023). doi:10.1093/nar/gkad1072.

Detailed balance from social rules: a model for the evolution of social relationships

Miguel A. González-Casado[1], Andreia Sofia Teixeira[2] and Angel Sánchez[1,3]

[1]Grupo Interdisciplinar de Sistemas Complejos (GISC), Departamento de Matemáticas, Universidad Carlos III de Madrid, Leganés, Spain

[2]Network Science Institute, Northeastern University London, London, UK

[3]Instituto de Biocomputación y Física de Sistemas Complejos (BIFI), Universidad de Zaragoza, Zaragoza, Spain

We study a longitudinal dataset of positive and negative personal relationships among the students of a secondary school. For more than 5 years, we reconstruct the temporal evolution of a directed, weighted and signed network of more than 1000 nodes, with tie weights ranging from strong negative (-2) to strong positive (+2) relationships. In recent work [1] we showed that this network sits in a dynamic equilibrium in the strict statistical-mechanical sense. The transition probabilities driving the network dynamics are stationary; the empirical distributions of edges, degrees, triangles and other structural metrics coincide with the expected stationary abundances under this dynamics; and detailed balance is satisfied for transitions between degrees, edges and triangles. Remarkably, this equilibrium persists despite roughly 100% node turnover, implying that this equilibrium is an emergent property of the mechanisms governing relationship dynamics, not of the particular individuals involved. This motivates the central question of the proposed talk: which microscopic, individual-level social mechanisms generate the observed macroscopic equilibrium, and to what extent can they be identified from data?

To address this, we build a generative, actor-driven model of the network dynamics. Each individual controls their own outgoing ties. At random moments in continuous time, an individual reconsiders one of their relationships and may change it, choosing the modification that maximizes an objective function plus a stochastic term. The objective function is a weighted sum of local network statistics, each encoding a candidate social mechanism; its weights are the model parameters and play the role of inverse temperatures conjugate to those statistics. This yields a Markovian dynamics whose stationary behavior can be compared directly with the empirical equilibrium. Some mechanisms we consider include (see Figure 1) reciprocity, triadic closure, structural balance between positive and negative ties, homophily along node attributes such as grade and sex, popularity and degree effects, and capacity constraints on the number of relationships an individual can sustain. Each mechanism is grounded in an established social theory, so that the parameters carry a direct sociological interpretation.

Our analysis proceeds in three stages. First, we fit the model to the data using simulation-based Bayesian inference, obtaining a full posterior distribution over the mechanism strengths. Second, we interpret the inferred parameters as the relative importance of each social mechanism and examine their correlations and trade-offs, connecting them back to the equilibrium structure of the empirical dynamics. Third, we use the posterior to explore the family of dynamics the model can produce beyond the single observed trajectory: we sample parameter sets compatible with the data, simulate the resulting dynamics, assess the identifiability of competing mechanisms, characterize degeneracies and compensations among them, and test whether the inferred local rules indeed reproduce the macroscopic equilibrium—stationarity and detailed balance—observed in the data. This lets us distinguish features that are tightly constrained by the observations from those that the data leave undetermined.

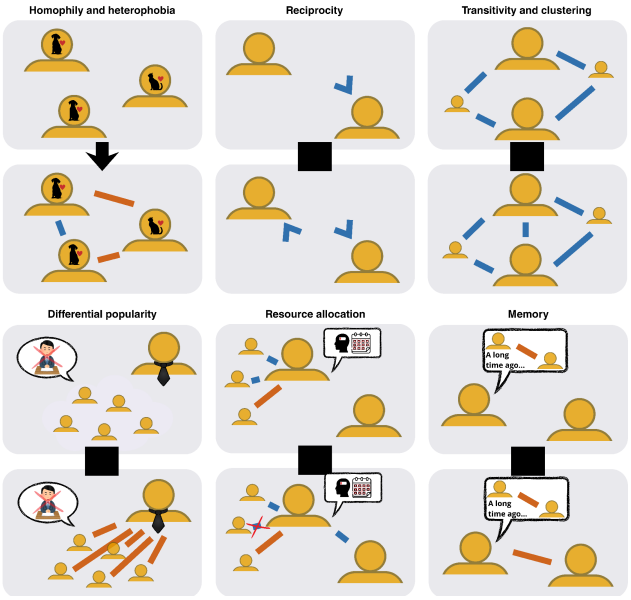

Fig. 1: Depiction of six exemplary mechanisms governing signed social network dynamics. Each mechanism is illustrated using two panels: the top panel shows the network state before the mechanism takes effect, and the bottom panel shows the resulting state after the mechanism operates.

[1] M. A. González-Casado, A. S. Teixeira, and A. Sánchez, *Evidence of equilibrium dynamics in human social networks evolving in time*, Communications Physics, **8(1)**, 227 (2025).

Kinetic theory of transport and segregation in confined granular mixtures

David González Méndez[1] and Vicente Garzó[1,2]
[1]Departamento de Física, University of Extremadura, E-06071 Badajoz, Spain
[2]Instituto de Computación Científica Avanzada de la Universidad de Extremadura (ICCAEx), E-06071 Badajoz, Spain

Confined granular mixtures, such as grains of different masses or sizes fluidized in vertically vibrated quasi-two-dimensional geometries, provide a paradigmatic example of driven nonequilibrium matter. Despite their relevance for granular transport, pattern formation, and segregation phenomena, a complete kinetic-theory description at finite density remains challenging, especially for mixtures with arbitrary composition.

In this contribution, we present a theoretical study of transport properties in a confined granular mixture at moderate densities. The system is described through a collisional model that mimics the transfer of energy from the vertical vibration of the walls to the horizontal motion of the grains, together with the inelastic revised Enskog kinetic equation. Starting from this framework, we derive the Navier-Stokes hydrodynamic equations for mass, momentum, and energy by means of a Chapman-Enskog expansion to first order in the spatial gradients.

The corresponding transport coefficients are formally determined by a set of coupled linear integral equations. Since their exact solution is highly involved for multicomponent systems, we focus on the relevant steady state and obtain explicit expressions within a leading Sonine-polynomial approximation. In particular, we determine the diffusion transport coefficients associated with the mass flux, as well as the shear and bulk viscosities for binary mixtures under quasi-two-dimensional conditions.

As an application, we use the diffusion coefficients to evaluate the thermal diffusion factor and analyze segregation driven by temperature gradients and gravity. The resulting criteria allow us to distinguish between Brazil-nut and reverse Brazil-nut behavior and show how density, inelasticity, and compositional asymmetry modify the segregation boundaries. Overall, this work provides a kinetic-theory framework for understanding transport and segregation in confined granular mixtures beyond both the dilute and tracer limits.

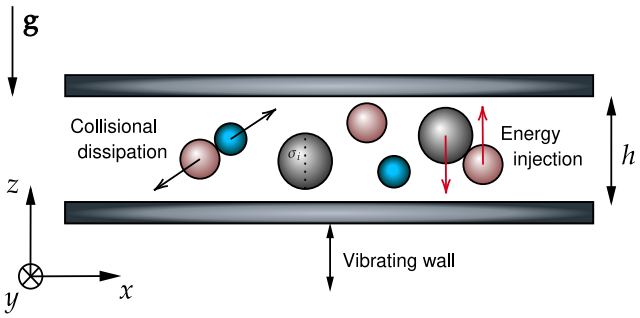

Fig. 1: Schematic illustration of the confined quasi-two-dimensional system. Vertical vibration is imposed on the box to inject external energy into the system. During non-planar collisions between grains, the vertical energy gained from the vibration of the plate is transferred to the *xy* components of the velocities. This kinetic energy is then dissipated and redistributed among the particles' horizontal degrees of freedom due to their collisions. It is important to note that, although our study aims to capture the phenomenology of confined systems, we are modeling an unconfined two-dimensional system where collisions are described by the Δ-model.

[1] D. González Méndez and V. Garzó, *Transport properties in a model of confined granular mixtures at moderate densities*, Phys. Fluids **38**, 033343 (2026).

[2] R. Brito, D. Risso, and R. Soto, *Hydrodynamic modes in a confined granular fluid*, Phys. Rev. E **87**, 022209 (2013).

Leveraging Complex Networks for Portfolio Optimization and Risk Management in Finance

M. Grande[1,3], J. Borondo[2,3]
[1]Grupo de Sistemas Complejos, Universidad Politécnica de Madrid, Madrid, Spain
[2]Departamento de Gestión Empresarial, Universidad Pontificia de Comillas ICADE, Madrid, Spain
[3]AGrowingData, Almería, Spain

Diversification is the cornerstone of risk-adjusted portfolio construction. Yet, despite being a well-established principle in finance, it has often been overlooked in pairs trading strategies. Pairs trading is a quantitative trading strategy that exploits historical price relationships between two assets, identifying opportunities where temporary divergences suggest profitable trades [1, 2]. The strategy involves simultaneously taking a long position in the underperforming asset and a short position in the overperforming asset, assuming that their historical equilibrium will be restored. Traditional approaches often focus on selecting top-correlated pairs, which can lead to over-concentration in assets influenced by the same underlying signals, thereby increasing systematic risk. To address this, we introduce a network science framework to improve diversification in pairs trading portfolios. In fact, assets—whether stocks, commodities, cryptocurrencies, or any other asset class—interact and form a complex network, with several assets clustering together. Understanding this structure is crucial for building effective, risk-diversified portfolios. To this end, we construct a structural network of assets based on cointegration and apply the Planar Maximally Filtered Graph (PMFG) [3] and Triangular Maximally Filtered Graph (TMFG) [4] methods to extract an effective market representation.

In this work [5], we show that constructing portfolios based on the properties of pairs within the underlying network enhance performance compared to solely selecting the top cointegrated pairs. By selecting pairs that include at least one of the most peripheral assets and ensuring the link is present in the filtered network (PMFG or TMFG), we systematically outperformed the portfolio composed of the top cointegrated pairs, particularly in terms of risk exposure. Additionally, our results show that portfolios formed by peripheral pairs outperform those formed by central ones.

Our results also reveal that portfolios containing pairs that serve as links across communities are less profitable and carry higher risk. While these weak ties act as bridges between otherwise disconnected parts of the market—facilitating spillovers across market communities—they also expose the pairs to diverse influences. A possible explanation is that, due to their bridging role, each asset in the pair is affected by distinct factors and market signals. Consequently, price movements in one community may not necessarily be mirrored in another, disrupting mean reversion. Since our findings suggest that such pairs should be avoided in pairs trading portfolios, identifying them is crucial for building a well diversified and profitable portfolio.

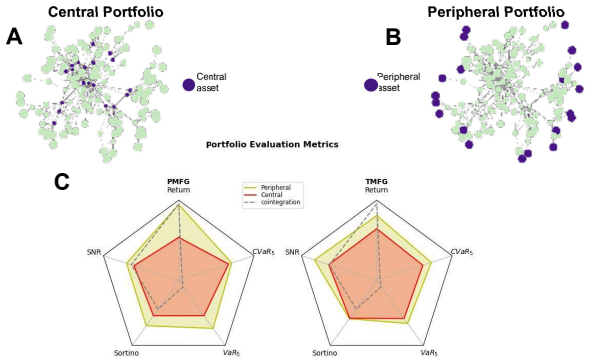

Fig. 1: (A) Visualization of an example of a central portfolio. Top central assets are marked in purple, and the pairs are formed by selecting one of the links connected to each of these assets. (B) Visualization of an example of a peripheral portfolio. Top peripheral assets are marked in purple, and the pairs are formed by selecting one of the links connected to each of these assets. (C) Radar plots comparing performance across central, peripheral, and classic cointegration portfolios, evaluated by five metrics: VaR_5, $CVaR_5$, *Sortino*, *SNR*, and average return. Lower values near the center indicate weaker performance, while larger ones in the exterior reflect stronger performance for each metric. The left plot corresponds to the PMFG network and the right to the TMFG network.

[1] Vidyamurthy, G. (2004). *Pairs Trading: quantitative methods and analysis.* John Wiley & Sons.

[2] Elliott, R. J., Van Der Hoek*, J., & Malcolm, W. P. (2005). *Pairs trading.* Quantitative Finance, 5(3), 271-276.

[3] Tumminello, M., Aste, T., Di Matteo, T., & Mantegna, R. N. (2005). *A tool for filtering information in complex systems.* Proceedings of the National Academy of Sciences, 102(30), 10421-10426.

[4] Massara, G. P., Di Matteo, T., & Aste, T. (2016). *Network filtering for big data: Triangulated maximally filtered graph.* Journal of complex Networks, 5(2), 161-178.

[5] Grande, M., & Borondo, J. (2025). *Embedding pairs trading in market networks: a network science approach to portfolio construction.* Humanities and Social Sciences Communications, 12(1), 1-11.

Stronger is Slower: Decoupling speed and pushing in evacuations through a bottleneck

Marta Grasa, Ángel Garcimartín, Laciel Alonso-Llanes, and Iker Zuriguel,
Depto. de Física y Matemática Aplicada, Facultad de Ciencias, Universidad de Navarra, 31080 Pamplona, Spain

When many bodies attempt to pass through a narrow opening simultaneously, it is common to see clogs appearing and the outflow slowing down as the desired speed increases . This effect has been observed in many discrete systems of different natures, and is commonly known in the literature as "Faster is Slower" [1, 2]. However, its origin is currently not well understood.

Our aim in this work is to study the effects of the desired velocity of the agents and their pushing force on the flow through a narrowing separately. To achieve this, we use an ensemble of self-propelled programmable robots equipped with various sensors (Fig. 1) to simulate evacuations thorough a bottleneck. This allows us to decouple and precisely control these two variables, which is not easy to achieve in most discrete systems.

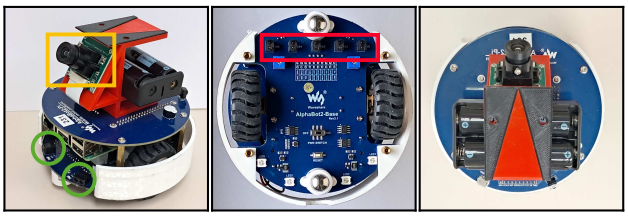

Fig. 1: Pictures of the robots used, with the sensors (front camera and IR proximity sensors in front, array of IR sensor at the bottom) highlighted. A red triangle on top facilitates tracking for later analysis.

We perform evacuation drills under different protocols: First, we program the robots to stop and wait if they find an obstacle directly ahead, preventing them from pushing each other or the existing clogs. We then instruct the robots set their motors to a determined power when their front IR sensors pick up an obstacle, thus pushing it with a fixed force. These evacuations were performed with two different pushing forces. All drills were repeated for two desired speeds.

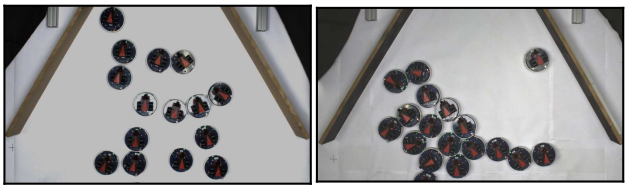

Fig. 2: Examples of the clogs which appear when the agents don't (left) and do (right) push each other. Both images correspond to experimental runs with $V = 35$ cm/s. The pushing force on the left is 0.7 N.

We see that clogs appear in all evacuation drills, both when pushing is present and when it is not, showing that pushing is not a necessary condition for their appearance. However, we do observe differences in their size and position (Fig. 2), even when the number of agents and desired speed are kept constant. When pushing is allowed, the clogs are larger and more dense, involving more robots.

This difference in the presence and magnitude of a pushing force also results in a difference in flow at the exit, as can be seen in the flow-density diagram shown in Figure 3. We see that removing the pushing by the agents results in lower densities within the arena, while increasing the maximum flow achieved at the bottleneck. The diagram also shows that and the effect of the desired velocity is highest when there is no pushing, and unexpectedly a higher desired velocity V results in a greater outflow when the pushing force is fixed.

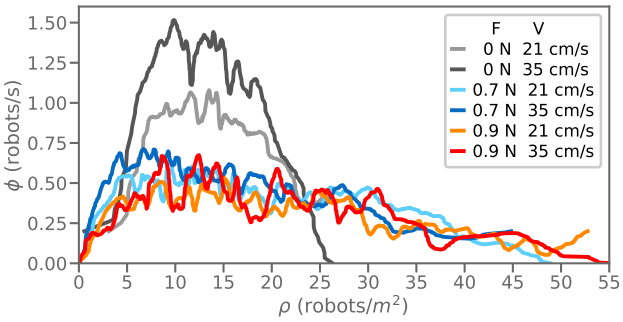

Fig. 3: Flow-density diagram at the exit for different pushing forces and desired speeds as shown in the legend.

This observed behavior indicates that it is not the higher desired speed which causes the flow to reduce, but the higher pushing force that this change implies in most systems where both variables are closely related to each other. We thus argue that the effect currently known as "Faster is Slower" would be more aptly called "Stronger is Slower". This exemplifies one of the many insights that the use of programmable robots can give us on the nature of discrete flow through a bottleneck.

[1] J.M. Pastor et al., *Experimental proof of faster-is-slower in systems of frictional particles flowing through constrictions*, Phys. Rev. E **92**, 062817 (2015).

[2] I. Zuriguel et al., *Clogging transition of many-particle systems flowing through bottlenecks*, Scientific reports **4**, 7324 (2014).

The role of space in explaining macroecological patterns of microbial abundance

Adrián Gutiérrez-Arroyo[1], Aniello Lampo[1], and José A. Cuesta[1]
[1]Universidad Carlos III de Madrid, Departamento de Matemáticas,
Grupo Interdisciplinar de Sistemas Complejos (GISC), 28911, Leganes, Spain.

Microbial communities inhabit remarkably diverse environments—from ocean waters to human guts and soils—yet their species abundance fluctuations share a universal statistical signature: they are well described by a gamma distribution [1]. This regularity has been interpreted as evidence of a hidden underlying mechanism, but its origin remains contested between two competing frameworks. Exogenous stochastic models reproduce the pattern via environmental noise acting on individual species, offering effective but mechanistically opaque descriptions [1]. Endogenous approaches based on generalized Lotka–Volterra (gLV) dynamics, by contrast, account for the complex interaction network of real communities but have consistently *failed* to reproduce the empirical distribution—predicting instead a power-law species abundance distribution $P(x) \sim x^{-1}$ arising from the chaotic turnover of species between rare and dominant states [2]. We have shown that *spatial structure* is the missing ingredient resolving this discrepancy [3]. We consider the open gLV model with constant migration,

$$\dot{x}_i = x_i\left(1 - x_i - \sum_{j\neq i}^{S} a_{ij}x_j\right) + \lambda, \qquad (1)$$

where $a_{ij} \sim \mathcal{N}(\mu, \sigma^2)$ are random interaction coefficients, and λ is the migration rate. For sufficiently large $\sigma\sqrt{S}$, this system enters a multiple-attractor chaotic phase where species alternate between low ($x \sim \lambda$) and high ($x \sim 1$) abundances. The resulting abundance fluctuation distribution (AFD)—defined from the standardized log-abundances [1] $z = (\log x - \langle \log x \rangle)/\mathrm{Var}(\log x)^{1/2}$—is bimodal and incompatible with a gamma in any parameter regime. We then embed the community in a fragmented landscape of M patches exchanging individuals through diffusion,

$$\dot{x}_i^u = x_i^u\left(1 - \sum_{j=1}^{S} a_{ij}^u x_j^u\right) + \sum_{v=1}^{M} D_{i,uv}(x_i^v - x_i^u), \qquad (2)$$

where patch-level interaction matrices are correlated with coefficient $\rho = 0.95$. At the local (single-patch) scale, dynamics remain chaotic with the same bimodal non-gamma AFDs. However, aggregating abundances globally across all patches, $x_i = \sum_u x_i^u$, eliminates turnover and yields AFDs in excellent agreement with the empirically observed gamma form across all explored parameter combinations and spatial configurations (Fig. 1). Crucially, this same result is obtained by aggregating M *independent* realizations of the constant-migration model (Eq. 1), each with a different interaction matrix drawn from the same distribution. This reveals that the gamma distribution could arise as a consequence of *statistical aggregation* [4] rather than the signature of any specific biological mechanism. The observed pattern may therefore be an artifact of the spatial coarse-graining inherent in metagenomic sampling: a fecal sample or a liter of seawater necessarily integrates microbial abundances over many effectively independent local communities. Our findings could have direct experimental implications. Experiments on spatially isolated, well-mixed communities should reveal bimodal log-abundance distributions and chaotic species turnover dynamics—signatures consistent with endogenous interaction-driven chaos rather than exogenous noise—whereas the standard bulk metagenomic sampling of the same system would recover the gamma. This prediction distinguishes sharply between the two competing explanatory frameworks and calls for new experiments with spatial resolution.

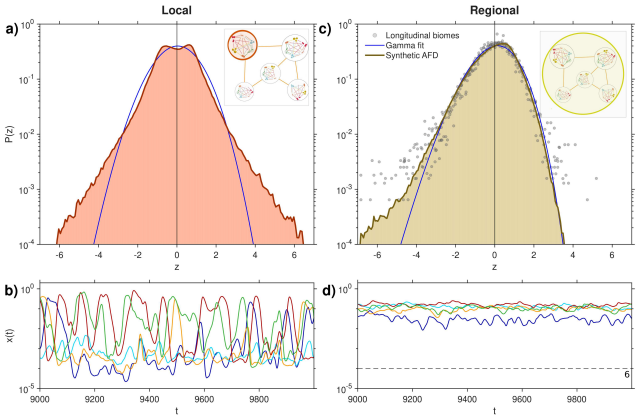

Fig. 1: Abundance fluctuation distributions and time series in the metacommunity model (Eq. 2, $M = 30$, $S = 250$). **(a)** Local AFD within a single patch: clearly non-gamma (red). **(b)** Local abundance time series showing chaotic species turnover. **(c)** Global AFD obtained by aggregating abundances across all patches: well described by the gamma distribution (black line), in agreement with empirical biome data (grey points) [1]. **(d)** Global time series: turnover disappears and species fluctuate steadily around their mean, as observed empirically.

[1] J. Grilli, *Macroecological laws describe variation and diversity in microbial communities*, Nat. Commun. **11**, 4743 (2020).

[2] T. Arnoulx de Pirey and G. Bunin, *Many-species ecological fluctuations as a jump process from the brink of extinction*, Phys. Rev. X **14**, 011037 (2024).

[3] A. Gutiérrez-Arroyo, A. Lampo, and J. A. Cuesta, *The role of space in explaining macroecological patterns of microbial abundance*, bioRxiv:2026.04.15.718693 (2026).

[4] M. Castro and J. A. Cuesta, *Beyond the central limit: universality of the gamma distribution from Padé-enhanced large deviations*, arXiv:2603.23567 (2026).

Delayed reproduction in fluctuating environments

Jorge Hidalgo[1,2], Lorenzo Fant[3,4], Rafael Rubio de Casas[5,6], and Miguel Á. Muñoz[7,2]
[1]Departamento de Física, Universidad de Córdoba, Spain.
[2]Instituto Carlos I de Física Teórica y Computacional, Spain.
[3]Istituto Nazionale di Oceanografia e Geofisica Sperimentale (OGS), Trieste, Italy.
[4]National Biodiversity Future Centre (NBFC), Palermo, Italy.
[5]Departamento de Ecología, Universidad de Granada, Spain.
[6]Research Unit "Modeling Nature" MNat, Universidad de Granada, Spain.
[7]Departamento de Electromagnetismo y Física de la Materia, Universidad de Granada, Spain.

The timing of reproduction is a key life-history trait, but delayed reproduction entails an intrinsic cost: individuals that reproduce later also contribute later to population growth. In this work, we ask whether such delays can be favored exclusively by environmental fluctuations, rather than by additional trade-offs. We address this question using a minimal delayed-logistic model in which reproduction occurs after a fixed maturation time α (see the upper panel of Fig. 1), while the birth rate fluctuates in a temporally correlated environment:

$$\dot{x}(t) = (b + \sigma\xi_\tau(t))\,x(t-\alpha)\left(1 - \frac{x(t)}{K}\right) - d\,x(t). \qquad (1)$$

Here $x(t)$ is the population density, b and d are the mean birth and death rates, K is the carrying capacity, σ controls the amplitude of environmental variability and $\xi_\tau(t)$ is a colored dichotomous noise with correlation time set by τ. A key ingredient is that births at time t depend on the population size at an earlier time $t-\alpha$, introducing demographic memory.

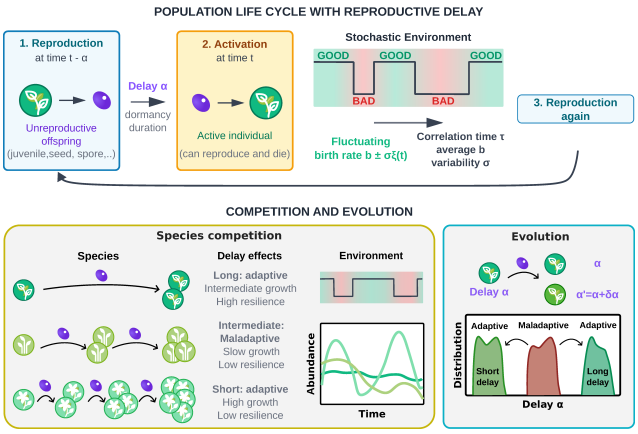

Fig. 1: Schematic representation of the delayed-reproduction model in a fluctuating environment. Lower panel shows an evolutionary scenario in which maturation time can evolve in time.

We study Eq. 1 using numerical simulations and analytical approximations, focusing on the mean growth rate G and the mean extinction time $\bar{T}$. Remarkably, we find that demographic memory and colored multiplicative noise make the system performance non-monotonic in the delay α [1].

Some of our results are summarized in Fig. 2: for small noise amplitudes, G decreases monotonically with α; above a threshold, it develops a global minimum at intermediate delays, corresponding to a saddle-node bifurcation, with an analogous effect when increasing τ. Despite the mathematical challenges of combining delay and colored noise, we derive a semi-analytical approximation that captures the key features of $G(\alpha)$ in good agreement with numerical simulations [1].

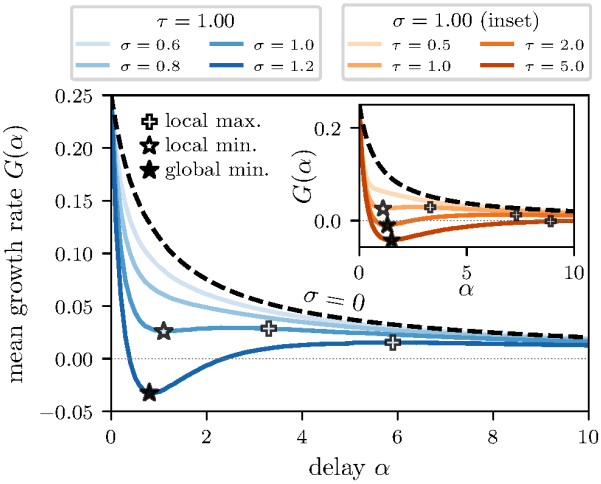

Fig. 2: Mean growth rate G: (main panel) as a function of the maturation time α for different noise amplitudes σ and fixed correlation time τ (inset: different τ and fixed σ).)

A comparison between G and the mean extinction time $\bar{T}$ reveals a clear trade-off: short delays maximize growth but shorten extinction times, whereas long delays reduce growth but enhance resilience [1]. Intermediate delays are disadvantageous in both respects, and thus emerge as "maladaptive" strategies. Additionally, we also implement an evolutionary algorithm in an agent-based model (as illustrated in the lower panel of Fig. 1), confirming the predicted bistability: populations evolve toward either short delays or long delays, while systematically avoiding intermediate delays.

Despite the simplicity of our minimal model, its core mechanism captures general effects that connect to diverse biological systems, including bimodal germination in plant seed banks, phenotypic diversification in microbial persisters, and cancer dormancy. Of course, system-specific details must be considered in each case. Nevertheless, this framework opens the door to more complex and realistic scenarios, which we leave for future work, such as evolutionarily stable distributions of lag times, multimodal bet-hedging strategies, and multiple populations sharing the same fluctuating environment. A full version of this work is available as an arXiv preprint [1] (under review).

[1] J. Hidalgo, L. Fant, R. Rubio de Casas, and M. A. Muñoz, *Fluctuating environments favor extreme reproductive delays and penalize intermediate ones*, arXiv:2512.05856, `https://arxiv.org/abs/2512.05856` (under review).

Memory-inspired acceleration of electro-orientation in nanoparticle suspensions

Miguel Ibáñez[1], Raúl A. Rica-Alarcón[1], and María L. Jiménez[1]
[1]Universidad de Granada, Department of Applied Physics and research unit 'Modeling Nature', Nanoparticle Trapping Laboratory, Granada (Spain)

When a system relaxes toward a new stationary state after a sudden change in a control parameter, the dynamics can be surprisingly complex [1, 2]. Attempting to shortcut this process by transiently driving the system beyond the target condition seems intuitively promising, but instead can trigger nonmonotonic, history-dependent responses: the hallmark of memory effects.

We use the electro-optical response of Brownian non-spherical nanoparticles dispersed in liquid as an experimental playground for these phenomena [3]. An applied AC electric field induces dipole moments that orient the particles, producing a measurable birefringence signal proportional to the nematic order parameter [4, 5]. The multiexponential character of the orientational relaxation makes this system particularly well-suited to explore memory effects such as the Kovacs anomaly [6–8]. In our experimental regime, it arises from polydispersity in the sample, but it is also present in monodisperse systems when permanent and induced dipoles coexist.

We show that the matched two-step (Kovacs) protocol, despite reaching the target order parameter at the switching time, fails to accelerate relaxation: the system overshoots and eventually merges back with the direct-protocol trajectory, with no net gain in the connection time. Building on a theoretical understanding of this failure, we design improved bang-bang protocols that sequentially suppress the slowest relaxation modes, achieving substantial reductions in connection time [7, 9, 10].

[1] Kumar, A., Bechhoefer, J. *Exponentially faster cooling in a colloidal system*. Nature **584**, 64–68 (2020).

[2] Ibáñez, M., Dieball, C., Lasanta, A., Godec, A. and Rica, R. A. *Heating and cooling are fundamentally asymmetric and evolve along distinct pathways*, Nature Physics **20**, 135-141 (2024).

[3] Ibáñez, M., Rica-Alarcón, R. A., and Jiménez, M. L. *Memory-aware acceleration of orientational dynamics in nanoparticle suspensions*. Accepted in Reports on Progress in Physics; arXiv:2603.12689 (2026).

[4] Arenas-Guerrero, P., Iglesias, G. R., Delgado, Á. V. and Jiménez, M. L. *Electric birefringence spectroscopy of montmorillonite particles*, Soft Matter **21**, 4923-4931 (2016).

[5] Felderhof, B. U. and Jones, R. B. *Kerr relaxation of anisotropic dielectric particles and Neel relaxation of anisotropic magnetic particles after a sudden change of field*, The Journal of Chemical Physics **115**,7852-7858 (2001).

[6] Kovacs, A. J., Aklonis, J. J., Hutchinson, J. M. and Ramos, A. R. *Isobaric volume and enthalpy recovery of glasses. II. A transparent multiparameter theory*, Journal of Polymer Science: Polymer Physics Edition **17**(7), 1097-1162 (1979).

[7] Patrón, A., Sánchez-Rey, B., Plata, C. A. and Prados, A. , Europhysics Letters **143**, 61002 (2023).

[8] Militaru, A., Lasanta, A., Frimmer, M., Bonilla, L. L., Novotny, L. and Rica, R. A. *Kovacs memory effect with an optically levitated nanoparticle*, Physical Review Letters **127**, 130603 (2021).

[9] Ibáñez, M., Patrón-Castro, A., Lasanta, A., Plata, C. A., Prados, A. and Rica-Alarcón, R. A. *The cost of speed: Time-optimal thermal control of trapped Brownian particles*, arXiv preprint arXiv:2602.14707 (2026).

[10] Patrón, A., Prados, A. and Plata, C. A. *Thermal brachistochrone for harmonically confined Brownian particles*, The European Physical Journal Plus **137**, 1-20 (2022).

Reducibility of higher-order to pairwise interactions: Social impact models on hypergraphs

Jaume Llabrés[1], Raúl Toral[2], Maxi San Miguel[1] and Federico Vázquez[1,2]
[1]Institute for Cross-disciplinary Physics and Complex Systems IFISC (CSIC-UIB),
Campus Universitat Illes Balears, 07122 Palma de Mallorca, Spain.
[2]Instituto de Cálculo, FCEN, Universidad de Buenos Aires and CONICET, C1428EGA Buenos Aires, Argentina.

Over the past decade, it has been emphasized that many biological, social, technological, and physical systems cannot be fully captured by models limited to pairwise (dyadic) interactions. In such systems, the fundamental units of interaction are often *polyadic*, involving groups of three or more entities, which are naturally represented by hypergraphs or simplicial complexes [1, 2]. Yet, the notion of higher-order interactions (HOI) is not foreign to Statistical Physics: the Mayer–Ursell cluster expansion already expresses many-body interactions in terms of diagrams analogous to hyperedges, showing that collective effects can emerge even within pairwise interaction frameworks. This raises a fundamental set of questions that motivate the present work: what precisely constitutes a higher-order interaction? Are group interactions truly irreducible, or can they be effectively represented as combinations of pairwise terms? Under what conditions can a dynamics defined on a hypergraph be reduced to an equivalent pairwise process?

In this work, we address the question of reducibility of HOI for social impact models on hypergraphs [3]. In these models, each agent holds a binary state variable and updates it according to the state configuration of its interaction group through a social impact function. We introduce a framework that guarantees that the group dynamics on a hypergraph can be exactly mapped onto an equivalent pairwise process on a weighted projected network. The link weights are defined so that the microscopic transition probabilities of both descriptions coincide, providing an exact dynamical equivalence between the higher-order and pairwise formulations.

Our main conclusion is that a general social impact model on an arbitrary hypergraph can be reduced, at the microscopic level, to a pairwise dynamics on a projected complex network with weighted links. These weights represent the effective probability of interaction between two nodes and, in general, depend on the instantaneous state configuration. As concrete examples, we introduce *hypergraph-voter models* as higher-order extensions of the voter models previously defined on a complex network. For the linear case, the equivalent pairwise dynamics occurs on a time-independent weighted projection, and the macroscopic evolution coincides with that of the standard voter model on the unweighted projected network. In contrast, the nonlinear case yields state-dependent, and hence time-dependent, weights. Additionally, we show that a minimal nonlinear voter model on the unweighted projected network provides an excellent effective description of the ordering dynamics of its hypergraph counterpart.

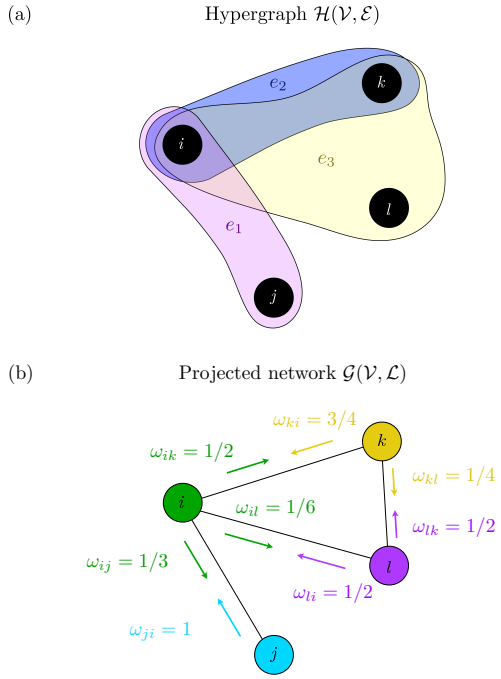

Fig. 1: Illustration of (a) a hypergraph $\mathscr{H}(\mathscr{V},\mathscr{E})$ and (b) its weighted projected network $\mathscr{G}(\mathscr{V},\mathscr{L})$ based on the mapping developed in our work [3].

[1] Bianconi, G., *Higher-Order Networks*, Elements in the Structure and Dynamics of Complex Networks, Cambridge University Press, 2021.

[2] Lambiotte, R., Rosvall, M., Scholtes, I., *From networks to optimal higher-order models of complex systems*, Nature Physics, **15**, 313–320, 2019.

[3] Llabrés, J., Toral, R., San Miguel, M., Vázquez, F., *Reducibility of higher-order to pairwise interactions: Social impact models on hypergraphs*, arXiv:2601.05169.

Collisional Cooling Induces Phase Separation Of Active Particles

Manuel Mayo[1], Lorenzo Caprini[2], María Isabel García de Soria[1], Umberto Marini Bettolo Marconi[3], Pablo Maynar[1], Luca Pizzoli[2] and Andrea Puglisi[2,4,5]
[1]Física Teórica, Universidad de Sevilla, Apartado de Correos 1065, E-41080 Sevilla, Spain
[2]Sapienza University of Rome, Physics Department, P.le A. Moro 2, Rome, Italy
[3]School of Sciences and Technology, University of Camerino, Via Madonna delle Carceri, Italy
[4]Istituto dei Sistemi Complessi - CNR, P.le A. Moro 2, Rome, Italy
[5]INFN, Sezione Roma2, Via della Ricerca Scientifica 1, I-00133, Rome, Italy

Motility-induced phase separation (MIPS) is a central collective phenomenon in active matter, theoretically established in the overdamped regime [1]. However, the role of inertia remains poorly understood, despite the large variety of active systems observed at macroscopic scales [3]. Here, we show that inertia fundamentally alters the dynamical origin of MIPS by introducing an effective cooling mechanism that is absent in overdamped active matter [2]. This conclusion is supported by an inertial extension of the direct simulation Monte Carlo method and by a kinetic theory for self-propelled inertial hard spheres derived directly from the microscopic dynamics. In contrast to the overdamped case, both approaches reveal that inertial MIPS does not rely on volume exclusion, but instead on a collective cooling mechanism coupling density, polarization, and temperature fields (see Fig. 1). This mechanism arises from the competition between self-propulsion and a density-dependent collision rate induced by spatial correlations between colliding particles. Our results establish a direct conceptual bridge between inertial active matter and granular physics, opening new perspectives for both fields.

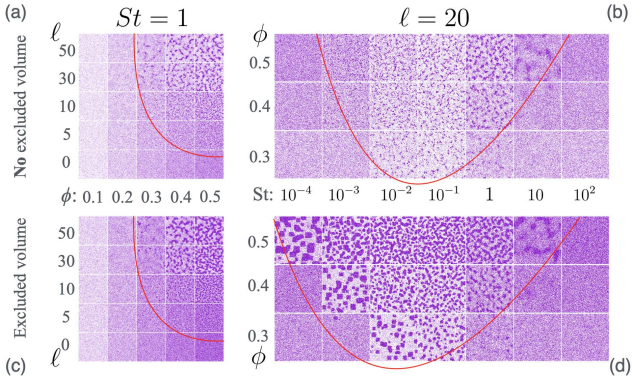

Fig. 1: Numerical results obtained using ADSMC with the Enskog collision rate. Panels (a)–(b) correspond to simulations without excluded-volume interactions, while (c)–(d) include excluded volume. Red lines serve as guides to the eye.

[1] M. E. Cates and J. Tailleur, *Motility-induced phase separation*, Annu. Rev. Condens. Matter Phys. **6**, 219 (2015).

[2] M. Mayo, L. Caprini, M. I. García de Soria, U. Marini Bettolo Marconi, P. Maynar, L. Pizzoli, and A. Puglisi, *Cooling mechanism controls motility-induced phase separation in inertial active liquids*, Phys. Rev. Lett. **136**, 188301 (2026).

[3] H. Löwen, *Inertial effects of self-propelled particles: From active brownian to active langevin motion*, J. Chem. Phys. **152**, 040901 (2020).

Beyond the Wisdom of the Crowd: How Network Topology Distorts Collective Perception

Giovanni Palermo[1], Vittorio Loreto[2], and Giulio Cimini[3]
[1]Department of Chemical Engineering, Universitat Rovira i Virgili, 43007 Tarragona (Catalonia)
[2]Sapienza University of Rome, Physics Department, Piazzale A. Moro 2, 00185 Rome (Italy)
[3]University Tor Vergata, Physics Department and INFN, 00133 Rome (Italy)

Classical theories of decision-making assume that people integrate information rationally, yet decades of behavioral research have revealed consistent cognitive biases driven by heuristics, bounded rationality, and limited attention. However, these individual mechanisms cannot fully explain the systematic errors that emerge at collective scales. As beliefs and information spread through social ties, they are filtered and amplified by network structure. Online echo chambers, homophily, and polarization provide remarkable examples of how network topology distorts human perception. Here we introduce a framework to quantify *network-induced perception biases*—systematic misperceptions of group attributes arising solely from the topology of social connections. We show that even when people are cognitively unbiased, their perception may be distorted, undermining the wisdom-of-the-crowd.

We model a population as a network with two communities, representing individuals with binary attributes (e.g., political orientation or belief). Each agent i holds an attribute $s_i = \pm 1$ and interacts with neighbors through edges defined by intra- and inter-group connection probabilities. Perception forms via a message-passing process: at each step, an agent updates her estimate of the global mean attribute m by averaging the perceptions of her neighbors. This yields a stationary perception μ that can be derived analytically through a mean-field approximation. We show that, in general, the mean perception μ does not match the real mean attribute m. We identify three drivers that cause this misperception: (i) *connectivity heterogeneity*, where more connected communities are overrepresented in perception; (ii) *community size imbalance*, causing minorities to appear larger and majorities smaller than reality; and (iii) *polarization*, where limited cross-group links prevent information flows and amplify intra-group misperceptions.

Simulations confirm that the mean stationary perception systematically deviates from the true population mean, even after averaging over all agents. This deviation quantifies a topological bias that does not cancel at the collective level, violating the wisdom-of-the-crowd principle. Analytical predictions derived from our mean-field theory closely match numerical results and extend to heterogeneous networks.

We validate these findings using survey data from Lee *et al.* [1], about social issues in Germany, the United States, and South Korea. Participants reported their own attribute, their social circle's attribute composition, and their estimate for the national population. The authors showed that the social circle correlates with the national estimate. We introduce a *message-passing estimator* that predicts population-level perception biases. Across all countries, this estimator outperforms the traditional social-circle method, confirming that longer-range network propagation better captures real-world misperceptions.

Our results demonstrate that the structure of social networks shapes how individuals and societies perceive themselves. Even without cognitive biases, network-driven biases can explain empirical phenomena such as the overestimation of minorities or false consensus effects.

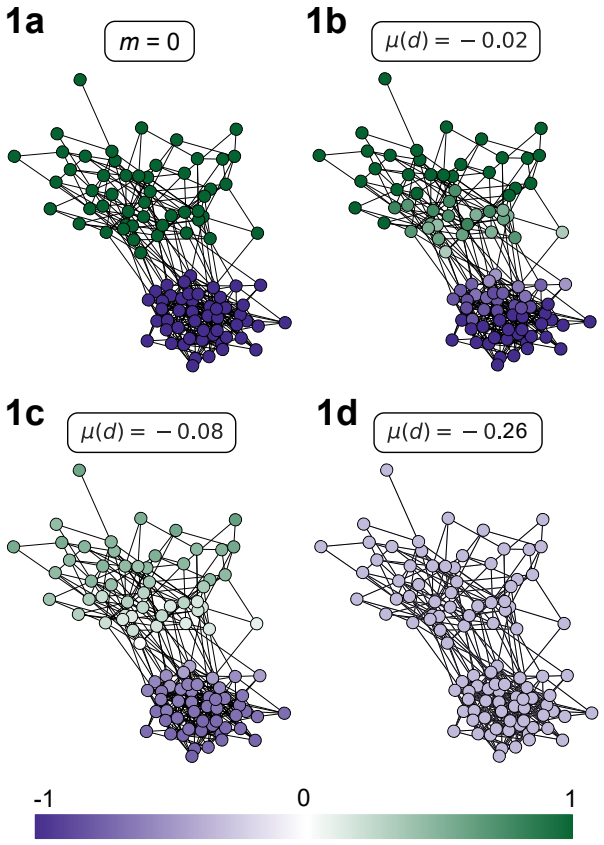

Fig. 1: (1a) We show an example of the message-passing algorithm, in which the information about a node's attribute may travel up to a distance d in the network. At $d = 0$, no propagation has occurred, so each node's perception corresponds to its own attribute. (1b) At $d = 1$, each node only gets messages from its neighbours, and nodes with neighbours in both communities develop a milder perception of the mean attribute. (1c) At $d = 5$, signals have reached nearly all nodes in the network. (1d) At $d = 30$, perceptions get close to stable values, which are not the same as m (the final average is -0.26, not 0), challenging the idea of the wisdom of the crowd. This happens because -1 nodes have more connections, so they share their views more widely.

[1] Lee, Eun and Karimi, Fariba and Wagner, Claudia and Jo, Hang-Hyun and Strohmaier, Markus and Galesic, Mirta, *Homophily and minority-group size explain perception biases in social networks*, Nature Human behaviour 10, (2019)

Towards the identification of principles for the design of stable microbial communities

Alberto Pascual-García[1],
[1]Spanish National Center for Biotechnology, C/Darwin 3, 28049, Madrid

Microbial communities play a fundamental role in a wide range of services related to health, the ecosystem and industry. However, many of these services require the management of complex communities, particularly those occurring in the natural environment. Consequently, there is growing interest within biotechnology in understanding the principles governing the relationship between composition (who), stability (how) and function (what).

To address this, one must consider hundreds of species that interact with one another, and these interactions in turn depend on the relationship with the environment. And one of the main problems in studying them is the lack of experimental results obtained under controlled conditions that allow for the minimisation of noise, to search for patterns, perform coarse-graining, and construct tractable mechanistic models.

In this presentation, I will begin by presenting large-scale experimental results on complex communities under controlled conditions with very high reproducibility [1]. Trajectories can be rationalised through the concept of the compositional landscape, similar to the fitness landscape in molecular biology. The results suggest that the landscape has distinct attractors, and the initial conditions of the communities determine the trajectory of their development.

To contextualise these findings, I will present theoretical results in which we identify a sufficient condition for the dynamic stability of complex communities, modelling the dynamics of taxa and their resources [2]. This condition also allows us to derive a function, the minimisation of which enables the design of the community's network of metabolite consumption and secretion.

We find that this optimisation maximises the number of functional groups, which translates into a reduction in effective competition. This result allows us to link to our previous macroecological findings, which explain the role of cooperation in sustaining biodiversity [3]. In turn, it raises questions about the scale of biological organisation at which selection is primarily operating, and supports the existence of metabolically cohesive consortia as building blocks of biodiversity [4].

Finally, I will show how we built on these findings to develop a computational tool for the design of feasible consortia using metabolic modelling [5]. With these models, we are able to observe niche expansion mediated by cross-feeding, identify functional groups, and model specific consortia of biotechnological interest.

In summary, our findings pave the way for understanding how to design complex communities with the potential to remain stable in changing conditions, such as those found in the natural environment

[1] Pascual-García A, Rivett D, Jones ML, Bell T. *Replicating community dynamics reveals how initial composition shapes the functional outcomes of bacterial communities.* Nature Communications. 2025;**16**(1):3002.

[2] Buchenel L, Bonhoeffer S, Pascual-García A. *A network optimisation condition uncovers the role of functional groups in the feasibility and dynamical stability of microbial model ecosystems.* bioRxiv. 2024; p. 2024–01.

[3] Pascual-García A, Bastolla U. *Mutualism supports biodiversity when the direct competition is weak.* Nature Communications. 2017;**8**:14326.

[4] Pascual-García A, Bonhoeffer S, Bell T *Metabolically cohesive microbial consortia and ecosystem functioning* Phil. Trans.Roy. Soc. B, 2020; **375**:1798,

[5] Ochsner N, San Román M, Jiménez-Fernández A, Bonhoeffer S, Pascual-García A. *misosoup: A metabolic modeling tool for identifying minimal microbial communities provides valuable insights into microbial ecology and biotechnological applications.* bioRxiv. 2025; p. 2025–08.

Beyond pairs: higher-order entanglement hyperlinks

Silvia N. Santalla[1], Sudipto Singha Roy[2], Germán Sierra[3], and Javier Rodríguez-Laguna[4]
[1]Dto. Física & GISC, Universidad Carlos III de Madrid, Spain
[2]Department of Physics, Indian Institute of Technology (ISM), Dhanbad, India
[3]Instituto de Física Teórica, UAM-CSIC, Universidad Autónoma de Madrid, Cantoblanco, Madrid, Spain
[4]Dto. Física Fundamental, Universidad Nacional de Educación a Distancia (UNED), Spain

Information and entropy are central concepts in statistical mechanics. Concretely, the mutual information between two parties is widely used to shed light into data obtained in many different scientific fields [1]. We may therefore ask about the amount of information shared between three or more parties which is not contained in any of the pairs. Higher-order information theory is a well developed branch of mathematics, but its application into physics is severely delayed. For example, concepts such as redundancy and synergy should play a more relevant role in our statistical analysis. In simple terms, three parties are said to show redundancy when knowing two of them makes the third unnecessary, while they show synergy when the full information about the system is only achieved when we know all of them, and no two of them will suffice [2]. Interestingly, synergy is strongly related to the quantum concept of monogamy [3].

On the other hand, our group showed in 2020 that the entanglement entropy (EE) of any bipartition of a pure state can be approximately expressed as a sum of entanglement links (ELs) [4]. In this work, we introduce their exact extension, i.e. the entanglement hyperlinks (EHLs), a type of higher-order mutual informations defined through the inclusion-exclusion principle, each of which captures contributions to the multipartite entanglement that are not reducible to lower-order terms [5].

We show that any EHL crossing a factorized partition must vanish, and that the EHLs between any set of blocks can be expressed as a sum of all the EHLs that join all of them. This last result allows us to provide an exact representation of the EE of any block of a pure state, from the sum of the EHLs which cross its boundary. In order to illustrate their rich structure, we discuss some explicit numerical examples using local ground states. The EHLs thus provide a remarkable tool to characterize multipartite entanglement in quantum information theory and quantum many-body physics.

[1] M. Mézard, A. Montanari, *Information, physics and computation*, Oxford University Press (2009)

[2] T.F. Varley, M. Pope, J. Faskowitz, O. Sporns, *Multivariate information theory uncovers synergistic subsystems of the human cerebral cortex*, Comm. Biol. **6**, 451 (2023)

[3] T.F. Varley, *Information theory for complex systems scientists: What, why, and how*, Phys. Rep. **1148**, 1 (2025)

[4] S. Singha Roy, S.N. Santalla, J. Rodríguez-Laguna, G. Sierra, *Entanglement as geometry and flow*, Phys. Rev. B **101**, 195134 (2020)

[5] S.N. Santalla, S. Singha Roy, G. Sierra, J. Rodríguez-Laguna, *The hyperlink representation of entanglement and the inclusion-exclusion principle*, arXiv:2601.17926

Stochastic resetting with limited information

Sanz-Arqué, Verónica[1], and Cao-García, Francisco J.[2]
[1]Universidad Complutense De Madrid, Madrid, Spain
[2]IMDEA Nanoscience, Madrid, Spain

Stochastic resetting refers to the random reinitialization of the position of a random movement, and to the overall resulting kinematics [1, 2]. The typical case is a Brownian motion that is instantly reinitialized to the starting position at exponentially distributed time intervals, given by a resetting rate. Several variations such as finite-time resetting [3, 5], partial resetting [4] and random amplitude resetting have been studied [6]. However, generally these studies assume that the position is precisely known, which can not be the case in experimental realizations.

Here, we address the case where position precision is finite, and therefore the position information is limited. We choose for our computations a discrete realization. We consider a jump process over a lattice with an exponential stochastic resetting. But where the position information for resetting is only known at a coarse-grained level. The problem is addressed from an agent- based perspective. The latter allows us to study the sequences of resetting actions and its correlations.

We have found the different scaling of the main characteristic magnitudes with the spatial position precision. These magnitudes include the conditional probabilities between resetting actions, the gathered information, the entropy reduction by information, the entropy change at resetting, the entropy of the sequence of resetting actions and its upper and lower boundaries [7, 8], all of them as a function of the resetting rate to jump rate ratio. Analytical results for the scaling are found in the slow and fast resetting limits. Furthermore, we analytically and numerically verify key information-theoretic inequalities, regarding the measurement and resetting events, confirming that the systematic entropy reduction due to resetting is strictly bounded by the coarse-grained measurement constraints [9].
These results provide a relevant insight into real world applications of stochastic resetting, where the position precision is finite.

[1] M. R. Evans, S. N. Majumdar, and G. Schehr, *Stochastic Resetting and Applications*, J. Phys. A Math. Theor. **53**, (2020), https://doi.org/10.1088/1751-8121/ab7cfe.

[2] S. Gupta and A. M. Jayannavar, *Stochastic Resetting: A (Very) Brief Review*, Front. Phys. **10**, 1 (2022), https://doi.org/10.3389/fphy.2022.789097.

[3] D. Gupta, A. Pal, and A. Kundu, *Resetting with Stochastic Return through Linear Confining Potential*, J. Stat. Mech. Theory Exp. **2021**, (2021), https://doi.org/10.1088/1742-5468/abefdf.

[4] O. Tal-Friedman, Y. Roichman, and S. Reuveni, *Diffusion with Partial Resetting*, Phys. Rev. E **106**, (2022), https://doi.org/10.1103/PhysRevE.106.054116.

[5] D. Gupta, *et al.*, *Stochastic resetting with stochastic returns using external trap*, J. Phys. A Math. Theor. **54**, 025003 (2021), https://doi.org/10.1088/1751-8121/abcc59.

[6] M. Dahlenburg, A. V. Chechkin, R. Schumer, and R. Metzler, *Stochastic Resetting by a Random Amplitude*, Phys. Rev. E **103**, (2021), https://doi.org/10.1103/PhysRevE.103.052123.

[7] F. J. Cao and M. Feito, *Thermodynamics of feedback controlled systems*, Phys. Rev. E **79**, 041118 (2009), https://doi.org/10.1103/PhysRevE.79.041118.

[8] J. Jarillo, T. Tangarife, and F. J. Cao, *Efficiency at maximum power of a discrete feedback ratchet*, Phys. Rev. E **93**, 012142 (2016), https://doi.org/10.1103/PhysRevE.93.012142.

[9] V. Sanz-Arqué, and F. J. Cao-García, *Stochastic resetting with limited information.*, in preparation (2026).

RBMs, powerful modeling machines

Giovanni Catania[1], Aurélien Decelle[2,4], Alfonso de Jesús Navas Gómez[3], Beatriz Seoane[3,4],
[1]Institute for Cross-disciplinary Physics and Complex Systems IFISC (CSIC-UIB),
Campus Universitat Illes Balears, 07122 Palma de Mallorca, Spain.
[2]Escuela Técnica Superior de Ingenieros Industriales, Universidad Politécnica de Madrid, 28006 Madrid, Spain.
[3]Departamento de Física Teórica, Universidad Complutense de Madrid, 28040 Madrid, Spain
[4]GISC - Grupo Interdisciplinar de Sistemas Complejos 28040 Madrid, Spain.

Restricted Boltzmann Machines (RBMs) are unsupervised machine learning models structured as bipartite neural networks. They capture statistical correlations in data through a Boltzmann weight derived from an energy function. In this talk, I will demonstrate how analyzing this energy function provides deep and interpretable insights into the data, establishing RBMs as powerful tools for inference.

Notably, the RBM's energy function can be mapped onto a model of interacting spins, analogous to those extensively studied in statistical physics. Unlike traditional pairwise interaction models commonly used in inverse statistical problems (such as maximum entropy approaches), this mapping inherently includes higher-order interactions. Importantly, this framework enables the inference of complex, higher-order interactions without requiring an explosion in the number of adjustable parameters. Beyond direct inference from data, this perspective also opens the possibility of training RBMs to reproduce the effective Hamiltonian of another statistical model, providing compact and flexible representations of complex interacting systems and enabling the study of emergent effective interactions across scales.

Furthermore, analyzing the evolution of the free-energy landscape's minima throughout the training process, approximated using mean-field techniques, uncovers hidden hierarchical relationships between data points. This approach provides a straightforward method for performing hierarchical clustering, enabling unsupervised classification and identifying key features that characterize distinct data groups. We illustrate these methods in two different contexts: large datasets of homologous protein sequences, where RBMs can identify functional and structural constraints encoded in sequence variability, and large-scale neural recordings from mice, where they uncover collective activity patterns and hierarchical organization in neural populations.

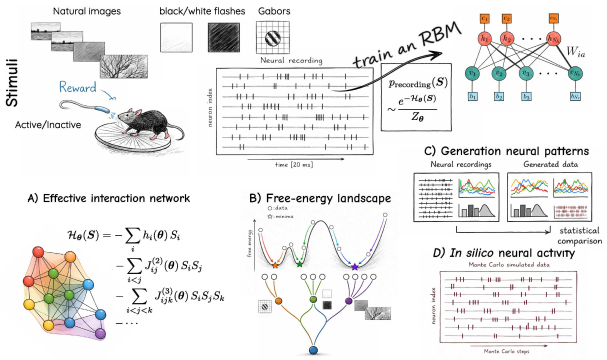

Fig. 1: Pipeline of the RBM-based inference procedure.

[1] A. Decelle, C. Furtlehner, A. de Jesús Navas Gómez, and B. Seoane, *Inferring effective couplings with restricted Boltzmann machines*, *SciPost Physics* **16** (2024) 095.

[2] A. Decelle, B. Seoane, and L. Rosset, *Unsupervised hierarchical clustering using the learning dynamics of restricted Boltzmann machines*, *Physical Review E* **108** (2023) 014110.

[3] A. Decelle, A. de Jesús Navas Gómez, B. Seoane, *Inferring High-Order Couplings with Neural Networks*, *Physical Review Letters* **135** (2023) 207301.

[4] N. Béreux, G. Catania, A. Decelle, F. Mignacco, A. de Jesús Navas Gómez, B. Seoane, *Uncovering statistical structure in large-scale neural activity with Restricted Boltzmann Machines*, *arXiv preprint* arXiv:2603.11032 (2026).

Learning and adaptive dynamics in bacteria controlled using microfluidics

Xavier Viader-Godoy[1], Jordi Garcia-Ojalvo[1]
[1]Departament de Medicina i Ciències de la Vida, Universitat Pompeu Fabra, Carrer del Doctor Aiguader, 80, 08003 Barcelona.

Biological systems are essentially dissipative active matter that must process information to navigate fluctuating environments. A central question in this field is whether single-cell organisms can "learn"—a process we define here as the systematic modification of a system's response due to repeated exposure to external stimuli[1]. This implies the emergence of memory effects and non-Markovian dynamics within the cell's internal state.

We investigate the potential for such learning by treating individual bacteria as stochastic systems driven by external chemical perturbations. Using a custom-built microfluidic platform, we grow bacterial colonies in a 2D configuration while maintaining high-resolution control over the extracellular medium. As shown in Figure 1, this setup allows us to precisely tune the chemical environment, varying nutrient or antibiotic concentrations, to deliver well-defined temporal stimulus profiles, ranging from single pulses to periodic oscillations.

By tracking gene expression via fluorescent reporters, we monitor the evolution of the cells' internal degrees of freedom in real-time. This approach allows us to quantify how environmental information is encoded within intracellular networks and how this encoding shifts the transition probabilities between different phenotypic states. Our goal is to determine if exposure history leads to measurable changes in cellular response, which would serve as evidence of information processing and learning in the simplest form of life.

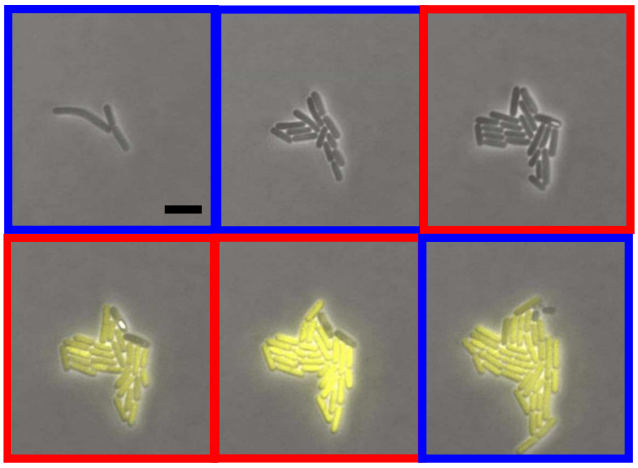

Fig. 1: **Single-cell response to dynamic environmental shifts.** Time-lapse sequence (16 hours total) showing the 2D growth of a *Bacillus subtilis* colony within a microfluidic chamber under a time-varying chemical environment. Initially, the colony grows for 8 h in medium A (blue frame). Upon switching to medium B—a yellow-fluorescence inducing medium (red frame)—for a 4-hour interval, the expression of the fluorescent reporter is triggered, and cellular growth is observed to stall. Following a switch back to the original medium A, growth is recovered, accompanied by a gradual attenuation of the fluorescent protein levels. Scale bar: 5 μm.

[1] Eckert, L., Vidal-Saez, M. S., Zhao, Z., Garcia-Ojalvo, J., Martinez-Corral, R., Gunawardena, J. (2024). *Biochemically plausible models of habituation for single-cell learning.* Current Biology, **34**(24), 5646-5658.e3.

Pósteres

Polarization and Locomotion Dynamics in Dictyostelium discoideum: A Study on Anomalous Diffusion

Sergio Alonso[1], Robert Großmann[2] and Carsten Beta[2]
[1]Department of Physics, Universitat Politecnica de Catalunya, Spain
[2]Institut für Physik und Astronomie, Universität Potsdam, Germany

Individual living cells, such as amoeboid cells, exhibit a remarkable ability to navigate complex environments to locate nutrients or capture bacteria. This movement is a two-step process: first, the cell undergoes polarization, triggered by internal biochemical patterns or external stimuli, and subsequently initiates locomotion in the direction established by that polarization. Modeling this coupling remains a significant challenge, as it represents a complex non-trivial free-boundary problem [1].

The central goal of this study is to determine whether the dispersion of actively crawling cells follows a Brownian or non-Brownian (anomalous) regime. While some literature suggests standard diffusion, recent studies indicate more complex stochastic behaviors that deviate from the classical Brownian model.

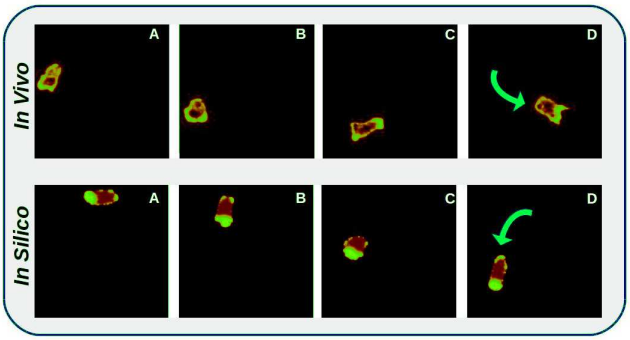

Fig. 1: Comparison of results from an in vivo cell and an in silico cell simulation. Top: Evolution of a Dictyostelium discoideum cell in vivo for four time points (A-D); bottom: evolution of a virtual Dictyostelium discoideum cell obtained through numerical simulations for four time points (A-D). Arrows in the final panels indicate the dynamics of the cell.

We have developed a specialized model based on a reduced stochastic reaction-diffusion model for the biochemistry of *Dictyostelium discoideum* polarization. Such model is intergrated in a phase field model for the cell shape, which account for the cell dynamics and in particular the cell locomotion [2] producing a *in silico* vesion of the cells. We employ this specialized model for the locomotion of *Dictyostelium discoideum* to systematically analyze the evolution of the Mean Squared Displacement (MSD) over time. Our approach integrates data from *in vivo* experiments with whole-cell computational models (*in silico*), see Fig.1, and active particle motion frameworks. By checking the time-dependent evolution of the displacement square, we characterize the nature of cell motility. Our findings contribute to the ongoing debate between reports of non-Brownian trajectories [3] versus standard Brownian observations [4].

We provide a detailed characterization of the conditions under which cells transition between different diffusive regimes, offering deeper insights into the underlying mechanisms of random cellular motion.

[1] Sergio Alonso, and Carsten Beta. *Mathematical and Computational Modeling of Amoeboid Cell Crawling* arXiv preprint arXiv:2603.15350 (2026).

[2] E Moreno, S Flemming, F Font, M Holschneider, C Beta, and S Alonso (2020). *Modeling cell crawling strategies with a bistable model: From amoeboid to fan-shaped cell motion*. Physica D: Nonlinear Phenomena, **412**, 132591.

[3] N Makarava et al. *Quantifying the degree of persistence in random amoeboid motion based on the Hurst exponent of fractional Brownian motion* Physical Review E, **90** (4) 042703 (2014).

[4] HU Boedeker et al. *Quantitative analysis of random ameboid motion*, Europhysics Letters, **90** (2), 28005 (2010).

Exploiting outer-membrane channel promiscuity to induce transient collateral sensitivity in *Pseudomonas aeruginosa*

Pablo Catalán[1,2], Saúl Ares[2,3], Beatriz Pascual-Escudero[4], Ioannis Kontos[3], Pablo Laborda[5], José Ramón Valverde[3], José L. Martínez[3], and Sara Hernando-Amado[3]
[1]Universidad Carlos III de Madrid, Departamento de Matemáticas, Leganés
[2]Grupo Interdisciplinar de Sistemas Complejos (GISC)
[3]Centro Nacional de Biotecnología (CNB), CSIC, Madrid
[4]Universidad Politécnica de Madrid
[5]Department of Clinical Microbiology 9301, Rigshospitalet, 2100 Copenhagen, Denmark

One promising strategy against antibiotic resistance is to exploit *collateral sensitivity* (CS): situations where making a microbe less sensitive to one drug simultaneously makes it *more* sensitive to another. Most work has focused on stable, mutation-driven CS, but CS can also be *transiently* induced in *P. aeruginosa* by dequalinium chloride (DC), which upregulates the efflux operon *mexCD* and produces transient CS to the aminoglycoside tobramycin, an inhibitor of bacterial protein synthesis [1]. The molecular mechanism remained unclear.

We combine mass-action kinetics, Bayesian inference, molecular dynamics, and experiments on isogenic mutants to identify it [2]. *P. aeruginosa* tripartite efflux pumps (protein complexes that extrude antibiotics across the cell envelope) share outer-membrane channels: MexCD canonically assembles with OprJ to extrude ciprofloxacin (a fluoroquinolone targeting DNA gyrase), while MexXY assembles with OprM to extrude aminoglycosides such as tobramycin. We show that DC inactivates the repressor NfxB, raising *mexCD* expression. Coarse-grained molecular dynamics indicates that overexpressed MexCD also forms a stable complex with OprM. The resulting sequestration of OprM by MexCD reduces functional MexXY–OprM, lowering aminoglycoside efflux and producing CS to tobramycin, while raising ciprofloxacin resistance.

A minimal mass-action model of pump assembly, combined with a Hill-type dependence of growth rate on intracellular antibiotic, yields a single functional form for the minimal inhibitory concentration (MIC, the lowest external antibiotic dose that prevents bacterial growth) of both drugs,

$$\mathrm{MIC}([\mathrm{DC}]) = A\,\frac{1+C\,([\mathrm{DC}]/B)^2}{1+([\mathrm{DC}]/B)^2}, \qquad (1)$$

in which A sets the baseline, AC the saturation value, and B the crossover dose. The sign of $C-1$ alone discriminates resistance ($C>1$, ciprofloxacin) from CS ($C<1$, tobramycin), so the same expression captures opposite phenotypes. Bayesian inference on dose–response data recovers both trends. The model further predicts that loss of OprJ preserves DC-induced CS (MexCD recruits OprM), whereas loss of OprM abolishes it; both predictions are confirmed in PA14 mutants. Competition for a shared outer-membrane channel is therefore the proximal cause of DC-induced transient CS, and offers a general route to elicit CS by perturbing shared components of multidrug efflux systems.

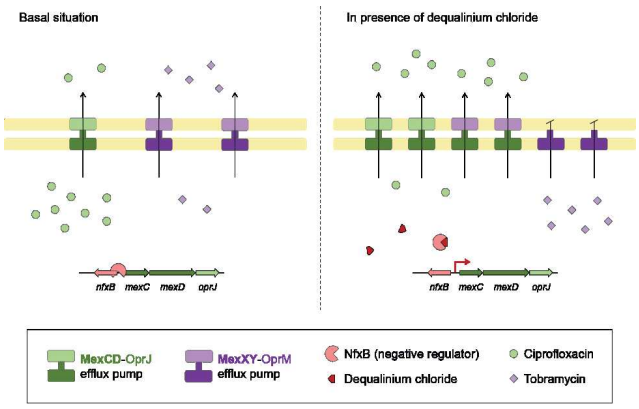

Fig. 1: Effect of dequalinium chloride (DC) on *P. aeruginosa* efflux pumps. DC binds NfxB, relieving its repression of *mexCD–oprJ*. Increased MexCD assembles with either OprJ or OprM, enhancing ciprofloxacin efflux; overproduced MexCD sequesters OprM from MexXY, compromising tobramycin extrusion.

[1] S. Hernando-Amado, P. Laborda, and J. L. Martínez, *Tackling antibiotic resistance by inducing transient and robust collateral sensitivity*, Nature Communications **14**, 1723 (2023).

[2] P. Catalán, S. Ares, B. Pascual-Escudero, I. Kontos, P. Laborda, J. R. Valverde, J. L. Martínez, and S. Hernando-Amado, *Exploiting outer-membrane protein promiscuity to induce transient collateral sensitivity via efflux pump competition*, bioRxiv 2026.05.12.724739 (2026).

Opinion dynamics under large-scale exogenous events

Gerard Argany[1], Lucila Alvarez-Zuzek[2] and Oriol Artime[1,3]
[1]Department of Condensed Matter Physics, University of Barcelona
[2]Fondazione Bruno Kessler, Trento, Italy
[3]Univeristy of Barcelona Institute of Complex Systems (UBICS)

Opinion dynamics models have successfully reproduced a wide range of collective phenomena arising from local social interactions, including consensus formation, polarization, and the persistence of minority opinions. Nevertheless, a major challenge remains in connecting microscopic interaction rules to abrupt, system-wide changes in public opinion. Real societies are frequently exposed to large-scale exogenous shocks—such as political scandals, coordinated misinformation campaigns, terrorist attacks, economic crises, or major scientific announcements—that can rapidly reshape the opinion landscape. These events may trigger sudden polarization, induce transitions toward previously minority viewpoints, or reinforce pre-existing beliefs in substantial fractions of the population, on timescales that interact nontrivially with those associated with local social influence mechanisms. Despite their empirical relevance, such phenomena remain largely absent from classical opinion dynamics models, where social influence is typically implemented through pairwise interactions producing at most one opinion update per event. As a consequence, existing frameworks struggle to capture the interplay between local imitation processes and abrupt macroscopic opinion shifts.

To address this limitation, we introduce a general and flexible framework that couples arbitrary local opinion dynamics to large-scale exogenous shocks. The framework allows shocks to possess tunable characteristics, enabling the modeling of a broad range of empirically motivated scenarios. Rather than replacing existing opinion models, our approach acts as an additional layer that can be incorporated into any local interaction dynamics, providing a unified methodology for studying the impact of external perturbations on collective opinion formation.

We first demonstrate the framework using the voter model as a reference case. The voter model is one of the most fundamental and analytically tractable models in sociophysics, capturing the role of pairwise imitation in the emergence of consensus. We show how the inclusion of exogenous shocks modifies its dynamical behavior and derive both qualitative and quantitative predictions for the resulting opinion trajectories. To highlight the generality of the approach, we further apply it to the noisy voter model (Kirman model), which incorporates spontaneous opinion changes and represents a widely studied extension of the voter framework.

While complete interaction networks provide the most transparent setting for analytical treatment, realistic social systems are characterized by nontrivial interaction topologies. To overcome this limitation, we employ a pair-approximation formalism that explicitly incorporates network structure and enables us to quantify how interaction patterns influence the response of the system to external shocks.

Using this framework, we investigate both equilibrium and non-equilibrium properties of the coupled dynamics, including stationary opinion distributions, full-time evolution, and first-passage statistics to consensus states (see Fig. 1). Our results reveal how large-scale perturbations interact with local social influence to generate behaviors that cannot be explained by either mechanism alone. More broadly, the proposed framework bridges a longstanding gap between traditional sociophysical models of opinion formation and the abrupt collective responses observed in real-world social systems.

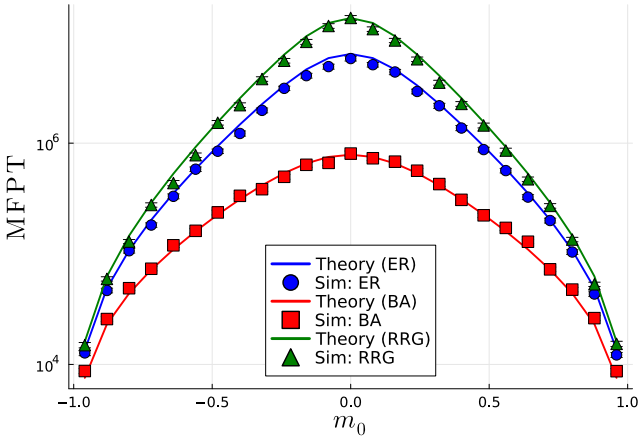

Fig. 1: **Mean first-passage time to consensus across different network topologies**. Theoretical predictions from the developed pair approximation (lines) and Monte Carlo simulations (symbols) for a Random Regular Graph (RRG), an Erdos-Renyi (ER) network, and a Barabási-Albert (BA) network, all with mean degree $\mu = 5$.

Mixing of a passive scalar in active nematic turbulence

Giacomo Bartolucci[1,2], Joan Térmens [1,2], Ido Lavi[3], and Jaume Casademunt[1,2]
[1]Departament de Fısica de la Materia Condensada, Universitat de Barcelona, Carrer de Martí i Franquès, 1, 08028 Barcelona, Spain
[2]Universitat de Barcelona Institute of Complex Systems (UBICS), Barcelona, Spain
[3]Center for Computational Biology, Flatiron Institute, 162 5th Ave, New York, NY 10010, USA

Active fluids are composed of units that continuously consume energy for propulsion and interact, yielding highly correlated flows. At high activity, active fluids typically exhibit spatio-temporal chaos. Such chaotic flows have been experimentally observed in a variety of systems, ranging from bacterial suspensions to cell monolayers. In all these cases, the chaotic patterns are reminiscent of classic inertial turbulence, despite they occur for Reynolds number for which inertia is negligible. For this reason, they are referred to as active turbulence [1]. In the case of active nematic fluids, i.e. if the elementary constituent are anisotropic, the flow can be characterised by long-ranged orientational order. Unlike classical turbulence, active nematic flows are endowed with an activity-dependent length scale, above and below which the velocity power spectrum features scaling laws with universal exponents independent of the material properties of the fluid. An important role in shaping active turbulent flows is played by topological defects. Topological defects are a non-local excitation of the orientation field in a polar or nematic fluid and have been linked to crucial functions in active fluids, ranging from tissue mechanics and morphogenesis to bacterial collective behaviour.

Here, we explore the potential role of active nematic turbulence in the mixing of a passive scalar field. The problem of mixing of a passive scalar by inertial turbulent flows combined with diffusion, is well-characterized. Surprisingly, however, the dynamics of mixing by active turbulent flows remains unexplored, despite it may be essential in biology, for example in the propagation of nutrients or morphogenic gradients.

We begin showing that the amplitude of concentration perturbations decays exponentially in time, while the statistical properties of the spatial correlations reach a steady state. Consequently, one can rescale the concentration in a time-dependent manner leading to a pseudo-stationary velocity spectrum at late times. We then show that, if diffusion over length scales characteristic of the turbulent flow is slow compared to advection speed, the pseudo-stationary concentration spectrum exhibits power law q^{-1}.

Secondly, we introduce noise correlated over large scales larger than the active length scale and characterize the corresponding steady state. We show that concentration fluctuations are injected and dissipated at different length scales, leading to a cascade in the concentration spectrum. In particular, concentration fluctuations are injected at large scales characteristic of the noise, while dissipation occurs also at scales comparable to the active length scale associated with the turbulent velocity spectrum.

Finally, we discuss the impact of topological defects in modulating the mixing rate. We show that, in the absence of defects, the mixing rate is related to the length scale characteristic of active turbulence. In the presence of defects, on the other hand, the mixing rate is controlled by the defect core length. Our findings can shed light on the mixing of chemicals via biological flows which exhibit turbulent behaviour, like bacteria or microtubules.

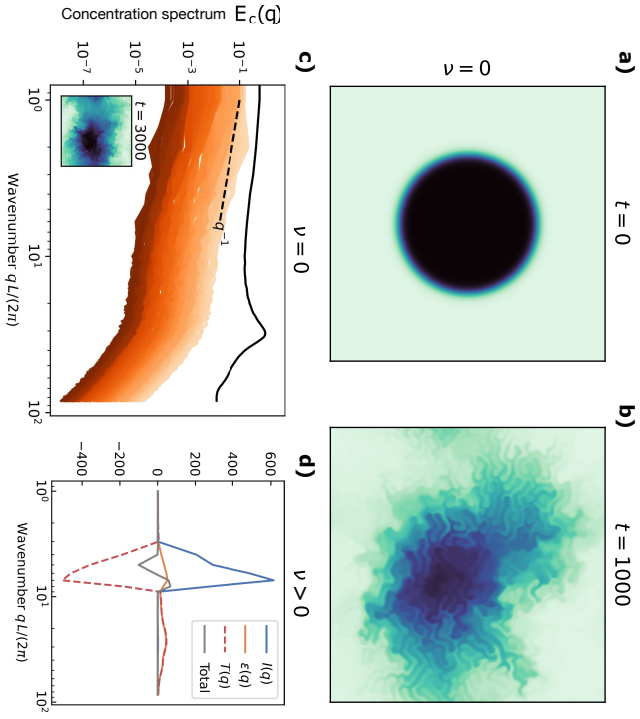

Fig. 1: **Mixing of a passive scalar via active turbulence** Concentration profiles in the a) initial state corresponding to a drop and b) mixed pseudo-stationary state. b) Concentration spectrum evolving in time, showing that, after an initial relaxation, the amplitude of fluctuations decay leaving unaltered the spatial patetrn. d) In the presence of noise, the contributions to the time evolution of the concentration spectrum balance. In particular, the injection $I(q)$ is peaked at low wavenumbers, while the dissipation $\varepsilon(q)$ exibits a second peak corresponding to the active length scale.

[1] R. Alert, J. Casademunt, and J.F.. Joanny, *Active Turbulence*, Ann. Rew. Cond . Mat.. Phys. **13**, 143-170 (2022).
[2] I. Lavi, R. Alert, J.F.. Joanny, and J. Casademunt, *Dynamical arrest in active nematic turbulence*, Phys. Rev Res. **8**, 013-294 (2026).

Mobility energetic balance as a driver of urban spatial organization

Federico Bellisardi[1], Enrique Cano Suñén[2], Ana Ruiz-Varona[3] and José J. Ramasco[1]
[1]Instituto de Física Interdisciplinar y Sistemas Complejos IFISC (CSIC-UIB), Campus UIB, 07122 Palma de Mallorca, Spain
[2]Human Openware Research Lab (HOWLab), Engineering Research Institute of Aragon (I3A), University of Zaragoza (UZ), Spain
[3]Arquitecturas Open Source (AOS) Research Group, School of Architecture and Technology, Universidad San Jorge, Zaragoza, Spain

Urban mobility entails costs in travel time, fuel consumption, fares, and physical effort. Yet mobility also takes place across uneven landscapes, where overcoming altitude differences requires a significant energetic investment. Here we introduce a terrain-aware energetic framework to quantify how topography shapes urban mobility and spatial organization across different urban systems.

We combine three empirical layers: (i) urban road networks (OpenStreetMap), (ii) high-resolution digital elevation models, and (iii) origin – destination (OD) mobility flows reconstructed from multi-year geolocated Twitter/X activity. Each city is represented as a directed spatial graph embedded on a real topographic surface. For every road segment, we compute both the longitudinal mobility cost and the uphill gravitational work associated with positive elevation gains.

For a trajectory τ, the total energetic cost is defined as

$$W_\tau = W_{\mathrm{Lon}} + W_{\mathrm{Alt}} = \lambda L_\tau + mg \int_\tau \max\left(0, \frac{dh}{d\ell}\right) d\ell,$$

where L_τ is the terrain-following path length, λ is an effective energetic cost per unit distance, and the second term accounts for the cumulative uphill gravitational work. Aggregating all trajectories weighted by empirical OD flows yields the total mobility energy of the city,

$$W_{\mathrm{Tot}} = \sum_{(O,D)} F_{OD} W_{OD}.$$

To isolate the role of spatial embedding from network topology, we generate ensembles of counterfactual urban configurations by applying pure geometric transformations, such as translations, rotations, and dilations, to the real road network while preserving its topology. These transformations reposition the same network over the surrounding terrain, modifying its alignment with elevation gradients without altering connectivity.

As shown in Fig. 1a for Atlanta and Fig. 1b for Santiago, the empirical urban configuration systematically minimizes the total mobility energy relative to translated, rotated, and rescaled alternatives. The same behavior is observed across all analyzed cities. Even small spatial perturbations produce significant energetic penalties, demonstrating that real cities occupy sharp minima of the energetic landscape.

At the microscopic level, the altitudinal energetic burden is highly heterogeneous. A small fraction of road segments concentrates most of the uphill mobility work, revealing the existence of high-work topographic corridors that structurally govern accessibility and energetic efficiency. This concentration explains the strong sensitivity of cities to geometric perturbations and highlights how terrain constraints organize mobility at the metropolitan scale.

Finally, we show how the same framework can be extended to evaluate urban densification scenarios. By introducing synthetic population growth and routing the induced mobility demand on the real road network, we identify locations that minimize the additional energetic burden associated with future urban expansion. The results demonstrate that terrain-aware energetic accounting provides a physically grounded criterion for evaluating accessibility and sustainable urban growth strategies.

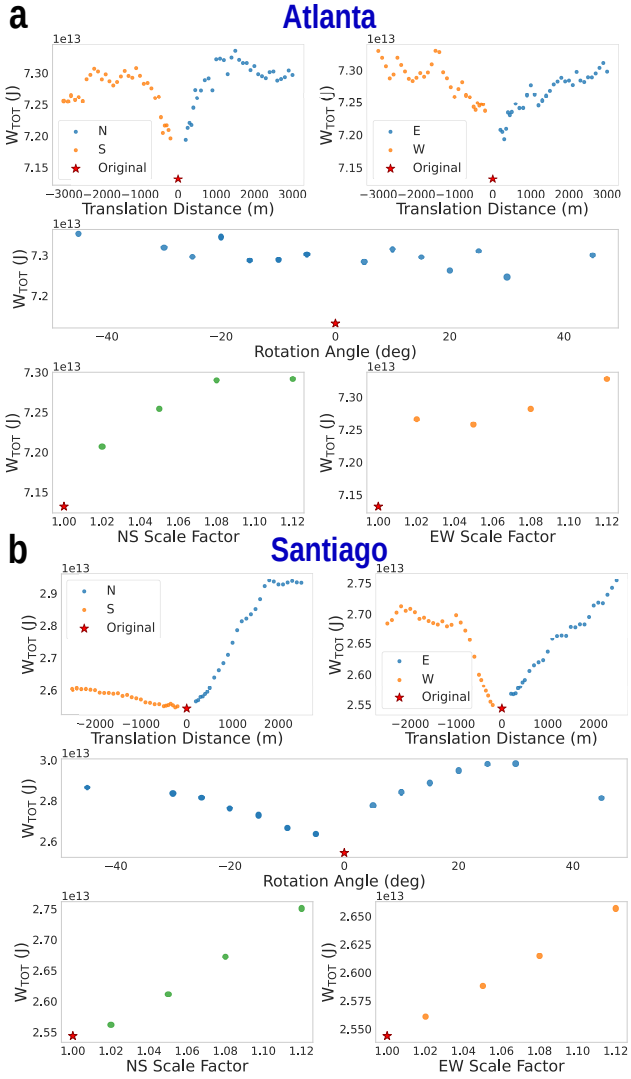

Fig. 1: **Energetic sensitivity to geometric transformations of urban form.** The empirical urban configuration systematically corresponds to the energetic minimum.

[1] M. Batty, *The New Science of Cities* (MIT Press, Cambridge, 2013).
[2] M. Barthelemy et al., *Surfacic networks*, PNAS Nexus **4**, pgae585 (2025).
[3] A.E. Minetti, et al., *Energy cost of walking and running at extreme uphill and downhill slopes*, J. Appl. Physiol. **93**, 1039–1046 (2002).

Correlaciones espacio-temporales en la localización de fuentes de gas bajo flujos estocásticos

Guillermo Benito-Calviño[1], Ahmed Boubrima[1], Alessandro Renzaglia[1] and Hervé Rivano[1]
[1]Inria, INSA Lyon, CITI, UR3720, Villeurbanne, France

La localización de fuentes de gas a partir de detecciones locales constituye un problema inverso de transporte estocástico cuya dificultad emerge de la intermitencia y correlación de los eventos de detección. Diversos trabajos han abordado este problema mediante modelos probabilistas de dispersión y medidas locales, siendo *Vergassola* [1] uno de los enfoques paradigmáticos. Sin embargo, gran parte de estos trabajos asumen observaciones independientes, ignorando las correlaciones espaciales inducidas por la dinámica del flujo. En este trabajo caracterizamos dichas correlaciones para observables binarios de detección simultáneos y estudiamos cómo incorporarlas en la inferencia de la posición de una fuente emisora.

Modelamos el campo de velocidades del flujo, asociado al viento, mediante un proceso de Ornstein–Uhlenbeck espacialmente uniforme,

$$\dot{\mathbf{w}}(t) = -a\,(\mathbf{w}(t) - \bar{\mathbf{w}}) + \sqrt{G}\,\boldsymbol{\eta}(t), \tag{1}$$

donde $\bar{\mathbf{w}}$ representa la velocidad media del viento, a^{-1} el tiempo característico de correlación y G la amplitud de las fluctuaciones. Este modelo introduce un tiempo de memoria finito en la dinámica, $\langle \mathbf{w}(t)\cdot\mathbf{w}(t+\tau)\rangle \sim e^{-a\tau}$, que constituye el principal mecanismo generador de correlaciones espaciales en las realizaciones de las plumas.

La propagación de partículas de gas se describe mediante el proceso advectivo-difusivo

$$\dot{\mathbf{p}}(t) = l\,\mathbf{w}(t) + \sqrt{2D}\,\boldsymbol{\xi}(t), \tag{2}$$

donde l cuantifica la transferencia de momento con el flujo y D representa la difusión efectiva local. La distribución de probabilidad $P_1(\mathbf{r},t)$ de encontrar una partícula en la posición $\mathbf{r}$ al tiempo t posterior a su emisión resulta gaussiana, con media $\boldsymbol{\mu}(t)$ y matriz de covarianza $\boldsymbol{\Sigma}(t)$ diagonal cuyos elementos vienen dados por

$$\boldsymbol{\mu}(t) = l\,\bar{\mathbf{w}}\,t + \mathbf{p}_0, \quad \Sigma_{ii}(t) = \frac{l^2 G}{a^3}(at - 1 + e^{-at}) + 2Dt. \tag{3}$$

La memoria temporal del viento induce además correlaciones entre trayectorias emitidas en instantes distintos. En consecuencia, la distribución conjunta de dos partículas $P_2(\mathbf{r}_1,\mathbf{r}_2;t_1,t_2)$, también gaussiana, presenta bloques cruzados no nulos en su matriz de covarianza,

$$\Sigma^{12}_{ii} = \frac{l^2 G}{2a}\left(2a\tau - 1 + e^{-a\tau} + e^{-a\Delta} + e^{-a(\Delta+\tau)}\right), \tag{4}$$

donde $\tau = \max(t_1,t_2)$, $\Delta = |t_1 - t_2|$, y el índice i recorre las coordenadas espaciales.

Para una fuente continua con tasa de emisión Q, aproximamos la concentración local de gas $C(\mathbf{r})$ mediante una distribución gamma. La concentración media se obtiene integrando la distribución unipartícula sobre el histórico de emisión, $\langle C(\mathbf{r})\rangle = \int_0^\infty Q P_1(\mathbf{r},t)\,dt$, mientras que la covarianza espacial entre la concentración en dos posiciones $\mathbf{r}_1$ y $\mathbf{r}_2$ se puede calcular gracias a P_2,

$$\mathrm{Cov}\big(C(\mathbf{r}_1),C(\mathbf{r}_2)\big) = \int_0^\infty\!\!\int_0^\infty Q^2 P_2(\mathbf{r}_1,\mathbf{r}_2;t_1,t_2)\,dt_1\,dt_2 - \langle C(\mathbf{r}_1)\rangle\langle C(\mathbf{r}_2)\rangle. \tag{5}$$

A partir de un umbral de concentración local, definimos observables binarios de detección $b_i \in \{0,1\}$. La probabilidad marginal de detección corresponde a la cola superior de la distribución gamma de la concentración. Utilizando estas estadísticas marginales, construimos la distribución conjunta de detección mediante una cópula gaussiana, cuya estructura correlacional viene determinada por la covarianza de la concentración (Ec. (5)).

En la Fig. 1 se compara la distribución conjunta de detección con la aproximación de independencia, mostrando la relevancia de las correlaciones espaciales para describir adecuadamente la estadística de los eventos de detección.

Finalmente, la distribución conjunta de detección se utiliza como verosimilitud en un esquema bayesiano de inferencia, explotando la estructura correlacional inducida por la dinámica del flujo en la estimación de la posición de la fuente emisora.

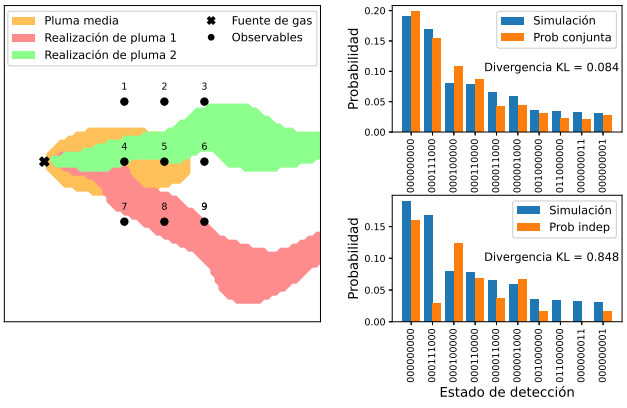

Fig. 1: **Izquierda:** Región del espacio donde la concentración de gas supera el umbral de detección, mostrada para el campo medio y dos realizaciones estocásticas con mismos parámetros. **Derecha:** Comparación entre la distribución conjunta de detección y la aproximación de independencia, utilizando como referencia simulaciones del modelo. En el eje x se representan los macroestados de detección más probables, definidos por el vector de respuestas binarias en cada punto de observación.

[1] M. Vergassola, E. Villermaux, and B. I. Shraiman, *Infotaxis as a strategy for searching without gradients*, Nature **445**, 406–409 (2007).

Rethinking Market Indicators with Network Science and Blockchain Data

M. Grande[1,5], S. Gómez[2], F. Borondo[3] and J. Borondo[4,5]
[1]Grupo de Sistemas Complejos, Universidad Politécnica de Madrid, Madrid, Spain
[2]Universitat Rovira i Virgili, Avinguda Països Catalans 26, 43007, Tarragona, Spain
[3]Departamento de Química, Universidad Autónoma de Madrid, Cantoblanco, 28049, Madrid, Spain
[4]Departamento de Gestión Empresarial, Universidad Pontificia de Comillas ICADE, Madrid, Spain
[5]AGrowingData, Almería, Spain

Cryptocurrencies and Decentralized Finance (DeFi) currently represent a fast-growing trend in finance, which enables financial services on public blockchains. In contrast to traditional financial markets, ruled by well-established corporations, DeFi is transparent, as it keeps publicly available records of all transactions that occur on the network. This availability of the data represents an opportunity to analyze and understand the market from the point of view of the complexity that emerges from the interactions among actors (users, bots, and companies) operating in the embedded market.

In this work [1], we focus on Ethereum, to show that the underlying transaction network bears further and useful information to forecast the evolution of the market. We aim to separate the non-redundant effects of the blockchain transaction network from technical analysis and social media trends in the future price of Ethereum. To this end, we build two machine learning models to predict the future trend of the market. The first model, serving as a baseline, considers the set of most relevant features according to the current scientific literature—including technical analysis and social media trends. The second model considers the features of the base model, but incorporates the network properties computed from the transaction network.

We find that the second model outperforms the baseline and can anticipate 46% more rises in the price and 19% more falls. Thus, we conclude that new indicators based on network properties provide valuable information to forecast the future direction of the market that cannot be explained either by technical analysis or social media trends alone. Hence, our results represent an important first step towards the definition of a new family of DeFi market indicators based on the complexity of the underlying transaction network.

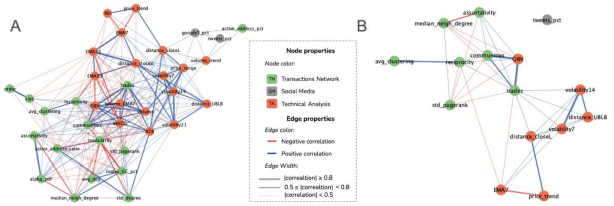

Fig. 1: Panel A shows the network resulting from the correlation between all features considered in our study. Only significant correlations, i.e., p-value < 0.05, have been included; the width of links is proportional to the absolute value of the correlation coefficient and the sign is color-coded (blue for positive values and red for negative ones). Panel B shows a filtered version of the network, only including the features selected by the FM.

[1] Grande, M., Gómez, S., Borondo, F. & Borondo, J. (2026). *Towards a New Generation of Market Indicators Driven by Blockchain Transaction Networks.* Chaos: An Interdisciplinary Journal of Nonlinear Science, 36(5).

Spatial Organization of Adhesion-Deficient Cells Modulates Mechanical Rigidity and Topological Dynamics in Epithelial Tissues

Natalia Briñas-Pascual[1], Víctor Manso[2], and Pilar Guerrero[1]
[1]Universidad Carlos III de Madrid, Departamento de Matemáticas, Grupo Interdisciplinar de Sistemas Complejos (GISC), Leganés, 28911, Madrid, Spain
[2]ProCURE, Catalan Institute of Oncology, Oncobell, Bellvitge Institute for Biomedical Research (IDIBELL), Campus de Bellaterra, 08908, L'Hospitalet del Llobregat, Barcelona, Spain

Epithelial tissues maintain their mechanical integrity through a delicate non-equilibrium balance between cell-cell adhesion and cortical contractility. While the disruption of adhesion-mediated junctions is widely recognized as a driver of epithelial-mesenchymal transition (EMT) and cancer progression [1], the physical mechanisms governing how local defects propagate to tissue-scale mechanical changes remain poorly understood.

Here, using a two-dimensional vertex model of active disordered networks [2], we demonstrate that the spatial arrangement of adhesion-deficient cells acts as an independent structural control variable that fundamentally alters the kinetics of cell removal and regulates the global and local mechanics of active cellular network. For identical fractions of adhesion-deficient cells, we uncover two divergent dynamical regimes governing the rate at which defective cells are eliminated via topological T_2 transitions. Randomly distributed mutants act as isolated defects that undergo rapid, uncorrelated removal, producing only short-lived shape-index fluctuations. Conversely, clustered mutants exhibit a significantly retarded, non-linear extrusion rate. Due to a reduced heterotypic interface density at the core, interior cells are physically shielded, delaying elimination and sustaining elevated shape-index signatures close to the rigid-to-fluid unjamming threshold ($p^* \approx 3.81$) [3]. Spatial aggregation thus acts as a structural amplifier, triggering localised unjamming transitions at lower mutant fractions than random distributions require (Fig 1).

Furthermore, we explicitly separate these geometric signals at local and global scales. We show that the initial mutant-neighbourhood cells experience severe shape-index elevations that precede any global network response. This local scale acts as an early topological indicator of mechanical instability driven by boundary-propagated T_1 and T_2 cascades, which is entirely quenched in random configurations. Remarkably, our analysis reveals that the coordinated removal of adjacent cells within a cluster leaves behind a permanent topological imprint. While random configurations are topologically reversible, clustered configurations freeze the network into a highly disordered state where topological defects endure long after full mutant clearance. This work provides a physical framework linking local adhesion defects to tissue-scale mechanics, identifying spatial organisation as a key determinant of epithelial behaviour.

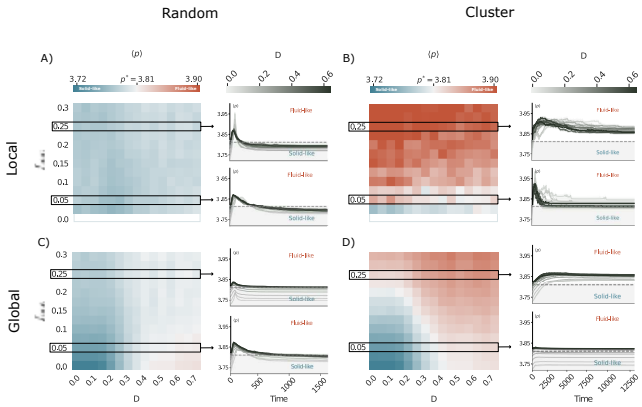

Fig. 1: Random configurations generate mostly transient shape-index deviations; clustered mutants produce systematically larger and more persistent elevations, particularly at the local scale, suggesting that shape-index perturbations originate at the cluster boundary and may extend to the tissue scale as the system ap proaches p^*.

[1] Soraia Melo et al., *The ECM and tissue architecture are major determinants of early invasion mediated by E-cadherin dysfunction*, Communications Biology 6, 1132 (2023). Doi: 10.1038/s42003-023-05482-x.

[2] Reza Farhadifar et al., *The Influence of Cell Mechanics, Cell-Cell Interactions, and Proliferation on Epithelial Packing*, Current Biology 17 (2007). Doi: 10.1016/j.cub.2007.11.049.

[3] Dapeng Bi et al., *A density-independent glass transition in biological tissues*, Nature Physics 11 (2014), Doi: 10.1038/nphys3471.

Biodiversity–ecosystem functioning relationships as spectra of aggregated interactions

Giulio Burgio, Alvaro Sanchez
Instituto de Biología Functional y Genómica (IBFG), CSIC-Universidad de Salamanca

Three decades of theory and experiment have established that biodiversity—the variety of life from genes to species—shapes key ecological processes such as productivity and nutrient cycling, and the stability of ecosystems [1]. Manipulations of species richness (number of species), especially in grassland and microbial systems, consistently find that biodiversity promotes functioning, yielding increasing and typically *saturating* biodiversity–ecosystem functioning (BEF) relationships [2]. Functioning arises from individual contributions as well as from pairwise and higher-order interactions among species, yet how BEF relationships emerge from them remain largely unexplored.

We approach this question through the concept of a composition-function map: an assignment of a collective function F (e.g., biomass, metabolic output) to each of the communities that can be assembled from a pool of N species [3]. Such a map is a scalar field on the Boolean hypercube $\{0,1\}^N$—a functional landscape—whose Fourier spectrum quantifies the interactions in the system: the Fourier coefficient ε_S associated to the species subset S of size $|S|=k$, is the average (k-th order) interaction among the species in S across all 2^{N-k} background communities to which these species can be added to [4]. The BEF relationship, $B(n)$, is the component of the map F that is invariant under species permutations, depending only on richness n.

The sprectral decomposition allows to express any BEF relationship as a unique combination of Kravchuk polynomials $\{K_k(n)\}_{k=0,\dots,N}$:

$$B(n) = \sum_{k=0}^{N} \binom{N}{k} (-2)^{-k} \varepsilon_k K_k(n), \qquad (1)$$

where $\varepsilon_k = \langle \varepsilon_S \rangle_{|S|=k}$ is what we term *aggregated interaction of order k*, namely the average of all k-th order average interactions [Fig. 1(a)]. Equation (1) provides an exact one-to-one correspondence that allows to derive the spectrum of aggregated interactions from a BEF relationship, and viceversa. We leverage it in various ways.

First, each ε_k is a double average—over background communities and over species subsets—so unless a mechanism enforcing sign coherence at order k is present, ε_k self-averages towards zero. Consistent with empirical observations, reporting only a very limited range of shapes (nearly-linear, saturating, or single-humped curves), $B(n)$ is thus expected to be a low-degree polynomial in n. Second, being invertible, Equation (1) turns into a falsifiable inference: a curve requiring degree ≥ 3 evidences sign-consistent—thus potentially detectable—higher-order interactions.

We perform Bayesian inference of Eq. (1) on several experimental landscapes, taking the total grown microbial biomass as the collective function. The landscapes are generated by growing every of the 31 combinations of 5 species in each of the 31 combinations of 5 carbon sources (replicated 4 times). In this way, we get 31 landscapes over species combinations, from which we measure (resources-mediated) species-species interactions, but also 31 landscapes over resources combinations, from which we extract (species-mediated) resource-resource interactions. We find that the effective degree d^* of $B(n)$, defined as the largest order k needed to explain most (99%) of the variance of $B(n)$, is generally low, yet its variation is structured [Fig. 1(b)]: assembling species produces systematically higher-order structure than assembling resources (median: $d^*=3$ vs. 1). Resource mixtures turn out to be near-additive, species mixtures show instead more complex patterns. Besides, the fraction of the variance of the full map F explained by richness alone is high for both (median: $R^2 \approx 0.5$) [Fig. 1(c)], confirming—at least for biomass—richness as an informative latent variable.

The framework requires only that a landscape can be defined, and so applies to any system—ecological or otherwise—in which a function is measured over combinations of components.

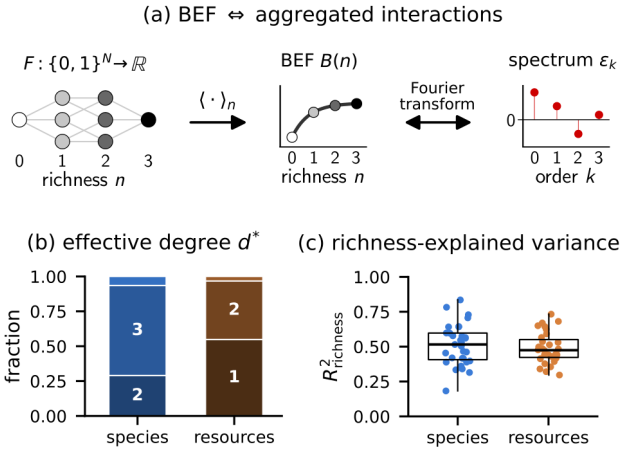

Fig. 1: (a) A composition-function map F on the hypercube projects, by averaging over richness, onto the BEF relationship $B(n)$; the projection is an exact Kravchuk transform of the aggregated-interaction spectrum $\{\varepsilon_k\}$, Eq. (1). (b) Effective degree d^* of $B(n)$ and (c) variance of F explained by richness over 62 experimental microbial landscapes, half of them assembled from species combinations and half from resources combinations, with F being total grown biomass.

[1] B. J. Cardinale *et al.*, Nature **486**, 59 (2012).
[2] D. Tilman *et al.*, Science **277**, 1300 (1997).
[3] A. Sánchez *et al.*, Mol. Microbiol. **122**, 3 (2024): 294-303
[4] R. A. Neher, B. I. Shraiman, Rev. Mod. Phys. **83**, 1283 (2011).

Unified Optimization Mechanism in Stochastic Resetting and Dynamic Redundancy

Daniel Campos, Javier Cristín, and Vicenç Méndez
Grup de Física Estadística, Departament de Física. Universitat Autònoma de Barcelona, 08193 Bellaterra (Barcelona), Spain

The First-Passage time T represents a universal and widespread magnitude to quantify the capacity of stochastic processes to explore their phase space. The probability distribution of T (or simply its average, the Mean First-Passage Time) provides practical information about how easily particular regions of that space can be reached/visited.

The extension of this idea to contexts where exploration is driven by multiple walkers or searchers, however, is not straighforward. First-passage time is still used as a significant measure of exploration efficiency in the context of N searchers simultaneously exploring a domain [1–4]. However, a different perspective is necessary if *efficiency* is to be understood in terms of the energetic costs and/or the resources deployed during such an exploration. Consider, for instance, a set of virtual bots exploring the nodes of the Internet for a particular item/information, or a social group of animals foraging for food through their habitat. For these and many other situations, search efficiency can be rather reformulated in terms of the Time Collective Cost [5] $T_C \equiv \int_0^T N(t)dt$, where $N(t)$ represents the number of active searchers at time t, so assuming then that this number can vary with time.

Consider for instance a situation in which *iid* Brownian trajectories (with diffusion coefficient D) emerge at random times $\{\tau_1, \tau_2, ...\}$ from the origin, trying to reach a *target* located at a distance r_0 from the origin. New trajectories are launched at a constant rate γ_b, so intermediate times $\{\tau_i - \tau_{i-1}\}$ are exponentially distributed. Likewise, each trajectory will be terminated at rate γ_d, so γ_d^{-1} represents the mean duration of trajectories.

Minimization of the first-passage time through the target can be accomplished in the limit $r_b \to \infty$, $r_d \to 0$ (so launching more and more trajectories to enhance detection probabilities), but this situation is not optimal if explicit costs of each trajectory are to be computed. At practice, minimization of the Collective Cost $\langle T_C \rangle$, involves nontrivial combinations of r_b and r_d. This has been termed as the 'dynamic redundancy' problem [5].

Surprisingly, when we explore numerically (through random-walk simulations) the average values of $\langle T_C \rangle$ for a large region of γ_b and γ_d values, we observe that the collective time cost gets minimized for a very broad range of combinations of these parameters. To understand this result, we will see how to exploit formal analogies between the dynamic redundancy problem and stochastic resetting to determine the optimal rates which minimizes the mean collective cost. Our results confirm the existence of a common optimization mechanism in stochastic resetting and dynamic redundancy. As we will argue, optimization in both cases is controlled by the value of the mean residual lifetime of the process without restart.

[1] G. H. Weiss, K. E. Shuler, and K. Lindenberg, Journal of Statistical Physics 31, 255 (1983).
[2] S. B. Yuste and K. Lindenberg, Journal of Statistical Physics 85, 501 (1996).
[3] S. D. Lawley, Physical Review E 102, 062118 (2020)
[4] J. B. Madrid and S. D. Lawley, Journal of Physics A: Mathematical and General 53, 335002 (2020).
[5] D. Campos and V. Méndez, Phys. Rev. E 109, 064109 (2024)

Ligand binding in crowded polymers

Juan Pedro García-Villaluenga[1] and Francisco Javier Cao-García[1,2],
[1]Universidad Complutense de Madrid, Madrid, Spain.
[2]IMDEA Nanociencia, Madrid, Spain.

Ligands change or modulate the physical and chemical properties of the bounded polymers. Ligand binding depends on the availability of the required binding sites. This feature greatly conditions the binding kinetics and the final coverage. The binding possibilities were computed generalizing the Mc Ghee – von Hippel counting methods [1, 2]. This procedure was shown to provide a result equivalent to the Tonks gas model [3] at equilibrium, and was applied also to derive the ligand coverage kinetics. The results show that ligand binding to multiple sites do not usually fully cover the polymer. Because the random binding leaves gapes that are too short for a new ligand binding. The ligands can bind non-cooperatively [4], where binding of the individual ligands is independent; or can bind cooperatively [5], where binding of a ligand to the neighboring is energetically favorable, leading to a more ordered ligand binding. Additionally, competitive ligand binding has illustrated the interactions between ligands of different sizes [6]. Competitive binding results show that small ligands have a strong impact in the inhibition of large ligand binding. Ligand binding size is revealed to a have a leading order compared to affinity. Ligand binding competition provides a key insight in a leading mechanisms that inhibits or enhances the presence of a ligand bound to a polymer, determining the ligand modulation of the physical and chemical properties of the polymer.

[1] J.D. McGhee, and P. H. von Hippel, *Theoretical aspects of DNA-protein interactions: co-operative and non-co-operative binding of large ligands to a one-dimensional homogeneous lattice.*, Journal of molecular biology 2, 469–89 (1974). https://doi.org/10.1016/0022-2836(74)90031-x

[2] J.D. McGhee, and P. H. von Hippel, *Erratum. Theoretical aspects of DNA-protein interactions: co-operative and non-co-operative binding of large ligands to a one-dimensional homogeneous lattice.*, Journal of molecular biology 3, 679 (1976). https://doi.org/10.1016/0022-2836(76)90228-X

[3] L. Tonks, *The Complete Equation of State of One, Two and Three-Dimensional Gases of Hard Elastic Spheres*, Phys. Rev. 10, 955-963 (1936). https://doi.org/10.1103/PhysRev.50.955

[4] J.P.G. Villaluenga, J. Vidal, and F. J. Cao-García, *Noncooperative thermodynamics and kinetic models of ligand binding to polymers: Connecting McGhee–von Hippel model with the Tonks gas model*, Physical Review E 102, 012407 (2020). https://doi.org/10.1103/PhysRevE.102.012407

[5] J. P. G. Villaluenga, and F. J. Cao-García, *Cooperative kinetics of ligand binding to linear polymers*, Computational and Structural Biotechnology Journal 20, 521–533 (2022). https://doi.org/10.1016/j.csbj.2021.12.043

[6] J. P. G. Villaluenga, D. Brunete, and F. J. Cao-García, *Competitive ligand binding kinetics to linear polymers*, Physical Review E 107, 024401 (2023). https://doi.org/10.1103/PhysRevE.107.024401

Social networks in online speech communities: An empirical analysis in the United Kingdom

David M. Carpio[1], José J. Ramasco[1], and David Sánchez[1]
[1]Institute for Cross-Disciplinary Physics and Complex Systems IFISC (UIB-CSIC), Campus Universitat de les Illes Balears, E-07122, Palma, Spain

Understanding how social interactions shape language use is a central problem in sociolinguistics, as everyday exchanges are the primary mechanism through which linguistic variants are transformed, transmitted, and reinforced [1]. Online social media provide an unprecedented opportunity to explore this question, as they generate vast amounts of data on users' interactions [2] and the linguistic content they produce [3]. In this work, we investigate how social interactions within online communities mediate both the languages employed and the prevalence of non-standard linguistic forms.

In particular, we analyze an extensive dataset of more than 500 million geolocated Tweets from the United Kingdom, collected between January 2015 and February 2021. From a complex systems perspective, we model interactions through replies and construct a directed, weighted network comprising over one million users, each assigned to a residence cell within the country. We then characterize the linguistic features of user-generated content and detect community structures within the network.

Regarding the languages employed, we found several communities where a minority language becomes dominant (as shown in Figure 1a). In particular, we identify communities exhibiting a strong social identity, where most members share the same minority language as their primary language (e.g., Figure 1b). In these communities, the use of the minority language is reinforced, with the vast majority of interactions occurring in that language. Other communities exhibit adaptive linguistic behavior, with individuals shifting from their primary language to a minority language when interacting within the community (e.g., Figure 1c).

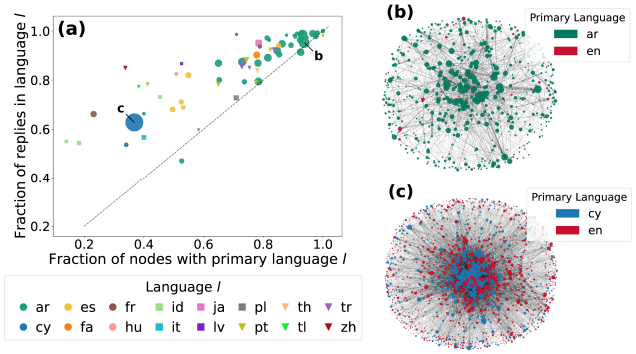

Fig. 1: (a) Communities with a dominant language other than English and containing at least 30 nodes. Each marker represents a distinct community, and the marker size is proportional to the community's size. Network visualizations of (b) a community predominantly composed of Arabic primary speakers (denoted by **ar** in green) and (c) a community characterized by the coexistence of Welsh primary speakers (denoted by **cy** in blue) and English primary speakers (denoted by **en** in red).

In the case of English, which is used by the vast majority of communities, we investigate how the use of non-standard features relates to the communities to which users belong. We quantify these features using two complementary measures: one based on the overall tweets generated by community members and another based on the replies exchanged within the community.

For the overall content, we compute the average frequency of non-standard features among the members of each community k, F_k^{nodes}. We compare the empirical results with a null model that preserves the size distribution of communities while randomizing their composition. We find a considerable number of communities exhibiting both lower and higher values of F_k^{nodes} than expected under the null model (Figure 2a). This finding suggests homophily, as users with similar linguistic behavior tend to cluster together.

Finally, we compute the frequency of non-standard features in all English replies exchanged within a community k, F_k^{replies}. We observe that communities whose members frequently employ non-standard features tend to amplify such practices through internal interactions, as evidenced by the strong correlation and the regression slope greater than one shown in Figure 2b. This process illustrates how social reinforcement within online communities contributes to the persistence and diffusion of linguistic variation.

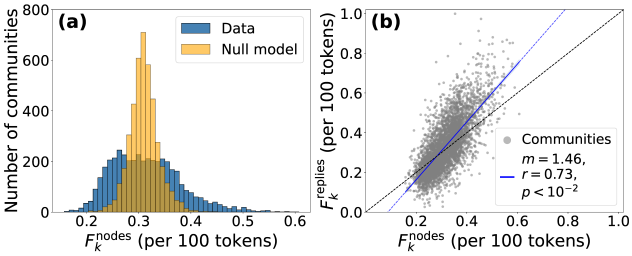

Fig. 2: (a) Comparison between the distribution of the average frequency of non-standard features in members' tweets, F_k^{nodes}, for the communities identified in the reply network (blue) and for the randomized null model (orange). (b) Correlation between the frequency of non-standard features in replies, F_k^{replies}, and F_k^{nodes}. Each point represents a community.

[1] J. Milroy and L. Milroy, *Linguistic change, social network and speaker innovation*, J. Linguistics **21**, 339–384 (1985)

[2] P. A. Grabowicz, J. J. Ramasco, E. Moro, J. M. Pujol, and V. M. Eguíluz, *Social features of online networks: The strength of intermediary ties in online social media*, PLoS ONE **7**, e29358 (2012)

[3] T. Louf, J. J. Ramasco, D. Sánchez, and M. Karsai, *When dialects collide: how socioeconomic mixing affects language use*, EPJ Data Sci. **14**, 47 (2025)

Lifetime patterns of reinfections: epidemic cohorts as traveling waves

Piergiorgio Castioni[1], Chiara Poletto[2], and Alex Arenas[1]
[1]DEIM, Universitat Rovira i Virgili, Tarragona, Spain
[2]Dipartimento di Medicina Molecolare, University of Padova, Padova, Italy

Infectious disease models that allow for reinfections, such as SIS or SIRS frameworks, often treat all infections as identical, neglecting the temporal structure of individual reinfection histories. This simplification obscures how immune memory evolves and influences epidemic dynamics. To address this limitation, we introduce a minimal "chain-SIR" model that explicitly tracks infection cohorts through successive SIR compartments, each representing individuals with a distinct number of past infections. Formally, the model reads

$$\begin{aligned} \dot{I}_i &= \lambda_{i-1} S_{i-1} - \gamma_i I_i - \mu_i I_i, \\ \dot{R}_i &= \gamma_i I_i - \delta_i R_i - \mu_i R_i, \\ \dot{S}_i &= \delta_i R_i - \lambda_i S_i - \mu_i S_i, \end{aligned} \tag{1}$$

where the letters S_i, I_i and R_i indicate susceptible, infected and recovered individuals with i cumulative reinfections (see Fig. 1). In this formulation, key epidemiological parameters β_i, γ_i, δ_i, and μ_i—transmission, recovery, immunity waning, and mortality rates, respectively—may vary with reinfection count i, enabling a more mechanistic link between infection history and population-level outcomes.

A rigorous coarse-graining of this model leads to an advection equation of the form

$$\frac{\partial N(x,t)}{\partial t} = -\frac{\partial}{\partial x}\left(\sigma(x) N(x,t)\right) - \mu(x) N(x,t), \tag{2}$$

where $N(x,t)$ indicates the fraction of people with x reinfections at time t, while $\sigma(x)$ and $\mu(x)$ are the reinfection and mortality rates, respectively.

Analysis of the system reveals that infection cohorts propagate as traveling waves in reinfection-count space, forming a structured ladder of successive exposures (see Fig. 1). This wave-like behavior enables us to derive several analytical results, including the stationary distribution of lifetime reinfections, the age-dependent reinfection rate, and the incidence risk ratio (IRR) across age groups.

We use these insights to fit real-world reinfection patterns derived from longitudinal cohort studies [1, 2]. For example, we find that the reinfection profile for a wide range of respiratory pathogens—including influenza A and B, respiratory syncytial virus (RSV), rhinovirus (RV), and human metapneumovirus (HMPV)— aligns closely with the prediction obtained using a reinfection rate $\sigma(x)$ that decreases exponentially with the number of prior infections. From this, we also able to quantify how much each new exposure reduces the infection risk for each of those virus.

Our approach provides a new physics-inspired framework for quantifying reinfection dynamics and immune-history effects, by mapping a complex epidemiological model to a simple advection equation. This work thus establishes a foundation for more accurate modeling of diseases characterized by partial and waning immunity.

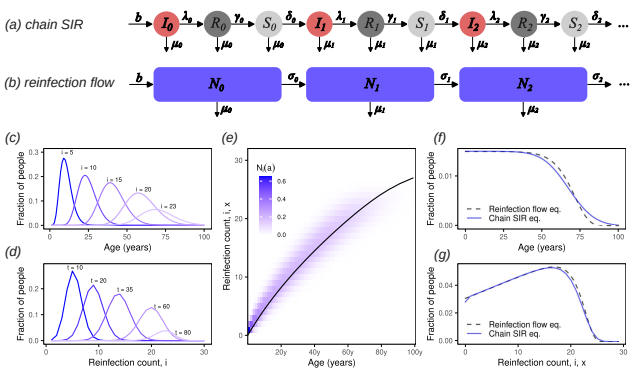

Fig. 1: **Overview of the chain SIR model.** In (a) and (b) we show diagrams of the chain SIR and its coarse-grained version. Here, $N_i = S_i + I_i + R_i$. Figure (c) describes the behavior of a single cohort, meaning the dynamic of the the coarse-grained model when initialized as $N_i(0) = \delta_{i0}$. The wave-like behavior of the system, together with its non-conservative nature due to the death rate μ_i, is even more apparent if we take snapshots at certain reinfection numbers (d) or at certain times (e). Finally, (f) and (g) portray the stationary distribution of the model in the age and reinfection domains, respectively (here the word "age" is used to refer to the time passed since the cohort was born). The black dashed line is the analytical expression derived from the PDE version of the model, while the solid red line was obtained by summing up all the cohorts for every number of reinfections i and age t, respectively.

[1] Hay, James A. et al., *Reconstructed influenza A/H3N2 infection histories reveal variation in incidence and antibody dynamics over the life course*, PLOS Biology **22**, 1545-7885, 2024.

[2] Monto, Arnold S. et al., *Respiratory Viral Infections From 2015 to 2022 in the HIVE Cohort of American Households: Incidence, Illness Characteristics, and Seasonality*, The Journal of Infectious Diseases **231**, 2025.

Modeling Polymeric Mixed Micelles via Coarse-Grained Single-Chain Mean Field Theory

Luis E. Castro-Anaya, and Allan D. Mackie
Departament d'Enginyeria Química, Universitat Rovira i Virgili, Avinguda dels Països Catalans, 26, 43007 Tarragona

Aqueous solutions of amphiphilic block copolymers exhibit rich phase behavior, notably self-assembling into spherical nanostructures called micelles above the critical micelle concentration (CMC). Understanding the thermodynamic stability and structure of these micelles is of significant interest for drug encapsulation and delivery applications [1]. In this contribution, we investigate the equilibrium properties of mixed micelles formed by binary mixtures of polyethylene oxide (PEO) and polypropylene oxide (PPO) block copolymers using Single-Chain Mean-Field (SCMF) theory [2] for binary systems with different total lengths and hydrophilic block lengths. Our SCMF scheme provides a self-consistent mean-field approximation for the configurational partition function, where intramolecular energies are computed explicitly and intermolecular interactions are modeled as interactions of every individual chain with fields. To achieve this, millions of self-avoiding chain configurations are randomly generated for each surfactant using the Rosenbluth algorithm $\{\alpha\}$, $\{\beta\}$, while concentric spherical fields are formulated inside a truncated octahedron box. A schematic diagram of a typical micelle structure is given in Fig. 1.

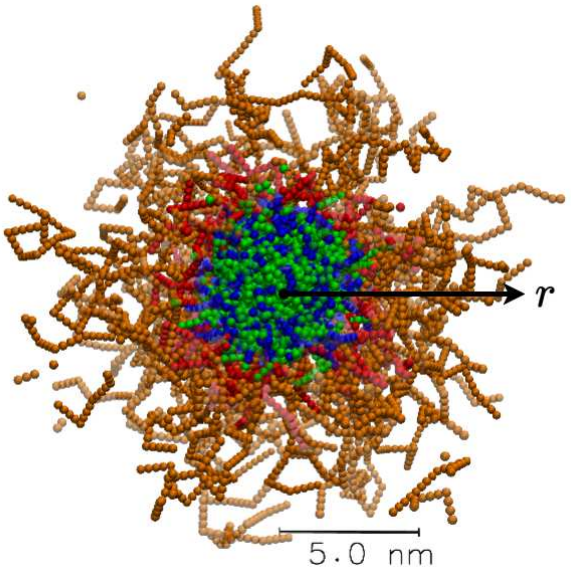

Fig. 1: Section of a micelle of the 200 most probable chain configurations for a 1:1 mixture of L64 and F87. Blue and green correspond to L64 and F87 PPO blocks. Red and orange to L64 and F87 PEO blocks.

The probabilities of each chain configuration in the system (Eq. 1), are calculated once the fields have converged. Water is treated as an implicit solvent under an incompressibility condition: all the space is occupied by solvent or polymer beads.

$$
\begin{aligned}
H[\alpha] &= U_{\text{intra}}(\alpha) + (N_A - 1) \\
&\cdot \varepsilon_{\text{EO,PO}} \int d\mathbf{r}\,(\Phi_{\text{EO}}(\alpha,\mathbf{r})\langle c_{\text{PO}}(\mathbf{r})\rangle + \Phi_{\text{PO}}(\alpha,\mathbf{r})\langle c_{\text{EO}}(\mathbf{r})\rangle) \\
&+ \varepsilon_{\text{EO},s} \int d\mathbf{r}\Phi_{\text{EO}}(\alpha,\mathbf{r}) c_{\text{s}}(\mathbf{r}) + \varepsilon_{\text{PO},s} \int d\mathbf{r}\Phi_{\text{PO}}(\alpha,\mathbf{r}) c_{\text{s}}(\mathbf{r}) \\
&+ k_{\text{B}}T \int d\mathbf{r} \left(\frac{\log \phi_{\text{s}}(\mathbf{r})}{v_{\text{s}}} \left[\phi_{\text{EO}}(\alpha,\mathbf{r}) + \phi_{\text{PO}}(\alpha,\mathbf{r})\right] \right)
\end{aligned}
\tag{1}
$$

By computing the standard chemical potentials of polymeric chains at varying total numbers of chains in the system (N_A, N_B) and coupling them with a mass action model, we estimate the CMC of the mixed systems. Our results reveal synergistic behavior in mixtures comprising polymeric chains with dissimilar hydrophilic block lengths (e.g., the L64-F87 mixture shown in Fig. 2). In contrast, near-ideal mixing is observed in systems with similar hydrophilic-to-hydrophobic proportions but different total chain lengths. These findings highlight the potential of using mixed copolymer systems to rationally tune and enhance micellar stability for targeted encapsulation purposes.

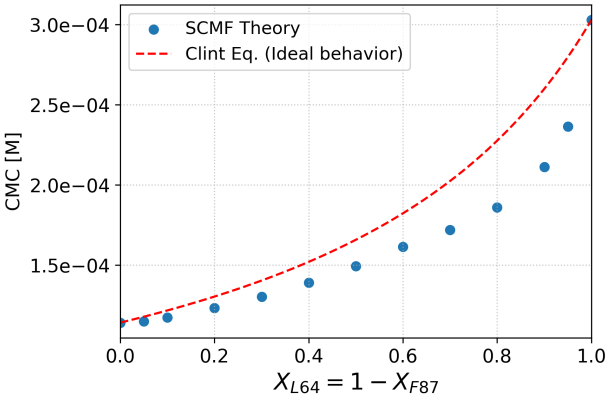

Fig. 2: Predicted CMC versus L64 mole fraction for L64 ($PEO_{13}PPO_{30}PEO_{13}$) and F87 ($PEO_{61}PPO_{40}PEO_{61}$).

[1] A. Naharros-Molinero, M. A. Caballo-González, F. J. de la Mata, and S. García-Gallego, *Direct and Reverse Pluronic Micelles: Design and Characterization of Promising Drug Delivery Nanosystems*, Pharmaceutics **14**, 2628 (2022).

[2] F. A. García Daza, A. J. Colville, and A. D. Mackie, *Mean-Field Coarse-Grained Model for Poly(ethylene oxide)-Poly(propylene oxide)-Poly(ethylene oxide) Triblock Copolymer Systems*, Langmuir **31**, 3596 (2015).

Information-Geometric Selection in T-Cell Receptor Cascades How Noise Shapes Ligand Discrimination

Juan Iribas de la Puerta[2] and Mario Castro[1,2],
[1]Instituto de Investigación Tecnológica (IIT), Universidad Pontificia Comillas, E28015, Madrid, Spain
[2]Grupo Interdisciplinar de Sistemas Complejos (GISC)

T cell recognition hinges on rapidly discriminating agonist from antagonist antigens in a noisy environment where target ligands are scarce. While kinetic proofreading explains how sequential phosphorylation improves specificity, a critical gap remains why do physiological T cell responses exhibit optimal activation at specific ligand dwell times and doses? We propose that the stochastic duration of T cell–APC encounters serves as a fundamental information-theoretic constraint. By treating the signaling cascade as a physical implementation of a Bayesian inference process, we show that discrimination is optimized when the encounter timescale matches the internal kinetics of the receptor's decision-making architecture.

We reformulate TCR signaling as a continuous inference process on a probability manifold defined by the cascade state distribution. The phosphorylation states evolve as a posterior distribution over ligand identity, updated by evidence accumulated from binding events.

Discrimination is governed by the interplay between three timescales; the ligand dwell time (τ), the limited signaling window ($1/\varphi$), and the stochastic encounter termination rate (μ). The mutual information $I(X;Y)$ between ligand identity X and the final signaling state Y exhibits an interior maximum at an optimal encounter rate μ. This explains why both extremely brief and excessively long contacts can degrade discrimination: brief contacts provide insufficient evidence, while long contacts allow the system to saturate or decay into non-signaling states.

The geometry of this inference process reveals fundamental differences between signaling architectures. In reversible cascades, the posterior distribution can fluctuate freely, leading to a stable but slower decision process. In contrast, architectures featuring an irreversible commitment step (absorbing states) create a "boundary collapse" in the information manifold. This mechanism forces the cell to commit to a decision, sharpening the discrimination between high-affinity agonists and low-affinity antagonists by preventing the accumulation of ambiguous evidence over time.

T cells do not merely count forward phosphorylation steps. Instead, the inference is multidimensional, incorporating information from both forward and backward transition rates. This explains why simple metrics like affinity (K_d) are often poor predictors of biological response: ligands with identical affinity but different kinetic signatures (the specific rates of phosphorylation and dephosphorylation) generate different information-geometric trajectories, leading to distinct cellular outcomes.

Our framework predicts a specific encounter rate that maximizes mutual information for a given receptor-ligand pair. For commitment-based architectures, this optimum occurs at shorter encounter durations compared to purely reversible ones. Furthermore, cascade architectures with an irreversible commitment state achieve higher peak mutual information, as the commitment state acts as a filter that locks in evidence, maximizing the divergence between agonist and antagonist signals.

This work connects stochastic contact dynamics to cellular information processing, revealing how evolution selects cascade architectures that optimize discrimination under time constraints. Our framework explains why physiological contact durations are conserved and provides a mathematical basis for predicting T cell responses to novel engineered receptors or therapeutic ligands.

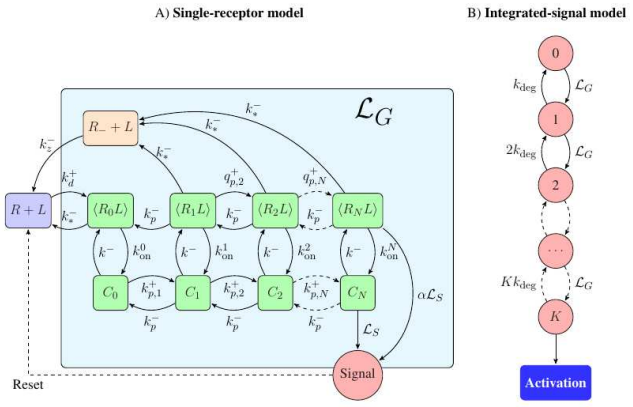

Fig. 1: Universal model of T-cell signalling.

[1] M. Lever, et al., "Phenotypic models of T cell activation", Nat. Rev. Immunol. 14, 619 (2014).
[2] J. Gálvez, et al., "Is TCR/pMHC affinity a good estimate of the T-cell response?" Front. Immunol. 10, 349 (2019).
[3] Morgan and Lindsay, "Modulation of antigen discrimination by duration of immune contacts", PLoS Comput. Biol. 19, e1011195 (2023).
[4] M. García-Sánchez, M. Castro, and J. Faro, (2023). B cell receptors and free antibodies have different antigen-binding kinetics. Proceedings of the National Academy of Sciences, 120(35), e2220669120.
[5] J. Faro, M. Castro, and C. Molina-París, C. (2017). A unifying mathematical framework for experimental TCR-pMHC kinetic constants. Scientific reports, 7(1), 46741.

Colloidal Monolayers: Compressible Hydrodynamics Breaks Fick's Law

M. Chamorro-Burgos[1] and A. Domínguez[1,2]
[1]Física Teórica, Universidad de Sevilla, Apdo. 1065, 41080 Sevilla, Spain
[2]Instituto Carlos I de Física Teórica y Computacional, 18071 Granada, Spain

Colloidal monolayers embedded in a bulk fluid exhibit long-ranged, effectively compressible hydrodynamic interactions (Fig. 1). Far from boundaries, these couplings lead to a breakdown of Fick's law beyond a characteristic length scale, producing anomalous, scale-dependent collective diffusion. This effect has been studied theoretically [1, 2] and observed experimentally [3], and can be described by a renormalized collective diffusivity

$$\frac{D^{(\mathrm{eff})}}{D} = 1 + \mathrm{Pe}, \tag{1}$$

where Pe is a scale-dependent Peclet number that diverges at large scales, and D is the single-particle diffusivity. So far, this anomalous diffusion has mainly been analyzed for monodisperse monolayers.

Here, we extend this framework to bidisperse monolayers composed of two particle species with different mobilities [4]. We show that interspecies hydrodynamic coupling strongly modifies collective transport and reveals a new regime when the two species are highly dissimilar. In this limit, the collective diffusivity of the large (slow) species is no longer determined solely by its own properties, but is instead renormalized by the diffusivity of the small (fast) species through hydrodynamic coupling.

This behavior is characterized by the scale-dependent Peclet numbers Pe_b and Pe_s of the big and small particles, leading to the modified anomalous-diffusion law

$$\frac{D_b^{(\mathrm{eff})}}{D_b} \approx 1 + \frac{\mathrm{Pe}_b}{1+\mathrm{Pe}_s}. \tag{2}$$

Figure 2 shows how the effective diffusion of the big particles depends on the scale-invariant ratio $\mathrm{Pe}_s/\mathrm{Pe}_b$, which is controlled by the diffusivities and concentrations of both species. Figure 3 summarizes the resulting dynamical regimes. In particular, the presence of small particles shifts the onset of diffusivity renormalization of the big particles to smaller length scales.

Our results identify a robust mechanism by which the transport of a slow component can be controlled indirectly by a fast one, despite the intrinsically non-Fickian character of the monolayer. They provide testable predictions for colloidal mixtures and membrane-like systems, and suggest strategies to tune multicomponent transport at soft interfaces by engineering hydrodynamic contrast.

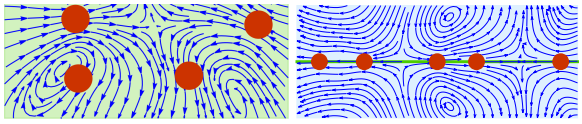

Fig. 1: Schematic of a monodisperse colloidal monolayer at a fluid interface. Left: effectively compressible in-plane flow. Right: incompressible embedding bulk fluid.

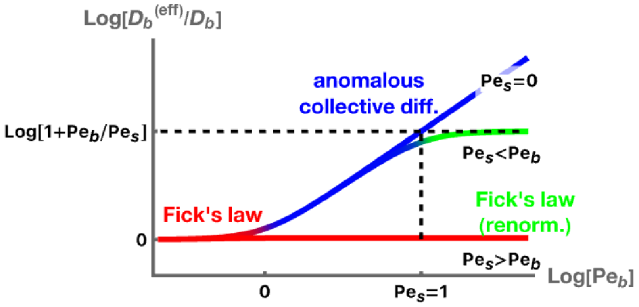

Fig. 2: Effective diffusivity of the big particles for three fixed values of $\mathrm{Pe}_s/\mathrm{Pe}_b$. As Pe_b increases, the system crosses over from Fickian to anomalous diffusion, or to a renormalized Fickian regime depending on the value of Pe_s.

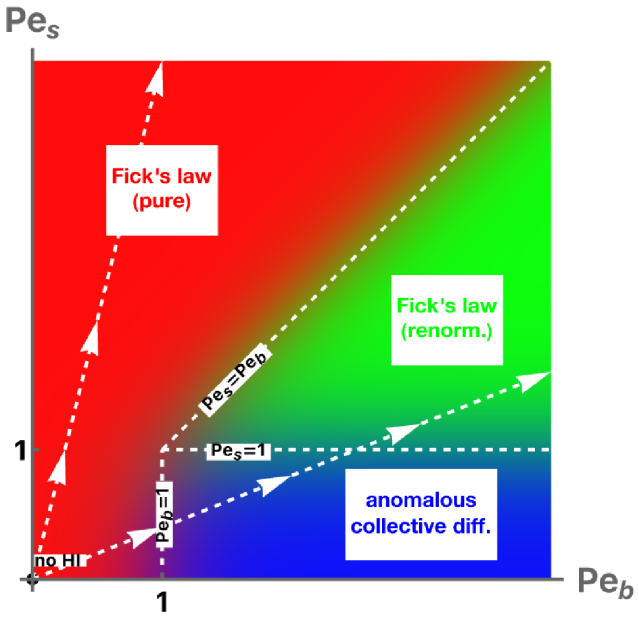

Fig. 3: Qualitative dynamical regimes of the big particles in the $(\mathrm{Pe}_b, \mathrm{Pe}_s)$ plane, showing the crossover between pure Fickian diffusion, anomalous collective diffusion, and a renormalized Fickian regime. The arrows indicate increasing length scale.

[1] J. Bleibel, A. Domínguez, F. Günther, J. Harting, M. Oettel, Soft Matter **10**, 2945 (2014).
[2] S. Panzuela, R. P. Peláez, R. Delgado-Buscalioni, Physical Review E **95**, 012602 (2017).
[3] B. Lin, B. Cui, X. Xu, R. Zangi, H. Diamant, S.A. Rice, Physical Review E **89**, 022303, (2014).
[4] M. Chamorro-Burgos, A. Domínguez, Physical Review E **113**, 055402 (2026).

Effect of size on transmission grid stability

Pere Colet[1], Kristóf Benedek[2,3], Geza Odor[2], and Damià Gomila[1]
[1]Instituto de Física Interdisciplinar y Sistemas Complejos, IFISC, CSIC-UIB, Palma, Spain
[2]Institute for Technical Physics and Materials Science, HUN-REN Centre for Energy Research, Budapest, Hungary
[3]Dpt. Theoretical Physics, Institute of Physics, Budapest University of Technology and Economics, Budapest, Hungary

Traditionally, large interconnected power systems with extensive synchronous zones have been assumed to provide higher reliability. In particular the Continental European Synchronous Area has been expanding along the years with recent additions being Ukraine in 2022 and the Baltic states in 2025.

However, large scale power flows such as those generated by high penetration of variable renewable energy sources, can put the stability of the European transmission grid at risk [2]. Furthermore, in large grids perturbations can propagate across the whole system following to the underlying topological connectivity. In particular, inter-area oscillations may arise as a consequence of the excitation of system's global modes triggered by a (local) perturbation [1]. Large grids formed by the addition of smaller (national) grids, such as the Continental European, are not specifically designed to maximize the damping of these modes. In extreme cases these modes can become unstable causing problems to system operations as it happen on the January 8, 2021 incident in which two parts of the European grid were separated [3]. Inter-area oscillations are associated to complex eigenvalues with small imaginary part. The undamping of these eigenvalues does not come through a Hopf bifurcation, rather they first become real (Belayakov-Devaney transition, BD). Once real, the two eigenvalues move apart very fast triggering a saddle-node (SN) bifurcation when one of them crosses zero. In parameter space SN and BD are very close, a similar scenario to that encountered for large scale power flows [2].

Here we analyze the dependence of grid stability on the the grid size, considering the imaginary part of the complex eigenvalues associated to the inter-area oscillations as indicator of how far in parameter space is the system from instabilities and using Continental European Synchronous Area (and parts of it) as a case study.

Acknowledgments: This work was suported by grant PID2024-157493NB-C22 financed by MCIN/AEI/10.13039/501100011033 (Agencia Estatal de Investigación, Spain) and FEDER (UE) and by María de Maeztu Program for units of Excellence in R&D, grant CEX2021-001164-M financed by MCIN/AEI/10.13039/501100011033 (Agencia Estatal de Investigación, Spain).

[1] Fritzsch, J., Jacquod, P. (2022). Long wavelength coherency in well connected electric power networks. *IEEE Access* 10: 19986. https://doi.org/10.1109/ACCESS.2022.3151687

[2] M. Martínez-Barbeito, D. Gomila, P. Colet, J. Fritzsch, P. Jacquod, *Transmission grid stability with large interregional power flows*, Phys. Rev. Res. **7**, 013137 (2025). https://doi.org/10.1103/PhysRevResearch.7.013137

[3] ENTSO-E. Final report on the separation of the Continental Europe power system on 8 January 2021. https://www.entsoe.eu/news/2021/07/15/final-report-on-the-separation-of-the-continental-europe-power-system-on-8-january-2021/

Thermodynamic Irreversibility and Abrupt Synchronization in Integrate-and-Fire Neural Population Model

Raúl Coterillo[1,2] and Miguel Aguilera[1,3]
[1] Basque Center for Applied Mathematics (BCAM), Bilbao, Spain
[2]University of the Basque Country (UPV/EHU), Bilbao, Spain
[3]Ikerbasque, Basque Foundation for Science

Understanding the nonequilibrium thermodynamics of large interacting systems remains a central challenge in statistical physics, with growing evidence that entropy production and temporal irreversibility are key signatures of neural function across cognitive states and disease [1]. While Markovian models have been extensively characterized through this lens [2], models containing refractory and synaptic integration effects remain largely unexplored.

In this work we propose a reinterpretation of the time-discrete, renewal approximation of the spike-response neural model [3] with uniform connectivity as a non-Markovian, kinetic spin model in which binary units $s_i \in \{0,1\}$ act as silent or firing neurons. Assuming an exponential-class integration kernel, the neuron potential is

$$u_{it} = \left(\alpha\left(J\sum_j s_{j,t-1} + I^{ext}_{t-1}\right) + (1-\delta(n))(1-\alpha)u_{i,t-1}\right) \tag{1}$$

where $n_i = t - \hat{t}_i \in \mathcal{N} \cup \{0\}$ is a "time since previous spike" counter, representing the number of timesteps since the last firing event $\hat{t}_i$ of each neuron. We solved the self-consistent dynamical mean-field equations describing the average firing rate using path-integral methods for a generating functional. Integration is described by age-structured population dynamics similar to the integral methods in [4], admitting closed-form fixed points and a tractable entropy production rate (EPR), our measure of thermodynamic irreversibility.

Since neurons with the same n_i are equivalent within the model due to the structure of (1), we can define an age-based potential u_{nt} and use the firing age distribution $p(n)$ as the state of our network. Assuming a noisy firing process yields a sigmoid $S(x)$ firing probability per age $\phi_t(n) = S(\beta h_{nt})$, $h_{nt} := u_{nt} - \theta$, where θ is the firing threshold and β a noise parameter, then $p(n)$ evolves as:

$$p_{t+1}(n) = \begin{cases} \sum_{n'}^{Q} p_t(n')\phi_t(n') & n = 0 \\ p_t(n-1)[1-\phi_t(n-1)] & 1 \le n < Q \\ \sum_{n'=Q-1}^{Q} p_t(n')(1-\phi_t(n')) & n = Q \end{cases} \tag{2}$$

where $m_t = p_t(n=0)$ is the activity of the network. Computing he EPR requires knowledge of the future state of the trajectory, which we encode in a "time until next spike" $n^\dagger$ variable obtained by projecting the future spikes into the current state. We project this variable into a joint distribution $p_t(n,n^\dagger)$ using survival statistics, allowing a population-average of instantaneous mean-field EPR σ:

$$\sigma_t = \sum_{n,n^\dagger} p(n,n^\dagger)\left(\phi_t(n)\beta(h_{nt} - h^\dagger_{n^\dagger t}) - \ln\frac{1+e^{\beta h_{nt}}}{1+e^{\beta h^\dagger_{n^\dagger t}}}\right) \tag{3}$$

where $h^\dagger_{n^\dagger t} := [u^\dagger_{n^\dagger t} - \theta]$ is the potential as in (1) of the reverse trajectory, integrating $u_{i,t+1}$ instead of $u_{i,t-1}$.

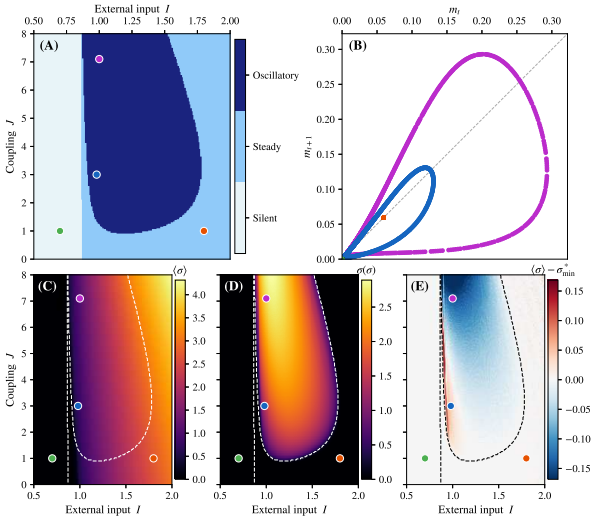

Fig. 1: **Phase diagram, return map, and EPR statistics.** **(A)** Phase diagram in the (I,J) parameter space, showing three dynamical regimes: silent (no activity), steady (constant firing rate), and oscillatory (rhythmic bursting). **(B)** Recursion plot selected parameter points. **(C-E)** EPR statistics across the phase diagram, with phase boundaries overlaid as dashed contours: mean $\langle\sigma\rangle$ *(C)*, standard deviation $\sigma(\sigma)$ *(D)*, and excess over the smallest fixed-point value $\langle\sigma\rangle - \sigma^*_{\min}$ *(E)*. We can observe an excess in EPR compared to random firing right in the phase boundary, right in the onset of synchrony from the steady random firing phase.

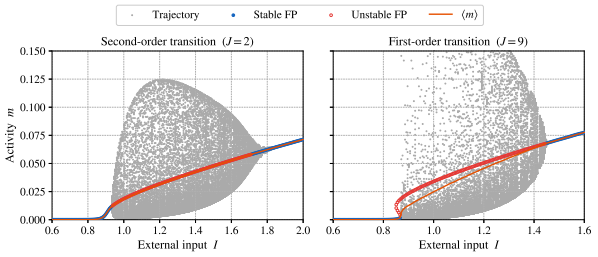

Fig. 2: **Continuous vs. abrupt synchronization.** Bifurcation diagrams for low $(J=2)$ and high $(J=10)$ synaptic coupling. Blue/red markers show stable/unstable fixed points; orange line is the simulated mean activity $\langle m\rangle$; dashed verticals bound the oscillatory region $(\sigma_m > \varepsilon)$. At low J the onset of collective firing is continuous, from steady activity to oscillations (second order); at high J the fixed point branch folds and the system jumps directly from silence to synchronization (first order).

[1] R. Nartallo-Kaluarachchi, M. L. Kringelbach, G. Deco, R. Lambiotte and A. Goriely, *Nonequilibrium physics of brain dynamics*, Physics Reports **1152**, 1 - 43 (2025)

[2] M. Aguilera, M. Igarashi and H. Shimazaki, *Nonequilibrium thermodynamics of the asymmetric Sherrington-Kirkpatrick model*, Nat. Comms. **14**, 3685 (2023)

[3] W. Gerstner *Time Structure of the Activity in Neural Network Models* Phys. Rev. E **1**, 738 (1995).

[4] W. Gerstner, W. M. Kistler, R. Naud and L. Paninski, *Neuronal Dynamics* (Cambridge University Press, 2014).

Information Propagation in Starling Flocks

Javier Cristín
Department of Physics, Autonomous University of Barcelona, Spain

Collective systems exhibit emergent transport phenomena in which local interactions give rise to propagating modes, from spin waves in magnetic systems to sound in fluids. Starling flocks provide a striking biological realization of this physics, as previous experiments have shown that collective turns propagate linearly across the group with negligible attenuation, indicating the presence of an underdamped sector in the dispersion relation [1]. Within the standard linear-response framework, however, propagating modes should also appear as so-called spin-wave peaks in the spectrum of spontaneous fluctuations.

Using new high-resolution experiments based on long-time stereoscopic tracking of natural flocks, we simultaneously analyze collective turns and spontaneous velocity fluctuations. While turning events display coherent wave-like propagation, the dynamical correlation function measured during straight flight exhibits a purely relaxational Lorentzian structure, with no evidence of propagating poles (so, without spin-waves). Experiments therefore reveal the coexistence of ballistic information transport and overdamped spontaneous fluctuations.

We show that this apparent contradiction cannot be resolved within the Inertial Spin Model (ISM) [2, 3], which constitutes the standard theoretical framework for flocks. We extend the ISM by introducing a quartic interaction term in the alignment dynamics, analogous to the anharmonic interaction of the Fermi–Pasta–Ulam–Tsingou (FPUT) model [4]. The resulting dynamics exhibit an amplitude-dependent crossover: spontaneous fluctuations remain overdamped, while sufficiently large perturbations dynamically activate an effective stiffness that supports underdamped propagation. Numerical simulations reproduce both the Lorentzian spontaneous correlations and the linear propagation observed experimentally during turns.

More broadly, these results provide an explicit example of amplitude-dependent transport in active matter and establish a direct connection between collective behaviour, nonlinear information propagation, and out-of-equilibrium statistical physics.

[1] A. Attanasi et al., "Information transfer and behavioural inertia in starling flocks," *Nature Physics* **10**, 691 (2014).

[2] A. Cavagna et al., "Flocking and turning: a new model for self-organized collective motion," *Journal of Statistical Physics* **158**, 601 (2015).

[3] A. Cavagna et al., "Discrete Laplacian thermostat for flocks and swarms: the fully conserved Inertial Spin Model," *Journal of Physics A: Mathematical and Theoretical* **57**,41 (2024).

[4] A. Cavagna et al., "Spin-Waves without Spin-Waves: A Case for Soliton Propagation in Starling Flocks," arXiv:2505.19665 (2026).

Modeling Protein Sequence Evolution as an Ornstein-Uhlenbeck Process in a Latent Space

Matteo De Leonardis[1]
Andrea Pagnani[1,2,3]
[1] DISAT, Politecnico di Torino, Corso Duca degli Abruzzi, 10129 Torino, Italy
[2] Italian Institute for Genomic Medicine, IRCCS Candiolo, SP-142, 10060 Candiolo, Italy
[3] INFN, Sezione di Torino, Via Pietro Giuria 1, Torino 10125, Italy

High-throughput directed evolution experiments generate longitudinal sequence libraries that are ideal for probing local fitness landscapes around a wild-type sequence, but their limited diversity often restricts their usefulness for global inference tasks such as structural contact prediction. We introduce an unsupervised inference framework that integrates directed-evolution sequencing time-series data with natural homologous sequences by modeling laboratory evolution as an Ornstein–Uhlenbeck (OU) process in a latent space learned from natural sequence variation [1].

We first construct a low-dimensional latent representation of protein sequence space by applying principal component analysis (PCA) to multiple sequence alignments of natural homologs. Experimental variants are then projected into this latent space, where the evolutionary trajectories generated during laboratory selection are described through OU dynamics combining diffusive motion due to stochastic mutations and a drift effect due to selective pressure. The analytical form of the OU transition probability allows direct maximum-likelihood estimation of the parameters that define the process using sequencing time-series data. The resulting stationary Gaussian distribution in latent space induces an effective Potts model in sequence space, providing a principled connection between laboratory evolutionary dynamics and statistical models of protein coevolution used in Direct Coupling Analysis (DCA) [2]. The inferred couplings improve structural contact prediction by combining global evolutionary constraints from natural homologs with local, experiment-specific signals.

We apply the framework to directed-evolution datasets of PSE1 β-lactamase and dihydrofolate reductase (DHFR), both evolved under antibiotic selection. Although the experimentally generated libraries explore only a restricted neighborhood around the wild type compared to natural homologs, the inferred latent dynamics capture additional evolutionary constraints that complement those encoded in natural sequence statistics alone. In particular, the couplings inferred from the OU equilibrium distribution improve structural contact prediction relative to low-rank covariance approximations and identify additional intermediate- and long-range contacts.

Our results show that this framework provides a unified probabilistic approach to combine local experimental exploration with global evolutionary information, opening new perspectives for integrating laboratory evolution data with statistical inference models of protein families.

[1] Adam J. Riesselman, John B. Ingraham, and Debora S. Marks, *Deep generative models of genetic variation capture the effects of mutations*, Nature Methods, vol. 15, no. 10, pp. 816–822, Sep. 2018. DOI: 10.1038/s41592-018-0138-4.

[2] Simona Cocco, Christoph Feinauer, Matteo Figliuzzi, Rémi Monasson, and Martin Weigt, *Inverse statistical physics of protein sequences: a key issues review*, Reports on Progress in Physics, vol. 81, no. 3, p. 032601, Jan. 2018. DOI: 10.1088/1361-6633/aa9965.

From semimicroscopic ion-channel simulations to effective Markovian cooperative dynamics

Alejandro Diaz-Moreno[1], Sergio Alonso[1], and L. Ramírez–Piscina[1]
[1]Departament de Física Aplicada, EPSEB, Universitat Politécnica de Catalunya, Avinguda Doctor Marañón, 44, E-08028 Barcelona, Spain

Voltage-gated ion channels are commonly modeled through Markov-state approaches, where the transition rates between open and closed states are introduced phenomenologically. While these models are computationally efficient, they usually lack a direct connection with the underlying microscopic ion-channel dynamics. In this work, we present a multiscale framework that bridges semimicroscopic stochastic simulations and effective Markovian descriptions of cooperative channel gating.

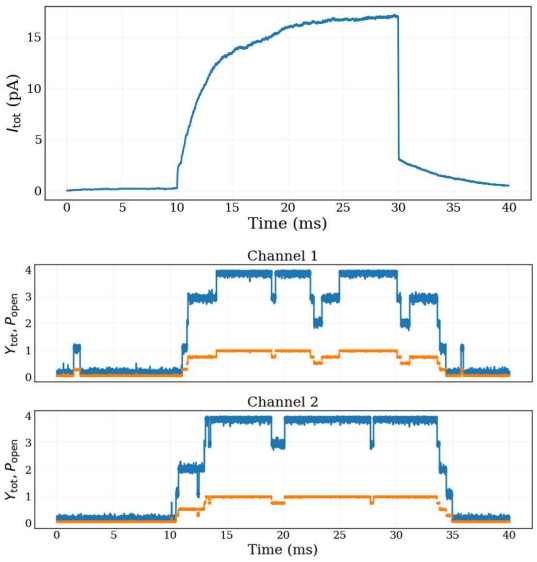

Fig. 1: Top: ensemble-averaged current under a voltage-jump protocol. Bottom: representative gating trajectories for two coupled channels, illustrating cooperative burst-like openings.

Our approach is based on a semimicroscopic Langevin model for tetrameric ion channels, where explicit ionic diffusion is coupled to the stochastic dynamics of the four channel subunits through a unified energy functional. The model incorporates membrane voltage, ion-gate interactions, and elastic coupling between neighboring subunits and channels. The resulting dynamics reproduce stochastic opening and closing events, subconductance states, and cooperative effects within channel clusters.

$$U_{\mathrm{tot}} = \sum_{c} \left[\sum_{i} V_E(x_{c,i}, \Delta V) + \sum_{j=1}^{4} \left(V_g(y_{c,j}) + V_s(y_{c,j}, \Delta V) + V_c(\{y_{c,j}\}) + \sum_{i} V_I(y_{c,j}, x_{c,i}) + V_{\mathrm{coup}}(y_{c,j}) \right) \right], \quad (1)$$

Using long stochastic simulations under different voltages and local channel configurations, we extract effective mean first-passage times associated with subunit opening and closing transitions. These transition times depend not only on the membrane potential, but also on the instantaneous state of neighboring subunits and adjacent coupled channels, providing an effective environment-dependent kinetic description.

The extracted transition rates are subsequently used to construct a coarse-grained Markov model capable of simulating large channel ensembles at significantly reduced computational cost.

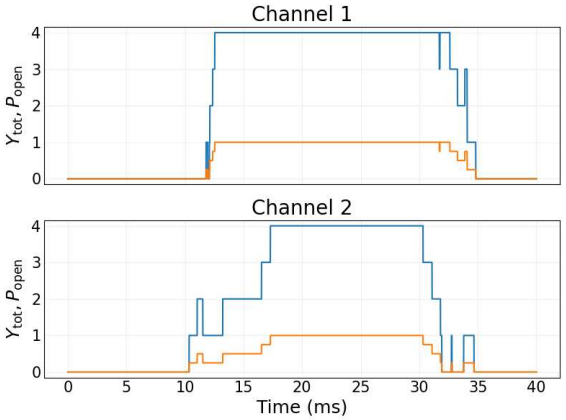

Fig. 2: Representative trajectories from the coarse-grained Markov model for two coupled channels under a voltage-jump protocol. The model reproduces the cooperative burst-like dynamics observed in the semimicroscopic simulations.

Despite the simplification, the Markovian description preserves the main dynamical trends observed in the semimicroscopic simulations, including cooperative activation and voltage-dependent collective kinetics.

This multiscale strategy provides a physically grounded route to derive effective channel kinetics directly from stochastic microscopic dynamics, offering a versatile framework for studying collective gating phenomena in large ion-channel assemblies.

[1] Ramírez-Piscina, L., "Fixed-Density Boundary Conditions in Langevin Models for Ionic Channels." *Phys. Rev. E* **98**, 013302 (2018).
[2] Ramírez-Piscina, L. and Sancho S.M., "Physical Properties of Voltage-Gated Pores." *Eur. Phys. J. B* **91**, 10 (2018).
[3] Ramírez-Piscina, L. and Sancho, J.M., "Subconductance States in a Semimicroscopic Model for a Tetrameric Pore." *Phys. Rev. E* **109**, 044402 (2024).

Assessing infrastructural resilience under extreme weather events: a case study of the Valencian DANA

Jonathan Diez[1,2], Aleix Nicolás Olivé[3], Eva Rifa[1,4], Emanuele Cozzo[1,2] and Oriol Artime[1,2]
[1]Universitat de Barcelona (UB), Gran Via de les Corts Catalanes, 585 08007 Barcelona
[2]Institute of Complex Systems (UBICS), Carrer de Martí i Franqués, 1 08028 Barcelona
[3] Universitat Pompeu Fabra (UPF), Ramon Trias Fargas, 25-27, 08005 Barcelona
[4] Eurecat, Av. Universitat Autònoma, 23, 08290 Cerdanyola del Vallès

On October 29, 2024, the DANA floods hit Valencia in an unprecedented manner. Rains in the region accumulated and led to large floods that resulted in physical damage, displacement and isolation, and the death of 230 people. The flooding lasted only a couple of weeks, but the effects are noticeable more than a year later. The disaster resulted in collapse of mobility, information flows, and social coordination. Roads became impassable, communities were isolated and fake news spread leading to the allocation of resources based on false information.

At the same time, a huge solidarity effort emerged. Thousands of people mobilized to remove debris and formed networks of mutual aid using digital platforms to coordinate and stay informed. [1]

In this project we analyze the collapse and the following recovery of these resources and networks during the DANA, that we conceptualize as three interdependent infrastructures and analyze them using satellite data, mobility data, and social media analysis. [2]

- Physical infrastructure: Reconstructing road network and travel times using satellite images and phone mobility data.
- Civic infrastructure: Coordination and communication between volunteers through Telegram groups and channels.
- Information infrastructure: Rapid share of public understanding through TikTok and Twitter.

We show how and when areas with damaged physical infrastructure are discussed in coordination channels of volunteers and how information is shared about these areas in social media. This allows us to understand how these different Infrastructures are corelated. With this we want to lie the basis for a general pipeline to analyze civic response to extreme weather events.

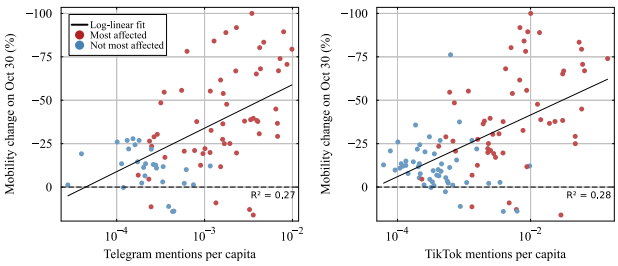

Fig. 1: Digital visibility and physical disruption after the Valencian DANA. Each point represents a municipality. The y-axis shows mobility change on October 30 relative to a weekday-matched baseline, while the x-axis shows Telegram or TikTok mentions per capita during the first response period. Red points indicate the most affected municipalities.

Our preliminary analysis compares municipality-level mobility decreases with mentions of Valencian municipalities on Telegram and TikTok. The results suggest a correlation between the physical impact of the disaster and social media activity: municipalities experiencing stronger mobility disruption tend to be more visible in volunteer coordination and information-sharing platforms. This shows that digital traces from civic and social media platforms may provide useful signals about affected areas during the response phase of an extreme weather event. At the same time, the analysis highlights important challenges, including delays in visibility, platform-specific biases, and the need to distinguish actionable information from noise or misinformation.

By connecting mobility data, volunteer coordination, and social media activity, this work contributes to the study of infrastructure resilience and crisis informatics. Fig. 1 shows how damaged physical infrastructure can be reflected in digital coordination channels and broader information flows, while also laying the groundwork for a generalizable pipeline to analyze civic resilience under extreme weather events. More broadly, the study demonstrates the value of integrating physical, civic, and informational infrastructures to better understand collective response during disasters.

[1] J. Martin-Moreno, E. Garcia-Lopez, M. Guerrero-Fernandez, J. Alfonso-Sanchez, and P. Barach, *Devastating "DANA" floods in Valencia: Insights on resilience, challenges, and strategies addressing future disasters*, Public health reviews, **46** (2025).

[2] O. Pasitselska, K. Buehling, and E. Gagrčin, *Chat groups as local civic infrastructure: A case study of "Solidary neighborhood help" Telegram groups during the COVID-19 pandemic in Germany*, new media & society (2025).

Evolutionary game dynamics as a mechanism for robust packet routing on scale-free networks

Francesca Dilisante[1,2], Pablo Gallarta-Sáenz[1,2], Jesús Gómez-Gardeñes[1,2], Luciano Stucchi[3] and Sandro Meloni[4,5,6]
[1]Department of Condensed Matter Physics, University of Zaragoza, 50009 Zaragoza, Spain
[2]GOTHAM lab, Institute for Biocomputation & Physics of Complex Systems, University of Zaragoza, 500018 Zaragoza, Spain.
[3] Universidad del Pacífico, Lima, Perú.
[4] Instituto de Física Interdisciplinar y Sistemas Complejos IFISC (CSIC-UIB), Campus UIB, 07122 Palma de Mallorca, Spain
[5]Istituto per le Applicazioni del Calcolo "Mauro Picone", Consiglio Nazionale delle Ricerche, 00185 Roma, Italy
[6]Centro Studi e Ricerche "Enrico Fermi" (CREF), 00184 Roma, Italy

Efficient packet routing in communication networks requires balancing two competing demands: minimizing path length and avoiding congested nodes. Pure shortest-path (SP) routing concentrates load at high-degree hubs, triggering a second-order jamming transition at comparatively low injection rates p_c^{SP}. Congestion-aware (CA) routing delays this transition to higher $p_c^{\mathrm{CA}} > p_c^{\mathrm{SP}}$ by dynamically redistributing load, but at the cost of a sharper, first-order-like collapse once capacity is saturated [1]. Neither paradigm alone constitutes a robust routing strategy.

We introduce an evolutionary game theory (EGT) framework in which a heterogeneous population of routing strategies, parameterized by a congestion-awareness parameter $h \in [0,1]$, competes for prevalence on a scale-free network, emulating realistic routing topologies. Strategies are updated across generations via selection pressure arising from differential routing performance, measured through two payoff metrics: a delivery-efficiency payoff, which penalizes packet accumulation, and a global-efficiency payoff, which jointly rewards instantaneous transit speed and delivery reliability.

This framework is analyzed under two complementary paradigms. In the *packet-centric* formalism, each packet is assigned a strategy at creation based on the current strategy distribution. In the *node-parent* formalism, strategy is instead anchored to the generating node, which applies it uniformly to all packets it produces, a more realistic model of router behavior. The node-parent formalism further admits local update rules (Moran process and Fermi) alongside the global replicator dynamics, capturing a crucial feature of real communication infrastructures: routing agents rarely have access to network-level performance information, operating instead under strict informational constraints with observational access limited to their own traffic state and coarse-grained signals from immediately adjacent neighbors.

Interestingly, across all paradigms, payoff metrics, and update rules, including the most realistic setting of local interactions with no global information, the evolutionary dynamics robustly achieve what neither pure paradigm can: by maintaining strategic diversity in the sub-critical regime, the system attains a higher jamming threshold p_c than fixed SP routing, and when congestion does set in, the transition avoids the violent first-order collapse of fixed CA strategies, settling instead at congestion levels comparable to SP routing (see Fig.1). This emerges spontaneously from purely local evolutionary exploration, without any centralized coordination. In the node-parent formalism, this robustness is not contingent on convergence to a unique strategy distribution: the fitness landscape contains multiple local minima, and different realizations settle into distinct strategy subsets, yet produce identical macroscopic congestion behavior.

Under local update rules, the fraction of nodes switching strategy per generation exhibits a pronounced peak near p_c, providing a node-level, locally accessible indicator of the jamming transition that requires no global knowledge of the network state. This suggests that a network operating under evolutionary local rules could detect the imminence of its own congestion transition through anomalous strategic volatility alone.

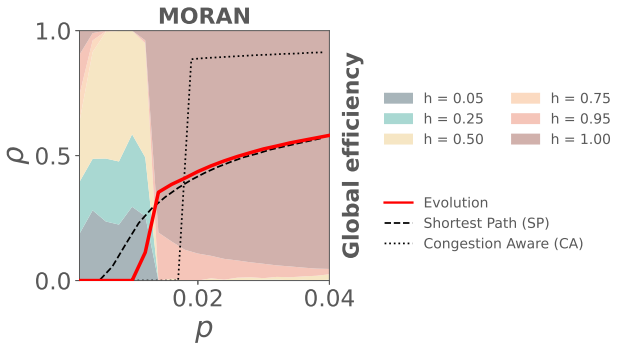

Fig. 1: Stationary strategy distribution $\{f_\alpha\}$ and order parameter ρ as a function of injection rate p under the node-parent formalism with Moran update rule and global-efficiency payoff. Dashed and dotted lines show the congestion baselines for fixed shortest path and congestion-aware routing, respectively. Results averaged over 100 independent realizations on a scale-free network with $N = 1000$ and $\langle k \rangle = 4$.

[1] P. Echenique, J. Gómez-Gardeñes, and Y. Moreno, Europhys. Lett. **71**, 325 (2005).

A look at the Gray-White matter Interface by diffusion MRI

Pablo F. Garrido[1,2], Paula Antelo-Riveiro[3,4], Markus H. Sneve[1], Anders M. Fjell[1,5], and Kristine B. Walhovd[1,5]
[1]Center for Lifespan Changes in Brain and Cognition, Department of Psychology, University of Oslo, Oslo, Norway
[2]Department of Physics, University of Oslo, Oslo, Norway
[3]Department of Organic Chemistry, CIQUS, Santiago de Compostela University, Spain
[4]Department of Applied Physics, Faculty of Physics, University of Santiago de Compostela, Spain
[5]Computational Radiology and Artificial Intelligence, Department of Radiology and Nuclear Medicine, Oslo University Hospital, Oslo, Norway

Magnetic Resonance Imaging (MRI) is a non-invasive technique used in the medical field to obtain high-resolution images of soft tissues, such as internal organs and muscles. MRI is widely used for clinical diagnosis by identifying morphological and functional alterations associated with a wide range of diseases. In our group, we use MRI-based neuroimaging as a tool to understand brain changes across the lifespan, from childhood to older adulthood.

MRI uses the magnetic properties of atomic nuclei (most commonly hydrogen) to characterize the tissues in which they reside. By modifying how we excite these nuclei and acquire their resonance signal, different pulse sequences can be designed, each sensitive to specific tissue properties. The most commonly used MRI sequences are structural, providing high contrast between tissue types and enabling clinicians to detect possible malformations. These sequences can be used to derive measurements such as volume and surface area, but are limited when characterizing tissue microstructure. To probe microstructural organization, diffusion MRI (dMRI) is used. dMRI is based on measuring the motion of water molecules within tissue, which is influenced by cellular and microstructural barriers. In neuroimaging, dMRI provides sensitive markers of brain microstructure, yet most analyses treat white matter (WM) and gray matter (GM) as homogeneous compartments, which can overlook the gray-white matter interface (GWI), a transitional region with rapidly changing microstructure that may carry biologically and clinically relevant information [1].

In this work, we propose a framework to characterize diffusion-related microstructural changes across the GWI by studying the profiles of the apparent diffusion coefficients perpendicular and parallel to the interface, and comparing them with the conventional diffusion tensor imaging (DTI) metrics (FA, MD, AD, RD) and advanced NODDI parameters (ICVF, ODI, ISO) [2]. Structural MRI data were processed with FreeSurfer to reconstruct the GWI and pial surface, and a set of intermediate surfaces was generated to sample different depths from the GWI into WM and into GM. Diffusion metrics were projected from the volume onto these surfaces, enabling the construction of microstructural profiles.

To interpret these findings, we introduce a biophysical model inspired by porous media theory, in which WM and GM are treated as distinct yet connected porous domains. Using concepts such as tortuosity and permeability, this model provides a conceptual link between measured diffusion signals and the underlying microstructural organization of tissue near the interface. Our results demonstrate that analyzing diffusion metrics across, rather than within, tissue compartments improves sensitivity to microstructural transitions. This approach offers a new perspective for studying cortical organization and may be valuable for investigating interface-related alterations across the lifespan.

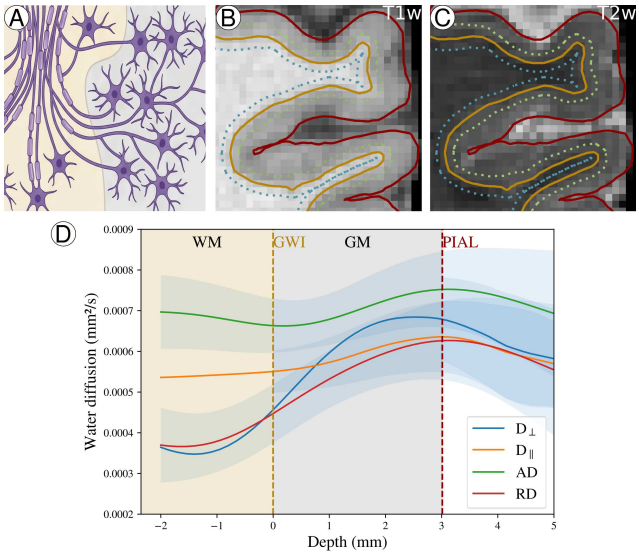

Fig. 1: A) Schematic representation of White Matter (WM) and Grey Matter (GM) microstrucutre. B) and C) Grey-White Interface (GWI) in yellow and Pial surface (red) over a T1w structural image (image B) and T2w structural image (image C). Dashed lines represent a surface 1 mm into the GW or WM. D) Evolution of perpendicular (blue) and parallel (orange) diffusion to the GWI from the WM to the pial, compared to the Axial Diffusivity (AD) and Radial Diffusivity (RD).

Keywords: MRI; diffusion MRI; neuroimage; brain microstructure.

Acknowledgements: This project has received funding from the European Research Council (ERC) under the European Union's Horizon 2020 research and innovation programme (grant agreement No 771355), the UiO:Life Science convergence environment fund, and was developed in collaboration with the Norwegian Twin Registry run by the Norwegian Institute of Public Health.

[1] D.H. Salat, S.Y. Lee, A.J. van der Kouwe, D.N. Greve, B. Fischl, and H.D. Rosas, *Age-associated alterations in cortical gray and white matter signal intensity and gray to white matter contrast*, NeuroImage **48**, 21-28 (2009).

[2] J. Y. Song, R. Fleysher, K. Ye, M. Kim, M. E. Zimmerman, R. B. Lipton, M. L. Lipton, *Characterizing the microstructural transition at the gray matter-white matter interface: Implementation and demonstration of age-associated differences*, NeuroImage **306**, 121019 (2025).

Epidemic Domains and Frontiers in Spatial Networks

Antonio F. Peralta[1], Daniel Ruiz-Reynés[1], Thilo Gross[2]
[1]Instituto de Física Interdisciplinar y Sistemas Complejos IFISC (CSIC-UIB), Palma de Mallorca, Spain
[2] Helmholtz Institute for Functional Marine Biodiversity at the University of Oldenburg, Oldenburg, Germany.

Epidemic spreading is a central problem in the study of dynamical processes on complex networks [1]. Among the most relevant models, the SIS (Susceptible-Infected-Susceptible) dynamics provides a minimal framework to investigate the interplay between disease transmission and the structure of the underlying contact network.

Consider the SIS model on a network with N nodes, where each node can be either susceptible (S) or infected (I). The dynamics is defined by the process rates $S+I \xrightarrow{\beta} 2I$ (infection) and $I \xrightarrow{\mu} S$ (recovery). A key feature of this model is the epidemic threshold β_c, i.e., the infection-rate value above which the epidemic spreads system-wide. Mean-field approximations, pair approximations, and spectral methods estimate this threshold from structural network properties such as the degree distribution or the spectrum of the adjacency matrix [1]. These approaches work well for weakly correlated networks, but spatial networks pose additional challenges because geometric constraints induce local correlations and clustering.

Random Geometric Graphs provide a paradigmatic example of spatial networks [2]. In this class of networks, nodes are distributed uniformly at random in space and are connected with probability p to other nodes within a sphere of interaction radius R. This geometry makes the epidemic dynamics intrinsically inhomogeneous. As a result, Random Geometric Graphs provide a natural framework for infections mediated by physical proximity, such as plant epidemics, where localized patches and infection fronts are often observed.

In this work, we derive an integro-differential dynamical equation for the SIS model on Random Geometric Graphs. This equation explicitly integrates over space and provides a theoretical description beyond classical homogeneous approaches:

$$\frac{\partial I(\mathbf{x},t)}{\partial t} = -\mu I(\mathbf{x},t) + \big(1-I(\mathbf{x},t)\big)\beta(\mathbf{x}) \int_{\mathbf{y}\in B^d(\mathbf{x},R)} \rho(\mathbf{y}) I(\mathbf{y},t) d\mathbf{y}. \qquad (1)$$

Here, $I(\mathbf{x},t)$ is the density of infected nodes, μ is the recovery rate, $\beta(\mathbf{x})$ is an effective infection rate, $\rho(\mathbf{y})$ is the spatial density of nodes, and $B^d(\mathbf{x},R) = \{\mathbf{y}\in\mathbb{R}^d : |\mathbf{y}-\mathbf{x}| \le R\}$.

The solution of Eq. (1) shows a highly accurate agreement with network simulations performed using the Gillespie algorithm [3], see Fig. 1. More importantly, the equation reveals epidemic domains in space and allows us to characterize their boundaries. In contrast with classical homogeneous approaches, SIS dynamics on Random Geometric Graphs gives rise to high-prevalence infection zones separated from low-prevalence susceptible regions. The characterization of these zones and their boundaries depends strongly on the network structure and therefore requires a precise theoretical analysis.

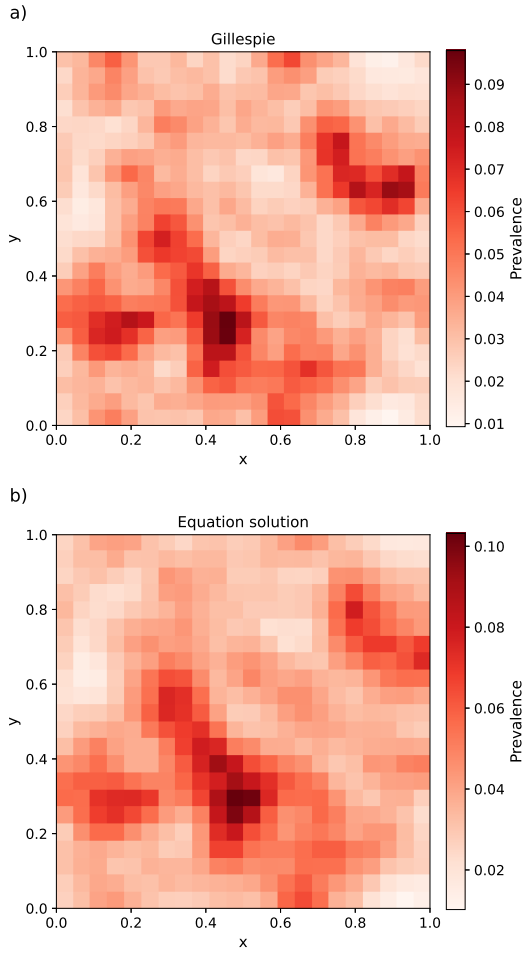

Fig. 1: Stationary prevalence $I(\mathbf{x}, t\to\infty)$ obtained from (a) Gillespie simulations and (b) the solution of Eq. (1). Parameters: $N = 256\times256$, $d = 2$, average degree $\langle k\rangle = 4$, connection probability $p = 0.01$, and $\beta = 1.05\beta_c$. For visualization, $I(\mathbf{x},t)$ is averaged on a 23×23 grid in both panels.

[1] R. Pastor-Satorras, C. Castellano, P. Van Mieghem, and A. Vespignani, *Epidemic processes in complex networks*, Rev. Mod. Phys. **87**, 925 (2015).

[2] J. Dall and M. Christensen, *Random geometric graphs*, Phys. Rev. E **66**, 016121 (2002).

[3] W. Cota and S. C. Ferreira, *Optimized Gillespie algorithms for the simulation of Markovian epidemic processes on large and heterogeneous networks*, Comput. Phys. Commun. **219**, 303 (2017).

Hydration water entropy controls sequestration in biomolecular condensates

Giancarlo Franzese[1,2]
[1] Institut de Nanociència i Nanotecnologia de la Universitat de Barcelona (IN2UB),
Martí i Franquès 1, Barcelona 08028, Spain
[2] Departament de Física de la Matèria Condensada,
Facultat de Física, University of Barcelona, Martí i Franquès 1, Barcelona 08028, Spain

Biological processes like the sequestration of superoxide dismutase 1 (SOD1) into biomolecular condensates, such as fused in sarcoma (FUS) and stress granules, are crucial for understanding disease mechanisms, including amyotrophic lateral sclerosis (ALS). Protein–crowder interactions within these condensates are fundamental to cellular phase separation and related diseases (condensatopathies). In vitro experiments show that heat shock-induced sequestration of SOD1 into FUS condensates depends on the type of crowder: PEG crowders replicate in vivo sequestration observed in cells, whereas bovine serum albumin (BSA) as a crowder reduces SOD1's partition coefficient (PC) into FUS condensates [1]. An implicit solvent model (OPEP) suggests this effect stems mainly from non-specific interactions [1]. By adding explicit water to the OPEP model, we demonstrated that hydration entropy plays a key role in reducing SOD1's PC (Fig. 1). Using the advanced CVF water model, which precisely captures hydrogen-bond networks at the molecular level [2–4], we explored water's influence on SOD1's behavior, residence times, and transition rates among states. Our findings offer new insights into how hydration entropy information affects biological function at molecular and cellular scales, supporting the idea that explicit water modeling enhances our understanding of cellular phenomena such as phase separation and condensatopathies [5].

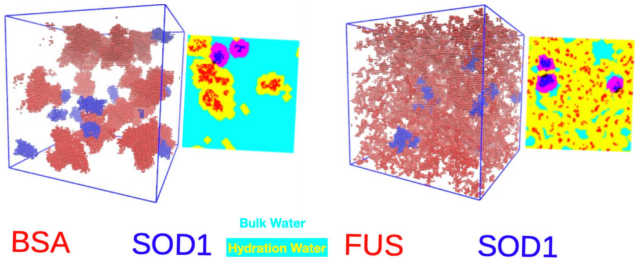

Fig. 1: Simulation snapshots of SOD1 in contact with BSA (left) and FUS (right) are shown in their 3D implicit- water representation (with SOD1 in blue and the other protein in red) or as 2D sections with water (turquoise for bulk and yellow or purple for hydration water).

[1] N. Samanta, S. S. Ribeiro, M. Becker, E. Laborie, R. Pollak, S. Timr, F. Sterpone, and S. Ebbinghaus, *Sequestration of Proteins in Stress Granules Relies on the In-Cell but Not the In Vitro Folding Stability*, J. Am. Chem. Soc. **143**, 19909 (2021).

[2] L. E. Coronas, and G. Franzese, *Phase behavior of metastable water from large-scale simulations of a quantitatively accurate model near ambient conditions: The liquid–liquid critical point*, J. Chem. Phys. **161**, 164502 (2024).

[3] L. E. Coronas, O. Vilanova, and G. Franzese, *A transferable molecular model for accurate thermodynamic studies of water in large-scale systems*, J. Mol. Liq. **434**, 128032 (2025).

[4] L. E. Coronas, O. Vilanova, and G. Franzese, *Efficient parallel algorithms for Monte Carlo simulations of millions of water molecules in the fluid phase*, Frontiers in Nanotechnology **7**, 1637828 (2025).

[5] L. E. Coronas, S. Timr, F. Sterpone, and G. Franzese, *Unveiling the entropic role of hydration water in SOD1 partitioning within FUS condensate*, J. Chem. Phys. **164**, 094910 (2026).

reserBUGS: A reservoir computing framework for probabilistic forecasting of ecological abundance time series

Miguel A. Mohedano-Muñoz [1,2], Javier Galeano [1,3], Juan M. Pastor [1,3],
Julia G. de Aledo [4], Ignasi Bartomeus [4], Alfonso Allen-Perkins [1,3]
[1]Grupo de Sistemas Complejos (GSC), Universidad Politécnica de Madrid, Madrid, Spain
[2]Departamento de Informática y Estadística, Universidad Rey Juan Carlos, Madrid, Spain
[3]Grupo Interdisciplinar de Sistemas Complejos (GISC), Madrid, Spain
[4]Estación Biológica de Doñnana (EBD-CSIC), Seville, Spain

Predicting how animal populations will change in the future is essential for biodiversity conservation, ecological management, and understanding the impacts of environmental change. Yet population dynamics arise from complex interactions among climate, habitat, species interactions, and stochastic processes, making reliable forecasts particularly challenging, especially when only short ecological time series are available [1]. We present reserBUGS [2], an open-source computational framework for probabilistic forecasting of insect population abundance whose analysis pipeline is shown in Fig. 1. The tool is based on reservoir computing [3], a machine-learning approach that uses a large network of randomly connected artificial neurons to capture complex temporal dependencies without the computational cost of training deep neural networks. Unlike conventional forecasting methods, reserBUGS produces full predictive distributions, allowing users not only to estimate future abundance but also to quantify forecast uncertainty and identify situations in which predictions are likely to be unreliable. We evaluated reserBUGS using thousands of insect population time series representing hundreds of species from around the world. Reservoir-based models consistently outperformed widely used statistical and machine-learning approaches in both point accuracy and probabilistic forecast quality. Incorporating environmental variables, including temperature and precipitation, further improved predictive performance, particularly at forecast horizons of three to four years. By combining accurate forecasts with explicit estimates of uncertainty and forecast reliability, reserBUGS provides ecologists and conservation practitioners with a practical tool for anticipating population change and supporting evidence-based management decisions under uncertainty.

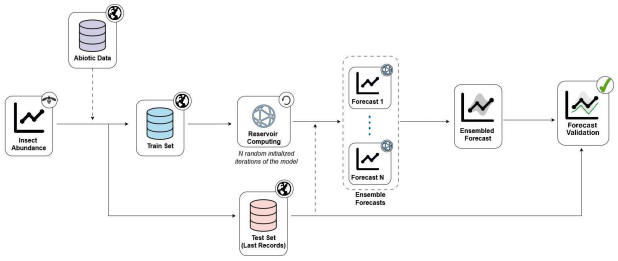

Fig. 1: Pipeline scheme followed in the reserBUGS prediction tool.

[1] M. C. Dietze, A. Fox, L. M. Beck-Johnson, J. L. Betancourt, M. B. Hooten, C. S. Jarnevich, T. H. Keitt, M. A. Kenney, C. M. Laney, L. G. Larsen, H. W. Loescher, C. K. Lunch, B. C. Pijanowski, J. T. Randerson, E. K. Read, A. T. Tredennick, R. Vargas, K. C. Weathers, and E. P. White, *Iterative near-term ecological forecasting: Needs, opportunities, and challenges*, Proc. Natl. Acad. Sci. U. S. A. **115**(7), 1424–1432 (2018).

[2] M. A. Mohedano-Munoz, A. Allen-Perkins, J. M. Pastor, J. Galeano, J. G. de Aledo, and I. Bartomeus, *reserBUGS: Reservoir computing for ecological forecasting* (PyPI, version 0.1.0, 2026), https://pypi.org/project/reserbugs/ (accessed 14 Jul 2026).

[3] M. Lukoševičius and H. Jaeger, *Reservoir computing approaches to recurrent neural network training*, Comput. Sci. Rev. **3**(3), 127–149 (2009).

Reproductive Strategy Transitions in Erysimum spp.: A Population Dynamics Approach Using a Generalized Interaction Model

Luciano Stucchi[1], Carlos Olmedo-Castellanos[2], Mohamed Abdelaziz[2], and Javier Galeano[3],
[1]Facultad de Ingeniería, Universidad del Pacífico, Lima, Perú
[2]Departament of Genetics, University of Granada.
[3]Complex System Group-Universidad Politécnica de Madrid

Reproductive strategies in flowering plants typically evolve over long evolutionary timescales. However, species within the Erysimum incanum complex—including E. incanum and E. wilczekianum—exhibit transitions between allogamy and autogamy on timescales far shorter than those predicted by standard evolutionary theory. While E. incanum relies on a mechanical self-pollination mechanism (anther rubbing), E. wilczekianum displays larger flowers associated with outcrossing, and populations across the complex show significant variation in mating system traits correlated with ploidy level. This raises a fundamental question from the perspective of statistical physics: what dynamical mechanisms, operating at the population level, can drive and sustain such rapid transitions between reproductive states?

We address this by adapting the generalized population dynamics model of Stucchi et al. [1], which unifies inter- and intraspecific interactions under a single polynomial functional framework that extends the classical Verhulst logistic equation. Crucially, intraspecific terms—typically neglected in standard ecological formulations—introduce new free-equilibrium solutions and substantially richer dynamical landscapes. We represent autogamous and allogamous reproductive strategies as distinct population states and model their coexistence and transitions as a function of intrinsic growth rates, inbreeding depression coefficients, and pollinator-mediated interaction terms.

Our analysis shows that the generalized model admits bistable regimes in which both strategies correspond to stable fixed points separated by an unstable equilibrium. Environmental perturbations or shifts in pollinator availability can drive the system across this threshold, producing abrupt strategy transitions without invoking genetic substitution. The parameterization of intraspecific terms maps directly onto biological observables measured in Erysimum populations, such as the pollen-to-ovule ratio and herkogamy indices. This framework provides a physically motivated account of mating system plasticity as an emergent property of population-level dynamics, and opens the possibility of characterizing reproductive strategy transitions through the tools of bifurcation theory and nonlinear stability analysis.

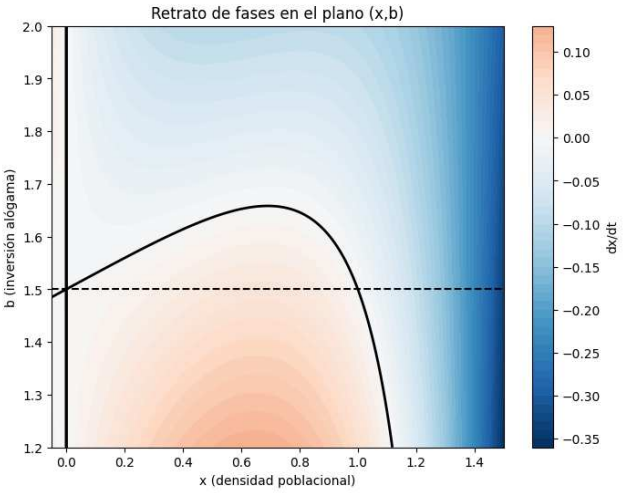

Fig. 1: Portrait of phases in the x,b plane

[1] Stucchi, L., Pastor, J. M., García-Algarra, J., Galeano, J. *A General Model of Population Dynamics Accounting for Multiple Kinds of Interaction*, Complexity **2020**, 1, 7961327, 2020.

Re-evaluating the acoustic niche hypothesis

Migual A. Mohedano-Muñoz[1], Javier Galeano[2], and Irene Mendoza[3]
[1]Escuela Técnica Superior de Ingeniería Informática, Universidad Rey Juan Carlos, Móstoles
[2]Complex System Group-Universidad Politécnica de Madrid
[3]Departament of Plant Biology and Ecology. University of Sevilla.

Birdsong is a key form of social communication and occupies a defined sound space within the natural environment. Sound propagation depends on habitat structure: understory species tend to emit lower-pitched songs, while canopy species use higher frequencies. Some adjust their signal to avoid interference from insects, traffic, or even aircraft noise. These adaptations led Bernie Krause to propose the Acoustic Niche Hypothesis [1], according to which species have co-evolved by distributing their sound emissions across time and the frequency spectrum to optimize communication and reduce overlap.

Three components can be distinguished in this definition of the acoustic niche: the structure of the song, reflected in its spectrogram; the time of signal emission, the temporal axis; and, more complex to assess, the evolutionary dimension that has led closely related species to occupy their own acoustic space to avoid overlap.

The Acoustic Niche Hypothesis was formulated without any mathematical measures, and although some local tests have been conducted, it still lacks large-scale, general validation with a more robust mathematical foundation. In this work, we aim to add measures that allow us to confirm or refute the predictions of the Acoustic Niche Hypothesis along habitat gradients and bird species diversity worldwide. To do this, we used 1-minute annotated audio recordings from the WABAD dataset [2], which includes more than 5,000 publicly available audio files from around the world. Local experts annotated, at the species level, the start and end times and the upper and lower frequencies of each bird vocalization identified in the recordings. We applied null models to test whether the acoustic signal distribution for each species was less or more aggregated than a random distribution based on Voronoi diagrams (Fig. 1). Our results showed that actual soundscapes do not differ from random distributions, offering weak support for the Acoustic Niche Hypothesis. Our results already indicate that bird species tend to overlap their songs across soundscapes, likely due to physiological limitations of their vocal system (syrinx) and other phylogenetic and environmental constraints. In this sense, the Acoustic Niche Hypothesis persists more as a paradigm entrenched in ecoacoustic research than as an empirically supported theory.

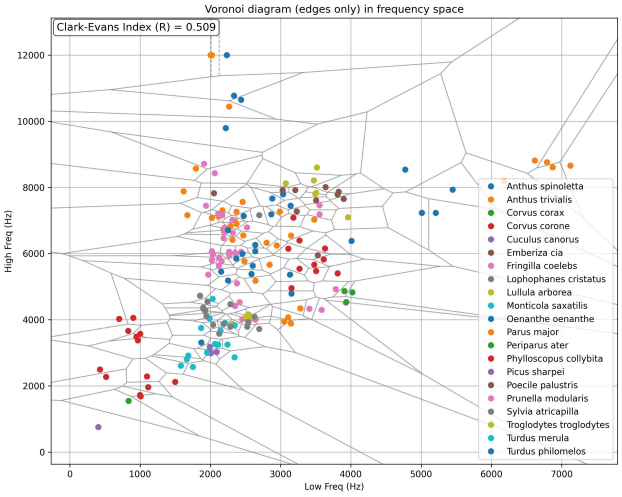

Fig. 1: Voronoi diagram showing the acoustic partitioning for the bird species singing in Doñana

[1] Krause, B., *The niche hypothesis: How animals taught us to dance and sing*, Whole Earth Review **57**, 14-16, 1987.

[2] Pérez-Granados, C., Morant-Etxebarría, J., Darras, K.F.A., Marín Gómez, O.H., Mendoza, I., Mohedano-Muñoz, M.A., Santamaría, E., Bastianelli, G., Márquez-Rodríguez, G., . . . , Sebastián-González, E. *WABAD: A World Annotated Bird Acoustic Dataset for Passive Acoustic Monitoring*, Ecology **107**,2, 2026.

Network structure and selective asymmetry drive coevolutionary fitness imbalances in antagonistic communities

Pablo Gallarta-Sáenz[1,2], Santiago Lamata-Otín[1,2], Jesús Gómez-Gardeñes[1,2] and Cecilia Siliansky Andreazzi[3]
[1] Departamento de Física de la Materia Condensada, Universidad de Zaragoza (Spain)
[2] GOTHAM lab, Institute for Biocomputation and Physics of Complex Systems (BIFI), Universidad de Zaragoza (Spain)
[3] Departamento de Biodiversidad, Ecología y Evolución, Universidad Complutense de Madrid (Spain)

Antagonistic interactions are fundamental drivers of ecological community structure and generate strong reciprocal selective pressures that shape the evolution of functional traits across interacting species. In this work [1], we develop a novel coevolutionary model for antagonistic communities that integrates network topology, trait evolution, and species fitness within a unified formalism. Both exploiters and victims evolve according to dynamical equations governed by two competing selective forces: an environmental selection towards a species-specific optimum, and a biotic selection arising from pairwise antagonistic interactions. The fundamental asymmetry of the system emerges not from the equations themselves but from the directionality of selection: exploiters are under pressure to match the functional traits of their victims, while victims evolve to maximize trait divergence and thereby escape exploitation. This construction gives rise to a rich landscape of emergent dynamical regimes whose transitions are governed by the relative magnitudes of the two selective forces: from rapid convergence to environmental optima under weak interaction pressure, to sustained nonlinear oscillations driven by the reciprocal feedback between chasing and escape strategies under strong bilateral selection (see Fig. 1).

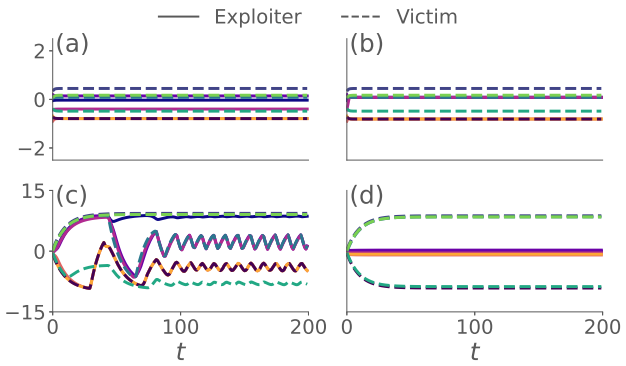

Fig. 1: Emergent dynamical regimes in the trait evolution of antagonistic communities. Temporal trajectories of functional traits for exploiters (solid lines) and victims (dashed lines) in a nested bipartite synthetic network of ten species (five exploiters, five victims), under four representative combinations of the selection strength parameters ξ_E and ξ_V: (a) $\xi_E = \xi_V = 0.1$, (b) $\xi_E = 0.9$, $\xi_V = 0.1$, (c) $\xi_E = \xi_V = 0.9$ and (d) ξ_E=0.1, ξ_V=0.9.

At the species level, connectivity plays a critical but asymmetric role in shaping evolutionary outcomes. For exploiters, the number of interaction partners is a primary determinant of fitness in a regime-dependent manner: generalist exploiters outperform specialists under weak interaction-driven selection, while specialists achieve superior fitness under strong antagonistic pressure. For victims, the connectivity–fitness relationship is weaker, more variable, and more sensitive to the specific structural and selective context, reflecting a fundamental difference in coevolutionary strategy between the two guilds. At the community level, a principal component analysis of 122 empirical antagonistic networks reveals that global network architecture is itself a structured and regime-dependent predictor of mean exploiter fitness: under strong reciprocal selection, modular and more species-rich communities with broader victim guilds sustain higher exploiter performance (see Fig. 2), while under weak bilateral selection this gradient reverses, with compact and densely connected networks marginally favoring exploiters. No equivalent structural predictor of fitness emerges for the victim guild across any selective regime, confirming that victim performance is governed primarily by local interaction dynamics rather than global network topology. Taken together, our results demonstrate how the interplay between selective asymmetry, connectivity heterogeneity, and network architecture generates complex and predictable fitness imbalances in antagonistic communities, with implications for the eco-evolutionary dynamics of host-parasite systems under anthropogenic change.

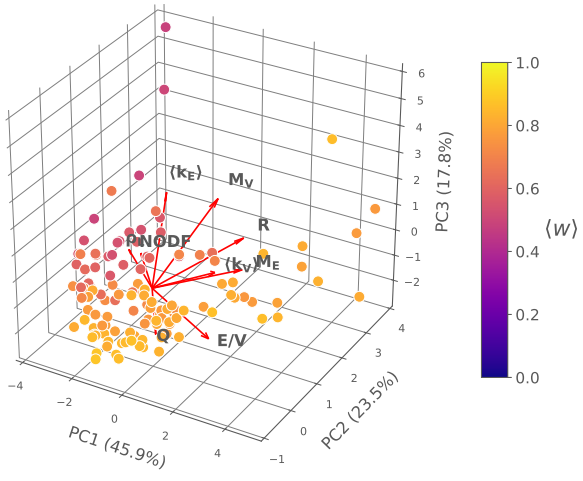

Fig. 2: Three-dimensional PCA projections of 122 empirical antagonistic networks, with each network represented as a point in the space spanned by the three dominant structural principal components (PC1: 45.9%, PC2: 23.5%, PC3: 17.8% of total structural variance). Point colour encodes mean exploiter fitness $\langle w_E \rangle$, averaged across all exploiter species under strong reciprocal selection ($\xi_E = \xi_V = 0.9$).

[1] Pablo *et al*. In preparation (2026).

Characterizing anisotropy in excitable media using spatial permutation entropy

Juan Gancio[1], Cristina Masoller[1], and Ulrich Parlitz[2,3]
[1]1 Universitat Politècnica de Catalunya, Departament de Física, Rambla Sant Nebridi 22, Terrassa 08222, Barcelona, Spain
[2]Max Planck Institute for Dynamics and Self-Organization, Am Fassberg 17, 37077 Göttingen, Germany
[3]Institute for the Dynamics of Complex Systems, University of Göttingen, Friedrich-Hund-Platz 1, 37077 Göttingen, Germany

Reaction-diffusion (RD) systems are extensively used in different disciplines to model a wide variety of phenomena, such as pattern formation, spatiotemporal chaos, or spiral waves. This allows such models to be used to study vegetation fields, bacterial growth, chemical reactions, and heart tissue. Although the simplest models are isotropic, natural systems are usually anisotropic: there is a preferred direction in which the system diffuses faster. Being able to estimate this direction from the observation of propagating waves, especially if their are irregular, i.e., chaotic, could be critically important when trying to uncover properties of the substrate or a living tissue. The spatial permutation entropy (SPE) [1] is a quantifier based on the ordinal analysis [2] and provides information of the nonlinear spatial structure. SPE has been used to characterize textures, art paintings, vegetation fields, and brain dynamics. Recently, SPE has been generalized to deal with anisotropic systems, showing that it can extract more information if the different possible orientations are considered [3].

In this work, we propose a new quantity based on SPE, the entropy ratio, that takes into account the spatial structure along the two orthogonal directions of a grid. We show that this quantity can be related to the underlying orientation of the fastest diffusion direction in several 2D RD systems. Furthermore, we show that the relationship between the angle of orientation of this direction and the entropy ratio does not depend on the specific RD system but only on the anisotropy ratio. Additionally, we propose an expression for the entropy ration given the anisotropy ratio and the angle, which under certain conditions can be inverted to obtain an expression for the angle. Although our results are based on numerical simulations, we believe that they represent a fundamental stepping stone in the analysis of real data, especially in applications related to the detection of fiber directions in cardiac tissue.

[1] Ribeiro H. V., Zunino L., Lenzi E. K., Santoro P. A., & Mendes R. S. (2012) Complexity-Entropy Causality Plane as a Complexity Measure for Two-Dimensional Patterns. *PLOS ONE* 7(8): e40689.

[2] Bandt, C., & Pompe, B. (2002). Permutation entropy: a natural complexity measure for time series. *Physical review letters*, 88(17), 174102.

[3] Gancio, J., Masoller, C., & Tirabassi, G. (2024). Permutation entropy analysis of EEG signals for distinguishing eyes-open and eyes-closed brain states: Comparison of different approaches. *Chaos: An Interdisciplinary Journal of Nonlinear Science*, 34(4).

Information transfer between spatially separated fish schools

Elena G. de Lamo[1], Oscar Sánchez[1], M Carmen Miguel[2,3], and Romualdo Pastor-Satorras[1]
[1]Dept. de Física, Universitat Politècnica de Catalunya, Campus Nord B4, 08034 Barcelona, Spain
[2]Dept. de Física de la Matèria Condensada, Universitat de Barcelona, Martí i Franquès 1, 08028 Barcelona, Spain
[3]Institute of Complex Systems (UBICS), Barcelona, Spain

Social animals rely on precise, rapid coordination to execute collective tasks [1]; for example, schooling fish utilize complex interaction networks to optimize navigation, locate resources, and collectively evade predators. It is well established in the field that vision is the primary driver of this local synchronization [2], allowing individuals to align their motion even under very dim lighting conditions [3]. However, what happens when a cohesive population is physically divided? If two spatially separated groups must choose between synchronizing with a distant cohort or merely following the local decisions made by their immediate neighbours, how does collective decision-making evolve? Is inter-group information transfer still possible when visual connectivity is severely degraded by distance and occlusion?

To shed light on these fundamental questions, we designed a partitioned experimental arena. A single tank is divided into three compartments, where a group of schooling fish is introduced into each of the two outer sections, see Fig 1, leaving the central compartment completely empty. This enforced physical gap creates a controlled "visual bottleneck," inherently degrading the quality of visual information and making it difficult for individuals to see past the empty space. In addition, the geometry of the tank introduces important dynamical constraints. By confining the fish within a rectangular arena, the system acquires a preferred direction of motion along the long axis of the tank. Consequently, the collective movement of each group becomes effectively one-dimensional. Therefore, by analysing the macroscopic directional motion of both groups across this spatial divide, we study their natural movement in their section of tank and their capacity to synchronize, understanding this alignment as a direct, quantifiable measure of information transfer.

These experimental observations can be understood by a coarse-grained model capable of reproducing this distance-dependent phenomenology. By bridging biological data with this physical framework, we demonstrate that vision remains critical for inter-group synchronization. Furthermore, we can compute the critical threshold at which this coordination lessens, quantifying how the flow of information decays as a function of increasing distance and visual occlusion. Ultimately, this work provides new insights into the spatial limits of collective intelligence and the robustness of biological active matter.

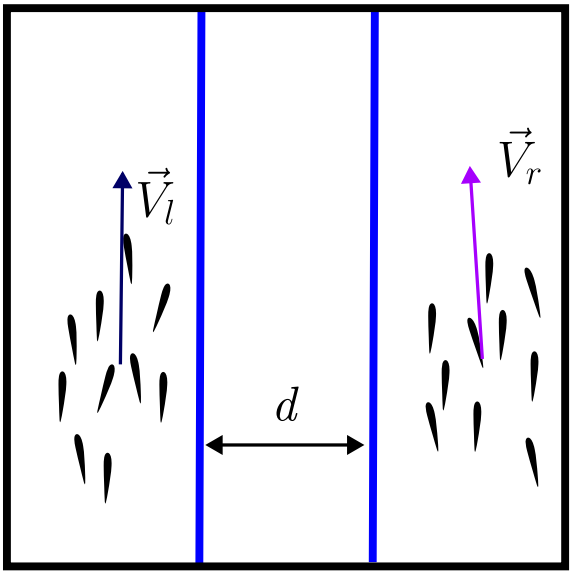

Fig. 1: Experimental tank divided in three sections with a group of ten fish at each outer section. Blue lines show transparent walls separated by an adjusted distance d, arrows indicate the velocity of the centre of mass of the groups.

[1] T. Vicsek and A. Zafeiris, *Collective motion*, Physics Reports **3**, 517 (2012).

[2] S. B. Rosenthal, C. R. Twomey, A. T. Hartnett, H. S. Wu and I. D. Couzin, *Revealing the hidden networks of interaction in mobile animal groups allows prediction of complex behavioral contagion*, Proceedings of the National Academy of Sciences **15**, 112 (2015).

[3] E. Shaw, *Schooling Fishes: The school, a truly egalitarian form of organization in which all members of the group are alike in influence, offers substantial benefits to its participants*, American Scientist **2**, 66 (1978)

Amyloid fibril elasticity through thermal fluctuations in molecular dynamics simulations

Jorge García-Inglés[1,2], Linda A. Zotti[1,2], and Salvatore Assenza[1,2]
[1]Departamento de Física Teórica de la Materia Condensada, Universidad Autónoma de Madrid, E-28049 Madrid, Spain
[2]IFIMAC, Universidad Autónoma de Madrid, E-28049 Madrid, Spain

Amyloid fibrils are proteinaceous aggregates in which peptides assemble into extremely long, stable chains with a well-defined supramolecular architecture (Fig.1a). They are involved in several neurodegenerative diseases, including Parkinson's and Alzheimer's, although their precise pathological roles remain hotly debated and many proposed therapeutic strategies focus on inhibiting or reversing the protein aggregation process [1].

Beyond disease, amyloid fibrils have emerged as promising biofunctional nanomaterials. Their appeal stems from the ease with which they can be synthesized in vitro from inexpensive proteins [2] (β-Lactoglobulin is a popular example), as well as their exceptional mechanical properties and stability. These qualities have enabled the creation of a wide range of amyloid-based technologies such as hybrid membranes for water purification [3] and scaffolds for tissue engineering [4].

Although new amyloid-based technologies are constantly emerging [5], the relationship between the structure and mechanical properties of amyloid fibrils at the atomic level still leaves room for exploration due to atomic resolution amyloid structures being only recently available. This structure-mechanics relation is central both to the rational design of amyloid-based materials and to our understanding of the energetics and dynamics of aggregation in biological environments. Experimental techniques such as AFM and optical tweezers can probe bulk elastic properties but offer limited insight into molecular-level deformation mechanisms. Atomistic simulations can bridge this gap, revealing structure–elasticity relationships at the atomic scale and thereby aiding both the characterization of amyloid growth and the tailoring of material properties.

In this study, we investigate experimentally deposited structures of Aβ40 and Aβ42 fibrils, closely associated with Alzheimer's disease, using standard atomistic molecular dynamics simulations. We establish a protocol for obtaining fibril conformations that remain stable on the microsecond timescale and, adopting a DNA-inspired local Cartesian coordinate system, characterize their equilibrium structural parameters (Fig.1b,c). Using the equipartition theorem, thermal fluctuations away from these equilibrium configurations are then used to extract elastic moduli governing bending, twisting, and stretching deformations.

We apply this analysis to amyloid fibrils with a variable number of residues and filaments, thus examining the role of different regions of the fibril in the elastic behavior and how the elastic moduli change with the number of constituent filaments. We gain quantitative insight into the tunability of amyloid mechanical properties and the energetics underlying the hierarchical assembly of fibrils from smaller subunits.

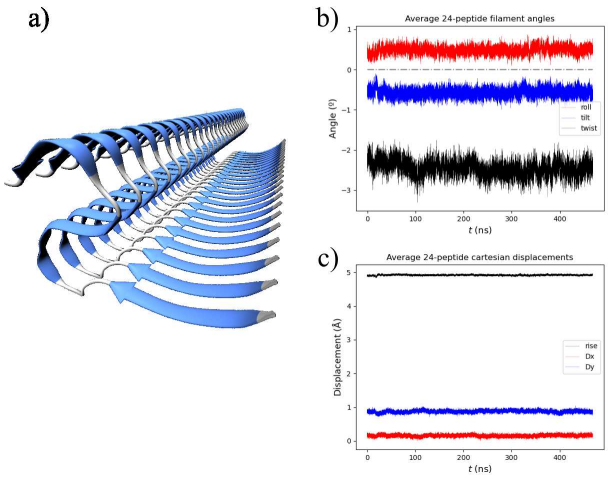

Fig. 1: a) One of the simulated Aβ42 filaments. b,c) Average relative angles and displacements of peptide pairs along the molecular dynamics trajectory.

[1] E. Karran, and B. De Strooper, *The amyloid hypothesis in Alzheimer disease: new insights from new therapeutics*, Nat. Rev. Drug Discov. **21**, 306 (2022).

[2] Y. Cao and R. Mezzenga, *Food protein amyloid fibrils: Origin, structure, formation, characterization, applications and health implications*, Adv. Colloid Interface Sci. **269**, 334 (2019).

[3] S. Bolisetty, and R. Mezzenga, *Amyloid–carbon hybrid membranes for universal water purification*, Nat. Nanotechnol. **11**, 365 (2016).

[4] S. Das, R. S. Jacob, K. Patel, N. Singh, and S. K. Maji, *Amyloid fibrils: Versatile biomaterials for cell adhesion and tissue engineering applications*, Biomacromolecules **19**, 1826 (2018).

[5] B. Liu, H. Zhang, and X. Qin, *Amyloid fibrils and their applications: current status and latest developments*, Nanomaterials **15**, 255 (2025).

Physically motivated adsorption kinetics from the aqueous phase: hydrogen evolution and nitrate reduction to ammonia on transition metals

A. de Arcos-Cañamero[1,2], T. Brito[1,2], G. Novell-Leruth[1], J.V. Perales-Rondón[1], and R. García-Muelas[1],
[1]Iberian Centre for Research in Energy Storage - CIIAE FUNDECYT-PCTEx. Av. Universidad s/n, 10004 Cáceres, Spain.
[2]International Doctoral School, University of Extremadura, Palacio de la Generala, Pz. Caldereros 1, 10003 Cáceres, Spain.

Solid-liquid interfaces appear in many processes in heterogeneous catalysis and electrocatalysis. In the Langmuir-Hinshelwood mechanism, the catalytic cycle starts with adsorption of reactants, followed by surface-mediated reactions and desorption of products. The kinetics of these elementary steps can be wrapped into a microkinetic model centred on the active sites, Eq. 1. Yet, while the kinetics of desorption and surface reactions is well described by the Eyring equation, no *ab initio* equivalent exists for adsorption kinetics from the aqueous phase. A common workaround consists in adapting the Eyring equation for adsorption, Eq. 2, but this is inconsistent: r_i must carry units of s^{-1} whereas Eq. 2 yields $M{\cdot}s^{-1}$, and replacing concentrations by activities does not help, as the activity of liquid water (55.5 M) and of protons at pH=0 would both be unity.

Applied to the hydrogen evolution and oxidation reaction on Pt(111), with adsorption energies from density functional theory (DFT) incorporated into a microkinetic model (Eq. 1), Eq. 2 shifts the experimental equilibrium line by 0.12 V (Figure 1-top). Replacing C_i by molar fractions x_i, as required by the statistical mechanics of the chemical potential in a mixture ($\mu_i = \mu_i^0 + k_B T \ln x_i$), makes Eq. 2 dimensionally consistent and uniformly applicable to solvent and solutes alike, thus restoring the equilibrium line (Figure 1-bottom)[3].

$$\frac{d\theta_j}{dt} = \sum_i \nu_{ij}\, r_i(\boldsymbol{\theta}, \mathrm{pH}, U, T), \qquad (1)$$

$$r_{\mathrm{ads},i} = \frac{k_B T}{h} \exp\left(-\frac{\Delta G_a^i}{k_B T}\right) C_i\, \theta_*\, S_0(T), \qquad (2)$$

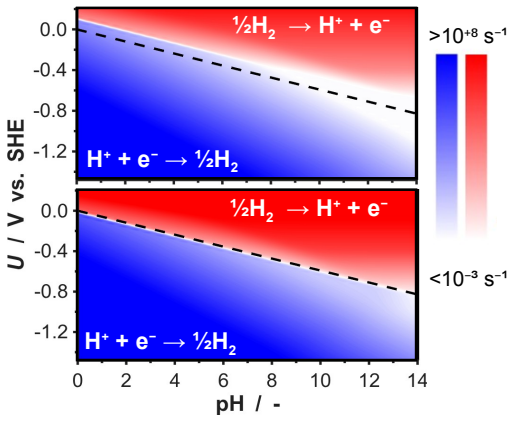

Fig. 1: Top: Hydrogen evolution/oxidation equilibrium under the traditionally-used Eyring equation, Eq. 2. Bottom: same equilibrium with molar fractions, x_i[3].

We then applied this framework to the nitrate reduction to ammonia (NRA). The electrochemical reduction of nitrate (NO_3^-), a pervasive water pollutant, to ammonia (NH_3) offers a sustainable alternative to the energy-intensive Haber-Bosch process, with Cu-based cathodes being highly selective towards NH_3[1, 2]. Most previous studies assume proton-coupled electron transfers without distinguishing whether hydrogenation proceeds via a proton from solution (Heyrovsky step, Eley-Rideal mechanism) or via adsorbed H* (Langmuir-Hinshelwood mechanism). We therefore calculated the full reaction network, including solvent-mediated protonation steps. There we found that the reduction starts by protonating adsorbed $*NO_3$, which is less activated than direct deoxygenation to $*NO_2$, consistent with experiments[2]. In general, direct protonation from the solvent is more likely at oxygen atoms or at N atoms bearing at most one oxygen.

With the present form, the kinetics of the full reaction mechanism can be fully assessed, including direct hydrogenations from protons in the solution.

We have shown that microkinetic models based on the concentration, Eq 2, are dimensionally inconsistent and fail to describe even basic equilibrium relations in heterogeneous electrocatalysis, as shown here for HER on Pt and NRA on Cu. Using molar fractions instead of concentrations or activities restores dimensional consistency and matches experimental equilibrium lines.

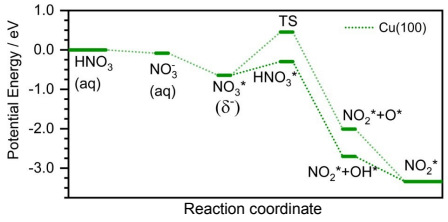

Fig. 2: First steps in nitrate reduction to ammonia on Cu(100)[4].

This work was funded by the InterGAmP project PID2023-152312OA-I00 funded by MCIU AEI 10.13039 501100011033 FEDER,UE, and the Spanish MICIU, and Junta of Extremadura through CIIAE Unit. **We gratefully acknowledge** the BSC-RES, COMPUTAEX, & CETA-CIEMAT for providing generous computational resources on MareNostrum, Lusitania & Turgalium clusters.

[1] J.V. Perales-Rondón, D. Rojas, W. Gao, M. Pumera, ACS Sust. Chem. & Eng. J., **11**, 6923-6931 (2023).
[2] L. Bai, B. Roldan Cuenya, et al., J. Am. Chem. Soc., **146**, 9665-9678 (2024).
[3] T. Brito, G. Novell-Leruth, L.A. Díaz, R. García-Muelas, In Prep.
[4] A. de Arcos-Cañamero, G. Novell-Leruth, J.V. Perales-Rondón, R. García-Muelas. In Prep.

Self-organization at multistability guiding pattern formation?

Enrique García-Ortiz[1,2], and Marta Ibañes[1,2]
[1]Departament de Física de la Matéria Condensada, Facultat de Física, Universitat de Barcelona (UB), 08028 Barcelona, Spain
[2]Universitat de Barcelona Institute of Complex Systems (UBICS), 08028 Barcelona, Spain

Pattern formation plays a key role in many different processes across biology, specially in cell fate specification during the development of numerous organisms. Such is the case of the liverwort *Marchantia polymorpha*, which experiences this kind of process at its gemma to determine which cells will form structures called rhizoids later in development. The emerging patterns are characterized by a scarcity of rhizoid precursors, a lack of periodicity, and purely localized development without lateral spread, among others (Fig. 1a). Within each cell of the gemma, a feedback loop arises between the rhizoid-specifying factor RLS1 (R) and a microRNA FRH1 (F) that suppresses it by cleaving the RSL1 mRNA (m) [1, 2]. The uniqueness of this system comes from the fact that, besides acting as a local repressor, F also mediates lateral inhibition [1, 2].

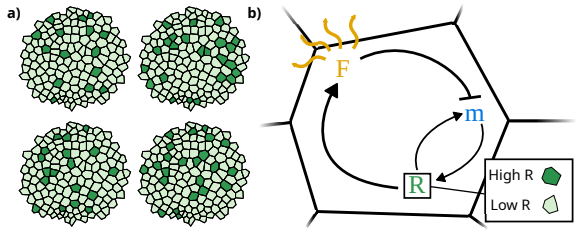

Fig. 1: **a.** Set of *M. polymorpha* gemmae displaying patterns resulting from simulations regarding the model from [3]. **b.** Schematic representation of the reaction-diffusion system that each cell in the gemma experiences.

Recent work from our group proposed that the lateral inhibition F enforces can be explained by its cell-to-cell diffusion (whereas R and m are unable to diffuse through the cell walls) (Fig. 1b) and further characterized the mechanism via mathematical modeling [3], formulating the following system:

$$\begin{cases} \dot{m}_i = \alpha_0 + \alpha \cdot \frac{{R_i}^n}{{R_i}^n + {k_R}^n} - k_c \cdot m_i \cdot F_i - d_m \cdot m_i \\ \dot{R}_i = \beta \cdot m_i - d_R \cdot R_i \\ \dot{F}_i = \gamma_0 + \gamma \cdot \frac{{R_i}^l}{{R_i}^l + {k_F}^l} - d_F \cdot F_i + D \cdot \Delta F_i^a, \end{cases}$$

where the i subindex refers to each cell of the gemma. Although this model can successfully reproduce the patterns displayed by real gemmae, in order to do so the values for its parameters must lie within a certain narrow regime that is close to criticality [3].

In this work, we hypothesize that *M. polymorpha* employs a self-organizing mechanism of some sort that allows the dynamics of its pattern-forming process to remain at this critical regime in the parameter space. First, we refine the model allowing for stochastic bursts of R following [3]. We then build upon the concepts of self-organized criticality (SOC) and self-organized bistability (SOB), which are based in the feedback that an order parameter transmits to a control parameter [4, 5], with the aim of endowing the model with a plausible self-tuning mechanism. Moreover, we ponder the biological meaning of this feedback. As other evidences in the literature suggest [6], we expect that a competition over a certain shared resource can establish such a mechanism. Hence, we propose a similar modification of the model to account for this phenomenon. We look at the necessary requirements of this feedback and define an order parameter established by this resource competition. We next evaluate its effect when it feeds back on distinct order parameters. After selecting the most adequate order parameter, we characterize some of the properties of the self-organization mechanism, such as the self-tuning timescale compared to the patterning timescale. Finally, we propose mathematical definitions and biological interpretations for the involved order and control parameters and link them with the resource competition framework.

[1] Thamm, A., and Saunders, T.E., Dolan, L. (2020). MpFEW RHIZOIDS1 miRNA-Mediated Lateral Inhibition Controls Rhizoid Cell Patterning in *Marchantia polymorpha*. *Current Biology* 30: 1905-1915.

[2] Proust, H., Honkanen, S., Jones, V.A.S., Morieri, G., Prescott, H., Kelly, S., Ishizaki, K., Kohchi, T., Dolan, L. (2016). RSL Class I Genes Controlled the Development of Epidermal Structures in the Common Ancestor of Land Plants. *Current Biology* 26: 93–99.

[3] Mercadal, J., Ferreira-Guerra, M., Caño-Delgado, A.I., Ibañes, M. (2026).Cell-type specification at criticality underlies rhizoid patterning in the liverwort *Marchantia polymorpha*. *Cell Reports* 45: 116728.

[4] Buendía, V., Di Santo, S., Bonachela, J.A., Muñoz M.A. (2020). Feedback Mechanisms for Self-Organization to the Edge of a Phase Transition. *Frontiers in Physics* 8: 333.

[5] Graf, I.R., Machta, B.B. (2024). A bifurcation integrates information from many noisy ion channels and allows for milli-Kelvin thermal sensitivity in the snake pit organ. *Proceedings of the National Academy of Sciences of the USA* 121: e2308215121.

[6] Karin, O., Miska, E.A., Simons, B.D. (2023). Epigenetic inheritance of gene silencing is maintained by a self-tuning mechanism based on resource competition. *Cell Systems* 14: 24-40.e11.

How Pluralistic Ignorance and Social Norms Shape Public Support for Road Pricing

Alberto Antonioni[1], Alice Ciccone[2], Cloé Garnache[3], Sara Ghivarello,[1] Askill H. Halse[2], Francesca Lipari[4]
[1]Carlos III University of Madrid, Spain
[2] Institute of Transport Economics (TØI), Norway
[3] Centre of Economic Research (CER-ETH), ETH Zürich, Switzerland
[4]University Complutense of Madrid, Spain

Public opposition remains a key barrier to the implementation of economically efficient environmental policies. Distance-based road pricing—where drivers pay per kilometre with fees varying by time and location—is theoretically optimal [1] yet politically contentious.

We investigate the drivers of public support for distance-based road pricing using original data from two stated choice experiments conducted in the Community of Madrid in 2022 and 2023 ($N = 638$ residents). Respondents chose between two road pricing alternatives and a status quo representing current tolls, fuel taxes, and the Madrid Central low-emission zone. Policy alternatives varied along five dimensions: urban peak price, urban off-peak price, non-urban price, electric vehicle discount, and revenue allocation. Before completing the choice tasks, respondents were randomly assigned to one of five information treatments (congestion and pollution, public revenues, redistribution, road pricing framing, social norms) or a control group. The post-choice module elicited three social norm constructs following Bicchieri [4]: **empirical expectations** (EE, beliefs about actual car use), **personal normative beliefs** (PNB, own ideal car use level), and **normative expectations** (NE, beliefs about others' ideal car use). Those norms were used to elicit *pluralistic ignorance*: the systematic tendency of individuals to misperceive how widely pro-environmental preferences are shared in their social environment [2, 3].

Main results. We document four findings.

(i) Policy design dominates. Overall support is substantial—77% of choices favour a pricing alternative—but highly sensitive to design. Support declines with price stringency and increases markedly when revenues are earmarked for public transport and active travel (coefficient ≈ 0.79, $p < 0.01$), equivalent in utility to a 0.63EUR reduction in the urban peak price. Informational treatments produce no significant shift in support, suggesting that one-shot fact provision is insufficient to move entrenched preferences.

(ii) Substantial preference heterogeneity. Latent class analysis identifies four classes: *pro-policy* (16.8%), *anti-policy* (14.5%), *moderate pro-policy* (47.0%), and *mixed* (21.7%). These groups differ markedly in price sensitivity, valuation of revenue use, and demographic composition. Car users and right-leaning voters are more likely to belong to the anti-policy class, while higher institutional trust predicts membership in the pro-policy classes.

(iii) Pluralistic ignorance exists and predicts support. Respondents overestimate others' tolerance for car-heavy behaviour by 8 percentage points on average ($\bar{\text{NE}} = 34.0\%$ vs. $\bar{\text{PNB}} = 26.0\%$; $t(456) = 8.49$, $p < 0.001$). This misperception is positively associated with policy support: respondents who overestimate how pro-car others are show greater demand for formal regulation, consistent with a *substitution* between informal norm-based and formal policy-based governance. Personal normative beliefs are negatively associated with support ($\beta = -1.056$, $p < 0.05$), while the effect of pluralistic ignorance is attenuated among high-trust respondents.

(iv) Social norm influences on behaviour are largely null. A separate elicitation of individual-level sensitivity to empirical and normative expectations—via hypothetical car-use scenarios—reveals that the large majority of respondents (71%) are indifferent to peers' behaviour and beliefs, with no statistically significant effect on policy support.

Implications. Overall support is substantial, but highly sensitive to design. Successful policies should have low to moderate pricing and earmark revenues to public transport and active travel. The positive association between pluralistic ignorance and road pricing support points to an important asymmetry—correcting norm misperceptions may strengthen voluntary compliance but simultaneously reduce support for coercive instruments. Policymakers face a strategic choice in norm communication that has not been previously recognised in the transport acceptability literature.

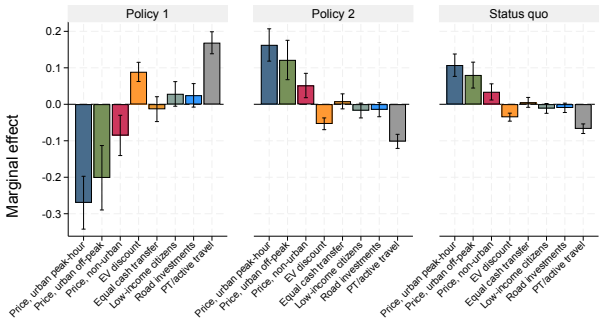

Fig. 1: Marginal effects of a change in Policy 1.

[1] A.C. Pigou, *The Economics of Welfare*, Macmillan, London (1920).
[2] G. Sparkman, N. Geiger, E.U. Weber, *Nature Communications* **13**, 4779 (2022).
[3] P. André et al., *Nature Climate Change* **14**, 253 (2024).
[4] C. Bicchieri, *The Grammar of Society*, Cambridge University Press (2005).

Self-Sustained Macroscopic Dynamics in an Asymmetric Hopfield Network with Plasticity

Gabriel Guzmán-Schiller[1,2], and Miguel Aguilera[1,3]
[1]Basque Center for Applied Mathematics (BCAM), Bilbao, Spain
[2]University of the Basque Country (UPV/EHU), Bilbao, Spain
[3]Ikerbasque, Basque Foundation for Science, Bilbao, Spain

Neural systems are capable of generating spontaneous self-sustained internal activity, a key phenomenon underlying cognitive processes such as habit formation and sequential processing [1]. How such autonomous low-dimensional dynamics can emerge from microscopic neural interactions and adaptive synaptic couplings remains an open question. Here, we study a minimal asymmetric model in which macroscopic activity stabilizes through synaptic plasticity.

To address this problem, we consider a network of binary spins evolving under stochastic Glauber dynamics

$$P(s_i \mid \mathbf{s}_{\setminus i}) = \frac{1}{2}\left[1 + s_i \tanh(\beta h_i)\right],$$

and interacting through a low-rank coupling matrix constructed from stored patterns,

$$h_i = \sum_{j,j\neq i} J_{ij} s_j, \qquad J_{ij} = \frac{1}{N}\sum_{\mu,\nu} \xi_i^\mu A_{\mu\nu} \xi_j^\nu .$$

In contrast to equilibrium Hopfield networks [2], which are typically associated with symmetric couplings, and static memory retrieval, the pattern-coupling matrix $A_{\mu\nu}$ is allowed to be asymmetric. This allows the emergence of non-equilibrium macroscopic dynamics [3]. At the macroscopic level, the network state is described by the overlaps m_μ between the spin configuration and the stored patterns. Defining $g_\mu(\mathbf{m}) = \frac{1}{N}\sum_i \xi_i^\mu \tanh\left[\beta \sum_{a,b} \xi_i^a A_{ab} m_b\right]$, the mean-field dynamics reads

$$\dot{m}_\mu = -m_\mu + g_\mu(\mathbf{m}).$$

The matrix A evolves according to a plasticity rule defined directly in terms of these macroscopic observables

$$\dot{A}_{\mu\nu} = \gamma g_\mu(\mathbf{m}) m_\nu - \kappa A_{\mu\nu}^3 .$$

The first term couples the expected postsynaptic response g_μ to the presynaptic macroscopic activity m_ν, thereby reinforcing directed couplings from ν to μ. It can be interpreted as a coarse-grained STDP-like plasticity term, while the cubic decay saturates the learned couplings. We study the conditions under which the balance between neural dynamics and synaptic plasticity generates autonomous macroscopic trajectories such as stable limit cycles.

Our results show that, under suitable conditions and in the absence of external stimuli, this learning rule can generate structured trajectories in overlap space, corresponding to self-sustained macroscopic neural activity, as shown in Fig. 1A. Moreover, the cyclic regime is accompanied by a positive entropy production rate (EPR) of the mean-field dynamics [4], which reaches an approximately constant plateau once the stable limit cycle is established, as shown in Fig. 1B. This provides a thermodynamic signature of sustained irreversible dynamics at the macroscopic level. After learning, A saturates while the overlaps remain periodic, suggesting that the cycle is supported by a learned dynamical memory. Thus, the cycle is not merely a transient of ongoing plasticity.

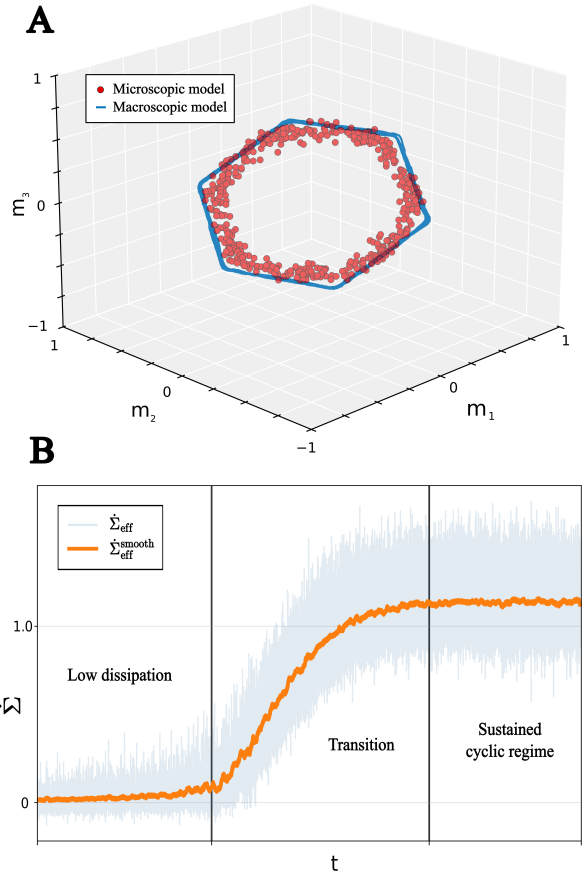

Fig. 1: **Self-sustained macroscopic dynamics and entropy production in an asymmetric Hopfield network with plasticity.** (A) Stable limit cycle in overlap space, comparing microscopic stochastic trajectories with the macroscopic mean-field dynamics. (B) Entropy production rate $\dot{\Sigma}_{\text{eff}}$ during learning, showing a positive plateau in the sustained cyclic regime.

[1] M. D. Egbert and X. E. Barandiaran, *Modeling habits as self-sustaining patterns of sensorimotor behavior*, Front. Hum. Neurosci. **8**, 590 (2014).

[2] J. J. Hopfield, *Neural networks and physical systems with emergent collective computational abilities*, Proc. Natl. Acad. Sci. USA **79**, 2554–2558 (1982).

[3] A. C. C. Coolen, *Statistical mechanics of recurrent neural networks II: Dynamics*, arXiv:cond-mat/0006011 (2000).

[4] M. Aguilera, D. De Martino, I. Garashchuk, and D. Sinelshchikov, *Nonequilibrium thermodynamics of associative memory continuous-time recurrent neural networks*, in *ALIFE 2025: Proceedings of the Artificial Life Conference 2025*, Vol. 37, Paper 55 (MIT Press, 2025).

Modelling the epidemiological impact of diagnostic performance on malaria transmission

Violeta Hernàndez Arnal, Max Puig, Sergio Alonso, Clara Prats and Daniel López
BIOCOM-SC, Department of Physics, Universitat Politècnica de Catalunya, Barcelona, Spain

Malaria is one of the leading causes of preventable death worldwide, yet the epidemiological impact of diagnostic performance on transmission dynamics is poorly understood. We study three compartmental models of increasing complexity – single-strain, two-strain, and spatially distributed – to quantify how the choice of diagnostic method and the geographical distribution of healthcare centers affect disease prevalence. Rapid Diagnosis Tests (RDT) are found to present a blind spot that allows an *hrp2*-deleted mutant strain to circulate silently at high prevalence, a phenomenon suppressed by switching to microscopy. The spatial analysis shows that diagnostic quality has a stronger influence on endemic prevalence than the size of the healthcare network.

Malaria transmission is driven by the coupled dynamics between human hosts and *Plasmodium*-infected mosquitoes [1, 2]. Fast detection is a key factor for disease control, protecting both the individual and the wider population from onward transmission. We use an extended SEITR–SI compartmental framework, calibrated to endemic malaria dynamics in Angola, to explore how the detection time T_D – the interval between the onset of infectiousness and treatment initiation – shapes transmission at three scales of increasing complexity.

Single-strain model: A five-compartment human population (Susceptible, Exposed, Infectious, Treated, Recovered) coupled to a two-compartment mosquito population reproduces the classical SEITR–SI dynamics. Simulations over the operational range of T_D – from Rapid Diagnosis Tests ($T_D = 3$ d) to clinical diagnosis ($T_D = 12$ d) – show that both the endemic equilibrium I^* and the initial epidemic peak grow monotonically, and drastically, with T_D (Fig. 1): clinical diagnosis reaches nearly six times the endemic prevalence achieved under RDT-based screening.

Two-strain model: We extend the framework to two competing strains: a wild-type, detectable by all methods, and an *hrp2*-deleted variant that evades RDT detection specifically. Under RDT-only screening the mutant strain accumulates silently, diverging from the reported incidence; switching to microscopy makes it fully trackable and its prevalence drops sharply. This confirms that the elevated burden of the *hrp2*-deleted strain under RDT is a diagnostic artifact rather than a true biological advantage.

Spatial model: Extending the two-strain model over a $140 \times 140\,\mathrm{km}^2$ territory, with detection time depending on distance to the nearest health facility, shows that increasing the number of healthcare centers reduces prevalence only marginally for the RDT-blind strain, regardless of network size: the diagnostic blind spot, not geographic inaccessibility, is the primary driver of the elevated disease burden.

Across all three scales, diagnostic performance has a crucial impact on the development of the disease. In populations where *hrp2*-deleted variants circulate, investments in diagnostic quality are likely to yield greater epidemiological returns than equivalent investments in healthcare infrastructure alone.

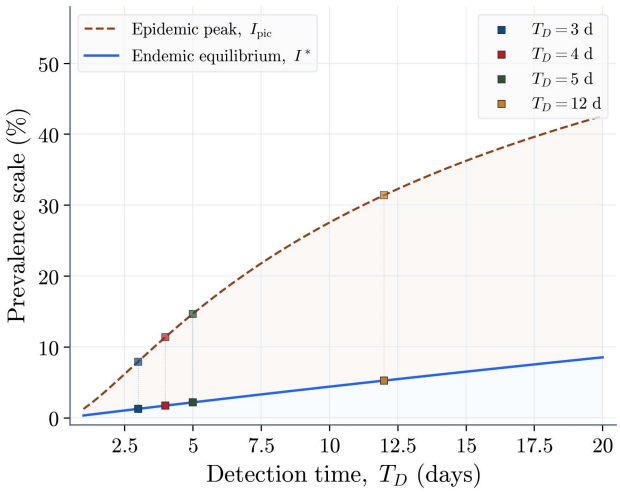

Fig. 1: Endemic equilibrium I^* (solid) and epidemic peak I_{peak} (dashed) as functions of the detection time T_D. Markers indicate the four diagnostic modalities: RDT, PCR, microscopy, and clinical diagnosis.

[1] S. Mandal, R. R. Sarkar, and S. Sinha, *Mathematical models of malaria – A review*, Malaria Journal **10**(1), 202 (2011).

[2] N. Chitnis, J. M. Cushing, and J. M. Hyman, *Bifurcation analysis of a mathematical model for malaria transmission*, SIAM J. Appl. Math. **67**(1), 24–45 (2006).

[3] L. Marquart *et al.*, *The in-vivo dynamics of Plasmodium falciparum HRP2: Implications for the use of rapid diagnostic tests in malaria elimination*, Malaria Journal **21**(1), 233 (2022).

[4] World Health Organization, *World Malaria Report 2023*, WHO Press, Geneva (2023).

Birth of Optical Linguistics: Bridging Quantitative Linguistics and Photonic Dynamics

Antoni Hernández-Fernández[1], Antonio J. Pons[1], and Andrés Aragoneses[2]
[1]Universitat Politècnica de Catalunya, Jordi Girona 31, 08034 Barcelona, Spain.
[2]Whitman College, Physics Department, 345 Boyer Avenue, Walla Walla, WA 99362, USA.

The influence of physics on biological scaling laws in communication systems emerges from optimization principles that constrain how energy, matter, and information are distributed across living systems [1–3]. In this work, we propose a unified framework for the investigation of linguistic-law analogues in non-biological physical systems, with a particular focus on photonic neurons operating under optical feedback. Building upon prior research on the physical underpinnings of linguistic regularities in human speech [4] and recent advances in the multiscale dynamics of photonic neuromorphic devices [5], we introduce the concept of *optical words* or *photowords* as discrete, symbol-like units derived from continuous optical intensity time series. Analogously to human languages, we defined *photonemes* as the constituents of these *photowords* (see Fig. 1 for an example).

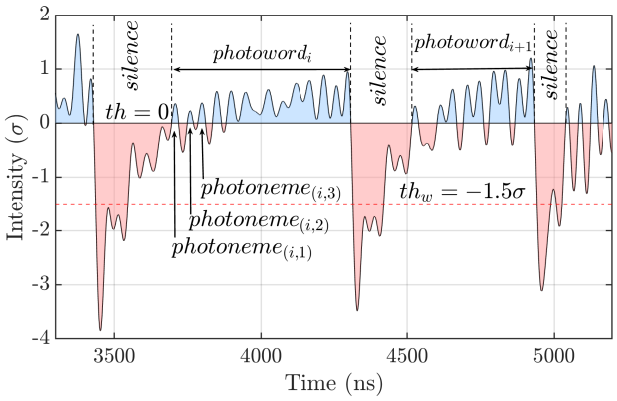

Fig. 1: Example of encoding the time series of a photonic neuron (laser diode with external optical feedback) into photowords and photonemes, applying the threshold method for the analysis of linguistic laws.

Using threshold-based segmentation [6], continuous photonic spike trains are transformed into these sequences of *photonemes* and *photowords*, enabling the application of mathematical tools from quantitative linguistics and time series [7, 8]. We then examine the emergence of well-known linguistic laws—including Zipf's law, the Herdan–Heaps law, the Brevity law, and the Menzerath–Altmann law—within these purely physical optical systems. Our results in photonic neurons indicate that some statistical regularities traditionally associated with human language can be considered a baseline and in some cases arise from the intrinsic dynamics of multiscale physical processes, without requiring biological or cognitive substrates.

Crucially, this framework opens a new research field, ***Optical Linguistics***, and a new perspective within complex systems physics by suggesting that such statistical signatures may serve as universal markers of structured information processing, as in other types of communication systems [9]. In this context, the identification of linguistic-law analogues in optical or electromagnetic signals could provide a novel methodological avenue for the detection and characterisation of non-random, potentially information-bearing signals of unknown origin, including those of possible extraterrestrial provenance [10].

Beyond introducing a formal definition of *optical units* in photonic communication systems, this work establishes a theoretical bridge between photonic neuromorphic platforms [5, 11] and quantitative linguistics [12]. More broadly, it supports the hypothesis that some linguistic-law-like distributions may emerge in multimodal communication as a consequence of fundamental constraints governing complex systems. This perspective offers new tools for signal analysis in domains where the distinction between noise and structured information remains an open challenge.

Acknowledgments: AHF acknowledges the support received through grant PID2024-155946NB-I00, funded by the Spanish Ministerio de Ciencia, Innovación y Universidades (MICIU), the Agencia Estatal de Investigación (AEI/10.13039/501100011033), and the European Social Fund Plus (ESF+), and also the grant AGRUPS-2026 from Universitat Politècnica de Catalunya. AA acknowledges support from the M.J. Murdock Charitable Trust through a College Research Program Natural Sciences Grant.

[1] R. Ferrer-i-Cancho, Europhys. Lett. **151**, 62001 (2025).
[2] R. Ferrer-i-Cancho, J. Quant. Linguist. **25**, 207 (2018).
[3] C. T. Kello, G. D. A. Brown, R. Ferrer-i-Cancho, J. G. Holden, K. Linkenkaer-Hansen, T. Rhodes, and G. C. Van Orden, Trends Cogn. Sci. **14**, 223 (2010).
[4] I. G. Torre, B. Luque, L. Lacasa, C. T. Kello, and A. Hernández-Fernández, R. Soc. Open Sci. **6**, 191023 (2019).
[5] A. Aragoneses, Sci. Rep. **16**, 1104 (2026).
[6] I. G. Torre, B. Luque, L. Lacasa, J. Luque, and A. Hernández-Fernández, Sci. Rep. **7**, 43862 (2017).
[7] L. Debowski, *Information Theory Meets Power Laws* (Wiley, Hoboken, 2020).
[8] K. Tanaka-Ishii, *Statistical Universals of Language* (Springer, Cham, 2021).
[9] A. Hernández-Fernández and I. G. Torre, Biol. Lett. **18**, 20220162 (2022).
[10] L. R. Doyle, B. McCowan, S. Johnston, and S. F. Hanser, Acta Astronaut. **68**, 406 (2011).
[11] J. P. Bannon, E. Main, T. Hill, and A. Aragoneses, Sci. Rep. **15**, 1391 (2025).
[12] E. Kelih, J. Mačutek, and M. Koščová, *Quantification in Linguistics and Text Analysis* (De Gruyter, Berlin, 2025).

Impact of fluctuations on particle systems described by Dean-Kawasaki-type equations

Nathan O. Silvano[1], Emilio Hernández-García[1], and Cristóbal López[1]
[1]Instituto de Física Interdisciplinar y Sistemas Complejos (IFISC), CSIC-UIB.
Campus Universitat de les Illes Balears, 07122 Palma de Mallorca

Dean-Kawasaki-type equations (DKTE) are stochastic partial differential equations that describe the density $\rho(\mathbf{x},t) = \sum_i \delta(\mathbf{x}-\mathbf{r}_i(t))$ of (possibly interacting) particle systems undergoing Brownian motion ($\mathbf{r}_i(t)$ are the particle positions). The very singular nature of the noise term present in them (of the conservative-multiplicative type $\nabla[\sqrt{D\rho(\mathbf{x},t)}\xi(\mathbf{x},t)]$) poses great challenges, both from the analytic and from the numerical point of view. In recent years several studies have established rigorous mathematical results from which reliable numerical algorithms can be developed [1–3],

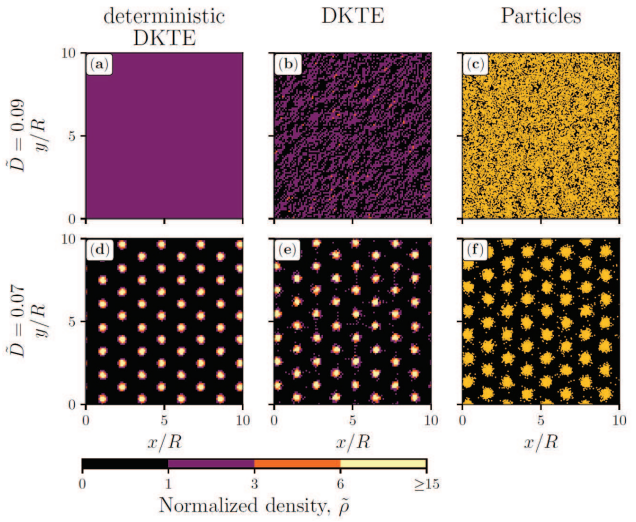

Fig. 1: Configurations at long times of a 20000-particle system interacting with a soft-core repulsive potential [4, 5] at two different values of the diffusion coefficient $\tilde{D}$ (one leading to quasihomogeneous distributions and the other to pattern formation). Results from the deterministic (mean-field) description, the stochastic DKTE partial differential equation, and the direct particle simulation are shown. In the last case all particle positions are shown, not a binned density.

For four models of increasing complexity, we compare microscopic particle simulations, the density-based DKTE stochastic partial differential equations, and their deterministic counterparts [4]. Our results confirm the consistence of the particle and DKTE results in the range of parameters for which the numerical algorithms are expected to be accurate. The comparison with the deterministic description identifies macroscopic quantities that can be altered by the conserved fluctuations present in the particle simulations and DKTE. We find that this noise enhances front-propagation speed in systems with density-dependent diffusivity, accelerates the onset of pattern formation in particle systems with nonlocal interactions, and reduces hysteresis in systems interacting via repulsive forces. In some cases, it accelerates transitions or induces structures absent in deterministic models. These findings illustrate that (conservative) fluctuations can have constructive and nontrivial effects, emphasizing the importance of stochastic modeling in understanding collective particle dynamics.

Figure 1 shows an example comparing configurations at long times for the dynamics of a system of 20000 particles interacting with a soft-core repulsive potential $V(r) \propto \exp[-|\mathbf{r}/R|^3]$ [4, 5] showing the similarities and differences between the direct particle simulation, the stochastic DKTE description and its deterministic approximation.

[1] F. Cornalba, J. Fischer, J. Ingmanns, and C. Raithel, *Density fluctuations in weakly interacting particle systems via the Dean–Kawasaki equation*, Ann. Probab. **54**, 155 (2026).

[2] F. Cornalba and J. Fischer, *The Dean-Kawasaki equation and the structure of density fluctuations in systems of diffusing particles*, Arch. Ration. Mech. Anal. **247**, 76 (2023).

[3] N. Wehlitz, M. Sadeghi, A. Montefusco, C. Schütte, G.A. Pavliotis, and S. Winkelmann, *Approximating particle-based clustering dynamics by stochastic PDEs*, SIAM J. Appl. Dyn. Syst. **24**, 1231 (2025).

[4] N.O. Silvano, E. Hernández-García, C.López, *Impact of fluctuations on particle systems described by Dean-Kawasaki-type equations*, Phys. Rev. E **113**, 044122 (2026).

[5] J.-B. Delfau, H. Ollivier, C. López, B. Blasius, and E. Hernández-García, *Pattern formation with repulsive soft-core interactions: Discrete particle dynamics and Dean-Kawasaki equation*, Phys. Rev. E **94**, 042120 (2016).

Catch bond me if you can: towards a unified view of B-cell receptor binding

Juan Iribas[1], Miguel García-Sánchez[2], José Faro[3], and Mario Castro[1]
[1]Universidad Pontificia de Comillas, Madrid, Spain
[2]NTT DATA Europe and Latam, Spain
[3]Universidade de Vigo, Vigo, Spain

As represented in Fig. 1, molecular bonds present two distinct behaviours when exposed to external forces: rapid rupture, known as slip bond, or enhancement of the bond's duration, known as catch bond. Slip bond behaviour is directly derived from Bell's theory [1]. As for catch bonds, multiple phenomenological mechanisms have been proposed, successfully fitting experimental lifetime-force curves. However, this variety and complexity of models shrouds the intrinsic assumptions and hinders the ability to extract meaningful information from the data.

In this work, we classify the aforementioned models and present our own cooperative force-driven proofreading model (CFPR); a mechanistic attempt to understand quantitatively both bond regimes in the context of B-cell receptors (BCRs), in which the pulling geometry enables additional bond formation. To illustrate our results, Fig. 2 highlights combinations of this model's parameters which induce slip bond and catch bond regimes.

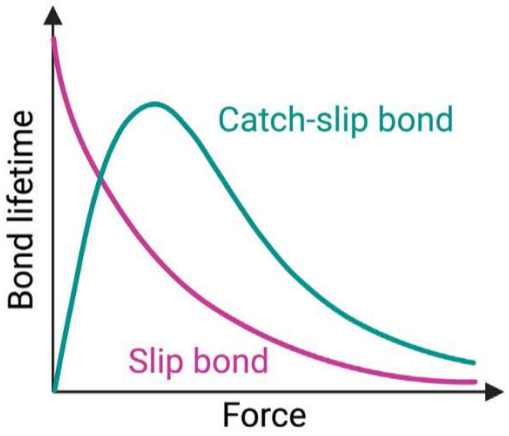

Fig. 1: Bond regimes

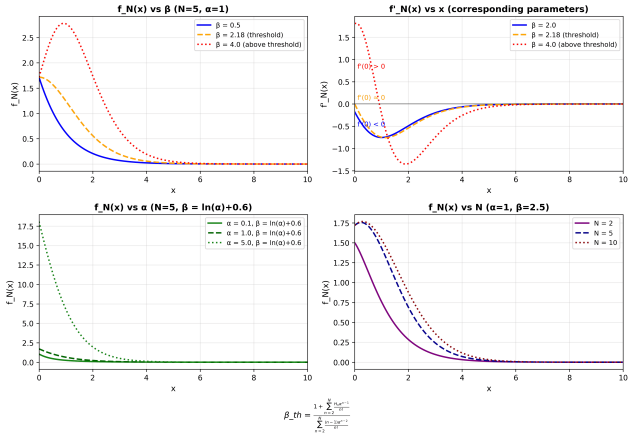

Fig. 2: Parameter combinations inducing bond regimes

[1] G. Bell, *Models for the Specific Adhesion of Cells to Cells*, Science **200**, 618–627 (1978).
[2] J. Rogers, A. Bajur, K. Salaita, and K. Spillane, *Mechanical control of antigen detection and discrimination by T and B cell receptors*, Front. Immunol. **123**, 2239 (2024).
[3] J. Faro, and M. Castro, *Affinity Selection in Germinal Centers: Cautionary Tales and New Opportunities*, Cells **10**, 1040, (2021).

Erlangian approximations of time-inhomogeneous continuous-time Markov chains with finite state space

Antonio Gómez-Corral[1], and Javier Jarillo[1]
[1]Department of Statistics and Operations Research, Complutense University of Madrid,
Plaza de Ciencias, 3, 28040–Madrid, Spain

We present a procedure for the numerical evaluation of transition probabilities at an arbitrary time-horizon T of continuous-time Markov chain (CTMC) models $\mathscr{X} = \{X(t) : t \geq 0\}$ with time-dependent transition rates $q_{x,x'}(t)$ and finite state space $\mathscr{S}$. The standard approach approximates the original CTMC by a piecewise time-homogeneous CTMC with constant transition rates over L intervals of equal length T/L, reducing the computation of transition probabilities to a product of matrix exponentials — an operation that becomes costly when the state space is large. We propose an alternative Erlangian approximation, where the time intervals have random exponentially-distributed lengths whose sum converges to T. Under this scheme, the transition probabilities are obtained via a product of matrix inverses rather than matrix exponentials, which is computationally more efficient, particularly for large state spaces. We illustrate this approach with numerical examples in SIS and SIR epidemic models, comparing both approximations against direct numerical computation. Both methods yield accurate estimates of the transition probabilities; the piecewise approximation typically requires fewer intervals but at a higher computational cost per interval, whereas the Erlangian approximation requires more intervals but each at a lower cost. For small state spaces either method suffices, but for large state spaces the Erlangian approximation may be more suitable.

Mobility-Induced Phase Separation in Binary Active Brownian Particle Mixtures

Daniel Jiménez Flores[1]
[1]Universidad de Sevilla

In this work, we report Brownian dynamics simulations of mobility-induced phase separation (MIPS) in a two-dimensional binary mixture of active soft Brownian particles. Particle interactions are modeled through non-additive Weeks–Chandler–Andersen potentials inspired by the Lennard–Jones interactions commonly used in glass-forming passive mixtures.

The structural properties of the coexisting phases are characterized by means of the radial distribution functions and the hexatic order parameter. Our results reveal that, unlike the monocomponent system, where the dense coexisting phase exhibits solid-like order, the high-density phase in the binary mixture remains spatially disordered.

To further characterize the dynamical properties of the system, we analyze the mean-square displacement of the active particles. We find that both the low-density and high-density coexisting phases display diffusive behavior at long times, indicating that the dense phase is liquid-like in the binary mixture. Interestingly, diffusive dynamics are also observed in the high-density solid-like phase of the monocomponent system. This behavior is associated with the presence of active topological defects, which promote particle transport within the ordered structure.

These findings show that binary interactions significantly modify the structural nature of the dense MIPS phase while preserving long-time diffusion, highlighting the rich interplay between activity, phase separation, and local ordering in active matter systems.

Chaos and its scalar embedding in neural network training

Pedro Jiménez-González[1], Miguel C. Soriano[1], and Lucas Lacasa[1]
[1]Institute for Cross-Disciplinary Physics and Complex Systems (IFISC, CSIC-UIB),
Campus UIB, 07122 Palma de Mallorca, Spain

Artificial neural networks define high-dimensional nonlinear dynamical systems whose optimization processes remain only partially understood. Despite their remarkable empirical success, the mechanisms governing how neural networks explore parameter space, converge towards minima, and generalize are still open questions from the perspective of dynamical systems theory.

Recent works have shown that neural network optimization can exhibit chaotic transient behavior, with sensitivity to initial conditions emerging in specific learning rate regimes and being closely related to efficient learning. In particular, in our recent work [1], we showed that neural networks trained close to the onset of chaos display positive Lyapunov exponents together with faster convergence towards high validation accuracy, suggesting a nontrivial connection between chaotic dynamics and optimization performance (see Fig. 1). These observations motivate the search for geometric representations capable of characterizing neural network optimization beyond conventional observables such as loss or accuracy.

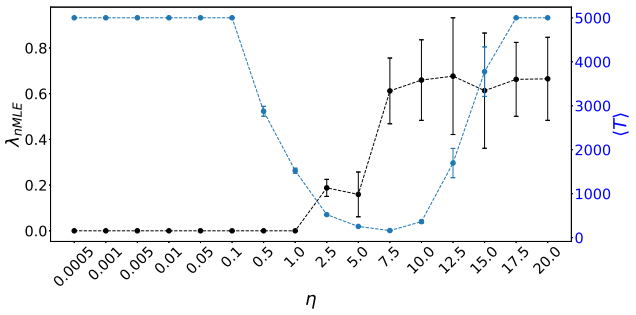

Fig. 1: Maximum Lyapunov exponent and average training time as functions of the learning rate. The left y-axis shows the average maximum Lyapunov exponent, estimated from perturbed training trajectories initialized within an ε-ball of radius $\varepsilon = 10^{-8}$ around a reference network initialization. The right y-axis shows the average number of training epochs required to reach a validation accuracy of 90% on the MNIST dataset. Results are averaged over 50 independent initial conditions. The figure highlights that the most efficient learning regimes coincide with the emergence of positive Lyapunov exponents.

Motivated by this connection between chaos and optimization, we use the scalar embedding framework introduced in [2] to study neural network training trajectories from a geometric and dynamical perspective. By constructing low-dimensional scalar representations of the evolution of the network weights, we analyze the divergence of nearby trajectories, define embedding-based decorrelation times, and investigate the organization of asymptotic training states (minima). We show that the scalar embedding captures the same qualitative dynamical regimes identified through the Lyapunov analysis in the high-dimensional parameter space while providing an interpretable representation of the training process. In particular, the scalar embedding allows us to characterize the statistical structure of the asymptotic training states through the spacings Δ between neighboring embedded minima. As shown in Fig. 2, although the raw spacing distributions vary across different initial conditions, an appropriate rescaling by the mean spacing leads to a collapse onto a common distribution. This result suggests the emergence of robust geometric organization and possible universal structure in neural network optimization dynamics [3].

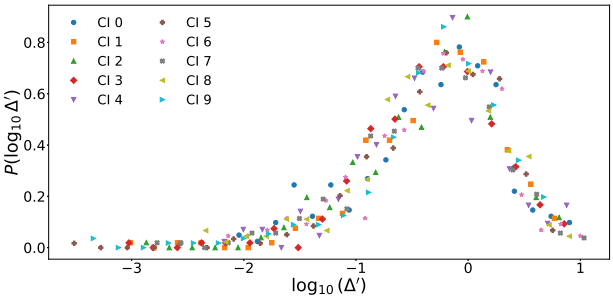

Fig. 2: Probability distribution of the rescaled spacings $\Delta' = \Delta/\langle\Delta\rangle$ between neighboring asymptotic embedded minima for different network initial conditions. While the raw spacing distributions display noticeable variability across initializations, the rescaled distributions collapse onto a common functional form, suggesting the emergence of universal statistical structure in the organization of neural network minima.

[1] P. Jiménez-González, M. C. Soriano, and L. Lacasa, *Leveraging chaotic transients in the training of artificial neural networks*, Phys. Rev. Res. **8**, L022032 (2026).

[2] L. Lacasa, F. J. Marín-Rodríguez, N. Masuda, and L. Arola-Fernández, *Scalar embedding of temporal network trajectories*, Chaos Solitons Fractals **199**, 116599 (2025).

[3] P. Jiménez-González, M. C. Soriano, and L. Lacasa, *Scalar representations of neural network training dynamics*, In preparation (2026).

Soluciones normales locales de la ecuación cinética de Boltzmann

Nagi Khalil[1,2] and Jorge Bravo-Gadea[1]
[1]Departamento de Física y Matemáticas, Universidad de Alcalá, 28805 Alcalá de Henares, España
[2]Grupo Interdisciplinar de Sistemas Complejos (GISC)

La Teoría Cinética proporciona un marco teórico que permite conectar la dinámica microscópica de un sistema de partículas con una descripción hidrodinámica del mismo, basada en unos pocos observables. Para un sistema clásico con N partículas idénticas, tal conexión se lleva a cabo a través de la ecuación cinética de Boltzmann (EB) para la función de distribución $f(\boldsymbol{r},\boldsymbol{v},t)$. Esta función es proporcional a la densidad de probabilidad de encontrar a una partícula cualquiera en la posición $\boldsymbol{r}$, con velocidad $\boldsymbol{v}$ en el tiempo t; y tiene norma respecto de $\boldsymbol{r}$ y $\boldsymbol{v}$ igual a N. Cuando la dinámica microscópica de las partículas viene dada por una evolución libre de colisiones salpicada de interacciones localizadas en el espacio y el tiempo, entonces las EB se pude escribir como

$$\partial_t f + \boldsymbol{v}\cdot\boldsymbol{\nabla} f + \boldsymbol{g}\cdot\boldsymbol{\nabla}_{\boldsymbol{v}} f = J,$$

donde $\boldsymbol{g}$ es un campo externo (fuerza por unidad de masa) y J es un operador de colisión: una función de $\boldsymbol{r},\boldsymbol{v}$ y t y un funcional de f. Esta ecuación supone la ausencia de correlaciones justo antes de las colisiones.

Asumiendo que las magnitudes hidrodinámicas son momentos de la función de distribución, es posible obtener sin mucha dificultad ecuaciones de balance a partir de la EB. Para la densidad de partículas $n = \int d\boldsymbol{v}\, f$, el campo de velocidad $\boldsymbol{u} = \frac{1}{n}\int d\boldsymbol{v}\,\boldsymbol{v} f$ y la temperatura $T = \frac{1}{d}\int d\boldsymbol{v}\,(\boldsymbol{v}-\boldsymbol{u})^2 f$, con d la dimensión del sistemas, las ecuaciones de balance son:

$$\begin{aligned}
&\partial_t n + \partial_{\boldsymbol{r}}\cdot(n\boldsymbol{u}) = 0,\\
&n\partial_t \boldsymbol{u} + n\boldsymbol{u}\cdot\partial_{\boldsymbol{r}}\boldsymbol{u} + \partial_{\boldsymbol{r}}\cdot P - n\boldsymbol{g} = \boldsymbol{0},\\
&n\partial_t T + n\boldsymbol{u}\cdot\partial_{\boldsymbol{r}} T + 2P:\partial_{\boldsymbol{r}}\boldsymbol{u} + \frac{2}{d}\partial_{\boldsymbol{r}}\cdot\boldsymbol{q} + \zeta T = 0,
\end{aligned}$$

donde se ha supuesto que las colisiones (y por tanto J) conservan el número de partículas, el momento lineal, pero no la energía en general. Las nuevas cantidades son el tensor de presiones P, el flujo de $\boldsymbol{q}$ y la tasa de enfriamiento ζ. La primera y la segunda se obtienen a partir de momentos de f mientras que ζ se puede expresar a partir del segundo momento de J.

Las ecuaciones de balance proporcionan una descripción hidrodinámica del sistema si somos capaces de expresar los nuevos términos, P, $\boldsymbol{q}$ y ζ, como función de los campos hidrodinámicos, n, $\boldsymbol{u}$ y T. Para ello, es suficiente con tener una **solución normal** $f[\boldsymbol{v}|n(\boldsymbol{r},t),\boldsymbol{u}(\boldsymbol{r},t),T(\boldsymbol{r},t)]$, esto es, una función de distribución solución de la EB cuya dependencia en $\boldsymbol{r}$ y t es a través de su dependencia funcional en los campos hidrodinámicos.

En este trabajo se identifican todas las **soluciones normales locales** de la EB con la siguiente propiedad de escala

$$f = n(2T)^{-\frac{d}{2}}\phi(\boldsymbol{c})$$

donde ϕ es una nueva función y $\boldsymbol{c} = (\boldsymbol{v}-\boldsymbol{u})/\sqrt{2T}$. Para ello, se supone que el operador de colisión cumple $J[\boldsymbol{r},\boldsymbol{v},t|f] = n^2(2T)^{(1-d)/2}J[\boldsymbol{c}|\phi]$. Esta forma de la solución normal es la más sencilla, pues se supone una dependencia funcional en los campos local (sin gradientes ni integrales).

Cada una de las soluciones normales locales identificadas está asociada a una hidrodinámica determinada, es decir, con una dependencia espaciotemporal de n, $\boldsymbol{u}$ y T concretas, lo que en algunos casos también determina la forma del potencial externo. En particular, para todas las soluciones, n y T sólo pueden variar espacialmente a lo largo de una dirección espacial, a lo sumo. Dependiendo de la forma concreta del operador de colisión, se pueden encontrar soluciones conocidas: la de equilibrio, el HCS y USF de gases granulares, etc.

Intermediate phenotypic heterogeneity creates an optimal coexistence window in bacteria–phage communities

Jung-Ho Kim[1], Mattia Mattei[1], David Soriano-Paños[1], and Alex Arenas[1]
[1]Departament d'Enginyeria Informàtica i Matemàtiques, Universitat Rovira i Virgili, Tarragona, Spain.

Phenotypic heterogeneity can expand ecological niche space even within a genetically homogeneous population. Recent experiments showed that growth-rate heterogeneity in a clonal bacterial host can stabilize coexistence among multiple phages [1]. Yet this discovery leaves unresolved whether increasing host heterogeneity monotonically promotes coexistence. Here we show that it does not. Using a trait-based bacteria–phage coexistence framework, we find that phage richness is maximized at an intermediate scale of host growth-rate heterogeneity, determined by the match between host phenotypic dispersion and phage niche width. Our results show that optimal phage diversity emerges from an ecological trade-off between two competing effects: increasing phenotypic heterogeneity enables niche differentiation but eventually reduces the host abundance in the preferred niche of each phage. Therefore, our findings predict that experimentally increasing host growth-rate variance at a fixed mean growth rate should produce a nonmonotonic phage richness response, providing a quantitative principle for how intraspecific phenotypic variation shapes biodiversity in microbial ecosystems.

[1] N. C. Pyenson, *et al*. *Diverse phage communities are maintained stably on a clonal bacterial host*, Science. **386**, 6727 (2024).

Genotype networks drive oscillating endemicity and epidemic trajectories in viral evolution

Santiago Lamata-Otín[1], Octavian C. Rotita-Ion[1], Alex Arenas[2]
David Soriano-Paños[2] and Jesús Gómez-Gardeñes[1]

[1]Department of Condensed Matter Physics, University of Zaragoza, Zaragoza, Spain
[2]Departament d'Enginyeria Informàtica i Matemàtiques, Universitat Rovira i Virgili, 43007 Tarragona, Spain

Rapidly evolving viruses persist in real populations through antigenic drift, continuously escaping host immunity [1]. Most eco-evolutionary models represent antigenic space as low dimensional, and this assumption is at odds with genomic surveillance data, which reveal that viral evolution should be better captured by complex genotype networks with modular and heterogeneous structure.

In our work [2,3], we introduce an eco-evolutionary epidemic framework in which viral mutation, immune memory, and cross-immunity dynamics are explicitly shaped by the topology of antigenic genotype networks.

Using synthetic genotype networks, we show how the topology of antigenic space alone can determine long-term epidemic behavior. In particular, modular genotype networks composed of interconnected mutant swarms naturally generate recurrent oscillatory endemic trajectories, whereas low-dimensional homogeneous lattice-like antigenic spaces lead to stable endemic equilibrium (see Fig. 1). Importantly, this qualitative difference emerges without requiring external seasonal forcing.

Then, we connect these results to real data by applying the model to the genotype network of Influenza A (H3N2). We show how its modular organization in mutant swarms gives rise to complex epidemic trajectories characterized by lineage turnover, closely resembling patterns observed in genomic surveillance data. Finally, we show that the model is able to partially reconstruct the empirical epidemic trajectory, recovering the temporal ordering of strain emergence observed in genomic surveillance data.

Overall, the topology of genotype networks is a key ingredient for describing and predicting long-term viral dynamics.

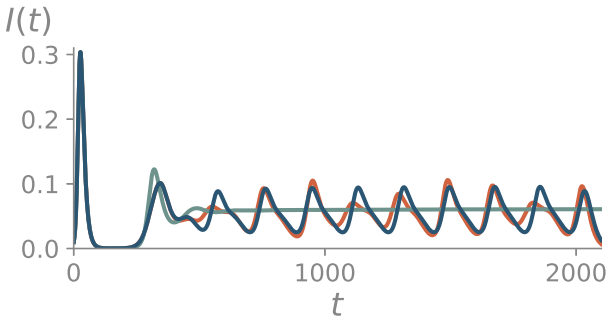

Fig. 1: Epidemic trajectories $I(t)$ obtained for synthetic antigenic genotype networks with different topologies. Modular networks formed by interconnected mutant swarms display sustained oscillatory endemic dynamics, whereas the homogeneous lattice approaches a stable endemic state.

[1] P. V. Markov et al., *The evolution of SARS-CoV-2*, Nature Reviews Microbiology **21**, 361–379 (2023).

[2] S. Lamata-Otín et al., *Genotype networks drive oscillating endemicity and epidemic trajectories in viral evolution*, Communications Physics **8**, 502 (2025).

[3] S. Lamata-Otín et al., *Interplay between evolutionary and epidemic time scales challenges the outcome of control policies*, arXiv:2603.18801 (2026).

Group dynamics shape contagion onsets and multistable active phases under collective reinforcement

Santiago Lamata-Otín[1,2], Federico Malizia[3], Leah A. Keating[2], Guillaume St-Onge[4]
Vito Latora[5], Jesús Gómez-Gard eñes[1] and Laurent Hébert-Dufresne[2]

[1]Department of Condensed Matter Physics, University of Zaragoza, Zaragoza, Spain
[2]Vermont Complex Systems Institute, University of Vermont, Burlington, VT, USA
[3]Department of Network and Data Science, Central European University, Vienna, Austria
[4]Laboratory for the Modeling of Biological and Socio-technical Systems, Northeastern University, Boston, MA, USA
[5]School of Mathematical Sciences, Queen Mary University of London, London, United Kingdom

In social systems, contagion processes strongly depend on group (higher-order) interactions, where peer influence plays a key role in the adoption of ideas, beliefs, and technologies. Previous studies have shown that changes in group synergy can lead to discontinuous transitions [1]; however, most works assume static interaction structures and rely on aggregated temporal data.

In this work [2], we introduce a mathematical model of complex contagion with group switching that explicitly accounts for the temporal evolution of higher-order interactions. Using Approximate Master Equations, we obtain numerical and analytical results describing how time-varying group structure shapes collective dynamics.

We first show that increasing group switching transforms the contagion transition from continuous to discontinuous, enlarging the bistable region. Remarkably, we have derived implicit analytical expressions for both the invasion threshold and the tricritical point separating continuous and bistable regimes. Notably, the invasion threshold interpolates smoothly between the quenched (static) limit [3] and the annealed (mean-field) limit.

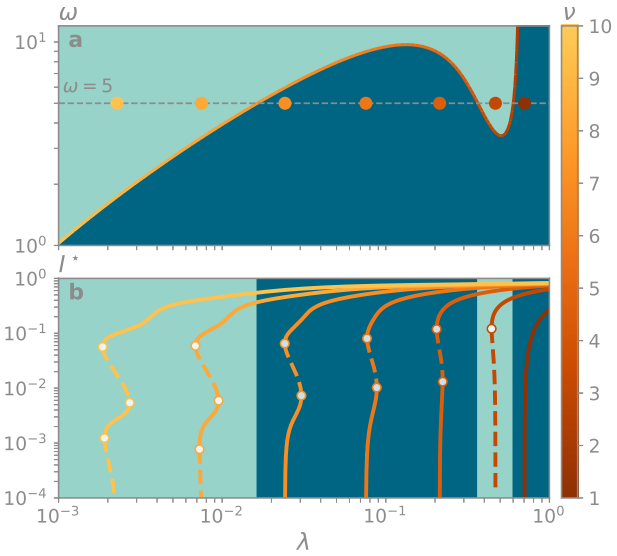

Fig. 1: **a** Phase portrait highlighting the tricritical line and the invasion threshold, using the group size distribution of the high school dataset. **b** Phase diagram showing the stationary prevalence ($I^\star$) as a function of the contagion rate (λ) and synergy (ν), for a group switching rate $\omega = 5$ and recovery rate $\mu = 1$. Solid (dashed) lines indicate the stable (unstable) branch.

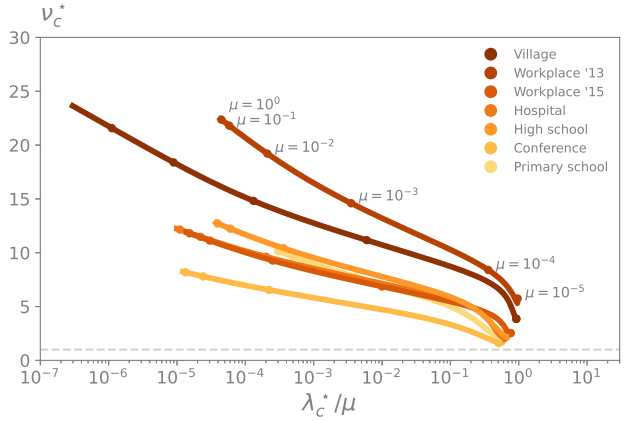

Fig. 2: Empirical tricritical points for different contagion timescales (determined by the recovery rate μ) and datasets. Colored curves show how the critical point moves as the group switching rate ω is swept from the quenched (static) to the annealed (mean-field) regime, and markers indicate the position corresponding to the empirically measured group switching rate.

We then incorporate key features of real interaction data, including heterogeneous group sizes and empirical switching rates. In this setting, multiple tricritical points can emerge for a given group switching rate (see Figure 1), separating four phases characterized by the combination of localized (large-group-driven) versus delocalized activity, and continuous versus discontinuous transitions. Remarkably, in localized regimes, we observe multistable active phases, where multiple endemic states coexist beyond classical bistability.

Finally, we assess the nonlinearities required for empirical datasets to exhibit discontinuous transitions (see Figure 2). We show that these critical values depend strongly on the timescale of the contagion dynamics and are systematically higher than those inferred in the literature from static, aggregated representations. This highlights how neglecting temporal group structure can lead to misleading predictions in contagion modeling.

[1] F. Malizia*, S. Lamata-Otín* et al., *Hyperedge overlap drives explosive transitions in systems with higher-order interactions* Nature Communications **16**, 555 (2025).

[2] S. Lamata-Otín et al., *Group dynamics shape contagion onsets and multistable active phases under collective reinforcement*, arXiv:2603.28566 (2026).

[3] G. St-Onge et al., *Influential groups for seeding and sustaining nonlinear contagion in heterogeneous hypergraphs* Communications Physics **5**, 25 (2022).

Probabilistic network alignment applied to brain connectomes

Teresa Lázaro[1], Roger Guimerà[1],and Marta Sales-Pardo[1]
[1]URV, teresa.lazaro@urv.cat

The network alignment problem, which seeks to find correspondence mappings between two or more graphs, is a widely studied open problem. Recent advances in connectomics have created a demand for tools to compare these datasets[1][2], since identifying mappings between neurons across brains is a challenging and non-trivial task. Current approaches to network alignment mainly focus on pairwise alignment, which, while useful, often fails to capture the full complexity and variability of multiple networks.

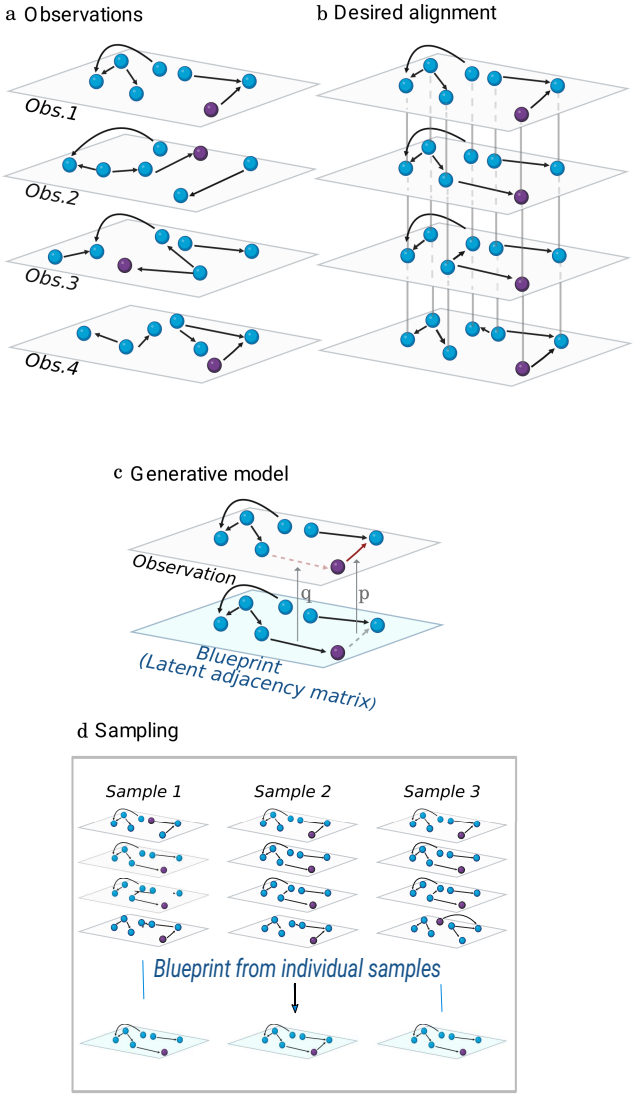

Fig. 1: (**a-b**) Scheme of the network alignment problem. **c** Proposed generative model for our Bayesian inference approach. **d** Sampling over some possible alignments during the maximization of the posterior.

Here, we address this limitation with a probabilistic method based on Bayesian inference, enabling the simultaneous alignment of multiple graphs. We assume the existence of an underlying blueprint for the connectome graph of a given species, $\mathbf{L}$, such that the brain of k of that species, $\mathbf{A}^k$, is a noisy copy of $\mathbf{L}$ with error level q and a permutation $\{\pi^k\}$ of its node labels. In this probabilistic framework, the problem of finding the best alignment reduces to maximizing the posterior probability $p(\mathbf{L}, \{\pi^k\}|\{\mathbf{A}^k\})$, derived from Baye's theorem. To sample this posterior probability we use a Markov chain Monte Carlo (MCMC) algorithm with Parallel Tempering.

Our method has been effectively applied to both weighted and unweighted graphs, achieving improvements over the current state-of-the-art. For example, in the case of four *C. elegans* connectomes with 224 neurons, our approach achieved an accuracy of 86.4%, surpassing the $56 \pm 2\%$ accuracy achieved by the multi-way KerGM[4]. Similarly, for the two hemispheres of the larval *D. melanogaster* with 1,235 neurons, our method achieved an accuracy of 79.2%. This results outperforms as well the $69.48 \pm 0.07\%$ of KerGM[4] and it is slightly better than the 79.2% accuracy of Fast QAP method[3], which is limited to pairwise network alignment.

Additionally, the interpretability of the Bayesian framework allows us for adapting the model to various scenarios, such as graphs with group annotations - feature particularly relevant for neuroscientists studying larger brains, like the adult *D. melanogaster*, highlighting the synergistic potential of this work. Furthermore, we have recently expanded our approach to handle networks with varying numbers of nodes and unannotated nodes. These advancements are particularly promising for real-world data, especially in neuroscience, where some neurons may be missing from brain to brain due to experimental limitations or biological variation accross individuals.

[1] Daniel Witvliet, et al. *Connectomes across development reveal principles of brain maturation.*, Nature, August 2021
[2] Winding M, Pedigo BD, et al. *The connectome of an insect brain.*, Science, 379(6636): eadd9330.
[3] Joshua T. Vogelstein, et al.*Fast Approximate Quadratic Programming for Graph Matching.*, PLOS ONE, April 2015.
[4] Dupé, Fet al. Proceedings of The 14th Asian Conference on Machine Learning, vol. 189 of Proceedings of Machine524 Learning Research, 311–326 (PMLR, 2023)

Coevolution of structure and function in cultured neuronal networks

I. Leyva[1,2], L.M. Ballesteros-Esteban[1,2], J.A. Almendral [1,2] and I. Sendiña-Nadal[1,2]
[1]Complex Systems Group & GISC, Universidad Rey Juan Carlos, Calle Tulipán s/n, Móstoles, 28933, Madrid, Spain
[2]Center for Biomedical Technology, UPM Campus Montegancedo, Pozuelo de Alarcón, 28223, Madrid, Spain

The interplay between structural organization and functional dynamics is a central problem in network science and neuroscience. However, experimentally tracking the simultaneous evolution of both structure and function in neuronal systems remains challenging. In this field, cultured neuronal networks (CNNs) have recently gained major relevance as an more controlled *in vitro* alternative to *in vivo* models.

In the present study, we monitored the coevolution of structural and functional connectivities of neuronal cultures grown on microelectrode arrays (MEAs), in a setup that allows the simultaneous recording of electrophysiological signals and microphotography detailed to the single-link level (Fig.1 (a)). Using an *ad hoc* image segmentation algorithm [1, 2], we detected neurons and neurites in real space (b) and mapped them into the electrode space (c), which can be represented as adjacency matrices that can be directly compared to their functional counterparts.

During the three-week development of the cultures, initially isolated neurons self-organize into a highly clustered circuitry of neuronal aggregates [1, 2]. In parallel, synchronization events extracted from electrode recordings reveal the emergence of coherent collective activity. The average synchronization reaches a maximum close to the structural percolation transition of the network. To quantify the structure–function relationship, we compare the physical connectivity with the functional network inferred from synchronized firing events. The correlation R between both layers peaks during the percolation stage, when approximately 15% of structural links support synchronous activity between electrodes. As cultures mature, the absolute correlation slightly decreases but its statistical significance increases (Fig. 1 (d)). At the local level, we find that the functional hubs that mainly sustain the coherent activity are not the structural hubs but nodes with intermediate degrees [2]. This result suggests that even in very simple cases such as the CNNs cultures, one should be cautious when extrapolating the functional features to the underlying unknown topology.

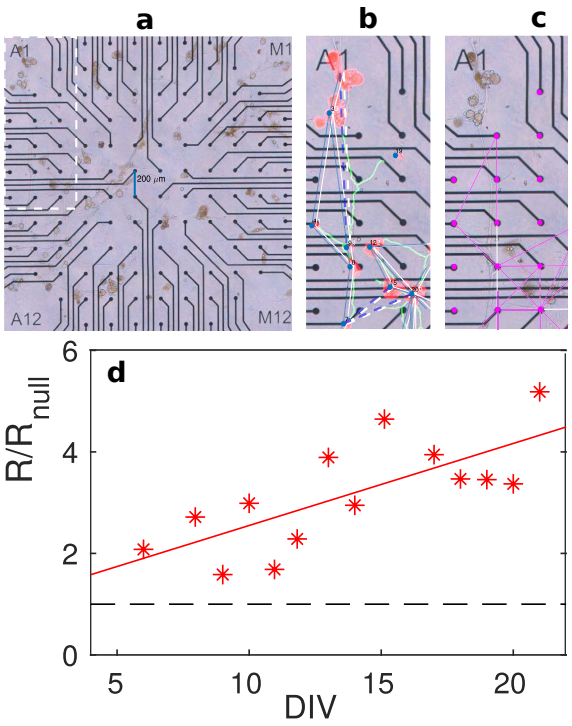

Fig. 1: (a) Snapshot of a neuronal culture grown on top of a microelectrode array (MEA) (b) Image segmentation of the marked region in (a), with detected neurons (red), neurites (green) and the proyected adjacency matrix (blue), (c) Electrode-space graph projection, (d) Null-normalized structure–function correlation vs. days in vitro

To the authors' knowledge, this is the first study of the coevolution of structure and dynamics in self-organized cultured neuronal networks to the level of single links. It opens the way for future investigations aimed at elucidating the intricate relationship between structure and function in other scenarios, including those mediated by external stimulation.

[1] D. de Santos-Sierra, I. Sendiña-Nadal, I. Leyva et. al. *Graph-based unsupervised segmentation algorithm for cultured neuronal networks' structure characterization and modeling*, Cytometry Part A **87**, 513, 2015.

[2] L.M. Ballesteros-Esteban, I. Leyva, J. A. Almendral, I. Sendiña-Nadal, *Self-organization and evolution of structure and function in cultured neuronal networks*, Chaos, Solitons & Fractals **173**, 113764, 2023.

Polarization patterns in ferroelectric materials

Juan M. López[1],
[1]Instituto de Física de Cantabria, CSIC-Universidad de Cantabria, Santander, Spain

There is an outburst of theoretical and experimental activity in the field of topological phases in ferroelectric superlattices [1]. These are nano-scale multilayer thin film systems exhibiting ferroelectricity with interesting emergent pattern formation phenomena [2]. The emergence of these polarization textures is driven by nonlinear instabilities controlled by parameters as elastic strain and external electrical field. The role of spin in ferromagnets is played by the local polarization in these ferroelectrics leading to ordered phases, domain walls, and large scale patterns, depending on strain and temperature. Interestingly, phases with long-range order include stripes, squares, hexagons, zig-zag structures, and labyrinths. Currently, there is great research activity, both experimental and numerical, to explain and control of all these patterns and forms [2]. These polarization textures remind of those that appear in nonlinear spatially extended systems driven away from equilibrium. In this contribution we start from the fundamental Devonshire hamiltonian of a ferroelectric crystalline solid and we derive a Ginzburg-Landau model for the polarization to describe the onset of instability and the emergence of polarization structures. The model correctly describes that the homogeneous state of zero polarization $\langle P \rangle = 0$ (paraelectric phase) is unstable to perturbations of a wavelength ξ_c. This mode can get excited by applying an external electric field. The simplest GL model able to describe ferroelectricity also predicts instabilities in the form of domains or stripes with alternating polarization, dots or bubbles organized in square and hexagonal lattices. The model complexity may be progressively increased to include elasticity, flexoelectricity, Dzyaloshinskii-Moriya interaction, etc to produce more complex structures.

Acknowledgments: This work was supported by Grant No. PID2021-125543NB-I00 funded by MCIN/AEI Spain

[1] Ramesh, R., Schlom D.G, Nat. Rev. Mat. **4**, 257–268 (2019). Creating emergent phenomena in oxide superlattices

[2] J. Junquera *et al.*, Rev. Mod. Phys. **95**, 025001 (2023). Topological phases in polar oxide nanostructures.

[3] Cross M.C. and Hohenberg P.C., Rev. Mod. Phys. **65**, 851 (1993). Pattern formation outside of equilibrium.

Transcriptional dynamics induced by competition for resources

Judith López Zancajo, José María Sancho and Marta Ibañes
Universitat de Barcelona, Facultat de Física, Carrer de Martí i Franqués, 1 - 11, 08028 Barcelona
Universitat de Barcelona Institute of Complex Systems (UBICS), Carrer de Martí i Franqués, 1 - 08028 Barcelona

What determines the dynamics of gene networks? The long-standing interpretation has been modular and, as such, the scientific community has focused on building a catalogue of minimal design principles that are able to produce specific transcriptional dynamics [1]. For instance, it is known that negative feedback loops can lead to oscillatory behaviour [1].

However, it is widely accepted that cells contain families of transcription factors that are able to participate in the same regulatory networks (redundancy) and, vice-versa, said transcription factors may take part in multiple regulatory networks (promiscuity). In a modular view, redundancy and promiscuity are commonly disregarded; it is assumed that shared resources are produced in such quantities that they are not limiting. Hence, gene circuits are thought to operate independently. But if the resource is not in abundance, then modules must compete for it and partitioning arises. This competition is known to modify transcriptional dynamics beyond the expectations of the design architecture of the network. As an example, when competing for a resource, pulsatile modules autoorganize to not pulse simultaneously [2].

Following this premise, we analyse how stochasticity and competition for resources reshape the dynamics of minimal circuits. Our results reveal that resource competition can lead to complex dynamical behaviours such as oscillations and excitability (behaviours not observed when the modules operate in isolation) and that stochasticity enhances said impact. Overall, our work aims to highlight the importance of taking into account promiscuity, redundancy and noise in the study of transcriptional dynamics.

Grant PREP2024-002668 funded by MICIU/AEI/10.13039/501100011033 and by "ESF+" to JLZ. Grant PID2024-161853NB-I00 funded by MICIU/AEI/10.13039/501100011033 and by "ERDF A way of making Europe" to MI.

[1] Alon, U. (2007). *Network motifs: theory and experimental approaches*. Nature Reviews Genetics, 8(6), 450–461.

[2] Park, J., Dies, M., Lin, Y., Hormoz, S., Smith-Unna, S. E., Quinodoz, S., Hernández-Jiménez, M. J., Garcia-Ojalvo, J., Locke, J. C. W., & Elowitz, M. B. (2018). *Molecular Time Sharing through Dynamic Pulsing in Single Cells*. Cell Systems, 6(2), 216-229.e15.

Dynamics of the Cournot-Stackelberg quantum game

J. Grau-Climent[1], L. Garcia-Perez[1], R. Alonso-Sanz[1], and Juan C. Losada[1],
[1]Complex Systems Group, Universidad Politécnica de Madrid, Avda. Puerta de Hierro 2, 28040 Madrid, Spain

In the standard Cournot duopoly [1], two firms choose quantities q_1 and q_2 simultaneously. The market price is given by a linear inverse demand function:

$$p = a - bQ, \quad Q = q_1 + q_2,$$

where $a > 0$ and $b > 0$. The profit (or utility) of firm i is $u_i = pq_i - c_i q_i = q_i(a - bQ - c_i)$, where c_i denotes the marginal cost of firm i.

The dynamical evolution of the quantities is governed by a bounded rational adjustment process given by

$$q_i(t+1) = q_i(t) + \alpha q_i(t)\Phi_i(t) = q_i(t) + \alpha q_i(t)\frac{\partial u_i(t)}{\partial q_i(t)},$$

where α is the speed of adjustment in the strategic decision-making process, and $\Phi_i(t)$ represents the marginal incentive based on local information.

In this work, we extend the classical model by introducing a sequential decision-making (Stackelberg structure) [2] and a quantum entanglement of strategies (Li-Du-Massar scheme) . Our model is formulated using backward induction at the level of expectations without introducing auxiliary variables such as aggregated announced quantities. The resulting dynamical system exhibits an intrinsic asymmetry: the leader's dynamics evolve independently of the follower, while the follower's dynamics depend explicitly on the leader's trajectory.

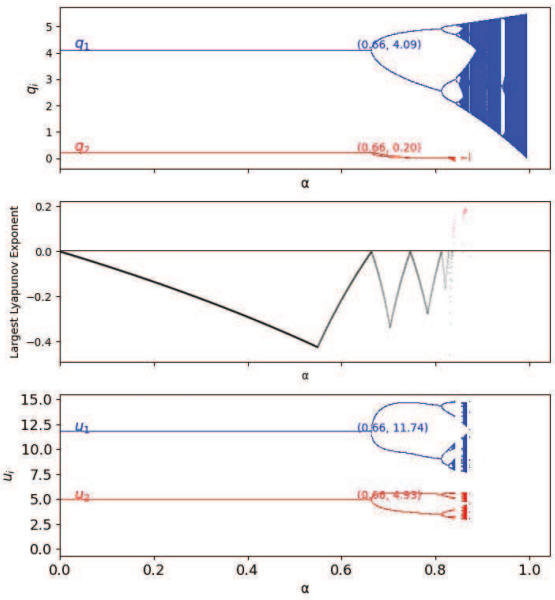

Fig. 1: Top: strategy bifurcation diagram; middle: Lyapunov maximum exponent; bottom: profit bifurcation diagram. $a = 10, b = 1, c_1 = c_2 = 1, \gamma = 0.4$.

The stability properties depend on the marginal costs c_1, c_2, the degree of entanglement γ, and the Cournot demand parameter a. When marginal costs are equal, both players lose stability simultaneously (see fig1). When costs differ, a rich variety of dynamical behaviors emerges, including asymmetric stability regions and bifurcation patterns (see fig2). In particular, the degree of entanglement can either enhance or reduce stability depending on the cost configuration, and in certain regimes the follower loses stability before the leader despite the Stackelberg hierarchy.

The interaction between sequential decision-making, quantum entanglement, and cost heterogeneity generates complex nonlinear dynamics that significantly extend the classical Cournot–Stackelberg results. Cost asymmetry plays a crucial role in shaping stability regions and bifurcation patterns, producing behaviors that are not present in the classical Cournot–Stackelberg setting.

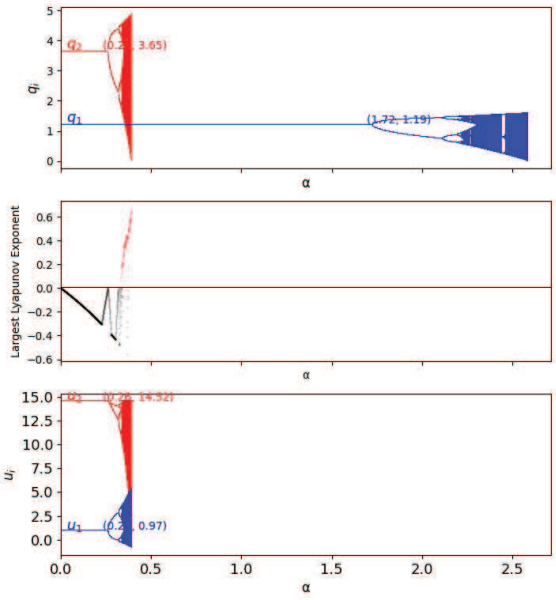

Fig. 2: Idem fig 1 whit $c_1 = 4.2, c_2 = 1, \gamma = 0.05$.

[1] Cournot, A. A. *Recherches sur les principes math´ematiques de la theorie des richesses* L. Hachette (1838).
[2] Von Stackelberg, H.F. *Marktform und Gleichgewicht*. J.Springer, Viena (1934).
[3] Li, H., Du, J., Massar, S. *Continuous-variable quantum games* Physics Letters A **306**, 73–78 (2002).

The Role of Saturation in Information Diffusion on Social Media

J. Atienza-Barthelemy[1], J.C. Losada[2], and R.M. Benito[2]
[1] Spanish National Research Council (CSIC), Madrid, Spain
[2]Complex Systems Group, Universidad Politécnica de Madrid, Avda. Puerta de Hierro 2, 28040 Madrid, Spain.

Online social networks have significantly transformed the way information is created, shared, and consumed. Since users can easily generate and disseminate news, opinions, and other content, the amount of information circulating on these platforms has increased enormously. As a consequence, users are exposed to an excessive volume of content, giving rise to the so-called saturation effect. In social networks, saturation refers to the overload of information that exceeds the cognitive processing capacity of individuals [1]. Understanding how this phenomenon influences information diffusion is therefore an important challenge [2].

In this work, we study information propagation on Twitter, currently known as X, where messages spread through a dynamic and decentralized followers network. Users can follow others without reciprocity, and each tweet becomes visible to all followers, who may further retweet it and propagate the content [3]. To analyze this process, we consider three case studies related to globally relevant events: the Fridays for Future protests in September 2019, the Spanish general elections in November 2019, and the U.S. presidential election in November 2020.

Our goal is to develop a model that connects user behavior with diffusion dynamics. Using data collected through the Twitter API, we investigate whether the saturation effect influences the probability that a user retweets a message. In particular, we analyze how this probability depends on the amount of information received by the user, which is assumed to be proportional to the number of accounts they follow.

The model focuses on the retweet rate Φ, defined as the probability that an Observer becomes a Spreader. In our framework, this quantity can be estimated as $\Phi = \frac{S}{O}$, where S and O represent the number of spreaders and observers, respectively. Since the level of saturation mainly depends on the incoming information flow, it is naturally related to the user's out-degree k_{out}. Figure 1 shows the relationship between k_{out} and the retweet rate Φ. Based on the empirical results, we propose a power-law dependence of the form $\Phi = ck_{out}^{\gamma}$, which provides a strong fit to the observed data.

We also examine the temporal profile of information spreading. Figure 2 shows the evolution of retweet activity over time. In all cases, retweet activity drops significantly after 16 hours, highlighting the short lifespan of tweets in a saturated environment. Our results underscore the competitive nature of information diffusion in social networks, where tweets have short useful life spans and are quickly replaced by new information.

These results confirm that saturation reduces the effectiveness of content dissemination and also influences the time scale and peak activity of cascades. Temporal analysis complements structural simulations by revealing how quickly attention fades.

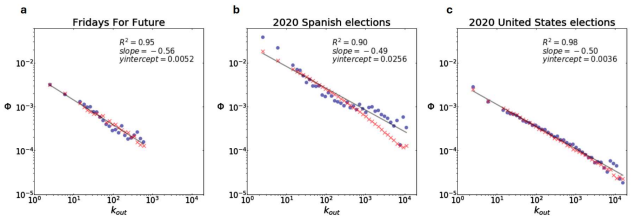

Fig. 1: The retweet rate Φ as a function of the number of people a user follows k_{out} for the experimental retweet network (blue dots) and the simulated retweet network (red x's). Then the straight line corresponds to the fit of the observed blue dots.

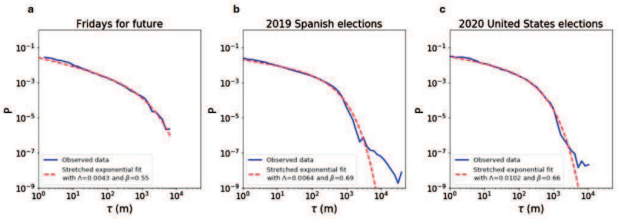

Fig. 2: Temporal evolution of the number of retweets. Each curve corresponds to the respective case study.

[1] Dhir, A., Kaur, P. & Chen, S. Social media fatigue and information overload: Understanding the effects on user behavior and mental health. Int. J. Inf. Manag. 40, 101–110 (2018).

[2] Atienza-Barthelemy, J.; Losada, J.C.; Benito, R.M. Modeling Information Diffusion on Social Media: The Role of the Saturation Effect. Mathematics 2025, 13, 963 (2025).

[3] Borondo, J., Morales, A. J., Benito, R. M. & Losada, J. C. Multiple leaders on a multilayer social media. Chaos, Solitons & Fractals 72, 90–98 (2015)

Non-equilibrium universality classes of interfaces in active phase coexistence

Raphaël Maire[0,1], Adhvik Jagannathan[1], Leonardo Galliano[2,3], Andrea Plati[1], Frank Smallenburg[1], Giuseppe Foffi[1], Ludovic Berthier[2,4]

[0]Departament de Física de la Matèria Condensada, Universitat de Barcelona, C. Martí Franquès 1, 08028 Barcelona, Spain
[1]Université Paris-Saclay, CNRS, Laboratoire de Physique des Solides, 91405 Orsay, France
[2]PSL Research University, CNRS, ESPCI Paris Gulliver, 75005 Paris, France
[3]Universita di Trieste, Dipartimento di Fisica Strada Costiera 11, 34151 Trieste, Italy
[4]Université de Montpellier, CNRS, Laboratoire Charles Coulomb (L2C), 34095 Montpellier, France

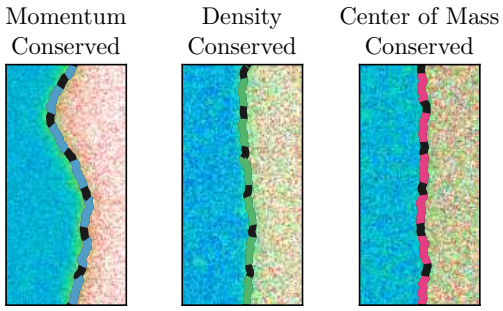

Fig. 1: Various interface fluctuation depending on the underlying conservation laws

In recent years, non-equilibrium interfaces such as those in motility-induced phase separation have attracted intense interest. Although striking non-equilibrium effects, including effective negative surface tension, have been reported, numerical studies have repeatedly found an apparently equilibrium-like interface spectrum, $S = \langle h_k h_{-k} \rangle \sim k^{-2}$.

In this talk, we introduce a new non-equilibrium particle system in which energy is injected during collisions. The particles are hard disks that dissipate energy through viscous drag during free flight, while acquiring variable energy upon impact. With interparticle attractions or density-dependent energy injection, the system phase separates, forming interfaces with a rich variety of non-equilibrium fluctuations.

Remarkably, when the two coexisting bulk phases are hyperuniform, interface fluctuations are strongly suppressed, giving $S \sim k^{-1}$ [1]. By tuning the driving mechanism and the underlying conservation laws, we also uncover regimes of enhanced fluctuations, $S \sim k^{-3}$, as well as behavior consistent with the recently identified qKPZ universality class (see Fig. 1) [2]. We further show that chirality can change the interface universality class. We fully explain this phenomenology by deriving an effective interface equation from the underlying order-parameter dynamics and using the renormalization group. All in all, we link the microscopic driving to emergent interfacial universality.

[1] Raphaël Maire, Leonardo Galliano, Andrea Plati, and Ludovic Berthier. Hyperuniform interfaces in nonequilibrium phase coexistence. *Physical Review Letters*, 135(22):227102, 2025.

[2] Raphaël Maire, Andrea Plati, Frank Smallenburg, and Giuseppe Foffi. Conservation laws and slow dynamics determine the universality class of interfaces in active matter. *Physical Review Letters*, 136(14):148301, 2026.

Optimising Seagrass Restoration Using Spatial Self-Organisation

Jorge Mampel Danta[1], Daniel Ruiz-Reynés[1], Núria Marbà[2], and Damià Gomila[1]
[1]IFISC (CSIC-UIB). Institut de Física Interdisciplinar i Sistemes Complexos, 07122 Palma, Mallorca
[2]IMEDEA (Institut Mediterrani d'Estudis Avançats) (UIB-CSIC), Miquel Marqués 21, 07190 Esporles, Mallorca

Seagrass meadows are declining globally due to anthropogenic pressures, making restoration a priority. Due to the logistical challenge of underwater work and the limited availability of shoots or seeds to plant, making the most out of this limited initial material is crucial. Meadows commonly develop spatial patterns driven by scale-dependent feedbacks which fundamentally alter the picture that might be given by linear or homogeneous models. We seek to include these dynamics to find the optimal distributions for a given initial amount of shoots, the one that best balances facilitation and competition, as well as non-local interactions. With this we will also explore thresholds relevant for restoratoin work.

We study this problem using a spatially extended model for shoot density $n \equiv n(\vec{x},t)$ [1]:

$$\begin{aligned}\partial_t n = & -\omega n + a n^2 - b n^3 + \varepsilon \nabla^2 n \\ & + \delta |\vec{\nabla} n|^2 + \alpha (\nabla^2 n) n + \beta (\nabla^4 n) n,\end{aligned} \tag{1}$$

where ω is the mortality rate, a and b encode local facilitation and competition, and the remaining terms capture spatial propagation and long-range interactions. The model is calibrated for *Cymodocea nodosa* using empirical growth and branching data.

The homogeneous bifurcation diagram of Eq. (1) features a bistable region between vegetated and bare-soil states, bounded by a saddle-node bifurcation at $\omega_{SN} = a^2/4b$. Above a Turing point ω_T, the homogeneous vegetated state destabilises and the system self-organises into spatial patterns. This extends resilience beyond the homogeneous tipping point through a sequence of patterned states — from periodic patterns to isolated localised patches — each corresponding to a distinct branch in the bifurcation diagram (Figure 1).

In this spatially extended setting, the survival threshold is no longer a single density value but a manifold in the space of vegetation distributions, defined by the stable manifold of the unstable localised state. We use the total initial growth rate $R = \int F[n(\vec{x})]\, d^2x$ as a the optimisation objective and pose the problem variationally: find the spatial distribution that maximises R subject to a fixed total number of shoots B_0, enforced via a Lagrange multiplier.

The optimal distribution resembles a localised patch but achieves successful establishment with fewer shoots than the unstable localised state, which is conventionally taken as the threshold. Its characteristic width is set by the intrinsic spatial scale of the self-organised patterns, suggesting that aligning planting interventions with the natural length scale of the meadow is key. As B_0 increases, the optimal strategy transitions from a single patch to spatially separated patches or a ring structure, indicating that there is a point of diminishing returns when forcing all shoots onto a single patch.

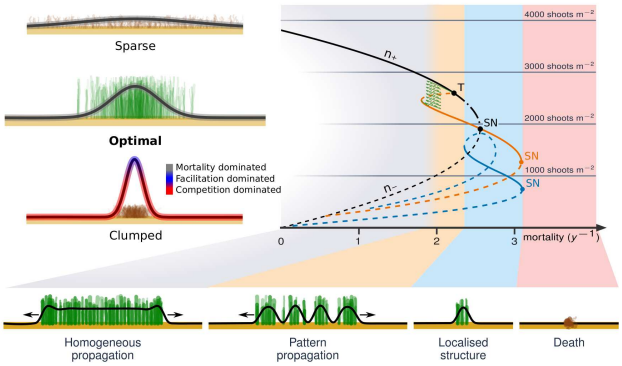

Fig. 1: Bifurcation diagram showing coexisting homogeneous, patterned, and localised states, and a sketch of how planting spread affects establishment outcome for a fixed number of shoots.

[1] D. Ruiz-Reynés et al., *Phys. Rev. Research* **2**, 023402 (2020).

From fiascos to sleeper hits: Predicting long-term movie reception patterns

Jaume Ojer[1], David March-Pons[2], and Michele Starnini[3],
[1]Institute for Cross-Disciplinary Physics and Complex Systems (IFISC, CSIC-UIB), 07122 Palma de Mallorca, Spain
[2]Dept. de Física, Universitat Politècnica de Catalunya, Campus Nord B4, 08034 Barcelona, Spain
[3]Department of Engineering, Universitat Pompeu Fabra, 08018 Barcelona, Spain

Understanding what drives the long-term success of creative works is a central challenge across the cultural industries. Throughout history, the evolution of art has been inseparable from the evolution of novelty: periods of heightened novelty redefined aesthetic norms, established new standards of artistic excellence, and reshaped audience expectations. Yet while certain works achieve enduring success by introducing novel styles and narratives, others fade despite showing technical mastery or cultural relevance [1]. Focusing on the cinematic industry, in recent years digital platforms and algorithmic recommendation systems have made audience attention an increasingly scarce resource, intensifying the interplay between novelty and success [2]. Most existing approaches measure cinematic success as a static quantity—typically box-office revenue captured at a single point in time or aggregated over a period—which does not always correlate with long-term audience opinion [3]. The temporal dimension of movie's reception, i.e. how audience engagement drifts over the years, remains largely unexplored.

Here, we propose a data-driven framework to classify and predict how movies are received by audiences over time, drawing on 62.5 million ratings of 8,855 films submitted over 26 years by more than 770,000 users on a major online platform. By constructing timeseries of both the volume of ratings (attention) and their numerical value (score), we identify five distinct attention classes and three score classes via supervised timeseries classification. Combining these temporal patterns with absolute measures of popularity and audience opinion, we define three reception classes — Fiasco, Success, and Sleeper hit — that capture the full trajectory of how movies are received over time. While audience attention typically decays after release as newly released items succeed them [4], the popularity of Sleeper hits grows years later, drawing an analogy with the "sleeping beauties" phenomenon observed in scientific citation dynamics [5].

Using movie metadata encompassing genres, box office, production details, content ratings, and runtime, we predict reception classes with a balanced accuracy of 0.84. Using SHAP, we study each feature impact on the prediction for each Reception Pattern—see Fig. 1—, revealing that box-office figures and runtime are the strongest predictors, with markedly different influences across classes: high-budget films with strong opening weeks but poor aggregated earnings tend to be Fiascos, while Successes show the opposite pattern. Additionaly, commercial blockbuster genres are strong indicators of Fiascos. Sleeper hits are characterized by low initial investment and modest revenues, and are disproportionately non-American dramas. Our framework offers a quantitative approach to understanding how cultural products achieve enduring impact, with potential applications beyond cinema to other domains of the entertainment industry.

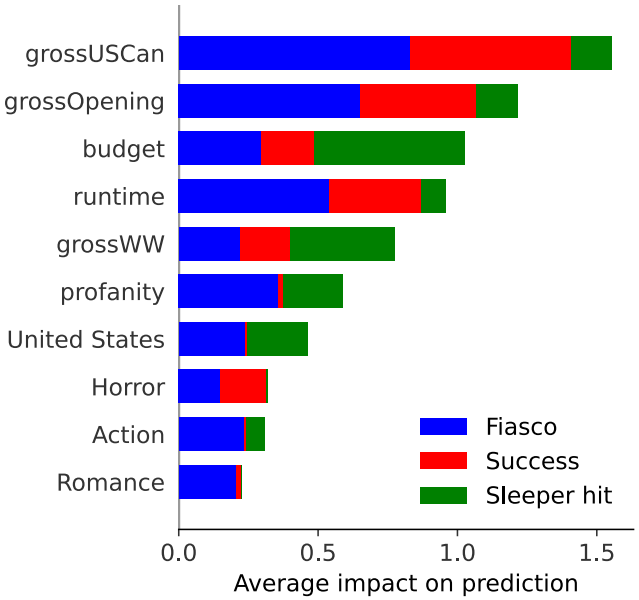

Fig. 1: SHAP summary plot showing the 10 features with the greatest impact on the Reception Patterns predictions. The different colors in each bar indicate each feature contribution for the prediction on that class.

[1] Samuel P. Fraiberger et al., Quantifying reputation and success in art, *Science* **362**, 825-829 (2018).
[2] M. S. Mariani et al., Collective dynamics behind success, *Nat Commun* **15**, 10701 (2024).
[3] M. Cook, 50 classic films that flopped when they where first released, *Bus. Insid.* (2024).
[4] C. Candia et al., The universal decay of collective memory and attention, *Nat. Hum. Behav.* **3** 82-91 (2019).
[5] Q. Ke et al., Defining and identifying Sleeping Beauties in science, *Proc. Natl. Acad. Sci. U.S.A*, **112** (24) 7426-7431 (2015).

Symmetry breaking in collective decision-making through higher-order interactions

David March-Pons[1], Romualdo Pastor-Satorras[1], and M. Carmen Miguel[2,3]
[1]Dept. de Física, Universitat Politècnica de Catalunya, Campus Nord B4, 08034 Barcelona, Espanya
[2]Dept. de Física de la Matèria Condensada, Universitat de Barcelona, Martí i Franquès 1, 08028 Barcelona, Espanya
[3] Institute of Complex Systems (UBICS), Universitat de Barcelona, Barcelona, Espanya

Collective decision-making in biological and artificial swarms often faces a fundamental challenge: symmetry breaking. When multiple alternatives are of equal value a the swarm may settle in a deadlock, unable to reach consensus for any option. Social insects such as honeybees overcome this through cross-inhibition signals, by which agents with different opinions inhibit each other [1]. In this work, we introduce a collective decision-making model inspired by the behavior of social insects, where agents autonomously discover and assess options' qualities, subsequently communicating their findings to the rest of the swarm; other agents can then observe these advertisements and, through social recruitment interactions, adopt an option already being advertised. Such behavior has been extensively used to study both theoretical and applied aspects of collective decision-making dynamics, setting the ground for the design of autonomous robot swarms [2, 4]. Our model shows that pairwise communication alone leads to decision deadlock in a symmetry-breaking task. This motivates the investigation in how group recruitment interactions—i.e. when information is received simultaneously by multiple members of the group rather than by the integration of multiple pairwise signals—provide an alternative mechanism to achieve symmetry breaking without relying on cross-inhibition signals.

Our model extends previous contagion models [2, 3] by incorporating multiple, mutually exclusive options and distinguishing between pairwise and higher-order social influences. Recent research has emphasized the role of group spreading in the adoption of social norms [3], showing how exchanges occurring at different group sizes produce new phenomena not observed when only considering pairwise connections. Using simulations and analytical mean-field solutions, we show that higher-order interactions are essential for breaking symmetry in systems with equally valid options, allowing the system to overcome stalemates and reach consensus [5]. As can be seen in the mean-field phase diagram of the model, Fig. 1, different strengths of pairwise and group-interactions as modulated by (λ_1, λ_2), drive the system from deadlock to symmetry breaking through either a continuous or discontinuous transition.

We further characterize this behavior on higher-order communication networks, encoded as simplicial complexes, obtained from simulations of robot-swarm experiments. In this setting, where communication is limited to the nearest neighbors that robots observe in their vicinity, group communication provides a mechanism to attain higher levels of consensus than pairwise cross-inhibition signaling. This allows us to validate our theoretical findings in a realistic and embodied scenario. Overall, our work emphasizes the important roles of autonomous behavior and higher-order structures in collective decision-making, offering insights into emergent consensus dynamics in social systems and guiding the design of decision protocols for artificial swarms.

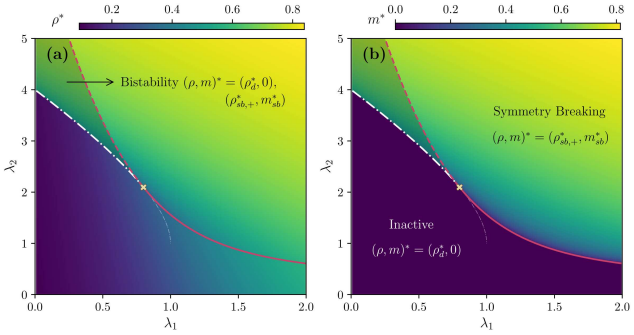

Fig. 1: Mean field results for two contagion spreading with spontaneous adoption, in the state space defined by pairwise spreading (λ_1) and higher order spreading (λ_2). **(a)** shows the active population and **(b)** the consensus order parameter (analogous to a magnetization). The dot-dashed line indicates the discontinuous transition while the continuous line marks a continuous transition. The dashed line marks the boundary of the bistability between the deadlock and symmetry-breaking solutions. The cross indicates the point where the nature of the transition changes. In both figures, the different regions are labeled according to their valid solutions, with the shaded area indicating the bistability region. Specifically, this region is colored based on the symmetry-breaking solution.

[1] Seeley, T. D. et al. *Stop Signals Provide Cross Inhibition in Collective Decision-Making by Honeybee Swarms*, *Science* **335**, 108-111 (2012).

[2] Reina, A., Marshall, J., Trianni, V., Bose, T. *Model of the best-of-N nest-site selection process in honeybees*, *Phys. Rev. E*, **95**, 052411 (2017).

[3] Iacopini, I., Petri, G., Barrat, A. et al. *Simplicial models of social contagion*,Nat Commun **10**, 2485 (2019).

[4] Valentini, G. et al. *The Best-of-n Problem in Robot Swarms: Formalization, State of the Art and Novel Perspectives*

[5] March-Pons, D., Pastor-Satorras, R. and Miguel M. C., *Symmetry breaking in collective decision-making through higher-order interactions*, *npj Complex* 3, 7 (2026)

Kuramoto dynamics with sign flipping interactions

Jonathan Diez[1,2], Dimitri Marinelli[1], Conrad J. Pérez-Vicente[1], and Albert Díaz-Guilera[1]
[1]Departament de Física de la Matèria Condensada and UBICS, Universitat de Barcelona, 08028 Barcelona, Spain
[2]Dresden Technical University (TUD), 01069 Dresden, Germany

Interactions in coupled systems are not always purely attractive. Neural populations combine excitatory and inhibitory influences, while social interactions may represent cooperation or antagonism. Moreover, the polarity of these interactions need not remain fixed: effective synaptic couplings can change their excitatory or inhibitory character, and social ties can evolve between agreement and opposition (see e.g. [1, 2]). Describing the interaction sign as a dynamical variable is therefore a natural extension of conventional synchronization models.

The Kuramoto model describes the phase θ_i of N coupled oscillators,

$$\dot{\theta}_i = \omega_i + \sum_{j=1}^{N} K_{ij} \sin(\theta_j - \theta_i). \tag{1}$$

We take identical oscillators, whose natural frequency can be absorbed in a rotating frame, and let the coupling carry a sign that evolves in time, $K_{ij} = K\, a_{ij}(t)$, with $a_{ij}(t) = +1$ for an excitatory link, -1 for an inhibitory one and 0 when i and j are not connected. Each link reverses its sign independently at the events of a Poisson process of rate λ, so that between flips the phases relax under the standard Kuramoto flow, while at each event one entry of the adjacency matrix changes sign and the phases remain continuous.

We study this dynamics on a ring, the simplest sparse topology in which multistability already appears, where only neighboring oscillators interact,

$$\dot{\theta}_i = a_{i+1,i}(t) \sin(\theta_{i+1} - \theta_i) + a_{i,i-1}(t) \sin(\theta_{i-1} - \theta_i), \tag{2}$$

with all indices taken modulo N. Besides full synchronization, the ring admits a family of twisted states, and with signed couplings the observable that labels them is the lag number

$$l(t) = \frac{1}{\pi} \sum_{i=1}^{N} \alpha_i(t), \tag{3}$$

where α_i is the gauged phase difference, equal to $\theta_{i+1} - \theta_i$ across a positive link and shifted by π across a negative one. The stable fixed points are the configurations with uniform $\alpha_i = \alpha$ and $|\alpha| < \pi/2$, and the parity of the number of negative links selects the even or the odd sector of l [3]. The volume of the corresponding basins of attraction follows a Gaussian law in l, but their shape remains an open problem: they are dominated by long tentacle like structures rather than by a compact region around the attractor.

We first use the flips deterministically, as a controlled probe of that landscape. Flipping one link while the system rests in a stable state with $l \neq 0$ sets off a perturbation that propagates around the ring and leaves the system, after relaxation, in a state with $|l| - 1$, independently of the initial lag and of the link chosen. Flipping a pair of links reduces the lag by two and is equivalent to shifting the phase of a single oscillator by π. Iterating the operation produces a cascade that drives any twisted state to full synchronization. Since the intervention connects points that are far apart in phase space to the same attractor, it supports the tentacle picture and suggests a nested, onion like organization of the basins.

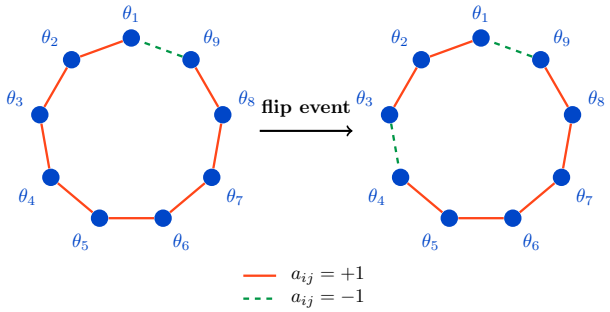

Fig. 1: **Single flip event changing the sign of one edge.**

We then let the signs switch stochastically and compare the mean time between flips in the ring, $1/(N\lambda)$, with the relaxation time of the phase dynamics, $\tau_E = N^2/(4K\pi^2)$. The invariant region $\mathscr{I} = \{\alpha_i \in (-\pi/2, \pi/2)\}$, known for the fully excitatory ring, survives when negative couplings are present and freezes the lag number, so that a flip must first eject the system from $\mathscr{I}$ before l can evolve. Only the flipped link leaves the region, the lag jumps by exactly one unit with a sign fixed by the local phase difference, and the system re enters $\mathscr{I}$ in a time of order $\log N$. The long time behavior follows from the competition of the two timescales: when flips are well separated the lag performs a biased walk toward the synchronized state, or toward its frustrated counterpart in the negative parity sector, whereas frequent flips arrive before the system relaxes and a broad set of non synchronized states is visited.

Sign flipping therefore plays a double role, as a deterministic probe of the basin geometry of the Kuramoto ring, for which no analytical description is available, and as a minimal model of interaction signs that change over time, as they do in neural and social systems.

[1] N. C. Spitzer, *Neurotransmitter switching in the developing and adult brain*, Annu. Rev. Neurosci. **40**, 1 (2017).
[2] F. Diaz-Diaz *et al.*, *Signed networks: theory, methods, and applications*, arXiv:2511.17247 (2025).
[3] A. Díaz-Guilera, D. Marinelli, and C. J. Pérez-Vicente, *Exploring the interplay of excitatory and inhibitory interactions in the Kuramoto model on circle topologies*, Chaos **34**, 043134 (2024).

Topological defects in vibrated monolayers of equilateral triangular prisms

Yuri Martínez-Ratón[1], Jorge Vega[2] and Enrique Velasco[2]
[1]Departamento de Matemáticas, Universidad Carlos III de Madrid
[2]Departamento de Física Teórica de la Materia Condensada, Universidad Autónoma de Madrid

We present experimental results in which a quasimonolayer of grains, shaped as equilateral triangular prisms, is vertically vibrated within circular and square confining cavities [1]. The system exhibits a fluid phase characterized by sixfold orientational order. However, the specific geometries of the cavities frustrate this order, leading to the excitation of topological defects that adhere to topological principles. We analyze the distribution of topological charges of these defects and their evolution as a function of the container geometry. In particular, we find that in the circular cavity, both the number and charge of defects remain constant in the steady-state regime, with only defects of charge +1 being excited [1]. In contrast, within the square cavity—with the same topology as the circular cavity—some defects become pinned to the corners of the cavity, developing charges of +1 or +2. Additionally, free defects with charges of ±1 can be excited. In Fig. 1 we show the 6-atic orientational order parameter field of different defect structures containing four pinned defects and a number of free defects observed in the granular monolayer. The order parameter is defined as $q_6 = \int_0^{2\pi} d\phi \cos(6\phi) h(\phi)$, with $h(\phi)$ being the orientational distribution function, i.e. the probability density of particle axis to be orientated with angle ϕ with respect to one of the six equivalent directors.

Notably, dynamic events occur, such as the fusion of two defects or the creation of two defects from a single one. These events are governed by the conservation of total charge within the cavity and give rise to various system configurations, with rapid transitions between them [1]. The observed dynamic fluctuations in topological charge are remarkable, influenced by both particle shape and cavity geometry. This system of vertically vibrated (dissipative) granular monolayers presents a unique and simple platform for studying topological phenomena, with potential implications for topological effects in equilibrium-oriented fluids.

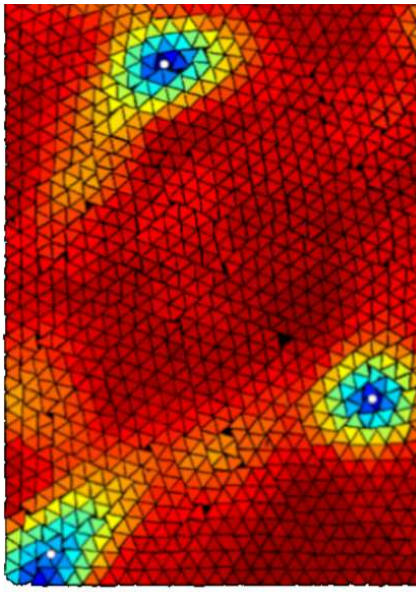

Fig. 1: Eight different defect structures of the 6-atic orientational order parameter field, q_6, found in experiments on vibrated monolayers of triangular prisms confined in square cavity. The charges of pinned and free defects are correspondingly shown.

[1] *Defects in vibrated monolayers of equilateral triangular prisms* , J. Vega, E. Velasco and Y. Martínez-Ratón, Phys. Rev. Research **7**, 043238 (2025).

Modeling and prediction of chemical paths using graph and recurrent NNs

Pedro Martínez Saiz[1], Marta Sales-Pardo[1], and Roger Guimerà[1]
[1]Departament d'Enginyeria Quimica, URV

Understanding how molecules transform along chemical trajectories is fundamental to drug discovery and metabolic engineering. However, the discrete, combinatorial nature of chemical space makes exploration challenging. We present a framework for modeling and predicting chemical reaction trajectories using graph convolutional networks (GCNs) and recurrent units (RUs). GCNs encode molecular graphs into continuous, interpretable latent representations where proximity reflects structural similarity, currently being mapped via Morgan fingerprints. RUs then capture sequential changes along trajectories, enabling prediction of next steps. Early results demonstrate that GCNs effectively preserve structural information for downstream decoding. Current work focuses on characterizing latent space geometry and introducing stochasticity to explore low-probability chemical regions.

The approach draws on Williams et al. [1], who showed that shallow recurrent decoders can learn latent representations of physical dynamics from sensor data, getting around computationally expensive PDE solvers. In the molecular domain, Tsai et al. [2] similarly combine an embedding layer with an LSTM to model molecular dynamics.

Fig. 1 details our twofold approach. Module A is a GCN variational encoder–decoder trained to reconstruct 2048-bit Morgan fingerprints. Morgan fingerprints are binary bit-vectors in which each active bit signals the presence of a specific substructure. Tanimoto similarity between reconstructed and true fingerprints thus quantifies how faithfully the latent space captures molecular structure. Once a well-posed latent space is established, module B introduces recurrent units to model sequential changes along chemical trajectories and predict subsequent steps.

The work is currently at the first stage (module A). Early results show that partitioning the 2048 fingerprint bits into separate ranges, each handled by an independent encoder–decoder, yields better per-range reconstruction quality than a single monolithic model. The full fingerprint is recovered by concatenating the partial representations. Reconstruction fidelity is measured via the Tanimoto score, and the reconstruction loss function is a binary cross-entropy $\mathscr{L}_{\mathrm{BCE}}$.

Each molecular graph is encoded to a Gaussian posterior $q(\mathbf{z}|\mathbf{x}) = \mathscr{N}(\boldsymbol{\mu}, \boldsymbol{\sigma}^2\mathbf{I})$, and a latent sample is drawn via the reparameterization trick of [3]:

$$\mathbf{z} = \boldsymbol{\mu} + \boldsymbol{\varepsilon} \odot \exp\left(\frac{\log \boldsymbol{\sigma}}{2}\right), \quad \boldsymbol{\varepsilon} \sim \mathscr{N}(\mathbf{0}, \mathbf{I}) \tag{1}$$

The Gaussian prior regularizes the latent space, encouraging smooth interpolation and enabling principled sampling of novel molecular structures. Its KL divergence against the prior $\mathscr{N}(\mathbf{0}, \mathbf{I})$ has a closed form:

$$\mathscr{L}_{\mathrm{KL}} = -\frac{1}{2} \sum_{j=1}^{d} \left(1 + \log \sigma_j^2 - \mu_j^2 - \sigma_j^2\right) \tag{2}$$

The final loss function then becomes

$$\mathscr{L} = \mathscr{L}_{\mathrm{BCE}} + \beta \cdot \mathscr{L}_{\mathrm{KL}} \tag{3}$$

where β is a hyperparameter (β-VAE formulation [3]) that balances reconstruction accuracy against latent space regularity.

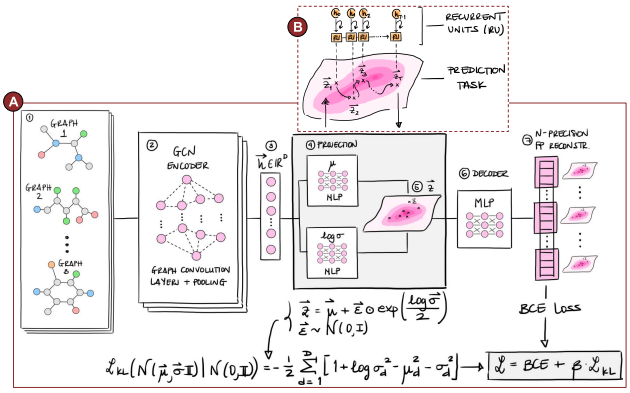

Fig. 1: (**A**) Graph Convolutional Network (GCN) for learning latent representations of molecular structures. (**B**) Recurrent Units (RUs) for modeling sequential changes along chemical trajectories.

Future work will characterize the geometry of the full latent space, in particular the proximity structure of molecular embeddings, and couple the learned representations with recurrent units to model and predict chemical trajectories end-to-end.

[1] J. P. Williams, O. Zahn, and J. N. Kutz, *Sensing with shallow recurrent decoder networks*, Proc. A **480**, 2298 (2024).

[2] ST. Tsai, EJ. Kuo, and P. Tiwary, *Learning molecular dynamics with simple language model built upon long short-term memory neural network*, Nat. Commun. **11**, 5115 (2020).

[3] D. P. Kingma and M. Welling, *Auto-Encoding Variational Bayes*, arXiv:1312.6114 (2013)

Inference of Atrial Conduction Properties from Activation Time Measurements Using Computational Modelling and Finite Element Methods

Marina Martins Cano[1], Enrique Alvarez-Lacalle[1], Jean Bragard[2] and Blas Echebarria[1]
[1] Universitat Politècnica de Catalunya, Barcelona, Spain
[2] Universidad de Navarra, Pamplona

Atrial conduction properties play a key role in the initiation and maintenance of cardiac arrhythmias, yet their quantitative characterization in human tissue remains challenging. In particular, quantitative estimates of the effective diffusion governing electrical propagation are highly relevant for characterizing atrial conduction. This work addresses the inverse problem of inferring diffusion properties from experimentally measured activation times in human atria.

Our experimental data consists of activation times recorded at different locations across the atria (Figure 1). Using these activation times defined at the nodes of a finite element mesh, we aim to reconstruct effective diffusion coefficients, with emphasis on anisotropic conduction along and across fiber directions. To account for the electrophysiological basis of propagation, cellular models, namely Fenton–Karma [1] and Grandi [2] formulations, are incorporated to link ion dynamics with tissue-level conduction. In the anisotropic case, fiber orientation is introduced using a rule-based method defined on a triangular mesh, allowing the distinction between longitudinal and transverse propagation.

The propagation of the membrane potential across cardiac tissue is described by (eq.1):

$$C_m \frac{dV}{dt} = \nabla \cdot (\mathbf{D} \nabla V) - I_{ion} \tag{1}$$

In (eq.1), $(\nabla \cdot (D\nabla V))$ is the diffusion term, with $\mathbf{D}$ acting as the diffusion tensor that describes how fast and in which direction the electrical wave travels through the anisotropic tissue. The velocity of propagation of a wavefront across the cardiac tissue is described by (eq.2) in terms of its curvature, K [3].

$$c = c_o - C_1 \cdot K \tag{2}$$

In (eq.2), c_0 is the velocity of a planar wavefront. The values of c_0 and C_1 depend on the effective diffusion coefficient in the propagation direction. By measuring the velocity and curvature of a wavefront, we can infer the effective value of the diffusion coefficient in the propagation direction. Using the spectral decomposition of the diffusion tensor, the diffusion along and across fiber direction can be deduced, if fiber direction is known.

To facilitate the development and validation of the methodology, we first consider simplified one-dimensional and two-dimensional isotropic and anisotropic problems solved using finite difference methods. These reduced settings provide a controlled framework to gain insight into the behavior of the inverse problem and study the effects of anisotropic conduction before moving to the full FEM formulation.

Preliminary results in one and two-dimensional test cases solved using finite difference methods demonstrate the feasibility of the proposed inverse framework. In isotropic media, the diffusion coefficient can be successfully recovered from known activation times. For anisotropic conduction, assuming known fiber orientations, local wavefront velocity and curvature measurements allow the estimation of the effective diffusion coefficient along the propagation direction through (2). The recovered values show good agreement with the prescribed diffusion coefficients.

Building on these results, the same inverse problem is being extended to anatomically realistic atrial geometries using FEM, where the atrial surface is represented as a two-dimensional triangular mesh enclosing a volume. The goal is to first solve the problem in a simplified geometry, namely an icosphere, to later tackle the problem in a more realistic triangular FEM mesh, in order to finally use the available experimental recordings of activation times.

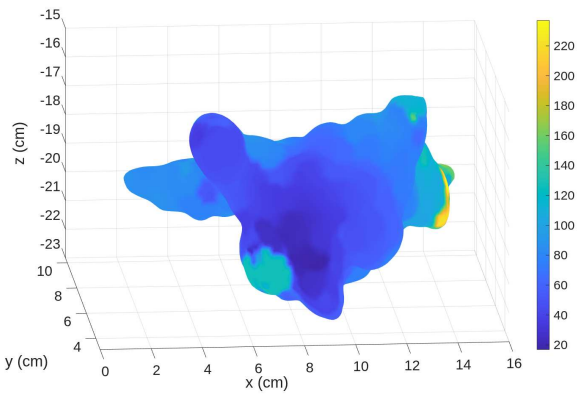

Fig. 1: Experimental measures of activation times on atrial surface.

[1] F. Fenton, A. Karma. *Vortex dynamics in three-dimensional continuous myocardium with fiber rotation: Filament instability and fibrillation.* Chaos. 1998 Mar;8(1):20-47.
[2] E. Grandi et al., *Human Atrial Action Potential and Ca^{2+} Model*, Circulation Research, vol. 109, no. 9, pp. 1055–1066, 2011.
[3] H. Dierckx, *Dynamics of Wave Fronts and Filaments in Anisotropic Cardiac Tissue*, Ph.D. thesis, Ghent University, 2010.

Thermal stress drives seagrass fragmentation in the Mediterranean Sea

Àlex Giménez-Romero[1,2], Tomàs Sintes[2], Carlos M. Duarte[3] and Manuel A. Matías[2]
[1]Centro de Estudios Avanzados de Blanes (CEAB-CSIC), Blanes, Girona, Spain
[2]Instituto de Física Interdisciplinar y Sistemas Complejos (IFISC, CSIC-UIB), Palma de Mallorca, Spain
[3]King Abdullah University of Science and Technology (KAUST), Thuwal, Saudi Arabia

Posidonia oceanica seagrass meadows are the ecological architects of Mediterranean coastal ecosystems. These ancient clonal plants—among the longest-lived organisms on Earth—provide indispensable services: blue carbon sequestration, sediment stabilisation, coastal protection, and nursery habitat. Yet sustained ocean warming is driving accelerated, poorly predictable spatial fragmentation across the basin, progressively eroding these services and the resilience of the ecosystems they sustain.

Classical thermal metrics—like the number of days above a threshold temperature, maximum temperature anomaly, marine heat wave (MHW) duration—fail to capture the cumulative sublethal damage from prolonged exposure below strict mortality thresholds. We introduce **Stress Degree Days** (SDD), defined as

$$\mathrm{SDD} = \int m(T(t))\,\mathrm{d}t, \qquad T > T_c,$$

where $m(T)$ is an experimentally validated [1] shoot mortality rate function and $T_c = 26$ °C is a lower critical temperature. This integral is evaluated from sea surface temperature (SST) time series at Mediterranean-wide scale. Fig. 1(a–b) illustrates the experimental mortality data and the resulting calibration of $m(T)$ against SDD. The steep nonlinearity of $m(T)$ above T_c amplifies the contribution of persistent moderate anomalies between T_c and the 50% lethal threshold $LT_{50} = 28.9$ °C that MHW-based metrics systematically underweight (Fig. 1(c)), grounding the index in measured plant physiology rather than statistical convention.

Global warming drives progressive mortality in Posidonia meadows, triggering a sequence of transitions to spatially patterned states of decreasing biomass—holes, stripes/labyrinths, and isolated spots [2]—before an irreversible transition to a barren seafloor. Combining SDD with large-scale *P. oceanica* distribution maps from remote sensing surveys, we identify a robust positive correlation with spatial fragmentation indices—patch isolation, gap density, meadow connectivity—not reproduced by simpler thermal metrics (Fig. 1(d)). This relationship holds across contrasting biogeographic sub-regions, establishing SDD as a basin-scale predictor of seagrass disintegration and confirming that exposure duration and intensity, not peak temperature alone, jointly govern fragmentation.

Under RCP8.5 (business as usual), meadow cover losses of ∼80% are projected by 2100, with near-total habitat suitability collapse in southern Mediterranean regions; under the more moderate RCP4.5, ∼40% losses are still expected. Fragmentation indices are projected to double or triple, disrupting clonal connectivity, sediment retention, and oxygen export—cascading far beyond direct thermal mortality. These trajectories imply that conservation windows for the most vulnerable meadows may close within decades under current emission trends. The approach is readily transferable to other seagrass species and thermal-stress contexts, with direct implications for conservation prioritisation, marine protected area design, and climate adaptation planning.

The SDD framework provides spatially resolved, mechanistically grounded diagnostics that identify current thermal hotspots and project fragmentation trajectories under realistic emission scenarios. Our results demonstrate [3] that the *timescale* of thermal accumulation—not peak temperature alone—governs *P. oceanica* fragmentation across the warming Mediterranean. SDD offers a physiologically grounded state variable that tracks the proximity of meadow ecosystems to critical transitions, opening the way for early-warning monitoring strategies and spatially targeted interventions before irreversible transitions set in.

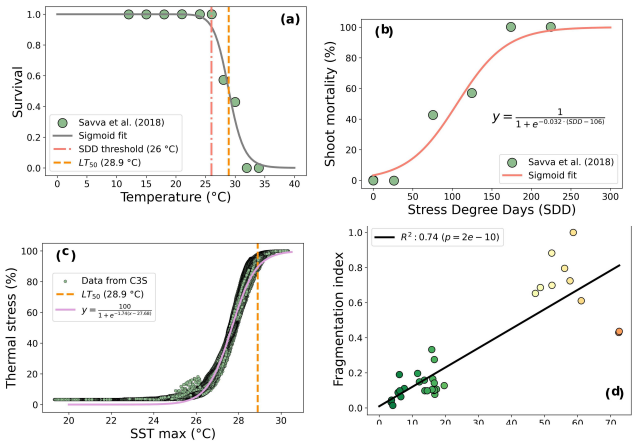

Fig. 1: Temperature-dependent mortality model for *Posidonia oceanica*. **(a)** Experimental survival of *P. oceanica* shoots after 25 days of exposure to constant temperatures [1]. **(b)** Logistic fit of experimentally measured shoot mortality after 25 days under constant temperature conditions to SDD. **(c)** Thermal stress as a function of the maximum SST across a 5 km grid in the Mediterranean Sea (green dots), showing that only the highest-stress sites in the Mediterranean exceed LT_{50}. **(d)** Relationship between thermal stress and *P. oceanica* cover.

[1] I. Savva, S. Bennett, G. Roca, G. Jordà, and N. Marbà, *Thermal tolerance of Mediterranean marine macrophytes: Vulnerability to global warming*, Ecology and Evolution **8**, 12032 (2018).

[2] D. Ruiz-Reynés, D. Gomila, T. Sintes, E. Hernández-García, N. Marbà, and C.M. Duarte, Science Advances **3**, e1603262 (2017).

[3] À. Giménez-Romero, T. Sintes, C.M. Duarte, and M.A. Matías, *Thermal stress is associated with fragmentation of Mediterranean Posidonia oceanica meadows*, Global Change Biology Communications (in press).

Salt-induced structural changes of alginate gels

Mara Maza-Cuello[1], Guillaume Briand[1], Órlaith Skelton[1], and Alberto Fernandez-Nieves[1,2,3]
[1]Department of Condensed Matter Physics, Universitat de Barcelona, Barcelona, Spain
[2]Institute for Complex Systems (UBICS), Universitat de Barcelona, Barcelona, Spain
[3]ICREA-Institució Catalana de Recerca i Estudis Avançats, Barcelona, Spain

Alginate-based gels are a valuable material for a variety of industries. In the medical and pharmaceutical domains, their inherent biocompatibility has led to applications in drug delivery and cell therapy, which require a deep understanding of the response of these materials to the physico-chemical conditions of the target environment.

Recently, it has been observed that alginate beads first swell and then deswell as [NaCl] is increased, a behavior explained by the ionic imbalance between the gel interior and the outside solution, which generates a non-monotonic osmotic pressure [1]. Experimentally, the size of the gels in pure water and at large concentrations of NaCl (1 M) is similar, rising the question of whether the gel structures in these two conditions are physically equivalent.

In this work, we present undergoing studies analyzing the effect of salt concentration on the gels structure. Remarkably, we have found that alginate beads show birefringence after manufacturing, meaning that the gel is not isotropic. With the aid of Jones calculus, we determine the structure of the alginate beads in the absence of salts using both linear and circular polariscopes. We find that the rise in [NaCl] leads to a more isotropic gel structure, as evidenced by a loss of birefringence. Whether this initial structure is recovered or not when [NaCl] is then decreased, depends strongly on [CaCl2]. For [CaCl2] = 1 mM, gels recover partially their original brightness. For [CaCl2] = 0.05 mM, the effect of the cycle is more dramatic: no brightness is recovered, and the gels swell to reach sizes well above the maximum swelling attained upon increasing [NaCl].

Our results indicate that alginate gels are birefringent and thus anisotropic right after gelation, but that their structure may change depending on the presence and the concentration of certain salts. A full characterization of the state of a bead cannot, therefore, be determined solely by its size, and the swelling and deswelling protocol can have an influence in the extent to which these changes are reversible or not.

[1] G. Briand *et al.*, *Salt-induced swelling and de-swelling of alginate gels*, J. Chem. Phys. **165**, 124908 (2026).

Dinámica colisional caótica controlada por fricción

Tomás de Navascues-Martinez[1], Diego Maza[1], and Mara Maza-Cuello[2]

[1] Departamento de Física y Matemática Aplicada, Facultad de Ciencias, Universidad de Navarra, E-31080 Pamplona, España.

[2]Department of Condensed Matter Physics, University of Barcelona, Carrer de Martí Franqués 1, Barcelona, 08028, Spain

La dinámica colisional de un cuerpo contra una base que oscila verticalmente fue considerada un ejemplo paradigmático de sistema caótico hacia finales de los años 90 [1]. No obstante, la aproximación a este problema se redujo con el tiempo a un ejemplo fundamentalmente académico, debido al gran número de variables incontroladas en el proceso experimental, lo que hace muy compleja su comparación con modelos teóricos que abarquen, aunque sea de forma parcial, el conjunto de variables implicadas en este proceso. Por otra parte, en fechas recientes se introdujo un nuevo mecanismo de transporte de partículas que permite controlar su velocidad cuando se encuentran sobre una base horizontal oscilante [2]. Utilizando este método de excitación, es posible, por tanto, controlar la velocidad colisional con la que interactúa el cuerpo oscilante, reduciendo el número de variables implicadas y permitiendo una comparación más detallada con los resultados predichos por diferentes modelos. En este trabajo mostramos resultados numéricos y experimentales sobre cómo es posible encontrar tanto regímenes periódicos como caóticos en sistemas de este tipo y discutimos sus posibles implicaciones en situaciones en las que interactúan varias partículas.

[1] Tufillaro, Nicholas B. and Abbott, Tyler and Reilly, Jeremiah, *An experimental approach to nonlinear dynamics and chaos* (Addison-Wesley,Redwood Cit, 1992).

[2] M. Maza-Cuello, D. Maza *Efficient Transport Controlled by Biharmonic Frictional Driving*, Phys. Rev. Lett. 133, 158201 – Published 9 October, 2024. DOI: https://doi.org/10.1103/PhysRevLett.133.158201 .

Inference of Interactions and Coexistence Regimes in Ecological Communities with Annealed Disorder

Alberto Megías[1], David Alonso[2], Vicente J. Ontiveros[2] and José A. Capitán[1]
[1]Complex Systems Group and Department of Applied Mathematics, Universidad Politécnica de Madrid. Av. Juan de Herrera 6, Madrid E-28040, Spain
[2]Ecology and Complexity, CEAB-CSIC, Centre d'Estudis Avançats de Blanes. Consejo Superior de Investigaciones Científicas. Acces Cala St. Francesc 14, Blanes E-17300, Spain

The study of population dynamics in large ecological communities is of fundamental importance for understanding biodiversity in complex ecosystems. Species interactions determine the conditions under which coexistence is possible. In this work, we focus on inferring the first two moments of the interaction matrix in large, complex ecological communities, as well as determining the coexistence regime in which the ecosystem operates. For that, we model an ecological community of S species with random interactions using the generalized Lotka–Volterra (GLV) equations. In addition, we incorporate environmental fluctuations into the dynamics. First, we analyze the model in the limit of a large number of species, $S \gg 1$, where different coexistence regimes emerge. We then develop an inference methodology to estimate the first two moments of the interaction matrix, together with the strength of environmental noise, enabling classification of the system according to its coexistence regime.

Under these assumptions, the evolution of population densities $x_i(t)$ is described by the following system of stochastic differential equations in the Stratonovich sense:

$$\frac{\dot{x}_i(t)}{x_i(t)} = r(t) - x_i(t) + \sum_{j\neq i} \alpha_{ij}(t) x_j(t), \qquad (1)$$

where $r(t)$ and $\alpha_{ij}(t)$ denote the growth rates and interspecific interactions, respectively, modeled as time-dependent random variables:

$$\begin{aligned} r(t) &= r - \sigma_{\text{env}}^2 + \sqrt{2\sigma_{\text{env}}^2}\,\xi_i(t), \\ \alpha_{ij}(t) &= \frac{\mu}{S} + \frac{\sigma_{\text{int}}}{\sqrt{S}} z_{ij}(t), \end{aligned} \qquad (2)$$

where r and σ_{env}^2 are the mean and variance of the growth rates, and μ/S and σ_{int}^2/S are the mean and variance of the interaction coefficients. The stochastic processes $\xi_i(t)$ and $z_{ij}(t)$ are Gaussian white noises with zero mean: $\langle \xi_i(t)\rangle = 0$, $\langle \xi_i(t)\xi_j(t')\rangle = \delta_{ij}\delta(t-t')$, $\langle z_{ij}(t)\rangle = 0$, $\langle z_{ij}(t) z_{k\ell}(t')\rangle = (\delta_{ik}\delta_{j\ell} + \rho\,\delta_{i\ell}\delta_{jk})\delta(t-t')$, where $-1 \le \rho \le 1$ quantifies the correlation between interaction coefficients.

In the limit $S \to \infty$, we analyze coexistence conditions using Dynamical Mean Field Theory (DMFT) [1]. This approach reduces the full system to an effective single-species dynamics. By studying the stationary distribution of abundances under annealed disorder, we identify three regimes: (i) *stable coexistence* (SC), where abundances fluctuate around an interior fixed point of the S-dimensional simplex; (ii) *unstable coexistence* (UC), where trajectories frequently approach the simplex boundaries; and (iii) *unbounded growth* (UG), an *artificial phase* characterized by diverging dynamics. These regimes are illustrated in Fig. 1.

Finally, based on the reduced dynamics, we construct a methodology to infer model parameters. We validate this method against simulated data from Eqs. (1)–(2), obtaining good agreement (see Fig. 2). We then apply the method to empirical datasets: the tropical forest of Barro Colorado Island (BCI) [2] and the zooplankton community of Lake Zürich (LZ) [3, 4]. Our results classify them, as expected, within the SC and UC regimes, respectively (see Fig. 1).

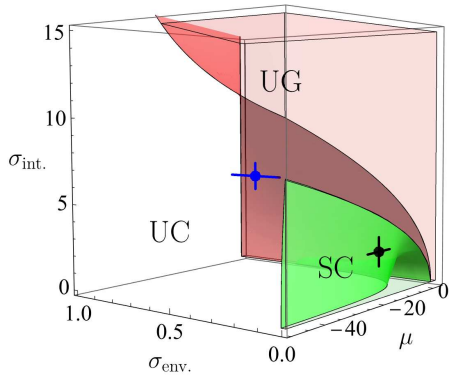

Fig. 1: Coexistence phase diagram for the GLV model with environmental noise under the rescaling $\sigma_{\text{int}}^2 \to r\sigma_{\text{int}}^2$ and $\sigma_{\text{env}}^2 \to \sigma_{\text{env}}^2/r$. Black and blue points correspond to inferred parameter values for BCI and LZ, respectively.

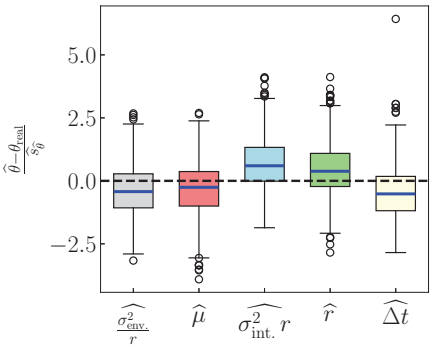

Fig. 2: Estimated parameter distributions obtained from 1000 simulations of Eqs. (1)–(2) with $S = 50$, $\mu = -2$, $r\sigma_{\text{int}}^2 = 1/4$, and $\sigma_{\text{env}}^2/r = 1/20$.

[1] D. Vollhardt, K. Byczuk, and M. Kollar, *Dynamical Mean-Field Theory*, in *Strongly Correlated Systems: Theoretical Methods*, edited by A. Avella and F. Mancini (Springer, 2012).

[2] R. Condit *et al.*, *Complete data from the Barro Colorado 50-ha plot: 423617 trees, 35 years, 2019 version* (2019).

[3] F. Pomati *et al.*, *Effects of re-oligotrophication and climate warming on plankton richness and community stability in a deep mesotrophic lake*, Oikos **121**, 1317 (2012).

[4] F. Pomati *et al.*, *Challenges and prospects for interpreting long-term phytoplankton diversity changes in Lake Zurich (Switzerland)*, Freshwater Biology **60**, 1052 (2015).

Anomalous heat transport in long-range chains of oscillators with conservative noise

Carlos Mejía Monasterio
Universidad Politécnica de Madrid, ETSIAAB, Ave Puerta de Hierro 2, 28040 Madrid

Heat and mass transport through a medium is a familiar thermodynamic phenomenon relevant to both basic physics and technology. From the point of view of statistical physics, the microscopic mathematical foundations of its macroscopic laws have challenged researchers for decades. In low-dimensional systems, heat transport remains a challenge in theoretical physics, and the possibility of anomalous energy transport and violations of Fourier's law have been thoroughly investigated.

We consider the non-equilibrium properties of a one-dimensional ring of N oscillators with long-ranged harmonic interactions, when it is perturbed by long-range conservative stochastic noise that exchange momenta of particle pairs[1–3]. We derive exact expressions for the deterministic contribution of the energy current-current correlation at equilibrium, based on the kinetic approximation of the normal mode dynamics [4].

In the thermodynamic limit the decay of the auto-correlation is algebraic, distinguishing four distinct regimes of correlation decay depending on the exponents δ and α, controlling the range of deterministic and stochastic interactions, as shown in Fig. 1. Surprisingly, the long-range noise breaks down the long-range correlations characteristic of low-dimensional models, suggesting a normal regime in which heat transport becomes diffusive. For finite systems, we also present exact expressions for the finite-size corrections to the algebraic decay of the correlation. In certain regimes, these corrections are considerably large, rendering it hard to estimate transport properties from numerical data for the finite chains. Our findings are tested against numerical simulations, performed with an efficient algorithm.

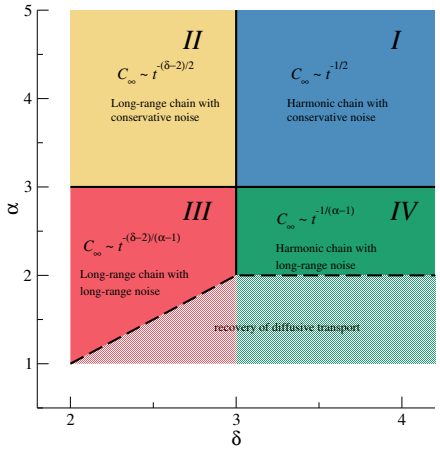

Fig. 1: Phase diagram of the different regimes of the model dynamics. Four different regimes are identified by colours and delimited by solid lines depending on the asymptotic decay of C_∞. The region below the dashed curve corresponds to the values of the range of the interaction δ, and the range of the noise α for which the thermal transport turns diffusive.

[1] S. Lepri, C. Mejía-Monasterio, A. Politi, *A stochastic model of anomalous heat transport: analytical solution of the nonequilibrium steady state*, Journal of Physics A: Math Theor., **42**, (2009) 025001:1-025001:15.

[2] S. Lepri, C. Mejía-Monasterio, A. Politi,, *Nonequilibrium dynamics of a stochastic model of anomalous heat transport*, Journal of Physics A: Math Theor., **43**, (2010) 065002:1-065002:22.

[3] L. Delfini, S. Lepri, R. Livi, C. Mejía-Monasterio, A. Politi, *Nonequilibrium dynamics of a stochastic model of anomalous heat transport: numerical analysis*, Journal of Physics A: Math Theor., **43**, (2010) 145001:1-145001:16.

[4] F. Andreucci, Stefano Lepri, C. Mejía-Monasterio, S. Ruffo, *Thermal Transport in Long-Range Interacting Harmonic Chains Perturbed by Long-Range Conservative Noise*, Journal of Statistical Physics, **192**:8 (2025) 1

[5] `http://http://noneq.etsiaab.upm.es`

Assessing Information Measures for Quantifying Spatial Heterogeneities in Laser Intensity Profiles Data

Oscar Ricardo Mejía Parra[1], and Cristina Masoller[1]
[1]Universitat Politècnica de Catalunya, Rambla St. Nebridi 22, Terrassa 08222, Barcelona, Spain

This work investigates the ability of information-theoretic measures to characterize and quantify spatial heterogeneities in broad-area semiconductor laser intensity profiles. We focus on filamentation phenomenon, where an initially smooth beam breaks into narrow, high-intensity structures. Shannon entropy (H) and Fisher information (F) are used to quantify the degree of filamentation in numerically and experimentally recorded beam intensity profiles. The results show that the Shannon-Fisher information (H-F) plane provides an effective tool for quantifying spatial heterogeneities at different laser operating regimes.

Introduction

Laser beam intensity profiles provide valuable insight into the spatial structure, stability, and performance of laser sources, but conventional characterization methods may fail to capture complex spatial features arising in nonlinear regimes. To address these limitations, we use an information-theoretic approach based on Shannon entropy (H) and Fisher information (F) [1, 2], analyzed in the Shannon–Fisher (H–F) plane. Every intensity point in a laser beam profile is normalized to fulfill $\sum_i p_i = 1$ and then treated as probability distributions. For a set of probabilities $\{p_1, p_2, \ldots, p_N\}$ obtained from a intensity profile, H and F are given by

$$H = -\sum_{i=1}^{N} p_i \log p_i \,, \tag{1}$$

$$F = F_0 \sum_{i=1}^{N-1} \left(\sqrt{p_{i+1}} - \sqrt{p_i}\right)^2 , \tag{2}$$

where F_0 is a constant. In this context, H provides a global measure of information, while F quantifies local gradients and fine-scale structures. Particularly, we apply this framework to filamentation phenomenon in broad-area semiconductor lasers, where an initially smooth beam breaks into narrow, high-intensity structures due to the interplay of diffraction, nonlinearity, and gain dynamics [3–5].

Analysis of Broad-Area Semiconductor Laser Beam Profiles

Fig. 1 shows the H–F plane analysis of experimental near-field beam intensity profiles of a single emitter (broad-area semiconductor laser) with a 200 μm contact width, obtained from a Monocrom laser bar and measured at different currents [6]. The H–F representation shows a clear evolution of beam profiles with current, where filamentation appears as a shift toward higher F and lower H, reflecting the formation of prominent and localized peaks. The weaker variation of H indicates that this transition is mainly driven by local gradients. Similar results were found for numerically obtained intensity profiles.

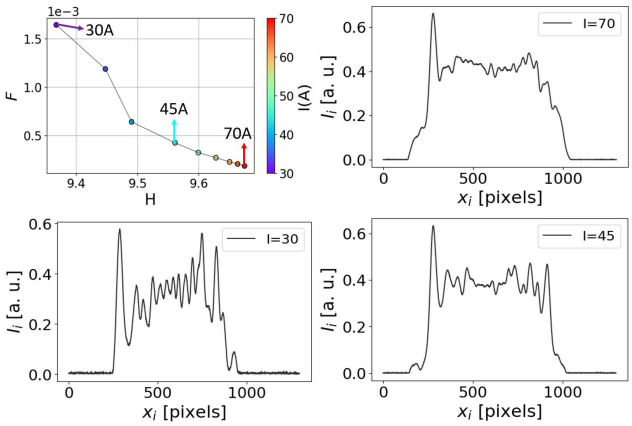

Fig. 1: Analysis of near-field intensity profiles of a broad-area semiconductor laser measured at different driving currents. Top left: H–F plane. Remaining panels: intensity profiles at three representative currents (30 A, 45 A, and 70 A). All profiles are normalized to $\sum_i p_i = 1$. The parameter F_0 in Eq. (2) is set to 4. The information measures are given in bits.

Conclusions

The H-F plane representation enables a clear discrimination between laser beam profiles at different operating regimes and can be a practical tool for quantifying spatial heterogeneities in broad-area semiconductor laser beam profiles.

Acknowledgements: Project funded by the Ministry for Digital Transformation and the Civil Service and by the European Union. Project funded by the State Secretariat for Telecommunications and Digital Infrastructures, financed by the European Union – Next Generation EU (TSI-069100-2023-0015). We acknowledge Dr. M. Facao and Monocrom staff for providing the data analyzed in this work.

[1] C. E. Shannon, A mathematical theory of communication, Bell Syst. Tech. J. **27**, 623–656 (1948).

[2] R. A. Fisher, Theory of statistical estimation, Math. Proc. Cambridge Philos. Soc. **22**, 700–725 (1925).

[3] A. Chen, W. Zhang, X. Zhou, J. Liu, and W. Zheng, Spatial coherence research and passive speckle suppression for edge-emitting broad-area semiconductor lasers, J. Opt. **26**, 045607 (2024).

[4] J. Ohtsubo, *Semiconductor Lasers: Stability, Instability and Chaos*, 4th ed. (Springer, Berlin, 2017).

[5] J. Albiol Serra, *Experimental Characterization of Filamentation Phenomena in Pressure-Mounted Diode Laser Bars*, M.Sc. thesis, Universitat Politècnica de Catalunya, Barcelona, Spain (2024).

[6] `https://monocrom.com`

Evolutionary adaptation through bet-hedging in finite populations under fluctuating environments

Marco Mendívil Carboni[1], and Luis Dinis[1] and Juan José Mazo[1]
[1]Grupo Interdisciplinar de Sistemas Complejos (GISC) and
Departamento de Estructura de la Materia, Física Térmica y Electrónica,
Universidad Complutense de Madrid, 28040 Madrid, Spain

Natural populations evolve under fluctuating environments and limited resources [1, 2], yet the combined effects of these factors on adaptation remain unclear. Here, we introduce a minimal agent-based stochastic model of a population undergoing a continuous-time birth–death process in a randomly switching two-state environment, where individuals inherit phenotypic strategies $s(\phi)$ that determine the distribution of phenotypes ($\phi \in \{A, B\}$) across generations. To study these dynamics exactly, we utilize the Gillespie simulation algorithm [5] while restricting the total population size to its initial value N_{ini} to impose an effective ecological carrying capacity that mimics continuous-culture conditions [4].

We first confirm that environmental variability can favor phenotypic diversity (bet-hedging) [6], and that the strategy maximizing the average growth rate $\langle \mu \rangle$ generally differs from the one minimizing the extinction rate r_{ext}. We then show that when evolution is enabled by introducing strategy mutations with a low probability p_{mut}, selection drives populations to converge to intermediate strategies that balance these competing objectives.

We further demonstrate that population size modulates the evolutionary outcome: large populations are immune to extinction and recover the classical growth-maximizing strategy [3], whereas smaller ones evolve toward more resilient, safer strategies. Finally, we show how a simple heuristic approximation captures these outcomes and clarifies the interplay between growth, extinction, and mutation. The stationary distribution of evolved strategies $p(\bar{s})$ is formulated as:

$$p(\bar{s}) \propto \frac{\exp(N_{\text{ini}} \cdot \langle \mu \rangle(\bar{s}))}{r_{\text{ext}}(N_{\text{ini}}, \bar{s}) + p_{\text{mut}} \cdot \langle \mu_b \rangle(\bar{s})} \tag{1}$$

where $\langle \mu \rangle$ represents the mean growth rate, $\langle \mu_b \rangle$ is the average birth rate, and the extinction rate decays algebraically as a power law ($r_{\text{ext}} \sim N_{\text{ini}}^{-\alpha}$) driven by adverse environmental episodes. This expression highlights the direct competition between the exponential amplification of growth differences at large populations and the dominance of the extinction risk in small populations.

Overall, our results highlight how environmental fluctuations and demographic constraints jointly shape adaptation, emphasizing the key role of extinction in finite populations.

[1] King's College, *Risk, Uncertainty and Evolutionary Strategies* (Cambridge University Press, Cambridge, 1982).
[2] E. Kussell and S. Leibler, *Phenotypic Diversity, Population Growth, and Information in Fluctuating Environments*, Science **309**, 2075 (2005).
[3] J. H. Gillespie, *Natural Selection for Variances in Offspring Numbers: A New Evolutionary Principle*, Am. Nat. **111**, 1010 (1977).
[4] The Economic Cell Collective, *Economic Principles in Cell Biology* (Online open access book, 2025).
[5] R. Toral and P. Colet, *Stochastic Numerical Methods* (Wiley, 2014).
[6] B. Xue and S. Leibler, *Bet Hedging against Demographic Fluctuations*, Phys. Rev. Lett. **119**, 108103 (2017).

Phase transitions in collective decision-making of social animals

M. Carmen Miguel[1], David March-Pons[2], and Romualdo Pastor-Satorras[2]
[1] Departament de Física de la Matèria Condensada, Universitat de Barcelona, Martí i Franquès 1, 08028, Barcelona, Spain
Institute of Complex Systems (UBICS), Universitat de Barcelona, 08028, Barcelona, Spain
[2] Departament de Física, Universitat Politècnica de Catalunya, Campus Nord B4, 08034, Barcelona, Spain

Collective decision-making in social animal groups often emerges from simple local interactions and can give rise to abrupt transitions between distinct behavioral states. In this work, we explore how group coordination, information transfer, and environmental constraints shape these transitions in animal collectives. Using controlled experimental systems combined with quantitative analysis, we investigate how groups integrate sensory information and social interactions to reach consensus and coordinate movement, particularly in constrained environments.

Our results highlight the key role of group interactions and sensorial cues in driving collective outcomes, revealing how small changes in environmental conditions or information accessibility can trigger qualitative shifts in group behavior, akin to phase transitions in physical systems. We further discuss how the interplay between individual behavior, group cohesion, and environmental structure governs the efficiency of collective decisions and navigation. These findings contribute to a broader understanding of active and living matter, bridging physics and biology, and provide new perspectives on how collective intelligence emerges in natural systems.

Thinking fast and slow: imitation, personal information and noise in the Voter Model

Daniela Molas[1], Daniel Campos[1]
[1]Universitat Autònoma de Barcelona, Statistical Physics Group, Department of Physics, Faculty of Sciences, Bellaterra, Spain.

We extend the classical Voter Model (VM) [1, 2] to incorporate accumulation-based imitation: each agent i among N possesses N_C internal criteria, each supporting either option A or B, which are updated through the observation of others' choices, called prospection (q), or through self-reinforcement $(1-q)$. At each step, agent i updates its choice either by direct imitation (p) or by applying a majority rule over its internal criteria $(1-p)$. This introduces a natural form of stubbornness: agents whose criteria are strongly aligned with one option resist change, unlike models with agents having a fixed probability of stubbornness.

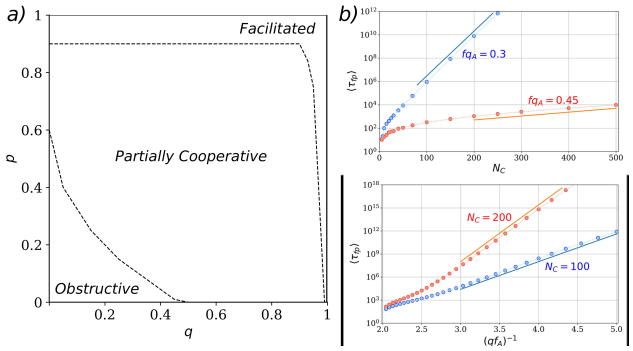

Fig. 1: a) Heatmap of the mean consensus time $\langle T \rangle$ as a function of p and q ($N = N_C = 100$, average over 3000 realizations). b) Mean switching time $\langle \tau \rangle$ vs. N_C (upper) and $(qf_A)^{-1}$ (lower) for $p = 0$. Solid lines show the theoretical scaling $\langle \tau \rangle \sim e^{N_C}$ and $\langle \tau \rangle \sim e^{1/qf_A}$ (average over 3000 realizations, $N = N_C = 100$).

The interplay between p and q produces three regimes (See Fig. 1 (a)): a Facilitated regime (high q, low-intermediate p) where both mechanisms cooperate and consensus is reached faster than in the classical VM; a Partially Cooperative regime; and an Obstructive regime (low p and q) where self-reinforcement dominates and frozen states with exponentially large consensus times appear.

For $p = 0$, the average time required for an individual to change opinion through the accumulation mechanism satisfies $\langle \tau \rangle \sim e^{N_C^2}$ and $\langle \tau \rangle \sim e^{1/qf_A}$. This result is obtained analytically from a first-passage problem and confirmed numerically (See Fig. 1 (b)). Quantifying the stubbornness induced by personal criteria shows that reintroducing direct imitation $(p > 0)$ is essential to escape frozen states, by generating fluctuations that destabilize the equilibrium $n_{i,A}/N_C = qf_A$.

Direct imitation drives consensus through fluctuations in the magnetization m, with a diffusion coefficient maximal at $m = 0$ and vanishing upon reaching consensus. In contrast, the majority rule generates an almost negligible deterministic drift near $m = 0$, but one that becomes self-reinforcing once partial consensus surpasses a threshold. This complementarity explains why the cooperative regime outperforms the classical VM.

Furthermore, as a natural extension, we introduce a noise term: with probability r, an agent spontaneously switches to the opposite opinion, independently of its social interactions, as in the classical noisy voter model [3]. However, in our model the noise acts only on the observable opinion and not on the accumulated internal criteria. This generates a discrepancy between the expressed opinion and the stored personal information, introducing a new relaxation mechanism absent in standard models.

After a noisy perturbation, the agent preserves internal criteria that continue favoring its previous state and may revert through the majority dynamics. In this way, noise no longer acts as a purely disordering mechanism and instead competes with an internal memory that tends to restore previous opinions. Preliminary numerical results show that the transition from a bimodal to a unimodal distribution is preserved, a characteristic of the classical noisy voter model previously studied, see [3] for more details, and furthermore show that the estimated critical noise (r_c) grows strongly with q, meaning that accumulated information acts as a shield against the effect of noise. Finally, we discuss how this framework naturally extends to multiple opinion states, where the interaction between the accumulation of personal information and noise is expected to enrich the phase structure beyond what is known for the standard multistate noisy voter model [4].

[1] S. Redner, *Reality-inspired voter models: A mini-review. Comptes Rendus Physique*,20(4):275–292, (2019).
[2] D. Molas and D. Campos, *The Mathematics of Movement: An Interdisciplinary Approach t o Mutual Challenges in AnimalEcology and Cell Biology*, edited by L. Giuggioli and P. Maini (Springer Nature Switzerland, 2026).
[3] A. Carro and R. Toral and M. San Miguel , *The noisy voter model on complex networks* (Scientific reports, 6(1), 24775, 2016).
[4] F. Herrerías-Azcue and T. Galla, *Consensus and diversity in multistate noisy voter models.* (Physical Review E, 100(2), 022304, 2019).

Emergence of orientational order in a confined hard-dumbbell fluid

Ana M. Montero,[1] Péter Gurin,[2] Szabolcs Varga,[2] and Andrés Santos[1,3]
[1]Departamento de Física, Universidad de Extremadura, Badajoz, E-06006, Spain
[2] Physics Department, Centre for Natural Sciences, University of Pannonia, P.O. Box 158, Veszprém H-8201, Hungary
[3] Instituto de Computación Científica Avanzada (ICCAEx), Universidad de Extremadura, E-06006 Badajoz, Spain

We present an exact theoretical study of a quasi-one-dimensional fluid of anisotropic hard dumbbells with continuous orientational degrees of freedom, which represents a minimal yet nontrivial model that captures the complex interplay between positional and orientational ordering under strong confinement [1]. In this system, the centers of the particles are constrained to lie along the x axis, while they are free to rotate in the xy plane (Fig. 1).

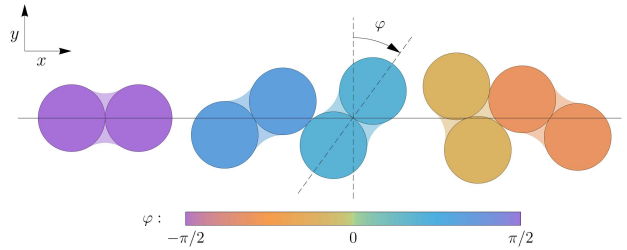

Fig. 1: Geometry of the q1D dumbbell system. The centers of mass are constrained to move along the x axis, while each dumbbell can rotate in the xy plane with orientation angle ϕ. Colors encode the dumbbell orientations. The light shading indicates the maximal admissible region that can connect the two disks of a dumbbell without affecting the contact distance between neighboring dumbbells, as illustrated in the rightmost pair.

By formulating the problem within a transfer-matrix framework, we obtain a fully analytical description of the system in terms of the spectral properties of an underlying integral operator. This approach allows us to go beyond approximate or numerical treatments and derive closed-form, exact expressions for key structural and thermodynamic quantities.

In particular, we derive exact results for the equation of state, the orientational distribution function, and both the partial radial distribution functions—defined between particles with specified orientations—and the total radial distribution function—defined between two particles regardless of their orientations. The asymptotic behavior of correlations is determined rigorously through the analytic structure of the Laplace-transformed correlation functions, whose poles, which can be either real or complex conjugates, define the positional and orientational correlation lengths. Our analysis reveals a rich phenomenology driven by volume-exclusion effects (Fig. 2). At intermediate and high densities, we identify an extended regime in which the radial distribution function exhibits an effective algebraic decay over several decades before crossing over to the exponential asymptotic decay dictated by the leading poles. Concurrently, the system undergoes a continuous crossover in orientational ordering, evolving from a weakly ordered, unimodal distribution to a strongly constrained, bimodal state. This structural evolution is accompanied by a nonmonotonic pressure relative to the Tonks gas and by a qualitative transition in correlation decay from oscillatory to monotonic behavior. In the high-pressure limit, near the close-packing density, we show analytically that positional and orientational fluctuations contribute equally to the pressure, yielding a universal result in which the pressure approaches twice that of the Tonks gas.

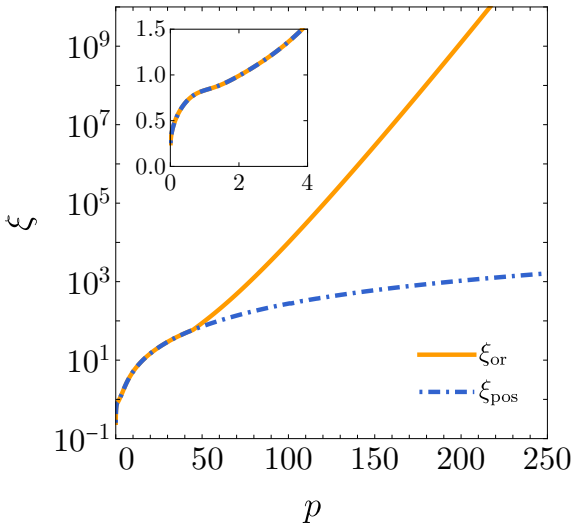

Fig. 2: Orientational correlation length $\xi_{\rm or}$ (solid line), and positional correlation length $\xi_{\rm pos}$ (dash-dotted line) as functions of pressure. Note that $\xi_{\rm or}$ exhibits a kink at $p \simeq 44.7$. The inset shows a magnified view of the curves for $p \leq 4$

Our results are corroborated by numerical solutions of the discretized transfer operator and supported by scaling arguments that rationalize the emergence of the observed regimes. Beyond providing a rare example of an interacting fluid model with exact, closed-form solutions for both structure and thermodynamics, this work establishes a benchmark for testing approximations and offers new insight into ordering phenomena in confined anisotropic systems.

[1] A. M. Montero, P. Gurin, S. Varga and A. Santos *Orientational ordering and correlations in a quasi-one-dimensional hard-dumbbell fluid*, Phys. Rev. E. **113**, 055404 (2026).

Probabilistic Cellular Automata: between deterministic Wolfram's rules 23, 77, 178 and 232

Francisco J. Muñoz[1] and Juan Carlos Nuño[1]
[1]Departamento de Matemática Aplicada, Universidad Politécnica de Madrid. 28040-Madrid. Spain

We study one-dimensional binary Probabilistic Cellular Automaton (PCA) that interpolate between Wolfram's classical rules 23, 77, 178 and 232 [1]. These rules are the only ones that satisfy two criteria: (i) in the case of a majority in the neighborhood states, the central site takes either the majority state or the opposite and (ii) if the neighborhood states are tied, the central site either changes its current state or keeps it. The PCA is defined by two Bernoulli random variables with parameters $p, r \in [0,1]$.

The probabilistic rule map can be written as:

$$\begin{aligned} f_{p,r}(x^{i-1},x^i,x^{i+1}) = \\ \mathscr{B}(r)\Big[(1-\mathscr{B}(p))f_{178}(x^{i-1},x^i,x^{i+1}) \\ +\mathscr{B}(p)f_{232}(x^{i-1},x^i,x^{i+1})\Big] \\ +(1-\mathscr{B}(r))\Big[\mathscr{B}(p)f_{77}(x^{i-1},x^i,x^{i+1}) \\ +(1-\mathscr{B}(p))f_{23}(x^{i-1},x^i,x^{i+1})\Big]. \quad (1) \end{aligned}$$

where $x_i \in \{0,1\}$, f_{23}, f_{77}, f_{178}, and f_{232} denote the local transition functions associated with Wolfram's elementary cellular automata rules 23, 77, 178, and 232, respectively [2], and $\mathscr{B}(p)$ and $\mathscr{B}(r)$ are Bernoulli random variables with expectations $E[\mathscr{B}(p)] = p$ and $E[\mathscr{B}(r)] = r$. Consequently, the expected value of $f_{p,r}$ is the convex combination of the deterministic rules with weights p and r (see Fig. 1).

We analytically solve small-size cases by using a Markov process formulation. We derive analytical expressions for the probability of asymptotically reaching each possible global configuration as a function of p and r, for all initial states. We show that for $0 < p, r < 1$, the asymptotic probability distributions of achieving any of the states for the PCA are independent of the initial conditions. This contrasts with the behavior of the deterministic Wolfram's rules 23 ($p = 0, r = 0$), 77 ($p = 1, r = 0$), 178 ($p = 0, r = 1$) and 232 ($p = 1, r = 1$), for which additional asymptotic states can occur, in particular periodic configurations. Finally, we discuss applying this kind of PCA to describe opinion dynamics involving hesitant agents.

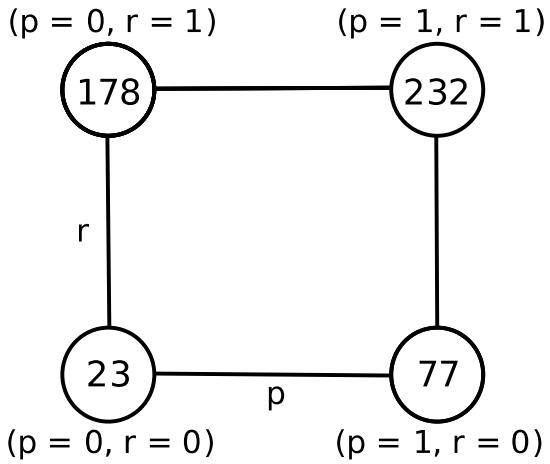

Fig. 1: Probabilistic parameter space defined by $p, r \in [0,1]$. The four vertices correspond to the deterministic Wolfram's rules: 23 ($p = 0, r = 0$), 77 ($p = 1, r = 0$), 178 ($p = 0, r = 1$) and 232 ($p = 1, r = 1$). The horizontal edges describe rules with non-standard ($r = 0$) and standard ($r = 1$) contagion in case of majority. Vertical edges represent rules that, in case of tie, keep the state of the central cell ($p = 0$) or change this state ($p = 1$). In the interior of the square, $0 < p, r < 1$, the PCA exhibits stochastic dynamics that depends on the probabilistic parameters.

This work has been partially published in [3].

[1] S. Wolfram. *Statistical mechanics of cellular automata*. Reviews of modern physics, 55 (3), 601–644 (1983).

[2] H. Fukś. *Nondeterministic density classification with diffusive probabilistic cellular automata*. Physical Review E, 66(6), 066106 (2002).

[3] F. J. Muñoz and J. C. Nuño, *Probabilistic cellular automata: between deterministic Wolfram's rules 23, 77, 178 and 232*, International Journal of Parallel, Emergent and Distributed Systems, 1–26. https://doi.org/10.1080/17445760.2026.2694339 (2026).

Assessment of protective mechanisms in the evolution of TB infection in rhesus macaques using a parameterized computational model

Fernando Muñoz[1], Martí Català[3], Beatriz Eguzkitza[4], Sally Sharpe[5], Clara Prats[1,2], Pere-Joan Cardona[6,7,8,9]
[1]Departament de Física, Computational Biology and Complex Systems (BIOCOM-SC), Universitat Politècnica de Catalunya.
[2]IRIS, Institute for Research and Innovation in Health, UPC
[2]Pharmaco- and Device epidemiology, NDORMS, University of Oxford.
[3]CASE - Physical and Numerical Modelling, Barcelona Supercomputing Center.
[4]Microbiologia Clínica i Experimental, Hospital Universitari Germans Trias i Pujol, Universitat Autònoma de Barcelona.

Tuberculosis (TB) is still a global health challenge. It is caused by *Mycobacterium tuberculosis* and is transmitted via infectious aerosols. Only a small fraction of inhaled bacilli establish pulmonary lesions, causing a minimal lesions that encapsulate rapidly. A subset of these lesions may progress to a size detectable via thoracic radiography, signaling an uncontrolled infection and significant tissue destruction that leads to clinical symptoms. This progression characterizes the transition to active pulmonary TB.

The Bubble Model (BM) is and agent-based model for TB lesion dynamics that captures how localized infections can escalate into widespread disease on a virtual lung [1, 2]. It identifies some key processes of infection evolution, including: lesion growth (governed by a logistic equation for the radius), coalescence of lesions that are close together to creating a bigger one, and endogenous reinfection (each lesion can produce $k \sim$ poisson daughters, and each travels a distance $d \sim$ exp through the bronquial tree). We also introduce an immune response of the host, reducing growth velocity and maximum size of lesions at a critical day, and the fact that lesion growth is limited by lung membranes, which trigger lesion encapsulation.

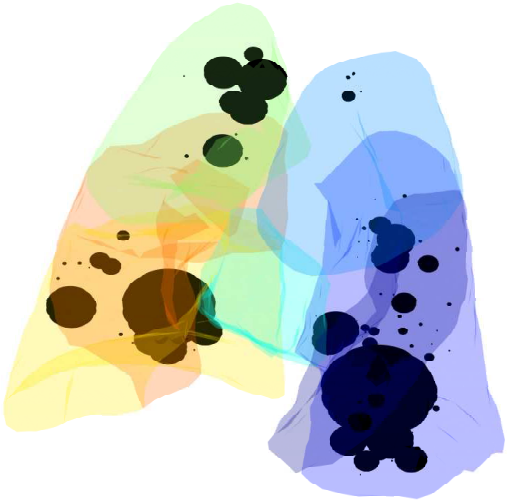

Fig. 1: Example of a simulation of the BM in the macaque virtual lung.

Each simulation of a single infectious process is not deterministic. By performing thousands of simulations with different initial conditions, we obtain an average output for a given fixed set of parameters. The output includes the number of consolidations (big lesions), micronodules (smaller lesions, which are classified as daughter or isolated), lung volume fraction occupied by consolidations, etc.

The parameters of the BM were fitted on a rhesus macaque lung to reproduce the experimental data of [3]. We successfully reproduced the macroscopic behavior of the infection during the initial weeks post-exposure. By taking this fit as a control scenario, we performed some virtual experiments. First, we evaluated the role of immune response strength through the simulation of an immunosuppressed host, revealing that without it, infection burden grows without limit. Second, we quantified the impact of the timing of immune activation, showing that an earlier activation offers some protection against infection burden. Finally, by introducing an artificial encapsulation of lesions within the pulmonary segments, we drew a parallel to human secondary lobules showing that these structures are an important defence mechanism in human infection.

These findings underscore the utility of the BM and high performance computing as tools for testing hypotheses of TB infection dynamics and predicting the impact of prophylactic and therapeutic interventions to control the disease.

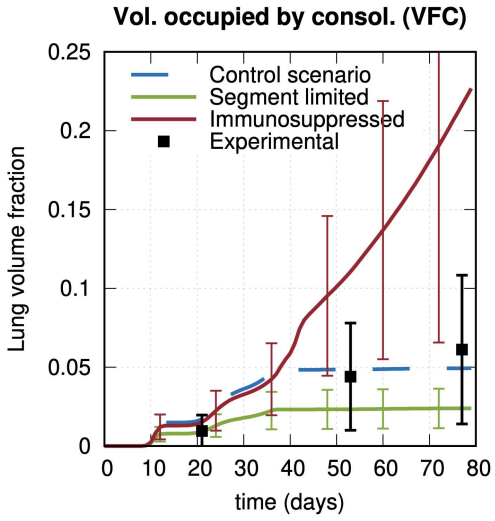

Fig. 2: Comparison of the lung volume fraction occupied by consolidations in the control scenario, immunosuppresed individual, and segment-limited experiment.

[1] Prats, C. *et al. Local Inflammation, Dissemination and Coalescence of Lesions Are Key for the Progression toward Active Tuberculosis: The Bubble Model*. *Frontiers in Microbiology* (2016).

[2] Català, M. *et al. Modelling the dynamics of tuberculosis lesions in a virtual lung*. *PLOS Computational Biology* (2020).

[3] Nogueira, I. *et al. Surveillance of daughter micronodule formation is a key factor for vaccine evaluation using experimental infection models of tuberculosis in macaques*. *Pathogens* (2023).

Thermodynamic inference in molecular motors: A martingale approach

Adrián Nadal-Rosa[1], and Gonzalo Manzano[2]
[1]Institute for Integrative Systems Biology (I2SysBio), CSIC-UV,
Catedrático Agustín Escardino Benlloch 9, 46980 Paterna, Spain
[2]Institute for Cross-Disciplinary Physics and Complex Systems (IFISC),
UIB-CSIC, Campus Universitat de les Illes Balears, E-07122 Palma de Mallorca, Spain

Molecular motors are in charge of almost every process in the life cycle of cells, such as protein synthesis, DNA replication, and cell locomotion, hence being of crucial importance for understanding cellular dynamics. However, given their size scales, in the nanometers range, direct measurements are rather challenging, and the information that can be extracted from them is limited. In this work [1] we proposed two novel strategies to infer thermodynamic properties of molecular motors based on martingale theory in stochastic thermodynamics.

In particular, we used two recent theoretical results about the statistics of entropy production. On the one hand, the integral fluctuation theorem at stopping times [2], and, on the other, a family of bounds to maximal excursions of entropy production [3].

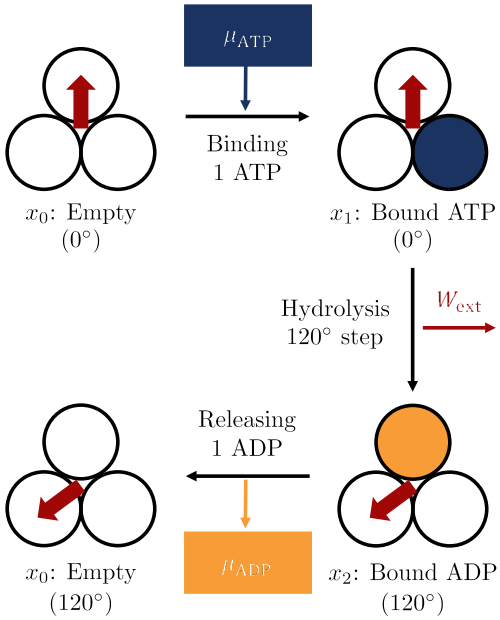

Fig. 1: **Three-states model for F1-ATPase.** A cycle in the hydrolisis (anticlockwise) direction is completed in three steps: (1) ATP binding ($x_0 \to x_1$), (2) ATP hydrolysis into ADP + P, accompanied by a 120° rotation against an external torque ($x_1 \to x_2$), and (3) ADP release ($x_2 \to x_0$). Reversed transitions are allowed and lead to ATP synthesis. The system and ATP and ADP reservoirs (colored squares) are embedded in a dissolution at a temperature T.

To illustrate our approach, we considered the rotary molecular motor F1-ATPase as a case study, which is responsible for the synthesis of ATP, the energy currency of life. We modelled its dynamics as a continuous-time Markovian process over a discrete set of states, each representing a different chemical configuration of the motor (see Fig. 1).

We simulated motor dynamics using the Gillespie algorithm with a stopping condition based on the first time that the motor completes a net number of rotations in either direction, hydrolysis or synthesis (see Fig. 2). Note that these two are the only observable transitions in the system.

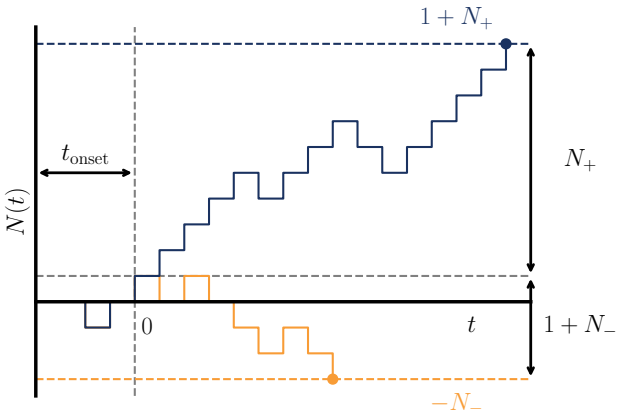

Fig. 2: **Stopping protocol.** The net current in the signaling transition $N(t)$ is monitored over time after the first transition is observed (at time t_{onset}). Trajectories are stopped either when the current reaches the threshold value $N_+ + 1$ (blue trajectory) performing N_+ cycles in the forward direction, or $-N_-$ (orange trajectory) corresponding to N_- cycles in the backward direction.

Using our two inference strategies, several key motor properties can be accessed. Remarkably, one can infer the work per step performed by the motor, the chemical potential difference of the ATP hydrolysis reaction, and the effective temperature of the environment. We focused on infering the work per step. The true value used in simulations was $W_{\mathrm{ext}} = 17\ k_{\mathrm{B}}T$. The IFT-based inference strategy gave an estimate of $17.02 \pm 0.06\ k_{\mathrm{B}}T$, compatible with the true value within one standard deviation and a relative deviation below 0.12%. The inference strategy based on the bounds to extreme statistics of entropy production gave an estimate of $16.6 \pm 0.2\ k_{\mathrm{B}}T$, compatible with the true value within two standard deviations and a relative deviation below 2.4%.

[1] A. Nadal-Rosa, and G. Manzano, *Thermodynamic inference in molecular motors: A martingale approach*, Phys. Rev. E. **112**, 3 (2025).
[2] G. Manzano, G. Kardeş, É. Roldán, and D. H. Wolpert, *Thermodynamics of Computations with Absolute Irreversibility, Unidirectional Transitions, and Stochastic Computation Times*, Phys. Rev. X. **14**, 2 (2024).
[3] G. Manzano, and É. Roldán, *Universal bounds to the maximal excursions of entropy production*, Phys. Rev. E. **105**, 2 (2022).

Periodic Input forces Synchronisation in Chaotic Neural Networks via Stochastic Resonance

Eduardo Nieto-Vargas[1], Rubén Calvo[1], Carles Martorell[1], and Miguel A. Muñoz[1]
[1]Departamento de Electromagnetismo y Física de la Materia
and Instituto Carlos I de Física Teórica y Computacional, Universidad de Granada, E-18071, Granada, Spain

During the last decades, neuroscience has benefited from the framework of complex systems theory. One example is a possible explanation for the chaotic behaviour observed in the neural cortex given by Sompolinsky et al. [1], where they explained that chaos can arise in randomly connected networks described by simple coupling equations. The original model has been extended to include a non-zero mean synaptic strength [2] and external noise [3], leading to three collective phases of the firing rates of the neural network. These phases are separated by phase transitions, of relevance to shed light on the brain criticality hypothesis [4].

To gain deeper insight into the response of this type of network to external inputs, we studied the case of a random non-reciprocal network subjected to a periodic input with a characteristic frequency, where the firing rate x_i of the ith neuron follows the equation

$$\dot{x}_i = -x_i + \tanh\left(g\sum_j J_{ij}x_j\right) + I_0\cos(\omega_i t + \theta_i)\,, \qquad (1)$$

where g is the global synaptic strength, J_{ij} is the synaptic strength of the effect of the jth neuron to the ith neuron, I_0 is the amplitude of the external forcing and ω_i and θ_i are respectically the frequency and phase of the external forcing in the ith neuron.

We discovered a resonance phenomenon where the complex Kuramoto order parameter has module close to one at a characteristic structure-dependent frequency (see Figure 1), revealing phase synchronization at the resonant frequency. We propose stochastic resonance between the intrinsic chaotic dynamics and the oscillatory input as a possible explanation for this event and analytically estimate the approximate theoretical resonance frequency, which is compatible with that observed in the simulations.

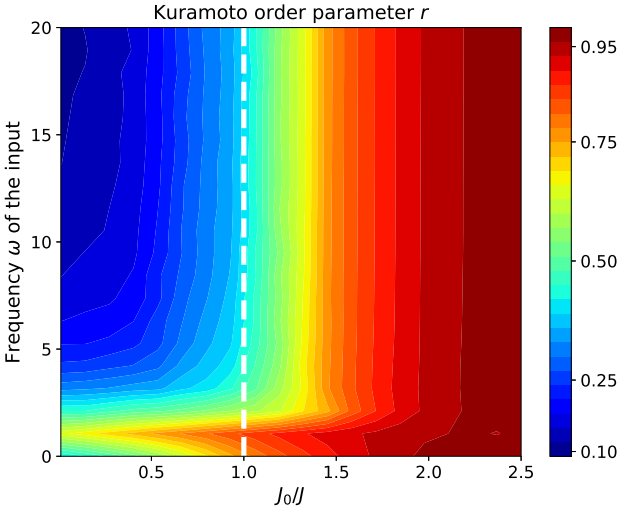

Fig. 1: Heat map of the average Kuramoto order parameter over several realizations of the random coupling strengths Jij of the networks as a function of the frequency ω of the input and the control parameter J0/J for J = 1.

[1] H. Sompolinsky, A. Crisanti, and H.-J. Sommers, Chaos in Random Neural Networks, Phys. Rev. Lett. 61, 259 (1988).
[2] Martorell et al., Dynamically selected steady states and criticality in non-reciprocal networks, Chaos, Solitons and Fractals 182, 114809, 2024.
[3] Calvo et al., Frequency-Dependent Covariance Reveals Critical Spatiotemporal Patterns of Synchronized Activity in the Human Brain, Phys. Rev. Lett. 133, 208401, 2024.
[4] Muñoz et al., Colloquium: Criticality and dynamical scaling in living systems, Reviews of Modern Physics. 90, 3, 2018.

Criticality in *in silico* neuronal networks

Mikel Ocio-Moliner[1,2], Eulàlia Canals[1] and Jordi Soriano[1,2]
[1]Departament de Física de la Matèria Condensada, Universitat de Barcelona, 08028 Barcelona
[2]Universitat de Barcelona Institute of Complex Systems(UBICS), 08028 Barcelona

Neuronal networks are hypothesized to operate near a critical point [1]—an intermediate regime between a quiescent and an absorbing state—where dynamic range, information transmission, and computational capacity are maximized [2]. At this operating point, neuronal dynamics are expected to exhibit scale invariance, universal scaling relations, and well-defined critical exponents.

In this work we investigate whether these signatures of criticality emerge in biologically plausible neuronal networks across structural and dynamical scales, and shed light on the mechanisms shaping such criticality state. For that, we simulate spiking dynamics in spatially embedded neuronal networks constructed under different simple geometries, such as Random Geometric Graphs or Hierarchically Modular Networks, coupled with Izhikevich neuron dynamics [3]. By varying structural parameters (connection radius, modular organization) and dynamical parameters (excitation–inhibition ratio, E/I strength balance), we examine how spatial embedding and topological heterogeneity influence the location and nature of the critical point. The measured critical exponents satisfy established scaling relations but systematically deviate from classical mean-field values in a manner consistent with spatially constrained and modular connectivity.

Finally, we map experimental neuronal activity recorded via multielectrode arrays onto this parameter space to evaluate the biological validity of the explored regimes.

[1] Beggs, J. M., Plenz, D., *Neuronal avalanches in neocortical circuits*, Journal of neuroscience, **23**, 11167-11177, 2003.

[2] Beggs, J., *The Cortex and the Critical Point*, The MIT Press, 2022

[3] Izhikevich, E.M., *Simple model of spiking neurons*, IEEE Transactions on Neural Networks **14**, 1569-1572, 2003.

Noise structure shapes transition pathways in cell-type switching processes

Sara Oliver-Bonafoux[1], Javier Aguilar[2], Tobias Galla[1], and Raúl Toral[1]
[1] Instituto de Física Interdisciplinar y Sistemas Complejos IFISC (CSIC-UIB), Campus UIB, 07122 Palma de Mallorca, Spain
[2] The Abdus Salam International Centre for Theoretical Physics, 34014 Trieste, Italy

Cells are dynamical systems capable of transitioning between different phenotypic states through the coordinated activation and repression of genes. Since gene expression is inherently stochastic, these dynamics are commonly described using stochastic modeling frameworks. A central ingredient in such descriptions is the choice of the noise function, which determines how fluctuations depend on the cellular state. Many studies assume state-independent fluctuations, known as *additive* noise [1], due to their analytical and computational simplicity. However, growing experimental evidence indicates that fluctuations in gene expression are state-dependent, naturally giving rise to *multiplicative noise* [2].

In this work, we investigate the impact of noise structure on cell-type switching processes in a minimal gene regulatory network composed of two self-activating and mutually repressing genes. This regulatory motif captures the essential features of binary cell-fate decisions and supports multiple stable phenotypic states corresponding to differentiated and undifferentiated cell types. Within this framework, we consider several forms of noise, including additive noise and three forms of multiplicative noise (environmental, demographic, and a simplified version of demographic noise). In addition, we analyze a reaction-based model that provides a microscopic representation of the underlying gene regulatory dynamics.

In particular, we study the impact of noise structure on differentiation, dedifferentiation and transdifferentiation processes. For each case, we compute the most probable transition pathway (see Fig. 1) in the limit of infinitesimal noise under different noise structures. To complement this analysis and characterize transitions beyond the small-noise regime, we also provide ensembles of stochastic trajectories at finite noise intensities. Our results show that, while differentiation paths are robust across different noise models, dedifferentiation and transdifferentiation are highly sensitive to the type of noise considered.

Overall, these findings highlight the critical role of noise structure in shaping cell-type switching dynamics. More broadly, they underscore the importance of carefully selecting the stochastic description when modeling biological systems, as different noise assumptions can lead to qualitatively different dynamical behaviors.

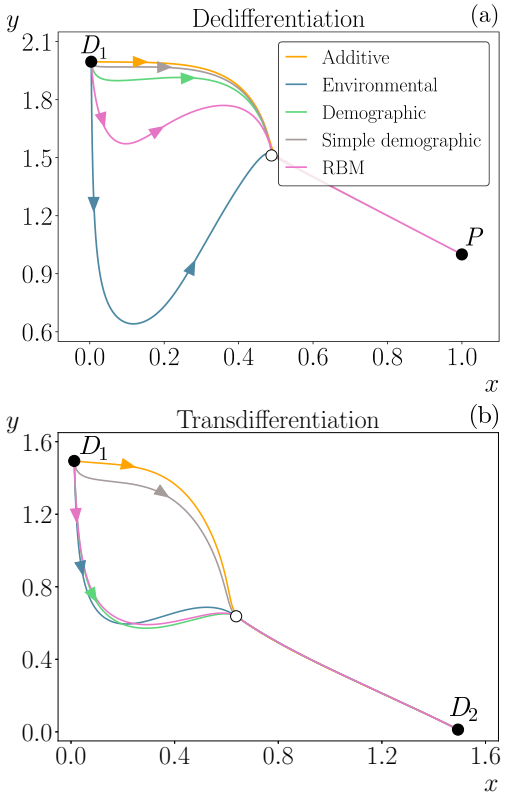

Fig. 1: Most likely transition paths in the small-noise limit for: (a) dedifferentiation from a (specialized) differentiated state D_1 to a progenitor state P, and (b) transdifferentiation from differentiated state D_1 to differentiated state D_2. In each case, optimal transition paths are computed under descriptions in terms of stochastic differential equations with additive, environmental, demographic, and simplified demographic noise, as well as under the corresponding discrete reaction-based model (RBM).

[1] J. Wang, K. Zhang, L. Xu, and E. Wang, *Quantifying the Waddington landscape and biological paths for development and differentiation*, Proceedings of the National Academy of Sciences **108**, 8257 (2011).

[2] A. Bar-Even, J. Paulsson, N. Maheshri, M. Carmi, E. O'Shea, Y. Pilpel, and N. Barkai, *Noise in protein expression scales with natural protein abundance*, Nature Genetics **38**, 636 (2006).

Anticipated synchronization in stochastic individual-based models

David Ortiz del Campo[1], Tobias Galla[1] and Raúl Toral[1],
[1]Instituto de Física Interdisciplinar y Sistemas Complejos IFISC (CSIC-UIB), Campus UIB, 07122 Palma de Mallorca, Spain.

Anticipated Synchronization (AS) describes counter-intuitive situations in which a system synchronizes with the future state of another, even though the coupling between the systems is perfectly causal. Thus, the driven system 'forecasts' the driver. Common setups include two identical copies of a system, coupled with a fixed delayed interaction. AS has been reported in chaotic [1], excitable [2] and spatially extended systems [3].

In this presentation, we extend the concept of AS to stochastic individual-based models. Previous studies [1–3] have considered systems of the form

$$\begin{cases} \dot{\mathbf{x}}(t) = \mathbf{f}[\mathbf{x}(t)], \\ \dot{\mathbf{y}}(t) = \mathbf{f}[\mathbf{y}(t)] + K\left[\mathbf{x}(t) - \mathbf{y}(t-\tau)\right], \end{cases} \tag{1}$$

where $\mathbf{x}$ and $\mathbf{y}$ denote the driver and driven systems, respectively, τ is the delay time, and $\mathbf{f}$ defines the intrinsic dynamics.

Here, instead of deterministic evolution equations, the dynamics are defined through stochastic reactions between particles of different species. The coupling is implemented through two additional reactions: particles in the driver system create particles in the driven system at rate K, while particles in the driven system are removed through a delayed reaction with the same rate K and delay τ.

We investigate two interpretations of the delayed reaction. In the *anonymous-target interpretation* (see [4, 5] for further details on the interpretation of delayed reactions), a delayed removal of an arbitrary (anonymous) target-type particle takes place provided that at least one target particle is present in the driven system after a time τ; otherwise, the event is discarded. In the deterministic limit (number of particles tending to infinity), this setup recovers Eq. (1). In the *active tagged-particle interpretation*, a specific particle is tagged when the delayed reaction is triggered and removed after a time τ, unless it disappears through another process before the delay expires.

We analyze the well-known Brusselator in two dynamical regimes: one in which the deterministic limit exhibits sustained oscillations, and another in which the deterministic dynamics converges to a fixed point while the stochastic system displays noise-induced oscillations.

For the anonymous-target interpretation, AS appears in the oscillatory regime for approximately the same coupling strengths and delays as in the deterministic description, although a minimum coupling strength is required due to demographic fluctuations. More interestingly, AS is also observed in the regime with noise-induced oscillations, as illustrated in Fig. 1(a,b). In this regime, linearization around the fixed point yields analytical expressions for the correlations, which agree well with simulations.

For the active tagged-particle interpretation, the driver and driven systems are no longer dynamically equivalent, although synchronization persists throughout the explored parameter region. In this case, one variable always lags behind the driver, while another may still exhibit AS, as shown in Fig. 1(c,d).

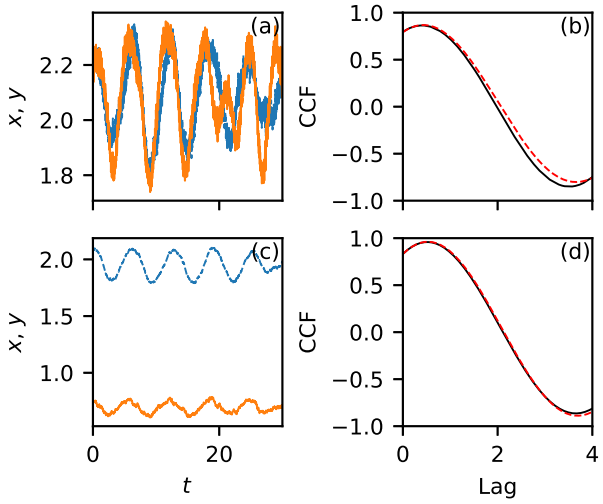

Fig. 1: Results for the stochastic Brusselator in the regime of noise-induced oscillations. Panels (a,b) correspond to the anonymous-target interpretation with parameters $K = 1$ and $\tau = 0.5$, while panels (c,d) correspond to the active tagged-particle interpretation with parameters $K = 10$ and $\tau = 0.15$. Panels (a) and (c) display a typical trajectory of the concentrations of a species X in the driver (dashed blue line) and Y in the driven system, (solid orange line). Panels (b) and (d) show the corresponding cross-correlation functions (CCFs). The existence of AS is indicated by the presence of a maximum of the CCF close to one and located at a positive lag value. Solid black curves are obtained from stochastic simulations, whereas dashed red curves correspond to the analytical predictions derived from the linearized theory.

[1] H. U. Voss, *Anticipating chaotic synchronization*, Physical Review E **61**, 5115-5119 (2000).

[2] M. Ciszak, O. Calvo, C. Masoller, C. R. Mirasso, R. Toral, *Anticipating the response of excitable systems driven by random forcing*, Physical Review E **90**, 204102 (2003).

[3] M. Ciszak, C. Mayol, C. R. Mirasso, R. Toral, *Anticipated synchronization in coupled complex Ginzburg-Landau systems*, Physical Review E **92**, 032911 (2015).

[4] L. F. Lafuerza, R. Toral, *Exact solution of a stochastic protein dynamics model with delayed degradation*, Physical Review E **84**, 051121 (2011).

[5] J. Miękisz, J. Poleszczuk, M. Bodnar, U. Foryś, *Stochastic Models of Gene Expression with Delayed Degradation*, Bull Math Biol **73**, 2231–2247 (2011).

Molecular simulation and modelling of thermoresponsive microgels

Arturo Moncho-Jordá[1,2], Alejandro Cuetos[3], Miguel Ángel Fernández-Rodríguez[1], Joe Dzubiella[4], Alessandro Patti[1,2]
[1]Department of Applied Physics, University of Granada, Avenida Fuentenueva, 18071 Granada, Spain
[2]Carlos I Institute of Theoretical and Computational Physics, Avenida Fuentenueva, 18071 Granada, Spain
[3]Center for Nanoscience and Sustainable Technologies (CNATS), and
Department of Physical, Chemical and Natural Systems, Universidad Pablo de Olavide, 41013 Sevilla, Spain
[4]Physikalisches Institut, Albert-Ludwigs-Universität Freiburg, Hermann-Herder Straße 3, D-79104 Freiburg, Germany

We introduce a coarse-grained theoretical and computational framework to describe the compression and assembly of thermoresponsive core–shell microgels in good solvent conditions. The approach builds upon a recently developed effective interaction formalism for responsive microgels that combines internal free-energy resolution with pairwise coarse-graining. The particle free energy is explicitly decomposed into core and shell contributions, each described through a Flory–Rehner-type theory with distinct elastic and swelling responses. Mechanical equilibrium between both regions is enforced, providing a self-consistent determination of particle size, internal redistribution of polymer density, and deformation under external constraints [1].

Interparticle interactions are mapped onto a size-dependent multi-Hertzian effective potential that explicitly incorporates the heterogeneous mechanical response of the core and corona. This formulation preserves the link between microscopic thermodynamics and mesoscale interactions, enabling a consistent description of compression-induced changes in both particle shape and effective interaction strength. Model parameters are calibrated against dynamic light scattering data for PNIPAM microgels across temperatures spanning the lower critical solution temperature, allowing quantitative reproduction of the swelling–collapse transition, including the non-trivial evolution of internal core dimensions and effective softness.

Building on this effective representation, Monte Carlo simulations of concentrated suspensions under compression are performed to explore structural, thermodynamic, and emergent collective properties. We analyze the evolution of size distributions, effective packing fraction, spatial correlations, and equation-of-state behavior as a function of temperature and concentration. In addition, we characterize the crossover from single-particle deformation to collective compression regimes and the onset of structural rearrangements driven by softness and internal heterogeneity. Our results demonstrate that responsiveness, compressibility, and internal architecture act in a coupled manner to govern the organization of dense microgel assemblies, providing a unified link between single-particle free-energy landscapes and emergent collective phenomena.

Acknowledgements
A.M.J. and A.P. thank grant no. PID2022-136540NB-I00 awarded by MICIU/AEI/10.13039/501100011033 and ERDF, a way of making Europe. A.M.J. also acknowledges the program Visiting Scholars funded by the Plan Propio of the University of Granada (Project PPVS2018-08). M.A.F.R. acknowledges funding from PID2020-116615RA-I00, PID2023-149387OB-I00, and PID2023-147135OB-I00 funded by MICIU/AEI/10.13039/501100011033 and by FEDER, EU, an EMERGIA grant with reference EMC21-00008 and project C-ING-208-UGR23 funded by Consejería de Universidad, Investigación e Innovación de la Junta de Andalucía, and by FEDER "Andalucía 2021-2027".

[1] A. Moncho-Jordá, A. Cuetos, M. Á. Fernández-Rodríguez, J. Dzubiella, and A. Patti, Macrmolecules **58**, 19, 10659 (2025)

A new experimental approach to study hemodynamic non-linear flows

Federico P. González[1] and Javier Burguete[1]
[1] Department of Physics and Applied Mathematics, University of Navarra, E-31008, Pamplona, Spain

Hemodynamic flows are a good example of non-linear systems in fluid-mechanics. Pulsatile flows and details of the geometries are specifics on each person and produce scenarios whose dynamics is largely unknown. For instance, vortices are created in bifurcations, as a compensation of the broken velocity profile. The origin of the pressure changes and recirculations are not completely understood.

Present hemodynamic models have become obsolete due to recent deveploments of medical techniques as MRI-based velocity acquisition. These tools provide data that point to the existence of a quasi-turbulent regime [1, 2]. Studies based on radiotherapy [3, 4] reveal the role of hemodynamic flows on determining blood dose rate, specifically on bifurcated arteries, where a temporal rich dynamics appears.

Recently, some authors [5, 6] underlined the importance of the sistolic pulse characteristics: changes on the shape of the temporal velocity profile, related to diseases or the age, maximize these dynamics [7].

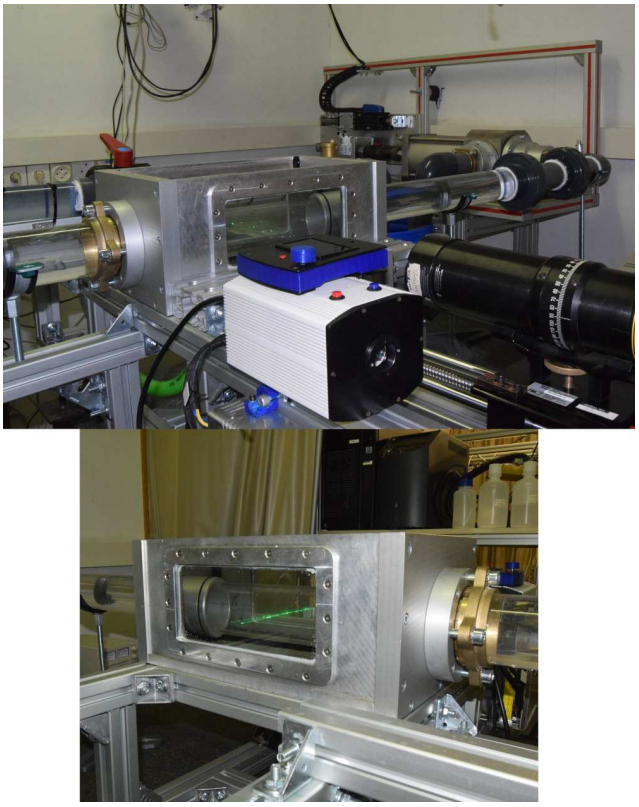

Fig. 1: Top Figure: Experimental set-up. Bottom Figure: Measurement zone.

We present a new experimental set-up, where the goal is to quantify the non-linear behaviour of the bifurcated arteries, to understand the dynamics and to correlate it to the temporal scale, (Top panel 1). We have built a closed loop with passive valves which are able to replicate the aortic and mitral valves. We produced a tailor-made axial pump (as a model of the left ventricule) to accurately control each parameter related to the shape of the velocity profile. In order to enhance the quality of the measurements, the geometry is scaled by a factor 3, increasing the period of the pulse and reducing the instantaneous velocity. The pump has the maximun capability to move $2.15L$ per pulse with a frequency of $0.82Hz$ and a minimun capability of $120ml$ with a frequency of $0.25Hz$. The design allows to analyze different bifurcations set-ups and a linear set-up, where no bifurcation exists. This linear set-up is basically a Poiseuille flow (Womersley), and is studied as a workbench to adapt the differentes techniques.

The measurement zone is located on a tank filled with the working fluid to regularize the optical properties of the set-up, Bottom panel 1. Measurements are obtained by optical techniques, specifically with a LDV system.

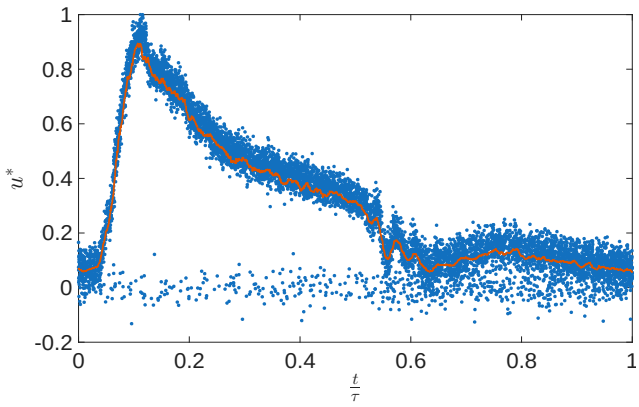

Fig. 2: Adimensional temporal velocity profile. τ correspond to the period.

We present preliminary results on a linear rigid domain testing different close-to-physiological velocity profiles. On figure 2, we show the adimensional temporal evolution of the velocity profile.

[1] K.M. Saqr, S. Tupin, S. Rashad, T. Endo, K. Niizuma, T. Tominaga, M. Ohta, Sci. Rep., **10**, 15492 (2020)
[2] K.M. Saqr, I.F. Zidane, Sci. Rep. **12** 13166(2022)
[3] M. García-Cardosa, C. Beekman, J. Burguete, H. Paganetti, Phys. Med. Bio. **71**, 9 (2026)
[4] Huesa Berral C., Whitrow R.J., Bertolet A., et al., Eur. J. Nucl. Med. Mol. Imaging, **50**, 2023
[5] M.C. Brindise, P.P. Vlachos, Phys. Fluids, **30**, 015111 (2018)
[6] J. Bürk, P. Blanke, S. Stankovic, et al., J. Cardiovasc. Magn. Reson., **14**, 84 (2012)
[7] D. Moron, D. Feldmann, M. Avila J. Fluid Mech. **948**, A20 (2022)

Stochastic Synchronization of Master-Slave Coupled Nonlinear Partial Differential Equations

Joaquín Míguez[1] and Inés P. Mariño[2]
[1] Universidad Carlos III de Madrid, Avenida de la Universidad 30, 28911 Leganés, Madrid, Spain
[2] Universidad Rey Juan Carlos, Calle Tulipán s/n, 28933 Móstoles, Madrid, Spain

Synchronization of spatially extended nonlinear systems has traditionally been investigated for individual model equations. However, many nonlinear evolution equations arising in applications share a common semilinear structure, consisting of a Burgers-type quadratic convection term together with a polynomial differential operator accounting for both dispersive and dissipative effects. Motivated by this observation, we study a general family of one-dimensional nonlinear PDEs that encompasses, among others, the generalized Kuramoto-Sivashinsky, Kawahara, Benney-Lin, and Nikolaevskiy equations [1–5]. This common formulation provides a unified framework in which synchronization results can be established simultaneously for a broad class of nonlinear evolution equations rather than on a model-by-model basis.

Using periodic boundary conditions and a Fourier spectral representation, we construct master-slave coupling schemes for the whole class of equations and generalize the local synchronization result previously established for the deterministic generalized Kuramoto-Sivashinsky equation [1] to this broader framework. The proposed formulation shows that the synchronization mechanism is not specific to a particular equation, but is shared by the entire family through a common quadratic nonlinear interaction, while the differences between models are entirely captured by the polynomial linear operator. The Fourier representation also yields a common finite-dimensional modal formulation, in which the nonlinear dynamics retain the same quadratic convolution structure independently of the particular equation under consideration, while the linear dynamics are completely characterized by the polynomial differential operator.

We then extend the analysis to stochastic dynamics by considering a deterministic master system observed through additive noise and a corresponding stochastic slave obtained by coupling the master with noisy observations. After applying a Fourier spectral truncation, the resulting dynamics are represented by a finite-dimensional system of stochastic differential equations governing the evolution of the retained Fourier modes. This formulation naturally leads to a probabilistic notion of synchronization based on the stability of the synchronization error process. Using stochastic stability techniques, we derive conditions under which the slave remains close to the deterministic master with high probability despite the presence of observational noise. The analysis further provides quantitative finite-time estimates for the synchronization error and identifies a subclass of equations for which stronger global stability properties can be established.

To illustrate the proposed methodology, we present numerical experiments for the stochastic Nikolaevsky equation. Figure 1 shows the evolution of the synchronization error field, which rapidly decreases and subsequently remains confined to a small neighbourhood of zero despite the stochastic perturbations. These results are consistent with the theoretical analysis and demonstrate the robustness of the proposed stochastic synchronization framework.

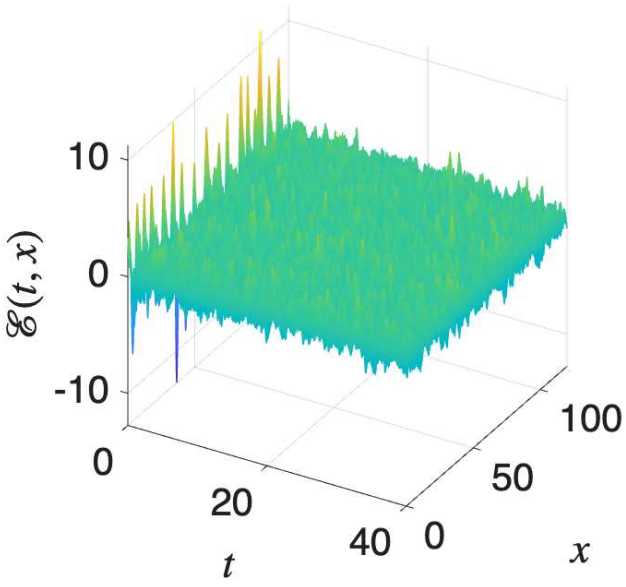

Fig. 1: Evolution of the synchronization error field for the stochastic Nikolaevskiy equation. Despite the stochastic perturbations induced by noisy observations, the synchronization error rapidly decreases and subsequently fluctuates around zero, illustrating successful stochastic synchronization.

[1] J. Míguez, H. Molina-Bulla, and C. Author3, *Master-slave coupling scheme for synchronization and parameter estimation in the generalized Kuramoto-Sivashinsky equation*, Phys. Rev. E **110**, 054206 (2024).
[2] J. Topper and T. Kawahara, *Approximate equations for long nonlinear waves on a viscous fluid*, J. Phys. Soc. Jpn. **44**, 663–666 (1978).
[3] D. J. Benney, *Long waves on liquid films*, J. Math. Phys. **45**, 150–155 (1966).
[4] S. P. Lin, *Finite amplitude side-band stability of a viscous film*, J. Fluid Mech. **63**, 417–429 (1974).
[5] E. Simbawa, P. C. Matthews, and S. M. Cox, *Nikolaevskiy equation with dispersion*, Phys. Rev. E **81**, 036220 (2010).

Emergent life-like dynamics in interacting Stochastic Cubic Autocatalytic Reaction–Diffusion Systems

Alberto P. Munuzuri[1,2], and Juan Pérez-Mercader[3]
[1]Group of Nonllinear Physics. Univ. of Santiago de Compostela, 15706 Santiago de Compostela (Spain)
[2]Galician Center for Mathematical Research and Technology (CITMAga), 15706 Santiago de Compostela, Spain
[3]Department of Earth and Planetary Sciences, Harvard University. Cambridge, MA 02138-1204 (USA)

A simple Stochastic Cubic Autocatalytic Reaction–Diffusion (SCARD) system composed of three coupled equations has previously been shown to generate solutions that reproduce, to a remarkable extent, several characteristic properties associated with living systems. These include self-organization, persistence of localized structures, and adaptive responses emerging from nonlinear dynamics. Such behavior suggests that relatively simple stochastic reaction–diffusion frameworks may capture essential mechanisms underlying the emergence of complex, life-like patterns[1].

In the present contribution, we extend this framework by introducing a systematic methodology to incorporate interactions between different populations or "species" within the SCARD model. The proposed formulation allows the coupling of multiple autocatalytic systems through interaction terms that represent competitive, cooperative, or predator–prey–like dynamics. This generalized approach provides a flexible platform for studying how interacting populations influence the spatiotemporal evolution of the system.

We analyze several representative interaction scenarios and investigate their impact on pattern formation, stability, and collective dynamics. Numerical simulations show that the inclusion of inter-species coupling enriches the dynamical behavior of the model, leading to phenomena such as coexistence, spatial segregation, and synchronized pattern evolution.

Overall, our results demonstrate that extending the SCARD model to include interacting populations produces dynamical behaviors that bear striking qualitative similarities to interaction mechanisms observed in real biological and ecological systems. These findings further support the potential of stochastic reaction–diffusion models as minimal frameworks for exploring the emergence of complex life-like dynamics.

[1] A.P. Muñuzuri J. Pérez-Mercader. *Unified representation of Life's basic properties by a 3-species Stochastic Cubic Autocatalytic Reaction-Diffusion system of equations* Physics of Life Reviews 2022; 41: 64-83.

Effect of particle morphology on margination dynamics in stenotic vessels: 2D and 3D simulations with red blood cells

Raquel Dapena-García and Vicente Pérez-Muñuzuri
CRETUS, Group of Nonlinear Physics, University of Santiago de Compostela, Spain

Cardiovascular diseases are a leading cause of death globally, with many cases linked to stenosis, an abnormal narrowing of blood vessels. Smart drug delivery systems based on micro- and nanoparticles offer promising minimally invasive therapeutic strategies. Several shear stress-sensitive drug vehicles have been proposed, where drug release is triggered by local shear changes [1]. However, no existing drug carriers are specifically guided to the vascular lesion by flow characteristics and wall shear stress changes, enabling both localized internalization in diseased cells and sustained therapeutic release. Understanding the factors governing margination in complex vascular geometries like stenotic arteries is therefore critical for advancing biomedical applications.

Particle migration and adhesion in a 2D constricted channel were studied using the lattice Boltzmann method [2, 3] to elucidate the combined effects of particle size, shape, flow conditions, and adhesion strength. Results show that medium-sized non-circular particles achieve significantly greater lateral margination than larger circular ones, demonstrating that shape and size jointly determine margination efficiency. Adhesion behavior [4] was strongly governed by local wall shear stress: increased adhesion strength favored earlier migration toward the boundaries, while high shear stress regions upstream of the stenosis substantially reduced the probability of stable particle attachment. A probabilistic model of particle detachment under varying shear conditions provided a more realistic assessment of the balance between particle retention and release.

Three-dimensional simulations in a stenotic vessel, incorporating deformable red blood cells (RBCs), confirmed and extended these findings. The presence of RBCs modified the lateral particle distribution, enhancing margination of non-circular particles toward the vessel wall in the post-stenotic region. The interplay between flow characteristics, particle geometry, cell rigidity, RBC-mediated hydrodynamic interactions, and wall shear stress was shown to critically determine lateral margination within the cell-free layer. These results provide design guidelines for nanoparticles in precision medicine, improving drug carrier effectiveness in regions of vascular pathology while minimizing occlusion risks associated with large particle sizes or high concentrations.

Acknowledgments: This research has been supported by the Xunta de Galicia (Grant No. 2025-PG025) and Ministerio de Ciencia e Innovación (Grant No. PID2022-141626NB-I00).

[1] Forouzandehmehr, M. et al. (2022). Particles in coronary circulation: A review on modelling for drug carrier design. *Materials and Design* **216** 110511. DOI: 10.1016/j.matdes.2022.110511.

[2] Krueger, T. et al. (2016). *The Lattice Boltzmann Method - Principles and Practice, Springer*. DOI: 10.1007/978-3-319-44649-3.

[3] Dapena-García, R., Pérez-Muñuzuri, V. (2026). Exploring the lattice Boltzmann method for two-dimensional turbulence simulation. *Am. J. of Phys.* **94**(4) 303–311. DOI: 10.1119/5.0303644.

[4] Decuzzi, P., Ferrari, M. (2006). The adhesive strength of nonspherical particles mediated by specific interactions. *Biomaterials* **27**(30) 5307—5314. DOI: 10.1016/j.biomaterials.2006.05.024.

Estudio de la criticalidad de las RBM usando AIS

A. Prat Pou[1], E. Romero[2], J. Martí[1] and F. Mazzanti[1]
[1]Departament de Física, Universitat Politècnica de Catalunya, Barcelona Tech, Campus Nord B4-B5, E-08034, Barcelona, Spain
[2]Departament de Ciències de la Computació, Universitat Politècnica de Catalunya, Barcelona Tech, Campus Nord B4-B5, E-08034, Barcelona, Spain

El estudio de las transiciones de fase y el fenómeno de la criticalidad constituye uno de los tópicos centrales de la física estadística, ya que proporciona un marco fundamental para comprender cómo los fenómenos macroscópicos emergen de las interacciones microscópicas. Diversos algoritmos de Monte Carlo han sido propuestos para abordar dicho problema. En este trabajo estudiamos el *Annealed Importance Sampling* (AIS) [1], un algoritmo que parte de una distribución de probabilidad inicial $p_0(\mathbf{x})$ y la transforma gradualmente hacia la distribuciń objetivo $p(\mathbf{x})$ a lo largo de N_β pasos intermedios. La clave del método reside en elegir una $p_0(\mathbf{x})$ de la que sea trivialmente posible obtener muestras, lo que permite generar configuraciones representativas de la distribución $p(\mathbf{x})$.

En este trabajo hemos aplicado el algoritmo AIS a una red neuronal conocida como *Restricted Boltzmann Machine* (RBM) [2], compuesta por dos capas de neuronas denominadas *visible layer* y *hidden layer*, con interacciones únicamente entre neuronas de capas distintas. La RBM es un modelo probabilístico en el que la probabilidad de cualquier estado viene dada por $p(\mathbf{x}) = e^{-E(\mathbf{x})/k_BT}/Z$. La energía E del sistema es:

$$E(\mathbf{x},\mathbf{h}) = -\mathbf{x}^T\mathbf{b} - \mathbf{h}^T\mathbf{c} - \mathbf{x}^T\mathbf{W}\mathbf{h}, \qquad (1)$$

donde $\mathbf{x}$ y $\mathbf{h}$ son los vectores asociados a los valores de las neuronas *visible* y *hidden* respectivamente, $\mathbf{W}$ es la matriz de pesos que describe la interacción entre ambas capas, y $\mathbf{b}$, $\mathbf{c}$ son los bias de cada capa. En este trabajo consideramos que las neuronas pueden adoptar únicamente estados binarios, $x_i \in \{0,1\}$ o $x_i \in \{-1,1\}$.

Una elección natural para $p_0(\mathbf{x})$ es la distribución de campo medio, en la que definimos la energía $E_0 = -\mathbf{x}^T\mathbf{B}$, lo que conduce a

$$p_0(\mathbf{x}) = \frac{e^{\mathbf{x}^T\mathbf{B}/k_BT}}{Z_0}. \qquad (2)$$

Para determinar el valor de $\mathbf{B}$, minimizamos la divergencia de Kullback-Leibler (KL) entre $p_0(\mathbf{x})$ y $p(\mathbf{x})$, lo que conduce a una expresión analítica para $\mathbf{B}$ en función de $\langle\mathbf{x}\rangle$, el valor medio de $\mathbf{x}$ bajo la distribución $p(\mathbf{x})$ de la RBM. Nótese que para $\mathbf{B} = 0$ se recupera la distribución uniforme.

La estrategia empleada para aproximar $\langle\mathbf{x}\rangle$, denominada *signs-h* (SGH) [3], consiste en generar aleatoriamente un conjunto de vectores $\mathbf{h}^i$ y, para cada uno de ellos, calcular el vector $\mathbf{x}^i$ que minimiza la energía asociada. El valor medio $\langle\mathbf{x}\rangle$ se aproxima entonces promediando sobre las distintas realizaciones $\mathbf{x}^i$.

En este trabajo hemos mostrado que, incorporando la mejora SGH, el algoritmo AIS es capaz de detectar transiciones de fase que, de otro modo, permanecen inaccesibles. La figura 1 ilustra un ejemplo con una RBM entrenada sobre el dataset MNIST, donde comparamos la función de partición obtenida con SGH, con la obtenida a partir de $\mathbf{B} = 0$, y con el resultado exacto. Se observa que SGH reproduce correctamente la tendencia del valor exacto, identificando claramente los distintos regímenes del sistema, mientras que la distribución uniforme no logra distinguirlos. Estos resultados sugieren que una inicialización informada de $p_0(\mathbf{x})$ es crucial para el correcto funcionamiento de AIS en sistemas con transiciones de fase, y abren la puerta al estudio sistemático de la criticalidad en modelos estadísticos con estructura de red neuronal.

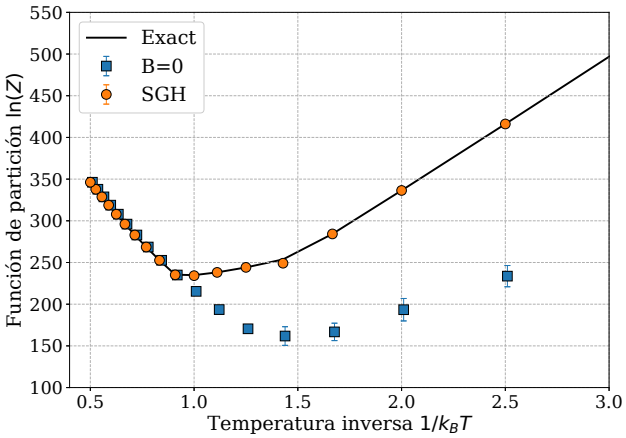

Fig. 1: Logaritmo de la función de partición en función de la temperatura para una RBM entrenada con el dataset MNIST, comparando las inicializaciones $\mathbf{B} = 0$ y SGH con el valor exacto.

[1] R. M. Neal, *Annealed importance sampling*, physics/9803008 (1998).

[2] N. Zhang, S. Ding, J. Zhang, and Y. Xue, *Neurocomputing 275*, 1186 (2018), ISSN 0925-2312, URL https://www.sciencedirect.com/science/article/pii/S0925231217315849

[3] Prat Pou, A.; Romero, E.; Martí, J.; Mazzanti, F. *Mean Field Initialization of the Annealed Importance Sampling Algorithm for an Efficient Evaluation of the Partition Function Using Restricted Boltzmann Machines*. Entropy 2025

Stochastic semi-microscopic modeling of different voltaje-gated channels

L. Ramírez–Piscina[1], and J.M. Sancho[2]
[1]Dep. de Física Aplicada, EPSEB, Universitat Politécnica de Catalunya, Av Doctor Marañón, 44. E-08028 Barcelona. Spain
[2] Universitat de Barcelona, Departament de Física de la Matèria Condensada, Martí i Franqués, 1. E-08028 Barcelona. Spain

The selective transport of ions across cellular membranes is governed by ion channels, complex macromolecular assemblies whose physiological function emerges from stochastic transitions between distinct conformational states. These transitions are fundamentally driven by thermal fluctuations and modulated by external thermodynamic forces, including transmembrane voltage, chemical gradients, and mechanical stress.

We model the single-channel dynamics of these systems using a semi-microscopic approach governed by stochastic differential equations. By using a reduced set of physical degrees of freedom, this framework reproduces key experimental behaviors in voltage-gated channels, including action potentials, pacemaker oscillations, and the "foot-in-the-door" effect [1–4]. Additionally, expanding the model to account for the channel's underlying tetrameric structure we have modelled K channels successfully [5] capturing the intermediate conductive states observed in experiments [6].

In contrast to K-V channels, the Na-V channel activates almost instantaneously in response to membrane depolarization, but it also inactivates very rapidly. This fast inactivation is typically a mechanical occlusion (often described as a "hinged-lid" or "ball-and-chain" mechanism) that physically blocks the pore even if the membrane remains depolarized.

On the other hand, whereas K channels are typically formed by the non-covalent assembly of four separate, usually identical, protein subunits, the Na channel is typically composed of a single, massive continuous polypeptide chain that folds into four distinct homologous domains (Domains I-IV). Because it is one continuous chain, the domains are not perfectly identical, which leads to asymmetric voltage-sensing and gating mechanics.

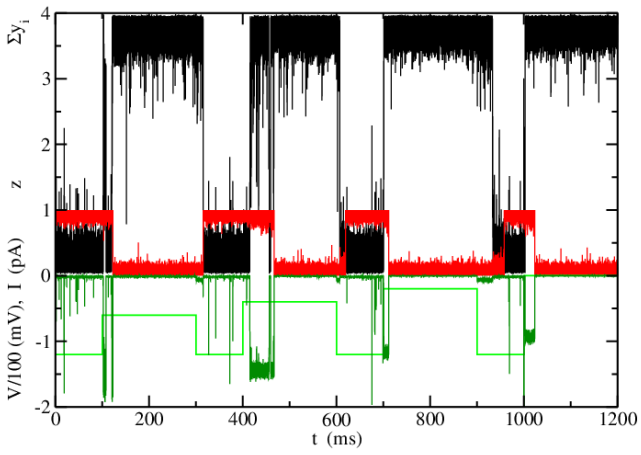

Fig. 1: Na channel under several voltage steps

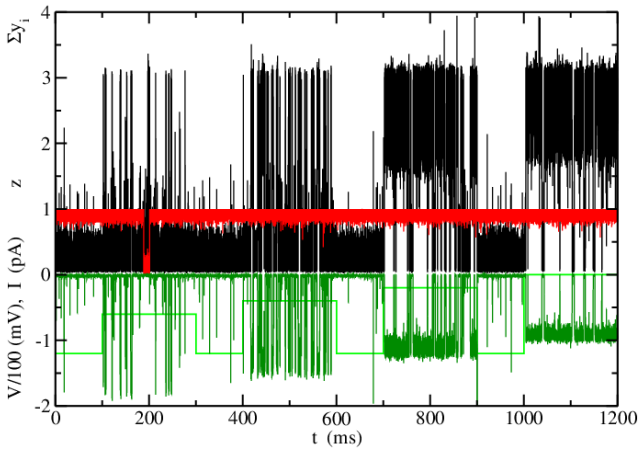

Fig. 2: Mutant Na channel, without fast inactivation, under the same voltage steps

We extend here our semi-microscopic modeling to the voltage-gated Na channel, implementing the pseudo-tetrameric structure and adding an additional inactivation gate. We compare the resulting Na-V channel model to experiments. Additionally, we also compare to experiments with mutant channels, in which the fast inactivation is suppressed [7], and consequently results are more sensitive to the internal model details.

[1] L. Ramírez-Piscina and J. M. Sancho, *Molecular Na-channel excitability from statistical physics*, EPL (Europhysics Letters) **108**, 50008 (2014).

[2] L. Ramírez-Piscina and J. M. Sancho, *Physical properties of voltage gated pores*, The European Physical Journal B **91**, 10 (2018).

[3] L. Ramírez-Piscina and J. M. Sancho, *Periodic spiking by a pair of ionic channels*, Physica A **505**, 345 (2018).

[4] L. Ramírez-Piscina, *Fixed-density boundary conditions in overdamped Langevin simulations of diffusion in channels*, Physical Review E **98**, 013302 (2018).

[5] L. Ramírez-Piscina and J. M. Sancho, *Subconductance states in a semimicroscopic model for a tetrameric pore*, Physical Review E **109**, 044402 (2024).

[6] J.S. Santos, S.M. Grigoriev and M. Montal, *Molecular Template for a voltage sensor in a novel K^+ channel III*, The Journal of General Physiology **132**, 651 (2008).

[7] M.P. Goldschen-Ohm, D.L. Capes, K.M. Oelstrom and B. Chanda, *Multiple pore conformations driven by asynchronous movements of voltage sensors in a eukaryotic sodium channel*, Nature Communications **4**, 1350 (2013).

Free-energy reconstruction from stable clusters (FRESC): A new method to evaluate nucleation barriers from simulation

A. Llamas-Jaramillo[1], I. Latella[1,2], and D. Reguera[1,3]
[1]Departament de Física de la Matèria Condensada, Universitat de Barcelona, 08028 Barcelona, Spain
[2]Universitat de Barcelona, Institute of Nanoscience and Nanotechnology (IN2UB), 08028 Barcelona, Spain
[3]Universitat de Barcelona, Institute of Complex Systems (UBICS), 08028 Barcelona, Spain

We present a simulation technique to evaluate the most important quantity for nucleation processes: the nucleation barrier, i.e. the free energy of formation of the critical cluster. The method is based on stabilizing a small cluster by simulating it in the NVT ensemble and using the thermodynamics of small systems to convert the properties of this *stable* cluster into the Gibbs free energy of formation of the *critical* cluster.

We demonstrate this approach using condensation in a Lennard-Jones truncated and shifted fluid as an example, showing an excellent agreement with previous Umbrella Sampling simulations [2]. The method is straightforward to implement, computationally inexpensive, requires only a small number of particles comparable to the critical cluster size, does not rely on the use of Classical Nucleation Theory, and does not require any cluster definition or reaction coordinate. All of these advantages hold the promise of opening the door to simulate nucleation processes in complex molecules of atmospheric, chemical or pharmaceutical interest that cannot be easily simulated with current techniques.

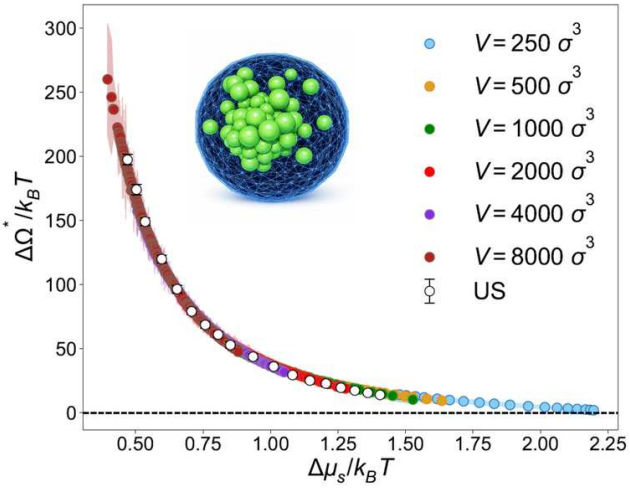

Fig. 1: Free energies of formation of the critical cluster $\Delta\Omega^*$ as a function of the supersaturation $\Delta\mu_s$ at $T = 0.625$ for a system of particles interacting with a Lennard-Jones (LJ) potential truncated and shifted at a reduced cut-off radius of $r_c = 2.5\sigma$ for simulations with different volumes: $V = 250\ \sigma^3$, $V = 500\ \sigma^3$, $V = 1000\ \sigma^3$, $V = 2000\ \sigma^3$, $V = 4000\ \sigma^3$, and $V = 8000\ \sigma^3$. The filled circles are the results of the simulations, and the open circles represent the values of previous Umbrella Sampling simulations of Ref. [2]. The shaded area represents the estimated standard deviation in $\Delta\Omega^*$.

[1] A. Llamas-Jaramillo, I. Latella, D. Reguera, *Free-energy reconstruction from stable clusters (FRESC): A new method to evaluate nucleation barriers from simulation*, J. Chem. Phys. **164**, 034102 (2026).

[2] A. Aasen, Ø. Wilhelmsen, M. Hammer, D. Reguera, *Free energy of critical droplets—from the binodal to the spinodal*, J. Chem. Phys. **158**, 114108 (2023).

Multiwell effects on inelastic confinement-induced resonances

Fabio Revuelta[1], and Alejandro Saenz[2]
[1]Grupo de Sistemas Complejos, ETSIAAB, Universidad Politécnica de Madrid, Avenida Puerta de Hierro 2, 28040 Madrid, Spain.
[2]AG Moderne Optik, Institut für Physik, Humboldt-Universität zu Berlin, Newtonstrasse 15, 12489 Berlin, Germany

Ultracold atoms loaded into optical lattices have emerged as an ideal platform for quantum simulation [1], offering an unprecedented degree of control over interparticle interactions and trapping geometries. In these highly confined systems, scattering properties can be drastically modified by the geometry of the external potential, leading to Confinement-Induced Resonances (CIRs) [2]. When these processes involve transitions between different vibrational states of the trap, they manifest as Inelastic Confinement-Induced Resonances (ICIRs). These resonances act as a powerful mechanism to tune interactions and couple external and internal degrees of freedom, opening new avenues for exploring novel quantum phases and few-body dynamics.

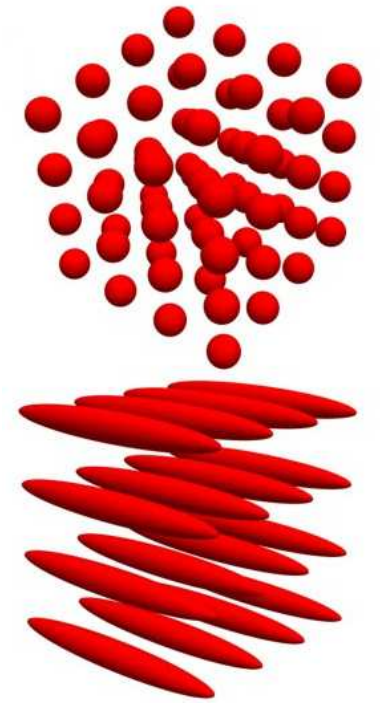

Fig. 1: Comparison of the scattering dynamics under different confinement geometries, as reported in Ref. [3]. (Top) In a three-dimensional optical trap, no dispersive features are observed. (Bottom) In a one-dimensional optical lattice, four distinct dispersive resonance features are detected.

Recently, resonance features associated with multiwell effects have been reported in a groundbreaking experiment conducted with a quantum simulator of ultracold atoms [3]. While the original results were explained through a superexchange mechanism that determines spin dynamics by allowing the virtual population of two particles on the same site, here we provide a complementary interpretation based on the aforementioned mechanisms.

In this work [4], we show that these resonance features can be fully understood as a consequence of ICIRs, manifested as avoided crossings in the two-particle spectrum. Our theoretical framework shows excellent agreement with the experimental data. By comparing the single- and double-well descriptions of the optical trapping potential, we confirm the multiwell origin of the observed features. Furthermore, we demonstrate that a double-well model is already sufficient to resolve the apparent symmetry violation found within the single-well approach. Finally, we discuss some intrinsic limitations of the harmonic approximation in this context.

[1] M. Lewenstein, A. Sanpera, and V. Ahufinger, Ultracold *Atoms in Optical Lattices: Simulating Quantum Many-Body Systems*, 1st ed. (Oxford University Press, Oxford, UK, 2012).

[2] E. Haller, M. J. Mark, R. Hart, J. G. Danzl, L. Reichsöllner, V. Melezhik, P. Schmelcher, and H.-C. Nägerl, *Confinement-Induced Resonances in Low-Dimensional Quantum Systems* Phys. Rev. Lett. **104**, 153203 (2010).

[3] Y. K. Lee, H. Lin, and W. Ketterle. *Spin Dynamics Dominated by Resonant Tunneling into Molecular States*, Phys. Rev. Lett. **131**, 213001 (2023).

[4] F. Revuelta, and A. Saenz, *Inelastic confinement-induced resonances in multiwell potentials* (in preparation).

Maximising the Mpemba effect in kinetic fluids

Antonio Patrón-Castro[1], Carlos Ríos-Monje[2], Carlos A. Plata[2], Bernardo Sánchez-Rey[3], and Antonio Prados[2]
[1]Department of Physics, Simon Fraser University, Burnaby, British Columbia V5A 1S6, Canada
[2]Física Teórica, Multidisciplinary Unit for Energy Science, Universidad de Sevilla, Apartado de Correos 1065, E-41080 Sevilla, Spain
[3]Departamento de Física Aplicada I, Escuela Politécnica Superior, Universidad de Sevilla, E-41011 Sevilla, Spain

The Mpemba effect [1] is a paradigmatic phenomenon of anomalous relaxation in nonequilibrium statistical mechanics [2]. Broadly speaking, it refers to the counterintuitive behaviour in which an initially hotter system cools faster than a colder one. Although this effect is present in a wide variety of physical systems, it requires the fulfillment of specific conditions to appear.

In this context, we investigate how to optimally prepare kinetic fluids, described at the one-particle level and coupled to a controllable thermal bath of temperature $T_s(t)$, in order to maximize the Mpemba effect. The dynamics are analysed using a Sonine expansion, in which the system is characterised not only by its kinetic temperature but also by a hierarchy of Sonine cumulants quantifying deviations from the Maxwellian velocity distribution. Since the cooling rate of the system depends explicitly on these cumulants, suitable preparations of nonequilibrium states with extreme values of such quantities can strongly enhance the Mpemba effect.

We formulate this problem within the framework of optimal control theory. In particular, we consider protocols with free final time and seek the driving $T_s(t) \in [T_{\min}, T_{\max}]$ that maximizes or minimizes a general objective functional built from the Sonine cumulants. The optimization problem is solved using Pontryagin's maximum principle [3].

The resulting optimal dynamics displays a rich phenomenology that strongly depends on both the choice of objective functional and the physical parameters of the system. In particular, different optimal protocols emerge depending on whether the target is maximised or minimised. We analyze in detail how the optimal solutions depend on the bounds imposed on the control and on the kinetic parameters of the fluid.

As a concrete illustration, we apply the general formalism to a molecular fluid subject to nonlinear drag within the first Sonine approximation. In this case, the dynamics are effectively described by the temperature and the excess kurtosis of the velocity distribution, allowing for an explicit characterization of the optimal protocols that maximize the Mpemba effect.

[1] Lasanta, A., Vega Reyes, F., Prados, A., and Santos, A., *When the Hotter Cools More Quickly: Mpemba Effect in Granular Fluids*, Physical Review Letters **119**, 148001 (2017).

[2] Patrón, A., Sánchez-Rey, B., Plata, C. A., and Prados, A., *Non-equilibrium Memory Effects: Granular Fluids and Beyond*, Europhysics Letters **143**, 61002 (2023).

[3] Liberzon, D., *Calculus of Variations and Optimal Control Theory: A Concise Introduction*, Princeton University Press, (2012).

Temperature-driven within-host pathogen dynamics reshapes epidemic invasion in vector-borne plant diseases

Juan Carlos Rodríguez Cabanillas[1], Manuel A. Matias[1], and Alex Giménez-Romero[2,1]
[1]Instituto de Física Interdisciplinar y Sistemas Complejos (IFISC, CSIC-UIB), Campus UIB, 07122 Palma de Mallorca, Spain
[2]Theoretical and Computational Ecology Group, CEAB (CSIC), Blanes, Catalonia, Spain

Epidemic models typically assume constant transmission rates or impose environmental forcing directly on model coefficients, a practical choice that sacrifices the connection between measurable within-host physiology and population-level dynamics. In plant epidemics, the within-host physiology is usually mediated by the temperature to which infected plants are subjected [1] and can be particularly relevant at the epidemic level.

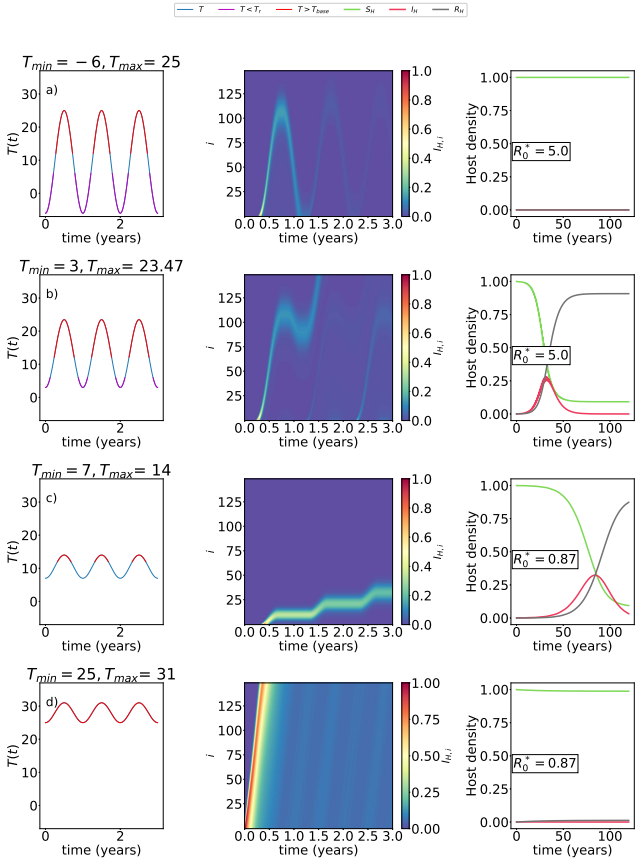

Fig. 1: (a–e) First column: sinusoidal temperature profiles. Red color indicates periods of pathogen progression ($T > T_{base}$); blue color, periods of thermal stasis in which neither progression nor regression occurs; purple color, periods of disease regression ($T < T_r$). Second column: distribution of infected hosts across infection stages, where color denotes the fraction of infected hosts in stage i at time t. Third column: corresponding host population dynamics, showing susceptible (S_H), infected (I_H), and removed (R_H) densities. The values of the remaining model parameters are represented by R_0^*.

Here we extend a vector-borne disease model [2] to incorporate *age of infection* through a stage-structured epidemic framework [3]. In this framework infectiousness emerges from within-host pathogen progression rather than being prescribed externally. Infected hosts progress through ordered compartments representing increasing pathogen load, with temperature-dependent progression and regression rates derived from experimentally measured thermal response functions. This construction generates time-varying infectiousness mechanistically, coupling the within-host pathogen dynamics to between-host disease transmission through thermal forcing. Applied to a vector-borne plant pathosystem (*Xylella fastidiosa*, Pierce's disease of grapevine), the model yields an analytically tractable approximation for the basic reproduction number R_0 whose temperature-dependent reveals a slow-growth paradox: the thermal optimum for within-host pathogen growth is not the thermal optimum for epidemic spread, because rapid progression shortens the effective transmission window, whereas mildly suboptimal temperatures can prolong infectiousness and sustain larger epidemics (see Figure 1 (c-d)) and also reveal how cold conditions can suppress invasion by either halting progression or inducing regression and recovery (see Figure 1 (a-b)).

We analyze epidemic invasion under constant, seasonal, stochastic, and empirical temperature regimes. Analytical expressions for the basic reproduction number under constant and seasonal forcing capture these mechanisms and accurately predict final epidemic size across diverse climatic regimes. Short-term temperature variability has its strongest effects near thermal thresholds, and empirical temperature series from invaded regions generate markedly different epidemic trajectories despite similar invasion suitability. These results show that neglecting the coupling between within-host physiology and transmission can lead to incorrect predictions of plant disease dynamics under climate variability and change.

[1] Giménez-Romero, A., Galván, J., Montesinos, M., Bauzà, J., Godefroid, M., Fereres, A., ... and Moralejo, E. *Global predictions for the risk of establishment of Pierce's disease of grapevines*. Communications Biology, **5**, 1389 (2022).

[2] Giménez-Romero, Flaquer-Galmés and Matías, M. A.*Vector-borne diseases with nonstationary vector populations: The case of growing and decaying populations.* Physical Review E. **106**, 054402 (2022).

[3] N. W. Landry, *Effect of time-dependent infectiousness on epidemic dynamics*, Physical Review E. **104**, 064302 (2021).

New and old Kibble-Zurek mechanisms in the quantum world

Javier Rodríguez-Laguna[1], Fernando J. Gómez-Ruiz[2], Ricardo Gutiérrez[3,4], and Silvia N. Santalla[2,4],

[1]Dto. Física Fundamental, Universidad Nacional de Educación a Distancia (UNED), Spain.
[2]Dto. Física, Universidad Carlos III de Madrid (Spain),
[3]Dto. Matemáticas, Universidad Carlos III de Madrid (Spain),
[4]Grupo Interdisciplinar de Sistemas Complejos (GISC), Universidad Carlos III de Madrid (Spain),

Crossing a phase transition can be a rough experience; crossing it too quickly can be downright traumatic. When a system is driven through such a transformation at a finite rate, it may be unable to coordinate its behavior across the whole system. Different regions independently select incompatible ordered states, leaving behind mismatches at their boundaries. The Kibble–Zurek (KZ) mechanism explains how these mismatches become frozen into defects. Remarkably, the density of such defects often follows universal scaling laws, revealing fundamental information about the critical properties of the transition.

Originally proposed in the field of cosmology [1], the KZ prediction is routinely applied in condensed matter physics and statistical mechanics [2], both in the classical and the quantum regimes [3]. The degree of universality found in practice is remarkable. Indeed, the density of defects when we cross a continuous phase transition is known to depend only on the crossing velocity v and two critical exponents: the dynamical exponent, z, and the exponent associated to the correlation length, ν.

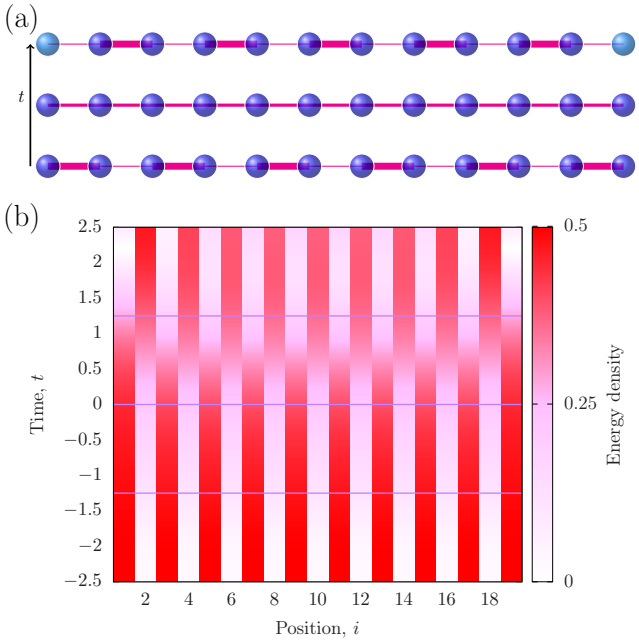

Fig. 1: (a) Illustration of interpolate between the two opposite dimerized free-fermionic chains. (b) Space-time diagram showing the time-evolution of the energy density of such a free-fermionic chain with open boundaries and $N = 20$ sites, illustrating KZ dynamics. Notice that for $t = -2.5$ the state is completely dimerized. As time evolves, we reach the homogeneous chain for $t = 0$ and an approximately opposite dimerization for $t = 2.5$.

As a relevant example, let us consider the interpolation between the two opposite dimerizations of a free-fermionic chain illustrated in Fig. 1(a). The space-time diagram of the energy density (i.e. the local correlation) is shown in Fig. 1(b), as the Hamiltonian evolves linearly between both extremes at $t = -2.5$ and $t = 2.5$. At $t = 0$ the instantaneous Hamiltonian is homogeneous, which would give rise to a nearly homogeneous energy density in the quasistatic limit.

The recent development of synthetic quantum systems has opened novel routes to explore KZ dynamics in engineered setups, such as the possibility to consider *inhomogeneous systems*, in which the physical parameters (such as the coupling constants) vary smoothly across the system [4]. Interestingly, inhomogeneous critical points can be described as if they took place on a *curved spacetime* [5], presenting very intriguing connections to black hole physics.

We therefore explore the wide variety of possible KZ dynamics on inhomogeneous systems, depending on the time-schedule taking us across the phase transition. Finally, we also consider KZ mechanisms in presence of disorder and strong inhomogeneities. This case presents very interesting applications to adiabatic quantum computation, since success is only guaranteed if the conditions of the adiabatic theorem hold, which implies that KZ dynamics should be inhibited.

[1] T.W.B. Kibble, *Topology of cosmic domains and strings,* J. Phys. A: Math. Gen. **9**, 1387 (1976). T.W.B. Kibble, *Some implications of a cosmological phase transition*, Phys. Rep. **67**, 183 (1980).

[2] W.H. Zurek, *Cosmological experiments in superfluid helium?* Nature **317**, 505 (1985).

[3] A. del Campo, G. de Chiara, G. Morigi, M.B. Plenio, A. Retzker, *Structural Defects in Ion Chains by Quenching the External Potential: The Inhomogeneous Kibble-Zurek Mechanism*, Phys. Rev. Lett. **105**, 075701 (2010). A. del Campo, W.H. Zurek, *Universality of phase transition dynamics: topological defects from symmetry breaking*, Int. J. Mod. Phys. A. **29**, 1430018 (2014).

[4] F.J. Gómez-Ruiz, A. del Campo, *Universal Dynamics of Inhomogeneous Quantum Phase Transitions: Suppressing Defect Formation*, Phys. Rev. Lett. **122**, 080604 (2019).

[5] N. Samos Sáenz de Buruaga, S.N. Santalla, J. Rodríguez-Laguna, G. Sierra, *Entanglement in non-critical inhomogeneous quantum chains*, Phys. Rev. B **104**, 195147 (2021).

Testing performance of Catch22 features in a time-series classification task

Consuelo Rojas[1], Ulrich Parlitz[2,3], and Cristina Masoller[1]
[1] Universitat Politècnica de Catalunya, Dept. of Physics, Terrassa, Spain
[2]Max Planck Institute for Dynamics and Self-Organization, Göttingen, Germany
[3] University of Göttingen, Institute for the Dynamics of Complex Systems, Göttingen, Germany

Accurate classification of short and noisy time series remains a challenge in many scientific applications. Feature-based approaches such as *Catch22*[1] aim to provide compact and interpretable representations that retain discriminative information while reducing dimensionality. However, it is not always clear whether such feature extraction methods offer advantages over simpler representations such as raw signals or Fourier-based features. In this study, we systematically compare these representations using synthetic sinusoidal and FitzHugh–Nagumo signals under varying levels of noise, resolution, class separation, and dataset size.

The datasets were generated from sinusoidal signals and FitzHugh-Nagumo (FHN) nonlinear dynamical model (Figure 1). To assess the robustness of each representation, we systematically varied signal duration, temporal resolution, noise level, class separation and the dataset size. Classification was performed using Support Vector Machine classifiers on six different representation: raw signals, Principal Component Analysis (PCA) applied to the raw signal, Fourier Transform (FFT) features, PCA applied to FFT features, *Catch22* features, and PCA applied to *Catch22* features.

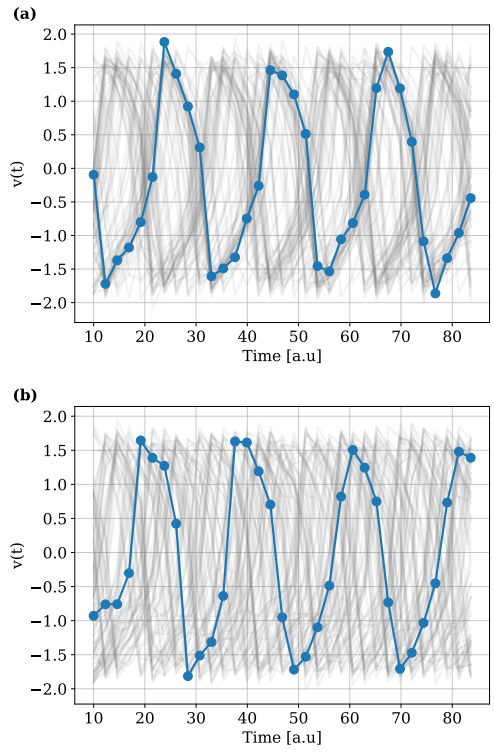

Fig. 1: Representation of FitzHugh-Nagumo signals generated for the experiment. (a) Signals with observational noise; (b) signals generated with dynamic noise.

Classification performance was assessed using the Area Under the ROC Curve (AUC). Across the experiments, *Catch22* features provided robust discriminative performance. For example, FHN signals containing only 21 sampled points remained separable when the parameter difference between classes was approximately 10–20%.

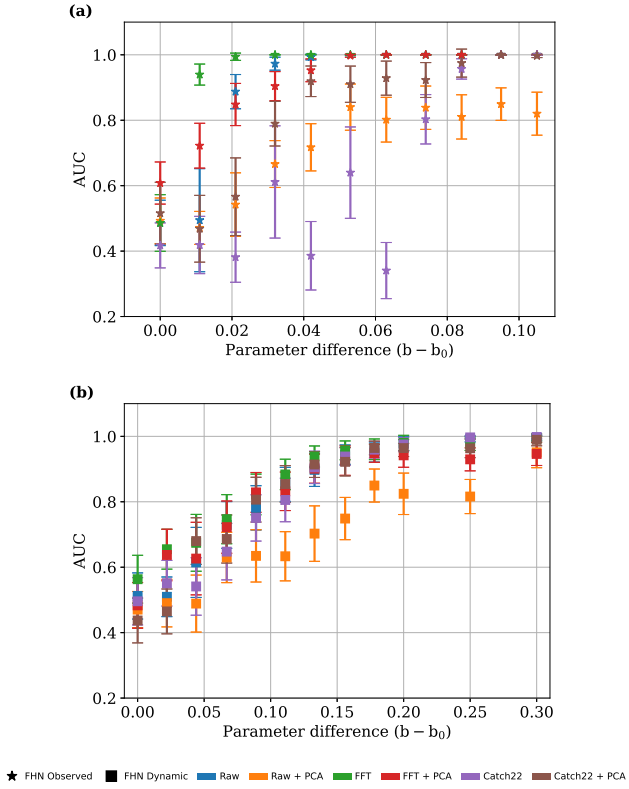

Fig. 2: AUC scores for classification performance for the FitzHugh-Nagumo generated signals. (a) Presents the dataset with observational noise. (b) Presents the results of the dataset generated with dynamic noise.

The results demonstrate that *Catch22* is effective for classification of short and noisy time series and remains applicable under severe data constraints. However, the observed performance gains over simpler representations are limited, suggesting that raw and FFT-based representations often preserve sufficient information for accurate classification. These findings indicate that representation complexity should be carefully balanced against computational cost and interpretability when designing time-series classification pipelines.

[1] C. H. Lubba *et al.*, *catch22: CAnonical Time-series CHaracteristics*, Data Min. Knowl. Discov. **33**, 1821–1852 (2019).

Analytic extension of Simon's model beyond the Zipf point

Pablo Rosillo-Rodes[1,2], Laurent Hébert-Dufresne[2,3], and Peter Sheridan Dodds[2,2,3]
[1]Institute for Cross-Disciplinary Physics and Complex Systems IFISC, Campus Universitat de les Illes Balears, Spain
[2]University of Vermont, Burlington, VT 05405, US
[3]Santa Fe Institute, 1399 Hyde Park Rd, Santa Fe, NM 87501, US

A vast array of evolving complex systems are composed of distinct component types of highly varying sizes: Species abundances within ecologies, market shares of corporations, populations of cities, and word counts in text corpora. A universal hallmark of such systems is that when types are ranked by decreasing size S, an inverse power law relationship appears: $S \sim r^{-\alpha}$ where r is rank. Zipf's law represents the observation that the exponent α for many such systems is close to 1.

Despite the prevalence of inverse power-law size rankings, their origin remains controversial.

Simon's formulation [1], the most influential and strongly debated explanation, fails to describe the $\alpha = 1$ regime. In this kind of models (rich-get-richer), existing elements are copied and new ones are added with some probability. This probability ρ is related to α in Simon's formulation as $\rho = 1-\alpha$. There is a catastrophic problem where $\alpha \to 1$ and $\rho = 1-\alpha \to 0$, as Simon's model produces a pathological first-mover advantage [2] rather than Zipf's law (see Fig. 1).

To address this limitation, we derive a generalized innovation rate $\rho(N,\alpha)$ that extends Simon's framework and correctly reproduces size–rank distributions of the form $f(r) \sim r^{-\alpha}$ for all $\alpha \geq 0$. The proposed innovation rate is given by

$$\rho(N,\alpha) = \frac{1-\alpha}{1+\alpha(1-\alpha)\zeta(\alpha)(N+1)^{\alpha-1}}, \qquad (1)$$

$$\rho(N,\alpha) \to \begin{cases} 1-\alpha & \text{for } \alpha \ll 1, \\ (\ln N+\gamma)^{-1} & \text{for } \alpha = 1, \\ [\alpha\zeta(\alpha)]^{-1} N^{-(\alpha-1)} & \text{for } \alpha \gg 1, \end{cases} \qquad (2)$$

where $\gamma \simeq 0.577$ is the Euler–Mascheroni constant. As seen in Fig. 1, this generalized mechanism eliminates the first-mover bias and reproduces the expected power-law profiles across all regimes. Moreover, we show [3] that the same scaling arises from purely non-mechanistic studies of growing systems [4], independent of the underlying mechanism that is making these systems grow, establishing a formal equivalence between the mechanistic and non-mechanistic origins of Zipf- and Heaps-like behavior.

Crucially, our analysis uncovers how Zipf's law emerges in a rich-get-richer system. The innovation rate must decay as $\sim 1/\log N$ where N, the number of different elements in the system, is large. This is intriguing, as $\log N$ is nothing more than the maximum entropy of a set of N distinct types. And a set of N distinct types is what the framework is modeling. We do not fully understand this result.

Our results unify preferential-attachment dynamics and sampling-based models under a single analytic framework, clarifying how generalized innovation controls the emergence of scale-free patterns in finite systems.

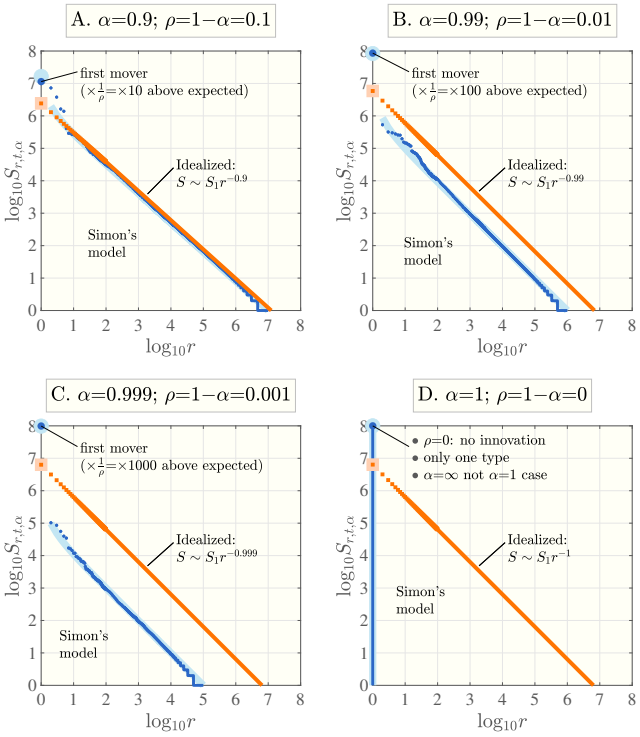

Fig. 1: Simon's model first-mover advantage effect (blue circles) and the result of our generalized innovation rate (orange squares) for different values of α. Here, ρ refers to Simon's fixed innovation rate.

[1] Simon, H. A., On a class of skew distribution functions, *Biometrika*, **42**:425–440, 1955.

[2] Dodds, P. S., Dewhurst, D. R., Hazlehurst, F. F., Van Oort, C. M., Mitchell, L., Reagan, A. J., Williams, J. R., and Danforth, C. M., Simon's fundamental rich-get-richer model entails a dominant first-mover advantage, *Phys. Rev. E*, **95**(5):052301, 2017.

[3] Rosillo-Rodes, P., Zimmerman, Julia W., Hébert-Dufresne, L., and Dodds, P. S., Simon's model does not produce Zipf's law: The fundamental rich-get-richer mechanism for any power-law size ranking, *arXiv*, arXiv:2604.13184, 2026.

[4] Rosillo-Rodes, P., Hébert-Dufresne, L., and Dodds, P. S., Complete asymptotic type-token relationship for growing complex systems with inverse power-law count rankings, *Phys. Rev. Research* **8**, L012029, 2026.

Prestige-driven dynamics to describe Pope name evolution

Dynamica praestigio impulsa ad evolutionem nominum pontificalium describendam

Pablo Rosillo-Rodes[1,3,*], Santiago Lamata-Otín[2,3,*], Laurent Hébert-Dufresne[3] and Peter Sheridan Dodds[3]
[1]Institute for Cross-Disciplinary Physics and Complex Systems IFISC, Campus Universitat de les Illes Balears, Spain
[2]Department of Condensed Matter Physics, University of Zaragoza, Spain
[3]Vermont Complex Systems Institute, University of Vermont, USA
[*]These two authors contributed equally

Naming practices constitute some of the most persistent and symbolic cultural processes in human history. Far from arbitrary labels, names encode social memory, institutional continuity, and collective values, providing a high-resolution window into cultural evolution [1]. Papal onomastics represent a unique, empirical paradigm of this phenomenon, extending back nearly two millennia and forming a long, discrete sequence of individual naming decisions produced within a remarkably enduring institution [2].

In recent decades, tools from statistical physics and complex systems have increasingly been applied to quantify historical, linguistic, and cultural trends. Generative frameworks, such as Simon's model of cumulative advantage [3], and preferential attachment in growing networks, have successfully mapped the universal emergence of heavy-tailed distributions, scaling laws, and the "rich-get-richer" dynamics across diverse natural and social systems.

In this work, we study papal onomastics with the formal language of stochastic choice processes, distinguishing three periods: First, Period I (32–751) reflects a phase of pure innovation driven by the cultural and linguistic diversity of early pontiffs. Then, Period II (752–913) marks a transition phase of declining innovation restricted to Italian popes. Finally, Period III (914–2013) initiates a systematic papal self-naming.

We show that Period I can be understood as a process of random extraction with replacement from a finite reservoir of names, which we refer to as the Chalice model. Within this framework, the expected number of distinct names does not grow indefinitely with the number of mentions. Instead, it increases rapidly at first and then progressively approaches a limit set by the effective size of the available name reservoir.

Then, Period II (752–913) marks a transition phase of declining innovation restricted to Italian popes. The slowdown in new name introductions is accurately described by a sublinear growth scaling law consistent with Heaps' law.

More importantly, the introduction of systematic papal self-naming initiates Period III (914–2013). To explain these dynamics, we introduce the *Divine Reinforcement Urn Model* (DRUM) [4]. Formulated within the framework of Randomly Reinforced Urns [5], DRUM formalizes name selection as a function of cumulative name prestige $x_i(t)$. At each papal election, names with greater accumulated prestige are correspondingly more likely to be selected, with each choice further reinforcing the prestige of the chosen name.

Upon selection, the chosen name's prestige is boosted by a random increment drawn from a heavy-tailed, scale-free reinforcement distribution. This choice of reinforcement explicitly combines highly probable low-prestige contributions with rare, high-prestige singular events.

The goodness of our results is demonstrated by DRUM's capability to reproduce multiple key macroscopic features of the historical sequence simultaneously. Crucially, the heavy-tailed reinforcement injection naturally captures the sudden popularity surges and the volatile, time-varying hierarchies seen in the empirical timeline (see Fig. 1a).

Furthermore, the model accurately predicts that the variance in the number of times a name n_i is used evolves quadratically in time as $\mathrm{Var}[n_i(t)] \propto \sigma^2/\mu^2 t^2$, with the growth rate governed by the mean μ and variance σ^2 of the prestige distribution.

As shown in Fig. 1b, this relation aligns tightly with the empirical variance, providing a substantially better description than random selection.

Finally, the simulated size–rank distribution matches the heavy-tailed inequality observed at the closing of Period III (Fig. 1c).

Overall, our results frame papal onomastics as a paradigmatic case of fitness-dependent cultural reinforcement, where new papal names depend on the accumulated prestige of previous names. The reproduction of the observed name cascades and scale-free patterns show that this long historical process can be explained by a small set of fundamental statistical laws combining innovation, reinforcement, and fitness heterogeneity.

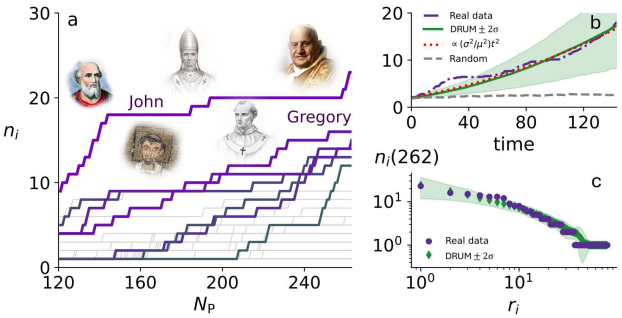

Fig. 1: (a) Number of pontiffs bearing each name across chronologically-ordered papacies. (c) Variance of name frequencies in the data (purple) compared with 100 DRUM simulations (green), with the analytical expression (red), and with a baseline in which each pontiff selects a name uniformly at random (gray). (d) Size–rank distribution of papal names at the end of Period III.

[1] J. Raaijmakers, *The Social Meaning of Names*, Writing Names in Medieval Sacred Spaces, Utrecht Studies in Medieval Literacy, 299 (2024).

[2] M. Baratto *et al.*. *The relationship between episcopal genealogy and ideology in the Roman Catholic Church*, arXiv preprint arXiv:2506.22108 (2025).

[3] H. A. Simon, *On a class of skew distribution functions*, Biometrika **42**, 425 (1955).

[4] P. Rosillo-Rodes*, S. Lamata-Otín*, *et al.*. In preparation.

[5] F. M. Hoppe, *Pólya-like urns and the Ewens' sampling formula*, J. Math. Biol. **20**, 91 (1984).

Instanton theory and fluctuation corrections to the thermal nucleation rate of a ferromagnetic superfluid

Enrique Rozas García[1] and Johannes Hofmann[1,2]
[1] Department of Physics, Gothenburg University, Sweden
[2]Nordita, Stockholm University and KTH Royal Institute of Technology, Stockholm, Sweden

When a system is quenched across a first-order phase transition into a metastable state, it relaxes to equilibrium via the nucleation and expansion of ground-state domains. While the theory of nucleation in classical and quantum systems has a long history—beginning with the work of Gibbs on the liquid-gas transition [1]—its predictions often differ from experimental measurements by orders of magnitude. This discrepancy is usually attributed to difficulties in sufficiently isolating experiments from impurities and external influences, as well as uncertainties in the underlying theoretical models.

Quantum gases have emerged as a promising experimental platform for studying nucleation, offering clean systems, precise experimental control, and well-established microscopic theoretical models. Recent measurements of the nucleation rate in a one-dimensional ferromagnetic superfluid [2, 3] provide the first look into the theoretical and technical challenges of describing nucleation in these systems.

We provide a field-theoretical description of thermal nucleation in a one-dimensional ferromagnetic superfluid [4], a quantum-gas analogue of false-vacuum decay. The rate Γ at which ground-state domains nucleate follows an Arrhenius law,

$$\Gamma = \frac{\sigma}{2\pi} e^{-\beta \Delta F}, \tag{1}$$

where the exponential factor is determined by the free-energy difference between the metastable state and a saddle-point of the energy functional: the critical droplet. The dynamical prefactor σ is given by the exponential rate of expansion of small perturbation from the critical droplet.

We evaluate both contributions over the full parameter space of the experiment, using a saddle-point approach to include both the critical droplet and the effect of quadratic fluctuations in our calculation of ΔF. This involves evaluating a functional determinant, which we do through the Gel'fand-Yaglom method. In addition, we obtain a closed-form expression for critical droplets close to the coexistence line, and use it to formulate an effective theory of domain nucleation and growth as a Kramers escape problem for the droplet size. Our results determine the parametric dependence of the nucleation rate and predict its signature in experimental images of a nucleating gas, increasing the rigor of comparisons between nucleation theory and experiment.

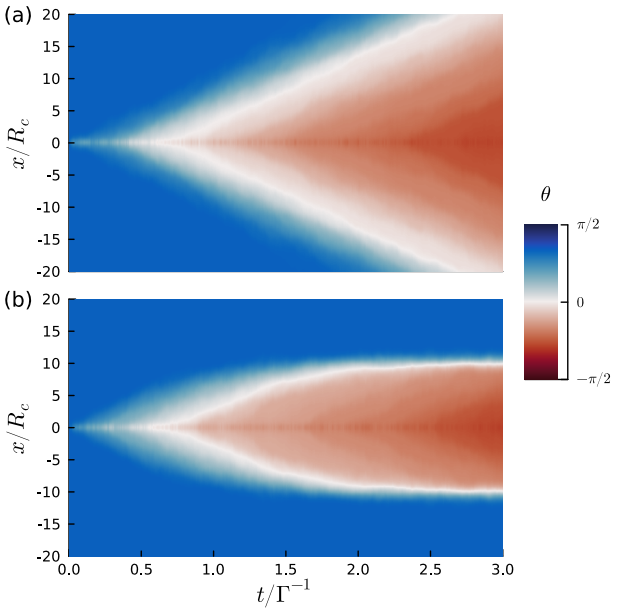

Fig. 1: Average polarization $\langle \theta(x,t) \rangle$ of a model quantum gas transitioning from a metastable phase (blue) to the stable phase (red), as obtained from 100 simulations of an effective Kramers problem. Panel (a) shows a homogeneous system, while panel (b) shows a system contained in an optical trap. Distances are in units of the critical domain size R_c which separates shrinking and growing domains, time is in units of the expected nucleation time Γ^{-1}.

[1] J. W. Gibbs, Transactions of the Connecticut Academy of Arts and Sciences 3, 416 (1876)
[2] Zenesini et. al., Nature Physics 20, 558 (2024)
[3] Cominotti et. al., Phys. Rev. Lett. 135, 183401 (2025)
[4] E. Rozas Garcia, J. Hofmann, arXiv:2512.20734 (2025)

Probabilistic Modeling of Colorectal Cancer Recurrence: A Bayesian Multicentre Study

Marta Sánchez-Díez[1], Carmen Ramírez-Castillejo[1] and Juan Manuel Pastor[2,3],
[1] CTB (CTB-UPM) Centro de Tecnología Biomédica, Universidad Politécnica de Madrid, 28223 Pozuelo de Alarcón, Spain.
[2] Grupo de Sistemas Complejos, Universidad Politécnica de Madrid, 28040 Madrid, Spain
[3] Grupo Interdisciplinar de Sistemas Complejos (GISC), Madrid, Spain

Colorectal cancer (CRC) remains a global health priority, representing the third most prevalent malignancy and the second leading cause of oncology-related mortality worldwide. Despite the clinical success of primary tumor resection and adjuvant therapies, long-term patient prognosis is frequently compromised by disease recurrence, which occurs in approximately 20–40% of patients within the first three years post-intervention. Recent breakthroughs in tumor biology highlight Cancer Stem Cells (CSCs) as the primary architects of this relapse due to their unique biophysical and functional plasticity, including a low metabolic division rate, self-renewal capacity, and a high proficiency for epithelial-mesenchymal transition (EMT). These traits allow CSCs to survive systemic treatments, enter the circulatory system, and colonize distant organs to form metastatic niches. However, a significant clinical hurdle remains: no single biomarker is exclusively expressed by CSCs, leading to diagnostic ambiguity and underscoring the urgent need for integrative, multi-parametric approaches that combine molecular signatures with clinical data.

Grounded in the synergy between molecular biology and computational intelligence, we constructed a predictive mathematical model for CRC relapse using a Bayesian computational framework that prioritizes probabilistic inference over traditional frequentist methods. After benchmarking several classical supervised learning architectures and identifying Logistic Regression as the most effective baseline model for our dataset, our optimized Bayesian application calculated risk through posterior distributions to provide a sophisticated quantification of uncertainty. Within an independent external validation cohort, the resulting framework demonstrated superior diagnostic performance, yielding a specificity of 85% and a sensitivity of 82%, thereby confirming its reliability in flagging high-risk patients while successfully limiting false-positive classifications.

To further validate its clinical utility, we integrated the model's probability outputs into a Kaplan-Meier survival analysis, which revealed a significant divergence in clinical outcomes, as patients assigned a high relapse probability exhibited markedly lower relapse-free survival. This robust discriminative capacity allowed for the prognostic stratification of the patient population into three distinct categories—low, intermediate, and high risk—that effectively mirror actual clinical events recorded in real-world patient trajectories.

Ultimately, this integration shifts oncological workflows from a reactive to a predictive paradigm, serving as a scalable tool for oncologists to enhance quality of life through targeted post-operative surveillance and personalized therapeutic strategies while sparing low-risk patients from unnecessary interventions.

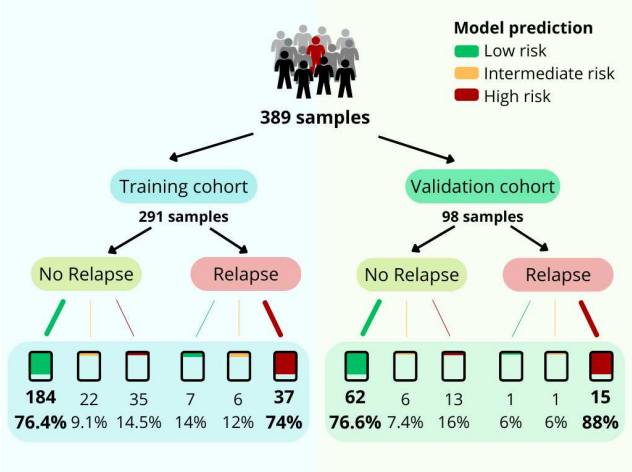

Fig. 1: Bayesian risk stratification and clinical outcome distribution. Samples were classified into three risk tiers based on the Bayesian posterior probability (p) of relapse: low risk ($p < 0.5$), intermediate risk (0.5 - 0.6), and high risk ($p > 0.6$). Data are presented separately for the training cohort (left) and validation cohort (right), sub-divided by patient relapse status. The distribution demonstrates the model's ability to concentrate non-relapsing cases within the low-risk category, while samples associated with clinical relapse are predominantly assigned to the high-risk tier.

Explainability in Machine Learning: Comparing White-Box and Black-Box Models for Alzheimer's Disease Detection

Juan Antonio Guevara Gil [1], Paula Sanchez Rego[2]
[1] Facultad de Estudios Estadisticos, Universidad Complutense de Madrid (UCM), Av. Complutense, s/n, Madrid
[2]Departamento de Matematicas, Universidad Carlos III de Madrid (UC3M), Avda. de la Universidad, 30, Madrid

Machine learning (ML) has become an increasingly relevant tool in the medical field, particularly for supporting diagnosis in complex diseases [1]. In this work, the objective was to apply its predictive capacity in order to compare white-box and black-box models in the binary classification of Alzheimer´s Disease (AD), a multifactorial neurodegenerative disorder influenced by genetic, cellular, clinical and environmental causes [2].

To achieve this, four supervised ML models were implemented: logistic regression and decision tree as white-box models, Bayesian Network (BN) as an intermediate model, and Support Vector Machine (SVM) as a black-box model. All of them were trained and evaluated using a common ML pipeline, including data preprocessing, hold-out splitting, 10-fold cross-validation, hyperparameter tuning and final assessment of their predictive performance on an independent test set [3].

However, when making predictions in a medical context, predictive performance alone is not enough. Experts also need to understand which variables are involved in the prediction in order to increase transparency and trust [4]. For that reason, interpretability was assessed across all models. Intrinsically interpretable models were analyzed directly, while Local Interpretable Model-Agnostic Explanations (LIME) were applied to the black-box model.

The results identified the decision tree as the model with the highest predictive capacity and the clearest transparency during classification, being the variables age, ApoE and family history the most relevant predictors. These findings suggest that, when predictive performance is similar, white-box models may be preferable in medical contexts, since they provide clearer explanations and greater transparency. Nevertheless, future research should validate these results using larger and more clinically detailed datasets, as well as additional white-box and black-box models.

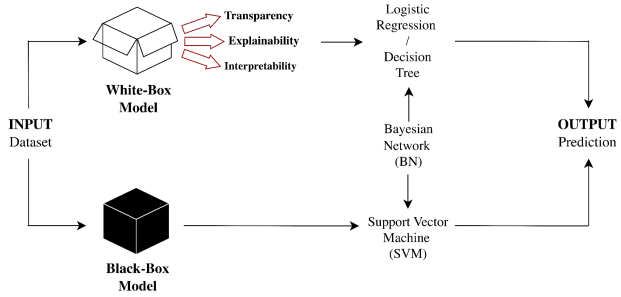

Fig. 1: Conceptual overview of the ML approach

[1] T. Jo, K. Nho, and A. Saykin, "Deep learning in alzheimer's disease: diagnostic classi- fication and prognostic prediction," Journal of Alzheimer's Disease, vol. 70, pp. S305– S323, 2019.

[2] X. Sun and Y. Zhang, "Amyloid hypothesis and alzheimer's disease," in Advanced Understanding of Neurodegenerative Diseases. IntechOpen, 2011. [Online]. Available: https://www.intechopen.com/chapters/25202

[3] Z.-H. Zhou, Machine Learning. Singapore: Springer, 2021.

[4] D. Doran, S. Schulz, and T. R. Besold, "What does explainable ai really mean? a new conceptualization of perspectives," 2017.

Delayed Thermal Relaxation and the Mpemba Effect in the Descartes Protocol

Andrés Santos[1]
[1]Departamento de Física and Instituto de Computación Científica Avanzada (ICCAEx),
Universidad de Extremadura, E-06006 Badajoz, Spain

The Mpemba effect, whereby a hotter system cools faster than a colder one under identical conditions, continues to stimulate theoretical and experimental interest as a paradigmatic example of anomalous nonequilibrium relaxation [1]. While most studies focus on systems brought into contact with a single thermal reservoir, recent works have shown that protocol design can strongly influence the occurrence and magnitude of the effect. In this poster I present a theoretical study of the Mpemba effect within the framework of the time-delayed Newton's law of cooling [2].

I introduce and analyze a three-reservoir scheme, termed the "Descartes protocol," in which two samples initially equilibrated at different temperatures are subjected to single-step quenches at different times before relaxing toward a common cold reservoir. This protocol provides a transparent way to disentangle the roles of three independent control parameters: the delay time (τ) associated with the thermal response, the waiting time (t_{w}) between the preparation of the samples, and the reduced intermediate (warm) reservoir temperature (ω). Using the exact solution of the delayed cooling equation [3], analytical conditions for the existence of both the direct and the inverse Mpemba effects under instantaneous quenches are derived. These conditions can be expressed as bounds on the normalized warm temperature for given values of the delay and waiting times, as shown in Fig. 1.

Within the admissible region where the Mpemba effect occurs, the magnitude of the effect can be optimized by a suitable choice of the protocol parameters. In particular, the value of the warm temperature that maximizes the effect for fixed delay and waiting times are determined, and compact and accurate approximations for both this optimal parameter and the corresponding maximal magnitude of the temperature difference between the samples are obtained. An especially simple result emerges for the global optimum: for a fixed delay time, the absolute maximum of the Mpemba effect is reached when the waiting time equals the delay time, $t_{\mathrm{w}} = \tau$.

The Descartes protocol also allows a direct comparison with previously studied two-reservoir schemes. Despite possessing an additional control parameter, the three-reservoir protocol is shown to yield a smaller maximal magnitude of the effect than the corresponding two-reservoir setup with the same delay time [3]. Finally, the analysis is extended to finite-rate quenches. In that case, strict equality of the bath conditions prevents a genuine Mpemba crossing, but an approximate effect persists when the time scale of the bath dynamics remains sufficiently short compared with the intrinsic delay time.

These results provide an analytically tractable framework for understanding how delayed thermal response and protocol design influence anomalous relaxation phenomena, and they suggest new ways to control and optimize Mpemba-type effects in simple thermal systems.

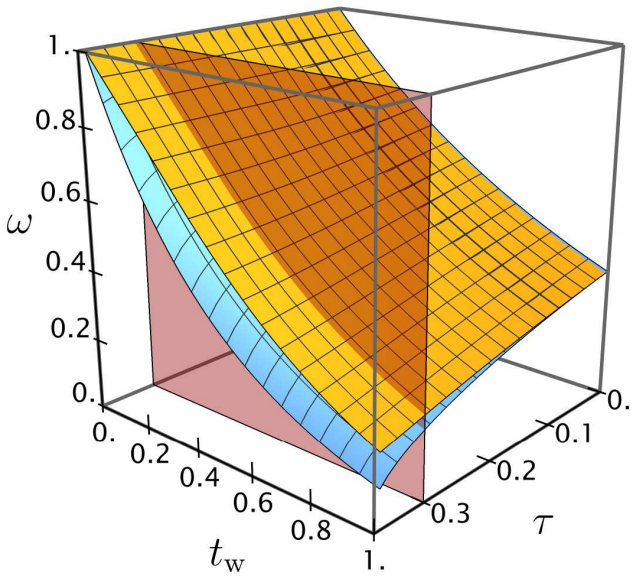

Fig. 1: Phase space for the direct Mpemba effect. The plane shows the particular case $\tau = 0.3$.

[1] G. Teza, J. Bechhoefer, A. Lasanta, O. Raz, and M. Vucelja, *Speedups in nonequilibrium thermal relaxation: Mpemba and related effects*, Phys. Rep. **1164**, 1 (2026)..

[2] A. Santos, *The Mpemba effect in the Descartes protocol: a time-delayed Newton's law of cooling approach*, J. Phys. A: Math. Theor. **59**, 145201 (2026).

[3] A. Santos, *Mpemba meets Newton: Exploring the Mpemba and Kovacs effects in the time-delayed cooling law*, Phys. Rev. E **109**, 044149 (2024).

Lost in averaging: from chaotic itinerancy to intermittent synchronization in complex networks

I. Leyva[1], I. Sendiña-Nadal[1], R. Sevilla-Escoboza[2], V. P. Vera-Ávila[3], and C. Letellier[4]
[1]Complex Systems Group & GISC, Universidad Rey Juan Carlos, Madrid, Spain
[2]Universidad de Guadalajara, Jalisco, Mexico
[3]Instituto Politécnico Nacional, Guanajuato, Mexico
[4]Rouen Normandie University-CORIA, Rouen, France

Many complex systems, from neural dynamics to reservoir computing, are thought to operate near criticality, where collective behavior emerges from the interplay between coherence and variability [1]. In this regime, intermittent synchronization has been widely reported and linked to functional adaptability as well as pathological states in brain dynamics [2]. However, its dynamical origin and relation to the underlying nodal behavior remain poorly understood, as standard approaches rely on global, time-averaged observables that can obscure the relevant mechanisms.

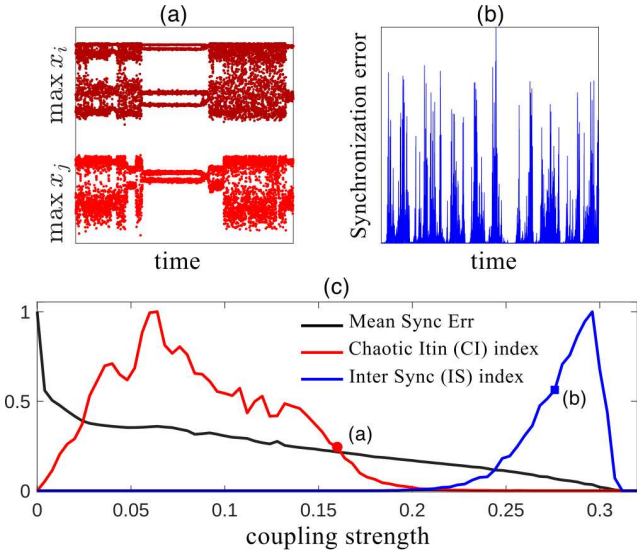

Fig. 1: Sequential transition from chaotic itinerancy (CI) to intermittent synchronization (IS) in a network of Rössler oscillators. (a) Time series in the Poincaré section of a pair of nodes in the weakly coupled regime, showing network-induced chaotic itinerancy among metastable regimes. (b) Global synchronization error in the strongly coupled regime, displaying intermittent alternations between coherent and incoherent phases. (c) CI and IS indices and global synchronization error versus coupling strength, with the red dot and blue square marking the coupling values in (a) and (b).

Here, we show that the route to synchronization in complex networks unfolds through a sequential transition between two distinct dynamical regimes: chaotic itinerancy (CI) and intermittent synchronization (IS), recently identified as successive stages along the synchronization process [3]. At weak coupling, the system exhibits CI, where nodes undergo irregular transitions among metastable regions of a high-dimensional attractor, reflecting a collective yet unsynchronized exploration of state space (Fig. 1(a)). The switching is network-wide but the dynamics remains node-dependent, making it functionally equivalent to the microstates observed in EEG signals [4]. As the coupling strength increases, this itinerant dynamics progressively collapses, reducing the effective dimensionality of the network attractor. Only beyond this point does IS emerge, characterized by irregular alternations between coherent and incoherent phases, as previously reported in complex networks [5]. This behavior is shown in Fig. 1(b), where the global synchronization error displays intermittent transitions between synchronized and desynchronized states.

To characterize these regimes, we combine a symbolic dynamics framework that captures node-level dynamical transitions with a threshold-based analysis of the global synchronization error. This approach reveals that CI and IS are mutually exclusive and occur in distinct coupling intervals, providing a dynamical explanation for intermittency as a network-level manifestation of the collapse of itinerant dynamics. The overall transition route is summarized in Fig. 1(c), which shows the evolution of the CI and IS indices and the global synchronization error with coupling strength, revealing a clear sequential crossover between the two regimes. These results uncover a multistage route to synchronization, bridging metastability, criticality, and collective behavior in complex networks.

[1] M.A. Muñoz, *Colloquium: Criticality and dynamical scaling in living systems*, Reviews of Modern Physics **90**, 031001 (2018).
[2] F.S. Borges, E.C. Gabrick, P.R. Protachevicz, et *al., Intermittency properties in a temporal lobe epilepsy model*, Epilepsy and Behavior **139**, 109072 (2023).
[3] I. Leyva, I. Sendiña-Nadal, R. Sevilla-Escoboza, V.P. Vera-Ávila, C. Letellie *From chaotic itinerancy to intermittent synchronization in complex networks*, Physical Review Research **8**, 013328 (2026).
[4] K.L. Rossi, R.C. Budzinski, E.S. Medeiros, B.R. Boaretto, L. Muller, U. Feudel, *Dynamical properties and mechanisms of metastability: A perspective in neuroscience*, Physical Review E **111**, 021001 (2025).
[5] V.P. Vera-Ávila, R. Sevilla-Escoboza, I. Leyva, *Complex networks exhibit intermittent synchronization*, Chaos **30**, 103119 (2020).

Synchronization of pulse-coupled oscillators in distributed power grid control

Ivan Sevostianov[1], Damia Gomila[1], and Pere Colet[1]
[1]IFISC, Palma de Mallorca, Spain

High penetration of renewable sources makes the power grid more fragile by reducing the fraction of controlled production, and, in extreme cases, triggers large-scale blackouts. The conventional way of balancing grid operation frequency are production adjustments according to the changes in consumption. Control capabilities could be significantly expanded by adding smart circuits that react to frequency fluctuations to ordinary devices such as heaters, coolers, chargers, etc. Their operations can be postponed or advanced, respectively decreasing or increasing demand whenever needed, namely acting as a virtual energy storage. Yet, simple algorithms may lead to synchronization of the operation cycles when recovering pending tasks, eventually triggering large frequency fluctuations [1]. These smart devices are, in fact globally coupled via the grid frequency. For devices that can only be in one of two states - ON or OFF - the reaction generates a frequency pulse when changing states. Pulse coupled oscillators appear in biology[2], but, as opposed to those models, here interaction is not direct from one oscillator to another. Rather, it is mediated by the grid frequency, which depends also on conventional power plant controls. In particular for a simple model of a house with heat pump we find that frequency deviations trigger a reaction only if applied during a small fraction of the phase-space cycle. For several houses we find that this coupling favors a sort of anti-phase synchronization: houses gather in groups each consisting of two subgroups separated by a constant phase difference.

We elaborate a theoretical model and use simulations of large oscillator ensembles to gather statistics about the stationary states they reach. With an insight from studying the behavior of oscillator pairs as dynamical system, we develop a method to detect groups of synchronized oscillators. Averaging over the initial conditions, we find a surprising result: probability distributions of group sizes have the same shape and scale linearly with the ensemble size N. With this in mind, we derive a convenient measure for coupling strength I that is independent of N. Synchronized groups produce simultaneous fluctuations in the grid frequency, thus by taking maximal group size for every stationary state (Fig. 1), we can infer the limits of control applicability. Besides, we obtain the mean fluctuation size as a function of coupling strength I for a small system, which in turn allows us to estimate the results for any N. These results are cross-checked with simulations of the full system of the power grid equations.

Moreover, we encounter a phase transition between a normal operation regime, where the temperature of the house changes periodically and the self-propelling phase where the smart device are triggered by their own fluctuations all the time and the temperature trajectory becomes aperiodic. The transition point is estimated analytically and verified numerically.

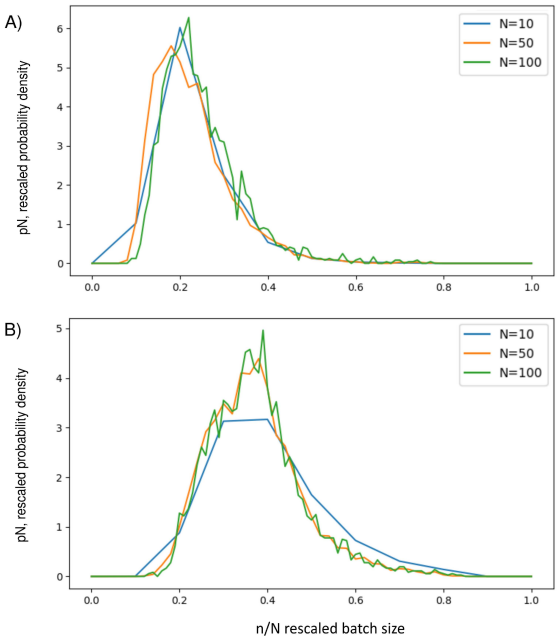

Fig. 1: The probability distribution density of synchronized batch sizes, measured in the stationary state for $N = 10, 50$ and 100 heat pumps/oscillators and coupling strengths A) $I = 5$, B) $I = 10$. The plots are rescaled to conserve the property of PDF $\int pdx = 1$.

[1] Tchuisseu, E. B. Tchawou and Gomila, D. and Brunner, D. and Colet, P., Effects of dynamic-demand-control appliances on the power grid frequency, *Phys. Rev. E*, **96**, 2017, 10.1103/PhysRevE.96.022302.

[2] Mirollo, Renato E. and Strogatz, Steven H., Synchronization of Pulse-Coupled Biological Oscillators, *SIAM Journal on Applied Mathematics*, **50**, 1990, 10.1137/0150098

Continuum description of active proliferating matter

Nathan Silvano[1], Emilio Hernández-García[1], and Cristóbal López[1]
[1]Institute for Cross-Disciplinary Physics and Complex Systems (UIB-CSIC), Palma, Spain

In active matter systems, a subject of interest is the emergence of *flocking* [1, 2]. While the emergent properties of interacting self propelled particles have been extensively studied, most theoretical frameworks assume a constant number of particles. This approximation breaks down in many biological contexts where birth and death processes are essential. Our work introduces a generalized model for proliferating active matter, exploring the emergent phenomena that arise when self propulsion is coupled with continuous individual reproduction, death, and spatially nonlocal competition. We provide a continuum approximation for the Active Brownian Bug (ABB) model [3], demonstrating that macroscopic flocking can be induced entirely by proliferation dynamics, without the need for explicit alignment interactions.

Starting from a lattice based microscopic master equation, we derive a macroscopic mean field continuum description. By applying a moment expansion to the angular distribution and truncating at the first order, we obtain a coupled set of dimensionless equations governing the scalar density of individuals $\rho(\mathbf{u},t')$ and the polarization vector field $\mathbf{p}(\mathbf{u},t')$:

$$\partial_t \rho = \boldsymbol{\nabla}^2 \rho - \mathrm{Pe}\,\boldsymbol{\nabla}\cdot\mathbf{p} + \mu\rho\,(1-(S*\rho))\,,$$

$$\partial_t \mathbf{p} = \boldsymbol{\nabla}^2 \mathbf{p} - \overline{D_r}\mathbf{p} - \frac{\mathrm{Pe}}{2}\boldsymbol{\nabla}\rho + \mu\mathbf{p}\,(1-(S*\rho))\,.$$

In this system: Pe is the Péclet number (activity/propulsion). μ is the normalized net growth rate. $\overline{D_r}$ is the normalized rotational diffusion. S represents the nonlocal spatial top-hat kernel, which models competition for resources within a finite radius.

Through linear stability analysis and numerical simulations in one and two dimensions, we identify that the homogeneous steady state is subject to two distinct instability mechanisms. These drive the system into three main dynamical regimes: Disordered Phase (D-phase): A homogeneous density distribution with no global polarization. Patterned Clusters (PC-phase): Driven by a Turing (stationary) instability, the system forms spatially periodic density patterns (e.g., hexagonal clusters in 2D) with zero global motion. Spatially Structured Flocking (SFF-phase): Driven by a Hopf (oscillatory) instability, the clusters break symmetry and transition into traveling patterns that migrate collectively, resulting in a non-zero global polarization.

We demonstrate that collective motion in this system does not rely on spontaneous polar ordering. Instead, local density gradients generate polarization at the edges of clusters. For sufficiently large activity (Pe) or growth (μ), this coupling causes individual clusters to drift. Nonlocal competitive interactions then synchronize these neighboring clusters, resulting in macroscopic, coherent transport.

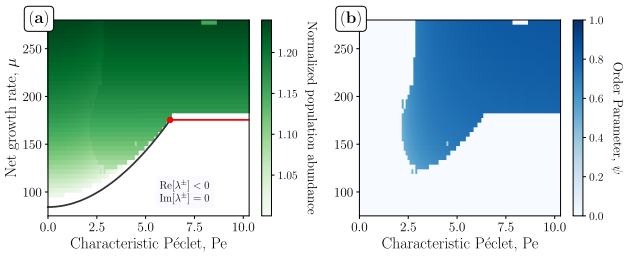

Fig. 1: Numerical simulations of the continuum equations revealing the parameter space spanned by the net growth rate μ and Péclet number Pe. The black line denotes the analytical Turing instability threshold (onset of pattern formation), while the red line indicates the Hopf instability boundary (onset of traveling waves). The contour maps display the normalized density abundance (a) and the global order parameter (b), clearly distinguishing the transition from stationary clusters to macroscopic flocking

[1] L. Dyson, C. Yates, C. Buhl, and J. McKane, *Onset of Collective Motion in Locusts Is Captured by a Minimal Model*, Phys. Rev. E **92**, 052708. (2015).

[2] F. Peruani, *Hydrodynamic Equations for Flocking Models without Velocity Alignment*, Journal of the Physical Society of Japan **86**, 101010 (2025).

[3] S. Takamura, N. Saito, *Title of article can optionally be included*, Phys. Rev. Res. **7**, 033299 (2025).

Ecological impact of the invasive Percnon gibbesi: A Model of Herbivory-Driven Halo Formation in Mediterranean Rocky Habitats

Sylvain Sylvestre Icaro Hamers[1], Eva Llabrés[1], and Tomás Sintes[1],
[1] Instituto de Física Interdisciplinar y Sistemas Complejos, IFISC (UIB-CSIC).
Campus Universitat de les Illes Balears, 07122 Palma de Mallorca.

Percnon gibbesi, commonly referred to as the urchin crab, was first documented in 1999 on Linosa and has subsequently expanded rapidly throughout the Mediterranean, reaching regions such as the Balearic Islands, Greece, Libya, Malta, and Israel. It is currently regarded as one of the most invasive decapod species in the Mediterranean basin [1, 2]. The species occupies rocky coastal habitats, typically sheltering among boulders, crevices, and rock fissures, where it is exposed to predation by both fishes and invertebrates. In contrast to most large infralittoral Mediterranean crabs, P. gibbesi is exclusively herbivorous, feeding primarily on filamentous and calcareous algae as well as corticated macrophytes.

In this study, we present a spatially explicit numerical model integrating algal growth dynamics with crab herbivory and fish grazing. Algae growth is solved with a PDE for vegetation density that incorporates the key characteristics of clonal growth together with the fundamental processes responsible for spatial self-organization [3]. The coupling between the crab population and the vegetation biomass is implemented through the algae mortality rate and the crab breeding probability.

The model is designed to investigate the ecological mechanisms underlying the formation of distinctive circular "halo" patterns surrounding occupied rocks, similarly to those observed around coral reefs [4, 5], and to provide a quantitative framework for estimating crab population densities and their ecological impact.

[1] Anton, Andrea; Bachot, Xavier; Pizarro-Borrull, Maria; Muñiz-Quintana, Sara and Puentes, Daniel. (2026). *Basin-wide patterns of abundance of a widespread invasive herbivore in the Mediterranean Sea*. Preprint, DOI: 10.21203/rs.3.rs-8523331/v1.

[2] Pizarro-Borrull, M., E.Font, N.Marbà, and A.Anton. (2025). *Prominent Grazing Rates and Feeding Preferences of an Abundant Exotic Benthic Herbivore in the Mediterranean Sea*. Ecology and Evolution 15, no. 7: e71686.

[3] Ruiz-Reynés, Daniel and Schönsberg, Francesca and Hernández-García, Emilio and Gomila, Damià. (2020) *General model for vegetation patterns including rhizome growth* . Phys. Rev. Res., 2, 2, 023402.

[4] E. Llabrés, E. Re, N. Pluma, T. Sintes, CM Duarte. (2024). *A generalized numerical model for clonal growth in scleractinian coral colonies*, Proceedings of the Royal Society B 291, 20241327 (2024).

[5] Llabrés, E., Innes-Gold, A.A., DiFiore, B., T. Sintes and Elizabeth Madin . (2025). *A spatial numerical model for seagrass–herbivore interactions and the formation of reef halos*. Coral Reefs 44, 1587–1599.

Self similarity in demonstrations online networks

Manuel Suarez-Roman[1,2,3], and M. Ángeles Serrano[4], and Yérali Gandica[5]
[1]Cátedra IA, UNIE Universidad
[2]Valencian International University (VIU)
[3]Universidad Carlos III de Madrid
[4]Universitat de Barcelona Institute of Complex Systems (UBICS), Universitat de Barcelona
[5]Autonomous University of Madrid

Online social mobilisation leaves digital traces of collective coordination, making it possible to analyse how interaction networks form and evolve during episodes of collective action. A natural question then arises: does peak mobilisation correspond merely to an increase in activity, or does it reflect a structurally distinctive network state? Previous studies have reported signatures of criticality during social movements, including peaks of collective attention and modular-to-nested transitions in user–hashtag interaction networks. To complete this picture, here we ask whether these critical phases also display multiscale self-similarity, and whether such self-similarity admits a geometric interpretation.

Here, we address this question by analysing Twitter hashtag activity during three large-scale mobilisation events: "No al Tarifazo" and "9n" in Argentina, and "Charlie Hebdo" in France. For each event, we construct temporal user–hashtag bipartite networks and hashtag co-occurrence networks. We identify the Critical Temporal Window (CTW) by combining activity peaks, modular-to-nested transitions, and the $\varepsilon_c^2(k)$ self-similarity test [1]. We then apply a degree-thresholding renormalisation procedure to the hashtag co-occurrence networks at the CTW, as schematically illustrated in Figure 1. This procedure generates a sequence of increasingly filtered subgraphs, allowing us to probe whether the same organisational principles persist across structural scales.

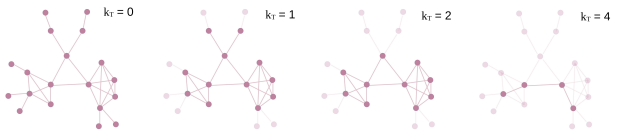

Fig. 1: **Degree-thresholding renormalisation procedure.** Starting from the original hashtag co-occurrence network ($k_0 = 0$), nodes with degree lower than or equal to a threshold k_t are successively removed, yielding a sequence of renormalised subgraphs at increasing structural scales.

Across the three events, the renormalised networks display clear signatures of multiscale k-cut self-similarity. As shown in Figure 2, their complementary cumulative degree distributions collapse after rescaling degrees by the average degree of each subgraph, and their clustering spectra collapse under the corresponding rescaling. This indicates that local hashtag co-occurrence patterns are preserved as progressively lower-degree nodes are filtered out, revealing a scale-invariant organisation that emerges specifically at peak mobilisation. These results suggest that the CTW is not only a period of maximal collective attention, but also a moment in which the underlying semantic and interaction structure becomes organised across multiple scales.

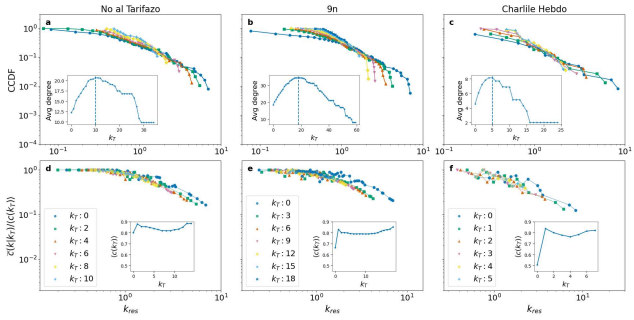

Fig. 2: **Evidence of multiscale k-cut self-similarity at the CTW.** At the Critical Temporal Window, renormalised hashtag co-occurrence networks exhibit a collapse of rescaled complementary cumulative degree distributions and clustering spectra, indicating that connectivity and local co-occurrence patterns are preserved across filtering scales.

In the conference talk, we will also show that these CTW networks admit accurate hyperbolic embeddings obtained with D-Mercator [2]. The resulting maps suggest that hashtag popularity and thematic similarity can be represented as latent geometric coordinates, with empirical connection probabilities closely matching those inferred from the model. This provides a complementary interpretation of the observed self-similarity, linking the persistence of co-occurrence patterns across renormalisation scales to an underlying latent metric structure.

These findings suggest that self-similarity and latent geometry provide a coherent framework for understanding how online collective action becomes rapidly amplified across scales during critical moments of mobilisation [3].

[1] Mariano G. Beiró, Ning Ning Chung, Lock Yue Chew, and Yérali Gandica. Signs of criticality in social explosions. *Scientific Reports*, 14(1), February 2024.

[2] Robert Jankowski, Antoine Allard, Marián Boguñá, and M. Ángeles Serrano. The d-mercator method for the multidimensional hyperbolic embedding of real networks. *Nature Communications*, 14(1), November 2023.

[3] M. Ángeles Serrano, Dmitri Krioukov, and Marián Boguña. Self-similarity of complex networks and hidden metric spaces. *Physical Review Letters*, 100(7):078701, February 2008.

Conditioning the Unlikely: Dynamics of Rare Events in Random Maps

Ángela Tajuelo-Valbuena[1], and Carlos Pérez-Espigares[1,2]

[1] Departamento de Electromagnetismo y Física de la Materia, Universidad de Granada, 18071 Granada, Spain
[2] Institute Carlos I for Theoretical and Computational Physics, Universidad de Granada, 18071 Granada, Spain

We investigate how rare dynamical fluctuations can be identified, analyzed, and effectively controlled in one-dimensional chaotic maps. In such systems, atypical trajectories — for example, those that transiently stabilize unstable periodic orbits or exhibit anomalously low or high finite-time Lyapunov exponents — usually require finely tuned initial conditions, which are notoriously hard to pinpoint because the dynamics is extremely sensitive to small perturbations. Using a large-deviation framework inspired by the generalized Doob transform in stochastic processes, we make use of an effective topologically conjugate map whose typical trajectories reproduce the statistics of these rare events [1]. This provides a way to "make rare events typical", to selectively realize prescribed dynamical behavior, and to probe dynamical phase transitions. We then move beyond purely deterministic maps and discuss random maps, with special focus on the Pelikan map [2]. This class of maps mixes a chaotic expanding branch with a stochastic selection mechanism, so that the resulting dynamics is neither purely deterministic nor purely random, providing a natural setting to extend this approach.

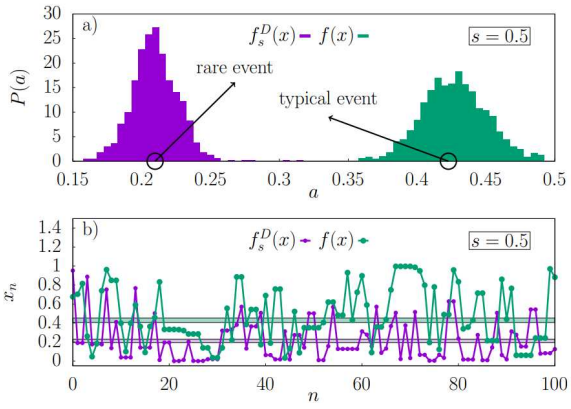

Fig. 1: Histogram and a typical trajectory of the observable $A = \frac{1}{N}\sum_{n=0}^{N-1} g(x_n)$, with $g(x_n) = x_n$ are shown for the Pelikan map and its corresponding Doob map with $p = 0.8$.

[1] Gutiérrez, R., Canella-Ortiz, A. and Pérez-Espigares, C., *Finding the Effective Dynamics to Make Rare Events Typical in Chaotic Maps*, Phys. Rev. Lett. **131**, 227201 (2023).

[2] Yan, J., et al., *Transition to anomalous dynamics in a simple random map*, Chaos **34**, 023128 (2024).

Breakdown of Hydrodynamics under Strong Confinement

Daniel Téllez[1], and M. Isabel García de Soria[1], Pablo Maynar[1], J. Javier Brey[1]
[1]Física Teórica, Universidad de Sevilla, apartado de correos 1065, E-41080, Sevilla, Spain

We investigate the hydrodynamic description of a dilute gas composed of hard spheres confined between two parallel, infinite plates. The confinement is characterized as ultra-confinement because the separation between the plates is of the same order as the particle diameter, which restricts the motion of the particles to being quasi-bidimensional (see fig. 1).

The foundation of this description is a kinetic theory based on a height-averaged distribution function. A Boltzmann-like equation for this function was previously derived through a formal BBGKY hierarchy, justifying its validity to first order in the density. This kinetic equation accounts for the specific geometry of the system by integrating over the allowed collision angles permitted by the narrow gap between the plates. It was also demonstrated that this description satisfies a version of the H-theorem and leads to a well-defined global equilibrium state for the confined fluid [1].

Using this kinetic equation as a starting point, we perform a formal Chapman–Enskog expansion to derive the governing hydrodynamic equations. In the initial approach, we describe the state of the fluid through four hydrodynamic fields: the two-dimensional number density, the parallel components of the flow velocity, and a single three-dimensional temperature. This derivation provides explicit analytical expressions for transport coefficients, including the thermal conductivity, dynamic shear viscosity, and bulk viscosity. Each of these coefficients depends on the plate separation distance. Notably, the bulk viscosity, which has a purely geometric origin in this system, exhibits a divergence as the gap width approaches the particle diameter. This divergence leads to non-physical predictions for the speed and absorption of sound in the limit of extreme confinement.

To address this issue, we propose an extended hydrodynamic description. In the regime of extreme confinement, the collision geometry only allows for nearly frontal impacts between the spheres. This restriction causes the kinetic energy associated with motion parallel to the plates to be approximately conserved during collisions. Consequently, the local isotropy of the temperature is broken, necessitating the use of separate temperature fields for the parallel and vertical directions. This leads to a five-field Chapman–Enskog expansion that eliminates the divergences and captures the transition of the transport coefficients from 3D to 2D values from first principles, in very good agreement with event-driven molecular dynamics simulations.

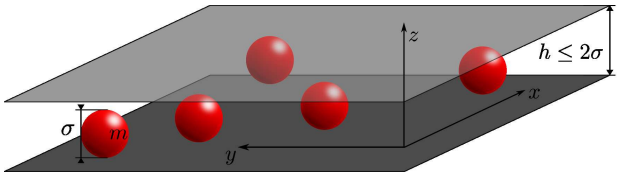

Fig. 1: Sketch of the system.

[1] J. J. Brey, M. I. García de Soria, P. Maynar, *Dynamics and kinetic theory of hard spheres under strong confinement*, Physical Review E **110**, 034127 (2024).

Biased Voter Models: From Persuasive Minorities to Partisan Network

Raúl Toral
Institute for Cross-Disciplinary Physics and Complex Systems IFISC (UIB-CSIC),
Campus Universitat de les Illes Balears, 07122 Palma de Mallorca, Spain

The voter model is a minimal framework for the study of opinion dynamics driven by social imitation. In its standard form, agents are neutral with respect to the two possible opinions and consensus is reached through fluctuation-driven ordering. This neutrality, however, is rarely realistic in social and political contexts, where individuals may have intrinsic preferences, asymmetric confidence, or persistent partisan predispositions. In this contribution I discuss a unified class of voter-like models in which bias is introduced at the level of the microscopic copying rule, and I focus on how the effect of this bias is mediated by the topology of the interaction network.

In the biased-voter model, only a fraction γ of the population has a preference for one of the two opinions, while the remaining agents are unbiased [1]. Biased agents copy changes towards and away from their preferred state with different probabilities, controlled by a bias parameter v. The central question is then not only how strong or numerous the biased agents are, but also how they are connected. In a complete graph the dynamics can be reduced to a one-dimensional biased random walk for the magnetization. For random initial conditions the relevant scaling variable is $\gamma v N$, or equivalently the product between the bias strength and the number of biased agents, and the probability of reaching the preferred absorbing state is a sigmoid function of this variable. The same analysis shows that the mean time to consensus grows as $\log N/(\gamma v)$, illustrating how even a small biased minority can dominate the final outcome when the system is sufficiently large.

This well-mixed result, however, gives only part of the picture. Pair-approximation theory and numerical simulations on Erdős–Rényi networks show that finite connectivity modifies the effective strength of the bias through the average degree μ. More importantly, when the network itself depends on the type of agents, the persuasive power of the biased group is strongly affected by its internal cohesion. Increasing the average number of links among biased agents, while preserving the global average degree, can substantially reduce the time needed to reach consensus and increase the probability that the system reaches the preferred absorbing state. By contrast, increasing only the number of contacts between biased and unbiased agents is not necessarily the most efficient strategy. Thus, persuasion is not only a matter of individual bias, but also of the mesoscopic organization of the biased subpopulation: who is biased matters, but who is connected to whom matters as well.

This network-based view of bias is further developed in the partisan voter model, where every agent has a fixed preferred opinion and the population is divided into two groups with opposite preferences [2]. In this case bias does not simply favor one global consensus state, but stabilizes coexistence between the two opinions. A pair approximation resolving the different classes of active links provides a mathematical description of the local ordering process beyond mean field. The relevant macroscopic variables are not only the magnetization or the density of satisfied agents, but also the densities of links joining agents with different combinations of state and preference. On uncorrelated networks, partisan bias leaves the total stationary density of active links unchanged but redistributes activity among these different link classes. When preferences also affect the formation of links, through homophilic or heterophilic attachment, structural correlations qualitatively modify the stationary state and the degree of local ordering [3].

The same link-resolved mathematical framework can be applied to both models. It allows one to separate the dynamical effect of bias, encoded in the transition probabilities, from the structural effect of connectivity, encoded in the densities of links between different classes of agents. From this perspective, the biased-voter model and the partisan voter model are two realizations of the same general problem: voter dynamics with quenched agent attributes that affect both the tendency to change opinion and the organization of social contacts. The resulting theory provides a common description of biased and partisan voter dynamics, and shows that the collective outcome of social influence depends crucially on the interplay between individual predispositions and the network organization of the agents carrying those predispositions.

[1] A. Czaplicka, C. Charalambous, R. Toral and M. San Miguel, *Biased-voter model: How persuasive a small group can be?*, Chaos Solitons & Fractals **161**, 112363 (2022).

[2] N. Masuda, N. Gibert and S. Redner, *Heterogeneous voter models*, Phys. Rev. E, **82**, 010103(R), (2010).

[3] J. Llabrés, M. San Miguel and R. Toral, *Partisan voter model on complex networks: Dynamics of local ordering*, manuscript in preparation.

Barrier pumping and basin erosion in slow-fast adaptive dynamics

Lluís Torres-Hugas[1], and Ivan Kryven[2] and Christian Bick[3]
[1]Departament d'Enginyeria Informàtica i Matemàtiques, Universitat Rovira i Virgili, Tarragona, Spain
[2]Mathematical Institute, Utrecht University, Utrecht, The Netherlands
[3]Department of Mathematics, Vrije Universiteit Amsterdam, Amsterdam, The Netherlands

Many adaptive systems recover after perturbations while their internal control variables are still changing. In the ideal limit of strong time-scale separation, the fast variables relax immediately and the slow variables move in an effective recovery landscape [1, 2]. In real finite-rate systems this reduction misses a simple physical effect: the fast variable can lag behind the adaptive coordinate. This lag behaves as a normal velocity and can inject or dissipate energy in the direction that separates recovery from escape.

We study this effect in a minimal deterministic model,

$$\dot{x} = -\gamma(x-\theta), \qquad \dot{\theta} = \varepsilon[-x+g(\theta)], \tag{1}$$

with $g(\theta) = \beta\theta^3 - \theta^5$. The coordinate $\theta = 0$ represents the recovered state. The associated potential

$$U(\theta) = \frac{1}{2}\theta^2 - \frac{\beta}{4}\theta^4 + \frac{1}{6}\theta^6 \tag{2}$$

has barriers separating this state from escape to outer attractors. Introducing the normal velocity $v = \dot{\theta}$ gives the exact lifted dynamics

$$\dot{\theta} = v, \qquad \dot{v} = (\varepsilon g'(\theta) - \gamma)v - \varepsilon\gamma U'(\theta). \tag{3}$$

Thus the adaptive system becomes a Liénard-type equation [3]: a conservative recovery force plus a state-dependent dissipative term. The recovery energy

$$E(\theta, v) = \frac{1}{2}v^2 + \varepsilon\gamma U(\theta) \tag{4}$$

satisfies the balance law

$$\dot{E} = (\varepsilon g'(\theta) - \gamma)v^2. \tag{5}$$

All changes in recovery energy are therefore caused by adaptive lag. In this sense, the problem becomes close in spirit to barrier-crossing physics: recovery is not determined only by the static barrier height, but also by the work performed on the barrier [4, 5].

Local anti-damping occurs where $\varepsilon g'(\theta) > \gamma$. However, local energy injection is not enough to destroy recovery. Basin erosion begins only when lag performs positive net work along the recovery barrier. We quantify this by the barrier-pumping number

$$\Pi = \frac{\varepsilon}{\gamma}\langle g' \rangle_b, \tag{6}$$

where $\langle g' \rangle_b$ is the feedback slope averaged along the frozen barrier with weight $[U(\theta_b) - U(\theta)]^{1/2}$. The threshold $\Pi = 1$ separates a dissipative barrier from a pumped barrier. For $\Pi > 1$, adaptive lag injects energy on average and the viable zero-velocity interval shrinks.

Numerical separatrix computations show that increasing the adaptation rate deforms the basin boundary even while the recovered fixed point remains locally stable. The mechanism is therefore not ordinary linear instability. It is a finite-rate, nonequilibrium erosion of the recovery basin caused by work performed by adaptive lag. This provides an internally driven analogue of rate-induced tipping [6], where the dangerous rate is generated by the feedback system itself.

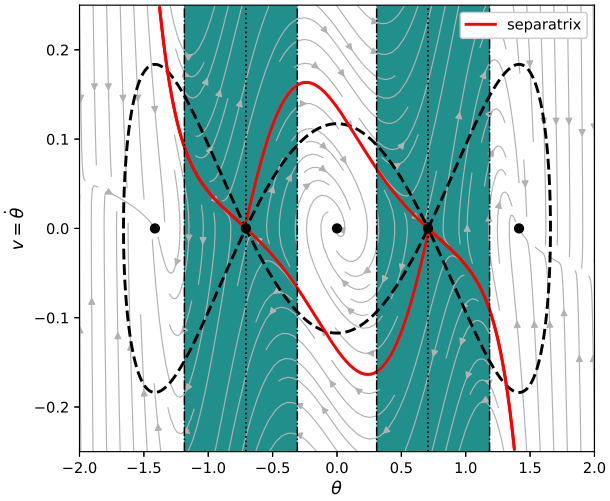

Fig. 1: Phase-space structure of the lifted adaptive dynamics. Grey streamlines show the flow, the red curve shows the separatrix of the recovery basin, the dashed curve shows the frozen recovery barrier, and shaded regions indicate local anti-damping, $\varepsilon g'(\theta) > \gamma$. Finite adaptation speed deforms the separatrix.

[1] N. Fenichel, *Geometric singular perturbation theory for ordinary differential equations*, J. Differential Equations **31**, 53–98 (1979).
[2] C. Kuehn, *Multiple Time Scale Dynamics* (Springer, Cham, 2015).
[3] A. Liénard, *Étude des oscillations entretenues*, Rev. Gén. Electr. **23**, 901–912, 946–954 (1928).
[4] H. A. Kramers, *Brownian motion in a field of force and the diffusion model of chemical reactions*, Physica **7**, 284–304 (1940).
[5] M. I. Freidlin and A. D. Wentzell, *Random Perturbations of Dynamical Systems*, 3rd ed. (Springer, Berlin, 2012).
[6] P. Ashwin, S. Wieczorek, R. Vitolo, and P. Cox, *Tipping points in open systems: bifurcation, noise-induced and rate-dependent examples in the climate system*, Philos. Trans. R. Soc. A **370**, 1166–1184 (2012).

Delay Mismatches Between Three Synchronized Lasers Characterized by Fourier Spectral Analysis

Sergi Torres-Serra[1], Mohammadreza Mokhtari[2], Cristina Masoller[1], Jordi Tiana-Alsina[3,4], Apostolos Argyris[2] and Miguel C. Soriano[2]

[1] Department of Physics, Universitat Politècnica de Catalunya, Rambla Sant Nebridi 22, 08222 Terrassa, Barcelona, Spain
[2]Institute of Cross-Disciplinary Physics and Complex Systems, IFISC (CSIC-UIB), Campus UIB, 07122 Palma de Mallorca, Spain
[3]Department of Applied Physics, Faculty of Physics, Universitat de Barcelona, Martí i Franquès 1, 08028 Barcelona, Spain
[4]Institut de Nanociència i Nanotecnologia (IN2UB), Universitat de Barcelona, 08028 Barcelona, Spain

We investigate the radio-frequency spectra (RFS) of a network of mutually coupled chaotic semiconductor lasers operating in the synchronized regime [1, 2]. The experimental system consists of four similar semiconductor lasers, differing mainly in their optical delay times τ_i (82.25 ns, 82.60 ns, 82.71 ns, and 82.88 ns). The lasers' indices are labeled according to increasing delay and studied in three-laser all-to-all coupled configurations.

An example of the synchronized temporal dynamics of the laser intensities is presented in Fig. 1. A distinctive feature of this synchronized dynamics is the appearance of well-defined peaks in the RFS of the intensity fluctuations. As shown in Fig. 2, the spectral distribution changes markedly depending on the selected laser subset. Although all configurations share the same mutual-coupling architecture, each exhibits a different spectral fingerprint, suggesting that these features originate from the small differences in the optical delays.

To investigate this behaviour, we perform numerical simulations based on the Lang–Kobayashi model [3], including delayed optical self-feedback and mutual optical injection. Using the experimentally measured delay times, the simulations accurately reproduce the measured RFS, correctly predicting both the spectral peak positions and their overall distribution.

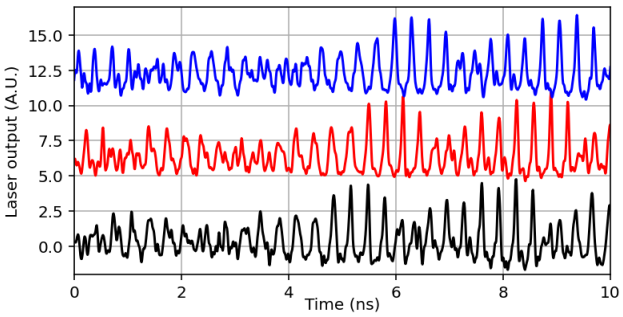

Fig. 1: Short segment of the experimental time series recorded from three synchronized semiconductor lasers. In this case, the lasers exhibit synchronized chaotic dynamics with a small time lag.

The analysis reveals that the delay mismatch is the dominant parameter governing the RFS. Each pairwise delay mismatch introduces a characteristic frequency given by $f_{ij} = 1/|\tau_i - \tau_j|$, and the observed spectra arise from the nonlinear interaction of these frequencies and their harmonics. For example, the main peak around 3 GHz in Fig. 2(a) results from the overlap of $f_{12} = 2.86$ GHz, $2f_{14} = 3.17$ GHz and $f_{24} = 3.57$ GHz, whereas in Fig. 2(b) the first peak near 4.5 GHz originates from the overlap of $2f_{13} = 4.35$ GHz and $3f_{14} = 4.76$ GHz, and the second peak at around 6.3 GHz results from the combination of frequencies $f_{34} = 5.88$ GHz and $3f_{13} = 6.52$ GHz.

Our results show that the delay mismatch in the network completely determines the spectral structure of the synchronized state. The different delay combinations define the set of characteristic frequencies that can contribute to the RFS, while the constructive overlap of their harmonics selectively enhances particular spectral components. Consequently, different subsets of synchronized lasers, despite sharing the same network topology, produce markedly different RFS simply because they contain different combinations of delay mismatches. This mechanism provides a straightforward physical explanation for the origin of the characteristic peaks observed experimentally and establishes the delay mismatch as the key parameter controlling the frequency content of synchronized chaotic semiconductor lasers [4].

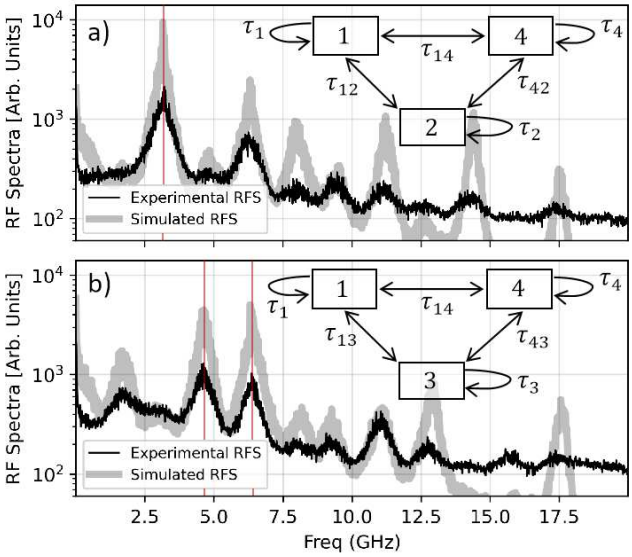

Fig. 2: Experimental radio-frequency spectra (black) of the synchronized chaotic time series for the (a) 124 and (b) 134 three-laser configurations. In light gray, we show the radio-frequency spectra of the simulated time series using the experimental values of the delays. Remarkably, replacing laser 2 with laser 3 leads to a substantial change in the spectral structure, despite the two configurations differing by only a single laser. The insets show the setup of each configuration, where τ_i is the delay time, and $\tau_{ij} = (\tau_i + \tau_j)/2$.

[1] M. C. Soriano, J. García-Ojalvo, C. R. Mirasso, and I. Fischer. Complex photonics: Dynamics and applications of delay-coupled semiconductor lasers. *Review of Modern Physics*, vol. 85, no. 1, pp. 421–470, 2013.

[2] Atsushi Uchida. *Optical Communication with Chaotic Lasers: Applications of Nonlinear Dynamics and Synchronization*. Wiley-VCH, 2012.

[3] R. Lang and K. Kobayashi. External optical feedback effects on semiconductor injection laser properties. *IEEE Journal of Quantum Electronics*, vol. 16, no. 3, pp. 347–355, 1980.

[4] M. Mokhtari, Adam C. Mackowiak-Pellon, M. Pflüger, M. C. Soriano, and A. Argyris. Experimental and numerical analysis of semiconductor laser network dynamics. In *Semiconductor Lasers and Laser Dynamics XII*, vol. 14090, p. 54, SPIE, 2026.

Irreversibilidad termodinámica en movilidad urbana

Lucas Trigal[1]
[1]Instituto de Física Interdisciplinar y Sistemas Complejos, IFISC (CSIC–UIB), Campus Universitat de les Illes Balears, E-07122 Palma, Spain

La movilidad cotidiana de una ciudad puede entenderse como una transformación estocástica entre dos distribuciones espaciales: la población nocturna, asociada a las zonas de residencia, y la población diurna, asociada a las zonas de trabajo. En esta contribución se propone una lectura de este proceso desde la termodinámica estocástica. A partir de datos origen–destino se construyen dos mapas de Markov: uno describe la redistribución residencia–trabajo y otro el retorno trabajo–residencia. Aunque ambos proceden de la misma matriz empírica de desplazamientos, no son equivalentes, porque se normalizan con respecto a poblaciones distintas.

El objetivo es inferir cuánta irreversibilidad contiene el ciclo diario de movilidad sin imponer una simetría artificial a los datos. Para ello se compara la probabilidad de los trayectos observados con la de sus trayectos inversos bajo una dinámica dual, construida a partir del estado estacionario de cada mapa. Esta comparación permite separar la parte asociada a la relajación estadística de la ciudad, incluso cuando existen enlaces de movilidad casi unidireccionales. Así, una tabla origen–destino deja de ser sólo una descripción de flujos y se convierte en un sistema dinámico sobre el que pueden definirse observables termodinámicos.

La aplicación a ciudades estadounidenses muestra que la irreversibilidad del ciclo residencia–trabajo–residencia se relaciona con la fracción de viajes unidireccionales, con la heterogeneidad espacial de la población diurna y con propiedades espectrales de los mapas de movilidad. Además, las ciudades más densas tienden a mostrar una reorganización diaria menos irreversible, compatible con una mayor mezcla entre residencia y empleo, mientras que ciudades menos densas presentan una separación funcional más marcada. El resultado es una caracterización termodinámica de la estructura urbana: la irreversibilidad del ciclo cotidiano actúa como una coordenada sintética para comparar regímenes de movilidad y localizar zonas con distinta función urbana.

Analysis of a mechanistic model of plant community dynamics based on replacement networks

Yolanda Valencia Díaz[1,3], and Julio M. Alcántara[2,3]
[1] Master's Degree in Advanced Physics, National University of Distance Education (UNED)
[2] Department of Animal Biology, Plant Biology and Ecology, University of Jaén
[3] Andalusian Institute for Earth System Research (IISTA-UJA), University of Jaén

The incorporation of complex network theory into ecology has transformed the study of biological interactions. However, in plant communities, most classical population models lack the necessary elements to explicitly incorporate empirical recruitment networks. In this project, we analyze the stability of the **Recruitment and Replacement (R&R) model** [1], which describes the dynamics of local communities through fundamental population rates and empirical interaction networks that encode recruitment patterns among species.

The abundance of species i is modeled through the following system of coupled difference equations:

$$x_i[t+1] = \kappa_i + \beta_{1,i}x_i[t] + \\ +\beta_{2,i}x_i[t]^2 + \sum_{j\neq i}\gamma_{j,i}x_j[t] + \beta_{2,i}x_i[t]\sum_{j\neq i}x_j[t] \qquad (1)$$

which incorporates intrinsic colonization potential (κ), intraspecific regulation (β) and net recruitment interaction effects (γ). Based on this formalism, we analyze local stability by studying the eigenvalues of the Jacobian matrix evaluated at viable equilibrium points.

This work is structured incrementally. In monocultures of annual species, the system reduces to linear dynamics with non-oscillatory asymptotic convergence, dominated by the colonization capacity in open spaces. The addition of perennial species introduces quadratic nonlinearities associated with vegetative growth, generating stability maps that are highly sensitive to external recruitment. In this regime, the saturation of the carrying capacity emerges as a buffering mechanism against perturbations.

By extending the formalism to two-species systems, analytical tools such as the Gershgorin circle theorem are applied. The results show that multispecies stability critically depends on the intensity of plant-soil feedbacks (PSFs) and accumulated interspecific effects. In particular, in asymmetric annual-perennial systems, the persistence of the annual species requires overcoming a critical threshold of external seed rain; below the threshold, its survival is contingent upon the facilitation exerted by the perennial species.

Currently, the model is being extended to three-species communities, with the aim of incorporating an explicit network theory approach and analyzing how topological asymmetries and intransitivities modulate the global resilience of the ecosystem [2].

[1] J. M. Alcántara, P. J. Rey, and A. J. Manzaneda, *A model of plant community dynamics based on replacement networks*, J. Veg. Sci. **26**, 524 (2015).

[2] J. M. Alcántara, M. Pulgar, and P. J. Rey, *Dissecting the role of transitivity and intransitivity on coexistence in competing species networks*, Theor. Ecol. **10**, 207 (2017).

Fitting power-law regimes with loglog-concave distributions

Núria Velasco Falguera[1], Isabel Serra[2], and Álvaro Corral[3,2;†]
[1]Centre de Recerca Matemàtica, Barcelona
[2]Departament de Matemàtiques, Universitat Autònoma de Barcelona
[3]Departament de Física, Universitat Autònoma de Barcelona
[†] alvaro.corral@uab.es

High variability is a fundamental phenomenon in statistical physics and complex-systems science. Important debates have taken place about how to characterize this high variability, and in particular, about if power-law distributions and power-law-tailed distributions are the best fits for particular real-world data sets. The "critical" issue is to find a threshold value of the variable from which a power-law fit works well. Several heuristic recipes have been proposed [1, 2], the most popular one being the Clauset-Shalizi-Newman method [1].

Here we propose a very different approach, introducing loglog-concave distributions. These are given by a probability density with the only restriction (appart from normalization) of being concave in a double logarithmic representation (concave in the mathematical convention, i.e., concave downwards). Loglog-concave distributions constitute a nonparametric family, encompassing many distributions widely used in complex-systems research, such as Pareto, Lévy-Smirnov, log-normal, Weibull, gamma, stretched exponential (including the exponential), and generalized extreme-value distributions. Remarkably, the power-law distribution is a limiting case of loglog-concavity (in the sense that it separates loglog-concavity from loglog-convexity).

We explore the maximum likelihood procedure applied to loglog-concave distributions, and explain how the resulting estimator takes the form of a piecewise power-law distribution. This estimator can be computed using an active set algorithm [3, 4]. This characterization provides the thresholds separating the different regions, together with their corresponding power-law exponents, which can be used as a criterion for identifying the ranges where the power-law distribution fit is appropriate.

We implement this approach using `R` and apply it both to simulated data and to representative datasets in extreme-value statistics and complex systems. An example of the output of the method can be seen in Fig. 1.

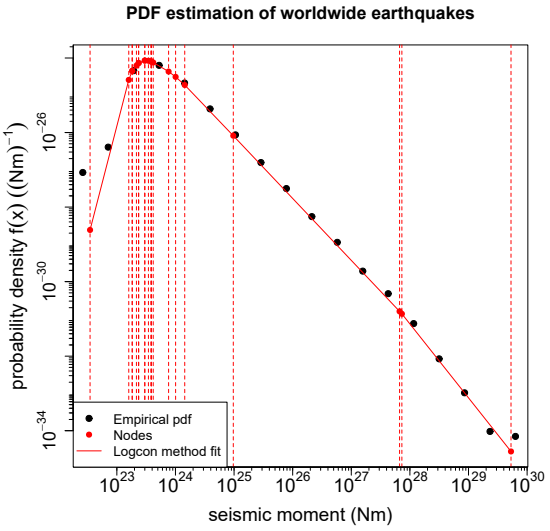

Fig. 1: Estimation of the probability density of the seismic moment of worldwide earthquakes data using the loglog-concave method. Black points indicate a histogram-like empirical estimation of the density (unrelated to the loglog-concave fitting method). Red points and vertical dashed lines indicate changes of power-law regimes. The most relevant regimes yield exponents 1.66 and 1.98.

[1] Clauset, A. et al., *Power-Law Distributions in Empirical Data*, SIAM Review **51**, 661–703, 2009.
[2] Corral, Á. & Deluca, A., *A practical recipe to fit discrete power-law distributions*, Acta Geophysica 61(6) 1351-1394, 2013.
[3] Pal, J. K., Woodroofe, M., & Meyer, M., *Estimating a Pólya frequency function*, Lecture Notes–Monograph Series 54, 239–249, 2007.
[4] Dümbgen, L., & Rufibach, K., *Active set and EM algorithms for log-concave densities based on complete and censored data*, arXiv:0707.4643, 2011.

Astrocyte-gated associative memory can produce self-attention through replicator dynamics

Arnau Vivet[1] and Alex Arenas[1 2]
[1]Departament d'Enginyeria Informàtica i Matemàtiques, Universitat Rovira i Virgili, 43007 Tarragona, Spain
[2]Complexity Science Hub Vienna, Metternichgasse 8, 1030 Vienna, Austria

Associative memory models explain how neural systems can store and retrieve information from partial or noisy cues, but classical formulations do not account for the active role of glial regulation in shaping neural computation. Astrocytes dynamically modulate synaptic transmission and network excitability, suggesting that memory retrieval may arise from coupled neuron–glia dynamics rather than from neuronal interactions alone. Here, we introduce a Hopfield-type associative memory in which effective synaptic connectivity is multiplicatively gated by astrocytic gains that evolve according to an entropy-regularized replicator equation. We show that the coupled neuron–astrocyte system admits a Lyapunov function, guaranteeing global convergence of the dynamics. At fixed points, astrocytic gains allocate resources through a softmax-normalized weighting of pattern similarity scores, thereby producing an emergent form of self-attention on the gain simplex. Across regimes of high memory load and strong interference, the model yields substantially higher retrieval accuracy than both classical Hopfield dynamics and recent neuron–astrocyte associative memory models. These results establish astrocyte-gated associative memory as a dynamical systems framework in which glial modulation supports competitive resource allocation and gives rise to attention-like computation.

Lista de participantes

Javier Aguilar Sánchez
The Abdus Salam International Centre for Theoretical Physics (ICTP), Trieste
jvrglrschz@gmail.com

Sergio Alonso Muñoz
Universitat Politècnica de Catalunya
s.alonso@upc.edu

Adolfo Alsina
Universidad Rey Juan Carlos
adolfo.alsina@urjc.es

Alberto Antonioni
Carlos III University of Madrid
alberto.antonioni@uc3m.es

Alex Arenas
Universitat Rovira i Virgili
alexandre.arenas@urv.cat

Saúl Ares
Centro Nacional de Biotecnología (CNB), CSIC
saul.ares@csic.es

Gerard Argany Herrera
Universitat de Barcelona Institute of Complex Systems (UBICS), Universitat de Barcelona
gerardargany@gmail.com

Lluís Arola Fernández
Universitat Rovira i Virgili
lluisarolaf@gmail.com

Oriol Artime Vila
Universitat de Barcelona
oartime@ub.edu

Giacomo Bartolucci
Universitat de Barcelona, Carrer de Mart í i Franquès, 1, 08028 Barcelona, Spain
bartolucci@ub.edu

Gemma Bel Bordes
Universitat Rovira i Virgili
gemma.bel@urv.cat

Federico Bellisardi
Institute for Cross-Disciplinary Physics and Complex Systems
fbellisardi@ifisc.uib-csic.es

Robert Benassai Dalmau
Universitat Oberta de Catalunya
rbenassai@uoc.edu

Guillermo Benito Calvino
Inria, INSA Lyon, CITI, UR3720, Villeurbanne, France
guillermo.benito-calvino@inria.fr

Rosa María Benito Zafrilla
Grupo de Sistemas Complejos. Universidad Politécnica de Madrid
rosamaria.benito@upm.es

José Manuel Blasco Losa
Centro Nacional de Biotecnología (CNB-CSIC)
jm.blasco@cnb.csic.es

Marián Boguñá Espinal
Universitat de Barcelona
marian.boguna@ub.edu

Josep Bonet Avalos
Departament d'Enginyeria Química, ETSEQ, Universitat Rovira i Virgili
josep.bonet@urv.cat

Javier Borge Holthoefer
Fundació per a la Universitat Oberta de Catalunya
jborgeh@uoc.edu

Javier Borondo Benito
Universidad Politécnica de Madrid
fj.borondo@upm.es

J. Javier Brey Abalo
Física Teórica. Universidad de Sevilla.
brey@us.es

Natalia Briñas
Universidad Carlos III de Madrid
nbrinas@math.uc3m.es

Javier Buceta Fernandez
Instituto de Biologia Integrativa de Sistemas (I2SysBio), CSIC-UV
javier.buceta@csic.es

Giulio Burgio
Instituto de Biologia Funcional y Genomica
giulioburgio@gmail.com

Daniel Campos Moreno
Depto de Física, Universidad Autónoma de Barcelona
daniel.campos@uab.cat

Francisco Javier Cao García
Facultad de Ciencias Físicas. Universidad Complutense de Madrid. & IMDEA Nanociencia
francao@ucm.es

José Ángel Capitán Gómez
Complex Systems Group and Department of Applied Mathematics, Universidad Politécnica de Madrid
ja.capitan@upm.es

David Mateo Carpio Rivas
Instituto: Instituto de Física Interdisciplinar y Sistemas Complejos IFISC (UIB-CSIC)
davidmateo@ifisc.uib-csic.es

Aleix Casals Cheng
Investigador predoctoral, Dept. d'Enginyeria Química, Universitat Rovira i Virgili
aleix.casals@urv.cat

Piergiorgio Castioni
Universitat Rovira i Virgili, Tarragona
piergiorgio.castioni@gmail.com

Luis Castro
Universitat Rovira i Virgili
luiseduardo.castro@urv.cat

Mario Castro Ponce
Instituto de Investigación Tecnólogica, Universidad Pontificia Comillas
marioc@comillas.edu

Miguel Ángel Chamorro Burgos
Física Teórica, Universidad de Sevilla, Apdo. 1065, 41080 Sevilla, Spain
mchamorro1@us.es

Pere Colet
Instituto de Física Interdisciplinar y Sistemas Complejos, IFISC (CSIC-UIB)
pere@ifisc.uib-csic.es

Alvaro Corral
Dept. de Fisica, Universitat Autonoma de Barcelona
alvaro.corral@uab.es

Raúl Coterillo Ruisánchez
Basque Center for Applied Mathematics (BCAM)
rcoterillo@bcamath.org

Emanuele Cozzo
Universitat de Barcelona
emanuele.cozzo@ub.edu

Javier Cristin
Profesor Lector en Universitat Autònoma de Barcelona
javier.cristin@uab.cat

Rodolfo Cuerno Rejado
Universidad Carlos III de Madrid, Dpto. de Matemáticas y Gpo. Interdisciplinar Sistemas Complejos
cuerno@math.uc3m.es

Jose Cuesta
Grupo Interdisciplinar de Sistemas Complejos - Universidad Carlos III de Madrid
cuesta@math.uc3m.es

Matteo De Leonardis
Dpto. de Física Teórica, Fac. de Ciencias Físicas, Univ. Complutense de Madrid (UCM), Madrid
matteo.deleonardis2@gmail.com

Merve Gozdenur Demirbek
Doctoral Student, Department of Chemical Engineering, Universitat Rovira i Virgili (Universitat Rovira i Virgili)
mervegozdenur.demirbek@urv.cat

Alejandro Diaz Moreno
Departament de Física, Universitat Politècnica de Catalunya
alejandrodimo95@gmail.com

Albert Diaz-Guilera
UBICS, Universitat de Barcelona
albert.diaz@ub.edu

Jonathan Diez
Fisica de materie condensada, Universitat de Barcelona, Institute of Complex Systems (UBICS)
Jonathan.Diez@ub.edu

Francesca Dilisante
Universidad de Zaragoza
francesca.dilisante.a@gmail.com

Virginia Dominguez Garcia
Estación Biológica de Doñana - CSIC
domgarvir@gmail.com

Jordi Duch
Departament d'Enginyeria Informàtica i Matemàtiques, Universitat Rovira i Virgili
jordi.duch@urv.cat

Blas Echebarria Domínguez
Dept. de Física i Institut de Recerca i Innovació en Salut, Universitat Politècnica de Catalunya
blas.echebarria@upc.edu

Iñaki Echeverría Huarte
Departamento de Física y Matemática Aplicada, Universidad de Navarra
iecheverriah@unav.es

Jordi Faraudo
Institut de Ciència de Materials de Barcelona (ICMAB-CSIC)
jfaraudo@icmab.es

Pablo Fernandez Garrido
Department of Physics and Center for Lifespan Changes in Brain and Cognition, University of Oslo
p.f.garrido@psykologi.uio.no

Antonio Fernández Peralta
Instituto de Física Interdisciplinar y Sistemas Complejos IFISC (CSIC-UIB), Palma de Mallorca, Spain
toni2.718@gmail.com

María José Franco Oñate
Departament de física de la matèria condensada, Universitat de Barcelona
mj.franco-onate@ub.edu

Giancarlo Franzese
Universitat de Barcelona
gfranzese@ub.edu

Javier Galeano
Universidad Politécnica de Madrid
javier.galeano@upm.es

Pablo Gallarta Sáenz
Universida de Zaragoza
pablogallarta00@gmail.com

Juan Gancio
Universitat Politècnica de Catalunya
juan.gancio@upc.edu

Elena García de Lamo
Universitat Politècnica de Catalunya
elena.garcia.de.lamo@upc.edu

María Isabel García de Soria Lucena
Física Teórica. Universidad de Sevilla.
gsoria@us.es

Jorge García Inglés
Departamento de Física Teórica de la Materia Condensada, Universidad Autónoma de Madrid
jorge.garciai@estudiante.uam.es

Jordi Garcia Ojalvo
Universidad Pompeu Fabra
jordi.g.ojalvo@upf.edu

Enrique García Ortiz
Universitat de Barcelona (UB), UB Institute of Complex Systems (UBICS)
enriquegarciaortiz@ub.edu

María Jinxue García Pantaleón Tarifa
Universitat Pompeu Fabra
mariajinxue.garciapantaleon@upf.edu

Rodrigo García-Muelas
Iberian Centre for Research in Energy Storage
rodrigo.garcia@ciiae.org

Sara Ghivarello
Universidad Carlos III de Madrid
sghivare@pa.uc3m.es

Adrià Gispert Fernández
Alephsys Lab, Dept. Enginyeria Informatica i Matemàtiques, Universitat Rovira i Virgili, Tarragona
adria.gispert.fernandez@gmail.com

Sergio Gómez
Universitat Rovira i Virgili
sergio.gomez@urv.cat

Jesús Gómez Gardeñes
Universidad de Zaragoza
gardenes@gmail.com

David González Méndez
Departamento de Física, Universidad de Extremadura
dgonzalezm@unex.es

Miguel A. González-Casado
Grupo Interdisciplinar de Sistemas Complejos, Universidad Carlos III de Madrid
miguelangel.gonzalezc@outlook.es

Mar Grande
Universidad Politécnica de Madrid
margrande45@gmail.com

Clara Granell Martorell
Universitat Rovira i Virgili
clara.granell@urv.cat

Marta Grasa Lainez
Dpto. de Física y Mat. Apl., Facultad de Ciencias, Universidad de Navarra, 31080 Pamplona, Spain
mgrasalaine@alumni.unav.es

Elvira Guardia
Departament de Física, Universitat Politècnica de Catalunya (UPC)
elvira.guardia@upc.edu

Pilar Guerrero Contreras
Universidad Carlos III de Madrid
pilar.guerrero@uc3m.es

Roger Guimerà
ICREA & Universitat Rovira i Virgili
roger.guimera@urv.cat

Adrián Gutiérrez Arroyo
Universidad Carlos III de Madrid, Departamento de Matemáticas, GISC
adgutier@math.uc3m.es

Gabriel Mallku Guzmán Schiller
Basque Center for Applied Mathematics
gguzman@bcamath.org

Violeta Hernandez Arnal
BIOCOM-SC, Departament de Física, Universitat Politècnica de Catalunya
vio.hernandez.arnal@gmail.com

Emilio Hernandez Garcia
IFISC, Instuto de Física Interdisciplinar y Sistemas Complejos (CSIC-UIB), Palma de Mallorca
emilio@ifisc.uib-csic.es

Antoni Hernández-Fernández
Institut de Ciències de l'Educació, Universitat Politècnica de Catalunya
antonio.hernandez@upc.edu

Jorge Hidalgo Aguilera
Universidad de Córdoba
jorge.hidalgo@uco.es

Marta Ibañes Miguez
Dept. Física de la Matèria Condensada, Facultat de Física, Universitat de Barcelona
mibanes@ub.edu

Miguel Ibáñez García
Departamento de Física Aplicada, Universidad de Granada
ibanez@ugr.es

Juan Iribas de la Puerta
Universidad Pontificia de Comillas
jiribas@comillas.edu

Javier Jarillo Díaz
Departamento de Estadística e Investigación Operativa, Universidad Complutense de Madrid
jjarillo@ucm.es

Daniel Jiménez Flores
Universidad de Sevilla
trabajosdani@outlook.es

Pedro Jiménez González
Instituto de Física Interdisciplinar y Sistemas Complejos
pjimenez@ifisc.uib-csic.es

Nagi Khalil Rodríguez
Departamento de Física y Matemáticas & GISC, Universidad de Alcalá
nagi.khalil@uah.es

Jungho Kim
Universitat Rovira i Virgili
jungho.kim@urv.cat

Lou Kondic
New Jersey Institute of Technology
kondic@njit.edu

Lucas Lacasa
IFISC (CSIC-UIB)
lucas@ifisc.uib-csic.es

Santiago Lamata Otín
Departamento de Física de la Materia Condensada, Universidad de Zaragoza
santiagolaot@gmail.com

Michela Lapenna
Universitat Rovira i Virgili
michela.11.lapenna@gmail.com

Teresa Lázaro Sánchez
Universitat Rovira i Virgili
teresa.lazaro@urv.cat

Inmaculada Leyva
Universidad Rey Juan Carlos
inmaculada.leyva@urjc.es

Jaume Llabrés Rubio
Instituto de Física Interdisciplinar y de Sistemas Complejos
jaumellabres@ifisc.uib-csic.es

Juan Manuel López
Instituto de Física de Cantabria - CSIC-UC
lopez@ifca.es

Judith López Zancajo
Universitat de Barcelona
jlopezzancajo@ub.edu

Juan Carlos Losada
Grupo de Sistemas Complejos. Universidad Politécnica de Madrid
juancarlos.losada@upm.es

Bartolo Luque Serrano
Profesor titular ETSI Aeronáutica y del Espacio de la UPM
bartolome.luque@upm.es

Allan Mackie Walker
Departament d'Enginyeria Química, Universitat Rovira i Virgili
allan.mackie@urv.cat

Raphaël Maire
Universitat de Barcelona
maire.raphael@yahoo.fr

Jorge Mampel
Institut de Física Interdisciplinària i Sistemes Complexos
jmampel@ifisc.uib-csic.es

Susanna Manrubia
Museo Nacional de Ciencias Naturales (CSIC). c/ José Gutiérrez Abascal 2, 28006 Madrid
smanrubia@mncn.csic.es

David March Pons
Departament de Física, Universitat Politècnica de Catalunya
david.march@upc.edu

Dimitri Marinelli
UBICS, Universitat de Barcelona
marinelli@ub.edu

Javier Martín Buldú
Universidad Rey Juan Carlos
jmbuldu@gmail.com

Johann Martinez
Universidad Rey Juan Carlos
johemart@gmail.com

Yuri Martínez Ratón
Departamento de Matemáticas (GISC). Universersidad Carlos III de Madrid.
yuri@math.uc3m.es

Pedro Martínez Saiz
Universitat Rovira i Virgili
pedro.martinez@urv.cat

Marina Martins Cano
BIOCOM-SC, Departament de Física, Universitat Politècnica de Catalunya
marina.martins.cano@upc.edu

Joan T. Matamalas
Universitat Rovira i Virgili
joantomas.matamalas@urv.cat

Manuel A. Matias
Instituto de Física Interdisciplianr y Sistemas Complejos (IFISC, CSIC-UIB)
manuel@ifisc.uib-csic.es

Mattia Mattei
Universitat Pompeu Fabra
mattia.mattei@upf.edu

Pablo Maynar Blanco
Física Teórica, Universidad de Sevilla
maynar@us.es

Manuel Mayo León
Física teórica, Facultad de Física, Universidad de Sevilla
mmayo@us.es

Mara Maza Cuello
Dept. of Condensed Matter Physics, Universitat de Barcelona, Spain
m.mazacuello@ub.edu

DIego Maza Ozcoidi
Departamento de Física, Facultad de Ciencias, Universidad de Navarra
dmaza@unav.es

Juan José Mazo Torres
Universidad Complutense de Madrid
jmazo@ucm.es

Alberto Megías Fernández
Grupo de Sistemas Complejos y Departamento de Matemática Aplicada, Universidad Politécnica de Madrid
alberto.megias@upm.es

Carlos Mejía Monasterio
ETSIAAB, Universidad Politécnica de Madrid
carlos.mejia@upm.es

Oscar Ricardo Mejía Parra
Universitat Politècnica de Barcelona
oscar.ricardo.mejia.parra@upc.edu

Marco Mendívil Carboni
Grupo Interdisciplinar de Sistemas Complejos (GISC), Universidad Complutense de Madrid
marcomc@ucm.es

María del Carmen Miguel López
Facultat de Física, Universitat de Barcelona
carmen.miguel@ub.edu

Manuel Miranda Barrado
Instituto de Física Interdisciplinar y Sistemas Complejos
m2bmanu@gmail.com

Daniela Molas
Universidad Autónoma de Barcelona (UAB)
danielamolas24@gmail.com

Ana Maria Montero Martinez
Dpto. de Física. Universidad de Extremadura
anamtr94@gmail.com

MIguel Angel Muñoz Martínez
Instituto Carlos I de Física Teórica y Computacional. Universidad de Granada
mamunoz@onsager.ugr.es

Francisco Javier Muñoz Ortega
Departamento de Matemática Aplicada, Universidad Politécnica de Madrid.
fcomunoz@alumnos.upm.es

Fernando Muñoz Puente
Biología computacional y Sistemas Complejos (BIOCOM-SC), UPC
fernandomunozpuente@gmail.com

Adrián Nadal Rosa
Instituto de Biología Integrativa de Sistemas, I2SysBio (CSIC-UV)
adrian.nadal@csic.es

Eduardo Nieto Vargas
Universidad de Granada e Instituto Carlos I de Física Teórica y Computacional
edunievar@onsager.ugr.es

Juan Carlos Nuño
Departamento de Matemática Aplicada. Universidad Politécnica de Madrid
juancarlos.nuno@upm.es

Mikel Ocio Moliner
Departament de Física de la Matèria Condensada, Universitat de Barcelona
mikelocio@ub.edu

Sara Oliver Bonafoux
Instituto de Física Interdisciplinar y Sistemas Complejos
saraoliver@ifisc.uib-csic.es

Simona Olmi
Istituto dei Sistemi Complessi - Consiglio Nazionale delle Ricerche
simona.olmi@cnr.it

David Ortiz del Campo
Instituto de Física Interdisciplinar y Sistemas Complejos (CSIC-UIB)
davidortiz@ifisc.uib-csic.es

Ignasi Pagonabarraga
UBICS, Universitat de Barcelona
ipagonabarraga@ub.edu

Giovanni Palermo
Universitat Rovira i Virgili
giovanni.palermo@urv.cat

Alberto Pascual-García
Spanish National Centre for Biotechnology (CSIC)
alberto.pascual.garcia@gmail.com

Alessandro Patti
Departamento de Física Aplicada, Universidad de Granada
apatti@ugr.es

Carlos Pérez Espigares
Departamento de Electromagnetismo y Física de la Materia. Universidad de Granada
carlosperez@ugr.es

Federico Pérez González
78987918f-179868-5
fperezgonza@alumni.unav.es

Ines Perez Mariño
Universidad Rey Juan Carlos, c/Tulipan s/n, Móstoles (Madrid), Spain
ines.perez@urjc.es

Alberto Perez Muñuzuri
Grupo de Física No Lineal. Facultad Físicas. Universidade de Santiago de Compostela
alberto.perez.munuzuri@usc.es

Vicente Pérez Muñuzuri
CRETUS. Grupo de Física No Lineal. Facultade de Físicas. Universidade de Santiago de Compostela
vicente.perez.munuzuri@usc.es

Arnau Prat Pou
Universitat Politècnica de Catalunya
arnau.prat.pou@upc.edu

Laureano Ramírez de la Piscina Millán
Dept de Física, Universitat Politécnica de Catalunya
laure.piscina@upc.edu

David Reguera
Departament de Física de la Matèria Condensada & UBICS, Facultad de Física, Universitat de Barcelona
dreguera@ub.edu

Fabio Revuelta Peña
Grupo de Sistemas Complejos, Universidad Politécnica de Madrid
fabio.revuelta@upm.es

Carlos Ríos Monje
Física Teorica, Universidad de Sevilla
crios1@us.es

Juan Carlos Rodríguez Cabanillas
Instituto de Física Interdisciplinar y Sistemas Complejos (IFISC, CSIC-UIB), Campus UIB, 07122 Palma
juancarlosrc@ifisc.uib-csic.es

Juan Manuel Rodriguez Parrondo
Universidad Complutense de Madrid y GISC
parrondo@fis.ucm.es

Javier Rodríguez-Laguna
Dto. Física Fundamental, UNED
jrlaguna@fisfun.uned.es

Adrián Roig Oliver
Universidad de Granada. Instituto Carlos I de Física teórica y Computacional
adriroig21@gmail.com

Consuelo Rojas Navarrete
Grupo de investigación en dinámica no lineal, óptica no lineal y lásers
consuelo.belen.paz.rojas@upc.edu

Pablo Rosillo Rodes
IFISC (UIB-CSIC)
prosillo@ifisc.uib-csic.es

Enrique Rozas Garcia
University of Gothenburg
enrique.rozas.garcia@physics.gu.se

Miguel Rubi
Departamento de Fisica de la Materia Condensada, Universidad de Barcelona
mrubi@ub.edu

Marta Sales Pardo
DEQ/ComSCIAM - Universitat Rovira i Virgili
marta.sales@urv.cat

Maxi San Miguel
IFISC (UIB-CSIC)
maxi@ifisc.uib-csic.es

Álvaro Sánchez de Andrés
Profesor investigación CSIC
alvaro.sanchez@usal.es

Marta Sánchez Díez
Universidad Politécnica de Madrid
marta.sdiez@upm.es

Paula Sánchez Rego
UC3M, Departamento de matemáticas, Grupo Interdisciplinar de Sistemas Complejos
paulasre@pa.uc3m.es

Anxo Sánchez Sánchez
GISC, Universidad Carlos III de Madrid
anxo@math.uc3m.es

José M. Sancho
Universitat de Barcelona
josemsancho@gmail.com

Silvia Santalla
Departamento de Física & GISC. Universidad Carlos III de Madrid
silvia.santalla@uc3m.es

Andrés Santos
Departamento de Física, Universidad de Extremadura
andres@unex.es

Verónica Sanz Arqué
Universidad Complutense De Madrid, Madrid, Spain
vsanz06@ucm.es

Pablo Sartori
GIMM
pablo.sartori@gimm.pt

Irene Sendiña Nadal
Complex Systems Group & GISC, Universidad Rey Juan Carlos, Madrid
irene.sendina@urjc.es

Beatriz Seoane Bartolomé
Departamento de Física Teórica, Universidad Complutense de Madrid
beseoane@ucm.es

M. Ángeles Serrano Moral
Universitat de Barcelona
marian.serrano@ub.edu

Ivan Sevostianov
Institute for Cross-Disciplinary Physics and Complex Systems, Palma de Mallorca, Spain
sevostianov@ifisc.uib-csic.es

Nathan Silvano
Institute for Cross-Disciplinary Physics and Complex Systems (UIB-CSIC)
nathanosilvano@gmail.com

Tomas Sintes Olives
Instituto de Física Interdisciplinar y Sistemas Complejos (IFISC). UIB-CSIC
tomas.sintes@uib.es

David Soriano Paños
Universitat Rovira i Virgili
sorianopanos@gmail.com

Ángela Tajuelo Valbuena
Universidad de Granada
atajuelo@correo.ugr.es

Pedro Tarazona Lafarga
Departamento de Fisica Teorica de la Materia Condensada, Universidad Autónoma de Madrid
pedro.tarazona@uam.es

Daniel Téllez Calle
Departamento de física atómica, molecular y nuclear, Universidad de Sevilla
dtellez@us.es

Raul Toral
IFISC, Universitat Illes Balears
raul@ifisc.uib-csic.es

Sergi Torres Serra
Universitat Politècnica de Catalunya
sergi.torres.serra@upc.edu

Lluís Torres-Hugas
Departament d'Enginyeria Informàtica i Matemàtiques, Universitat Rovira i Virgili, Tarragona, 43007,
lluis.torres@urv.cat

Núria Velasco Falguera
Centre de Recerca Matemàtica
nuriavelascofalguera@gmail.com

Xavier Viader Godoy
Departament de Medicina i Ciències de la Vida, Universitat Pompeu Fabra
xavier.viader@upf.edu

Arnau Vivet Parés
Universitat Rovira i Virigili
arnau.vivet@gmail.com

Iker Zuriguel Ballaz
Universidad de Navarra
iker@unav.es